

ULTRA-HIGH TEMPERATURE STEAM GASIFICATION OF BIOMASS

Qari Muhammad Khalid Waheed

**Submitted in accordance with the requirements for the degree of
Doctor of Philosophy**

**The University of Leeds
School of Process, Environmental and Materials Engineering**

October 2013

The candidate confirms that the work submitted is his own, except where work which has formed part of jointly-authored publications has been included. The contribution of the candidate and the other authors to this work has been explicitly indicated below. The candidate confirms that appropriate credit has been given within the thesis where reference has been made to the work of others

This copy has been supplied on the understanding that it is copyright material and that no quotation from the thesis may be published without proper acknowledgement.

The details of chapter 4 and chapter 5.3 of the thesis are based on the following published papers, respectively:

[1] WAHEED, Q. & NAHIL, M.A. & WILLIAMS, P.T. (2013) Pyrolysis of waste biomass: investigation of fast pyrolysis and slow pyrolysis process conditions on product yield and gas composition. *Journal of Energy Institute* 4 (2013) 233 - 241.

[2] WAHEED, Q. & WILLIAMS, P.T. (2013) Hydrogen production from high temperature pyrolysis/steam reforming of waste biomass: rice husk, sugarcane bagasse and wheat straw. *Energy & Fuel* 27 (2013) 6695 - 6704.

The candidate (Qari Waheed) performed the experimental work and prepared the initial draft along with the graphical and tabular presentation, calculation and summarization of the papers.

The co-author (Prof. Dr. P.T. Williams) supervised the work, proof read the drafts and made suggestions and corrections to the draft papers.

The co-author (Dr. M.A. Nahil) helped to perform slow pyrolysis experiments on his one-stage reactor in first paper.

ACKNOWLEDGEMENTS

“Praise be to Allah, the most beneficent and the most merciful”

I owe my deepest gratitude to the University of Engineering and Technology Peshawar, Pakistan and Higher Education Commission Pakistan for their financial support during my study abroad.

My heartily gratitude and appreciation go to my supervisor, Prof. Paul. T. Williams, for his continuous and constant support throughout this research. His kindness, patience, motivation, enthusiasm and guidance helped me a lot throughout the duration of this study.

I would like to thank Dr. Chunfei Wu, Dr. Jude Onwudili, Dr. Anas Nahil, Dr. Adrian Cunliffe, and Dr. Surjit Singh for their encouragement and guidance during this research. I would like to thank Mr. Ed Woodhouse for his continuous support from design and manufacturing of the reactor to various timely repairs and modifications. I am grateful to Eyub, Alfred, Naji, Rattana, Ruzinah, Faeiza, Safari, Brian, Ibrahim, Chidi, Paula, Eyup, Chika, Jonathan, Junizah, Amar, and Ramzi for their invaluable support and friendship they have shared with me. I am thankful to my friends Dr. Jafar Iqbal, Yameen Sandhu, Asim Ali, Safeer Haider, Dr. Shahid Maqsood, Dr. Bilal Ahmed, Dr. Shakoor, Mahabat Khan, Ali Arif and Imran Bashir for their help, support and encouragement.

I am very thankful to my parents, Muhammad Aslam and Ruqayya Aslam for their unconditional support during this research. I am thankful to my brothers and sisters for their time to time encouragement. Finally I am deeply thankful to my wife Sumiya for her unprecedented support, love, understanding and motivation during this research.

ABSTRACT

In this research, hydrogen production from conventional slow pyrolysis, flash pyrolysis, steam gasification and catalytic steam gasification of various biomass samples including rice husk, wood pellets, wheat straw and sugarcane bagasse was investigated at ultra-high temperature (~ 1000 °C). During flash pyrolysis of the waste wood, the gas yield was improved to ~ 78 wt.% as compared to ~ 25 wt.% obtained during slow pyrolysis. The addition of steam enhanced the hydrogen concentration from 26.91 vol.% for pyrolysis to 44.13 vol.% for steam gasification. The comparison of pyrolysis, steam gasification and catalytic steam gasification in a down-draft gasification reactor at 950 °C using rice husk, bagasse and wheat straw showed a significant increase in gas yield as well as hydrogen yield. The hydrogen yield was enhanced from ~ 2 mmoles g^{-1} for pyrolysis to ~ 25 mmoles g^{-1} during steam gasification using a 10 wt.% Ni-dolomite catalyst. The higher hydrogen yield was due to the enhanced steam reforming of hydrocarbons and thermal cracking of tar compounds at higher temperature. When compared with the other catalysts such as 10 wt.% Ni-dolomite, 10 wt.% Ni-MgO, and 10 wt.% Ni-SiO₂, the 10 wt.% Ni-Al₂O₃ catalyst showed the highest hydrogen yield of 29.62 mmoles g^{-1} . The investigation on gasification temperature showed that the hydrogen yield was significantly improved from 21.17 mmoles g^{-1} at 800 °C to 35.65 mmoles g^{-1} at 1050 °C. The hydrogen concentration in the product gas mixture was increased from 50.32 vol.% at 800 °C to 67.41 vol.% at 1050 °C. The increase in steam injection rate from 6 to 35 ml hr^{-1} enhanced the hydrogen yield from 29.93 mmoles g^{-1} to 44.47 mmoles g^{-1} . The hydrogen concentration increased from 60.73 to 72.92 vol.%. The increase was mainly due to the shift in the equilibrium of the water gas shift reaction as H₂:CO ratio increased from 2.97 to 7.78. The other process variables such as catalyst to sample ratio, carrier gas flow rate showed little or no influence on the gas yield and hydrogen yield. The steam gasification of residual biomass char was performed at 950 °C to recover extra hydrogen. The presence of 10 wt.% Ni-Al₂O₃ in the gasifier improved the hydrogen yield to ~ 47 mmoles per gram of biomass as compared to the other catalysts such as 10 wt.% Ni-dolomite and 10 wt.% Ni-MgO. The gasification temperature showed a positive influence on hydrogen yield from 750 °C to 950 °C. The increase in steam injection rate from 6 ml hr^{-1} to 15 ml hr^{-1} enhanced the hydrogen yield from 46.81 to 52.10 mmoles g^{-1} of biomass.

TABLE OF CONTENTS

ACKNOWLEDGEMENTS	iii
ABSTRACT	iv
TABLE OF CONTENTS	v
LIST OF TABLES	xii
LIST OF FIGURES	xiv
ABBREVIATIONS	xix
NOMENCLATURE	xx
Chapter 1 INTRODUCTION	1
1.1 World energy demand and resources	1
1.2 Biomass and organic waste	3
1.3 Hydrogen.....	6
1.3.1 Hydrogen economy	6
1.3.2 Hydrogen production	7
1.3.2.1 Steam methane reforming (SMR) of natural gas.....	7
1.3.2.2 Coal gasification.....	8
1.3.2.3 Biomass gasification.....	8
1.3.2.4 Electrolysis (Direct/Wind/Solar).....	9
1.3.2.5 Nuclear thermochemical.....	10
1.4 Energy from biomass	11
1.4.1 Biological methods	11
1.4.1.1 Fermentative hydrogen production.....	11
1.4.1.2 Anaerobic digestion.....	11
1.4.2 Thermochemical methods	12
1.4.2.1 Combustion	12
1.4.2.2 Pyrolysis	12
1.4.2.3 Gasification	13
1.5 Chapter references.....	15
Chapter 2 LITERATURE REVIEW	17
2.1 Biomass gasification	17
2.1.1 Gasification reactions.....	18
2.1.2 Syngas clean-up systems.....	19
2.1.3 Tar removal	19
2.2 Review of gasification conditions.....	21

2.2.1	Feedstock composition.....	22
2.2.2	Biomass particle size.....	28
2.2.3	The influence of gasification temperature.....	32
2.2.4	Steam to biomass ratio	36
2.2.5	The influence of gasifying agent.....	38
2.3	Gasification reactors.....	40
2.3.1	Fixed bed reactors	40
2.3.1.1	Up-draft fixed-bed reactors	40
2.3.1.2	Down-draft fixed-bed reactors	42
2.3.2	Fluidised bed reactors	43
2.3.2.1	Bubbling fluidised bed reactors.....	44
2.3.2.2	Circulating fluidised bed reactors.....	45
2.4	Catalytic gasification.....	47
2.4.1	Mineral-based catalysts.....	48
2.4.1.1	Dolomite.....	48
2.4.1.2	Olivine.....	49
2.4.2	Nickel based and other metal catalysts	50
2.5	Ultra-high temperature gasification of biomass.....	53
2.6	Research aims and objectives.....	54
2.7	Conclusions.....	56
2.8	Chapter references.....	58
Chapter 3 RESEARCH METHODOLOGY		67
3.1	Introduction.....	67
3.2	Materials.....	68
3.2.1	Biomass.....	68
3.2.2	Catalyst.....	73
3.3	Pyrolysis/gasification reactors	74
3.3.1	Up-draft ultra-high temperature fixed-bed reactor.....	74
3.3.1.1	Up-draft flash pyrolysis reactor.....	74
3.3.1.2	Standard operating procedure for up-draft flash pyrolysis reactor	78
3.3.1.3	Repeatability test for up-draft flash pyrolysis reactor	78
3.3.2	Down-draft ultra-high temperature fixed bed reactor	80
3.3.2.1	Down-draft catalytic steam gasification reactor.....	80

3.3.2.2	Standard operating procedure for down-draft gasification reactor	82
3.3.2.3	Repeatability test for down-draft catalytic steam gasification reactor	83
3.3.3	Single-stage fixed bed reactor	84
3.4	Analysis and characterisation	86
3.4.1	Gaseous products analysis	86
3.4.1.1	Gas analysis	86
3.4.2	Biomass and char characterization	87
3.4.2.1	Proximate analysis	87
3.4.2.2	Ultimate analysis	89
3.4.2.3	X-ray fluorescence (XRF) analysis of ash	90
3.4.3	Catalyst characterization	90
3.4.3.1	Temperature programmed oxidation (TPO)	90
3.4.3.2	Scanning electron microscopy (SEM)	92
3.4.3.3	Transmission electron microscopy (TEM)	93
3.4.3.4	Brunauer–Emmett–Teller (BET) surface area analysis ...	94
3.4.3.5	X-ray diffraction (XRD) analysis	95
3.5	Chapter references	96
Chapter 4	FAST AND SLOW PYROLYSIS OF BIOMASS	97
4.1	Introduction	97
4.2	Fast and slow pyrolysis of biomass at 850 °C	98
4.2.1	Product yield	98
4.2.2	Gas composition from fast pyrolysis and slow pyrolysis of biomass at 850 °C	102
4.3	The influence of temperature on product yield from fast pyrolysis	103
4.3.1	Product yield	103
4.3.2	The effect of fast pyrolysis temperature on gas composition	106
4.4	The influence of steam on the fast pyrolysis of biomass	108
4.5	Potential hydrogen production for fast pyrolysis	110
4.6	Conclusions	111
4.7	Chapter references	113
Chapter 5	TWO-STAGE PYROLYSIS GASIFICATION OF RICE HUSK, BAGASSE AND WHEAT STRAW	115
5.1	Introduction	115

5.2	Characterization of rice husk, sugarcane bagasse and wheat straw using thermogravimetric analysis	115
5.2.1	Comparison of biomass samples	116
5.2.2	The effect of heating rate	118
5.2.3	The effect of particle size	121
5.2.4	Kinetic parameters	125
5.2.5	Comparison of activation energy from literature	127
5.2.6	Conclusions for section 5.2	130
5.3	Hydrogen production from ultra-high temperature pyrolysis, steam gasification and catalytic steam gasification of rice husk, sugarcane bagasse and wheat straw	131
5.3.1	Characterization of fresh catalysts	132
5.3.2	Pyrolysis of rice husk, sugarcane bagasse and wheat straw.....	136
5.3.2.1	Product yield from pyrolysis	136
5.3.2.2	Gas composition and hydrogen production	138
5.3.3	Steam gasification of rice husk, bagasse and wheat straw	141
5.3.3.1	Product yield from steam gasification	141
5.3.3.2	Gas composition from steam gasification	142
5.3.4	Dolomite catalytic steam gasification of rice husk, bagasse and wheat straw.....	144
5.3.4.1	Product yield from dolomite catalytic steam gasification.....	144
5.3.4.2	Gas composition from dolomite catalytic steam gasification	146
5.3.5	10 wt.% Ni-dolomite catalytic steam gasification of rice husk, bagasse and wheat straw	146
5.3.5.1	Product yield from 10 wt.% Ni-dolomite catalytic steam gasification	146
5.3.5.2	Gas composition and hydrogen production	148
5.3.6	Characterization of reacted catalysts.....	150
5.3.7	Conclusions for section 5.3	153
5.4	The influence of process conditions on ultra-high temperature catalytic steam gasification of rice husk using 10 wt.% Ni-dolomite catalyst. ...	154
5.4.1	The influence of gasification temperature.....	154
5.4.1.1	Product yield.....	154
5.4.1.2	The influence of temperature on gas composition and hydrogen production	157
5.4.2	The effect of water/steam injection rate.....	162

5.4.2.1	Product yield.....	162
5.4.2.2	The influence of water injection rate on gas composition and hydrogen production.....	164
5.4.3	The influence of biomass particle size	168
5.4.3.1	Product yield.....	168
5.4.3.2	The influence of particle size on gas composition and hydrogen production	170
5.4.4	The influence of catalyst to sample ratio	171
5.4.4.1	Product yield.....	171
5.4.4.2	The influence of catalyst to sample ratio on gas composition and hydrogen production.....	173
5.4.5	The influence of carrier gas flow rate	174
5.4.5.1	Product yield.....	174
5.4.5.2	The influence of carrier gas flow rate on gas composition and hydrogen production.....	175
5.4.6	Conclusions for section 5.4.....	176
5.5	Chapter references.....	178
Chapter 6 CATALYST SELECTION & PYROLYSIS/GASIFICATION OF BAGASSE		186
6.1	Introduction.....	186
6.2	Catalyst selection for hydrogen production from pyrolysis-gasification of sugarcane bagasse	187
6.2.1	Characterisation of the fresh researched catalysts	187
6.2.2	Product yield	190
6.2.3	The influence of different catalysts on gas composition and hydrogen production	193
6.2.4	Characterisation of reacted catalyst	195
6.3	The influence of gasification temperature.....	201
6.3.1	Product yield	201
6.3.2	The influence of temperature on gas composition and hydrogen production	203
6.3.3	Characterization of reacted 10 % Ni-Al ₂ O ₃ catalyst.....	205
6.4	The influence of Ni loading	208
6.4.1	Product yield	208
6.4.2	The influence of Ni-loading on gas composition and hydrogen production	209
6.4.3	Characterization of reacted Ni-Al ₂ O ₃ catalysts.....	211

6.5	The influence of water/steam injection rate	214
6.5.1	Product yield	214
6.5.2	The influence of water injection rate on gas composition and hydrogen production	215
6.6	The influence of calcination temperature.....	217
6.6.1	Characterization of fresh catalysts	217
6.6.2	Product yield	219
6.6.3	The influence of calcination temperature on gas composition and hydrogen production	220
6.7	The influence of catalyst to sample ratio	222
6.7.1	Product yield	222
6.7.2	The influence of catalyst to sample ratio on gas composition and hydrogen production	224
6.8	Conclusions	226
6.9	Chapter references.....	228
Chapter 7 CHAR GASIFICATION		231
7.1	Introduction.....	231
7.2	Characterization of char from rice husk wheat straw and sugarcane bagasse pyrolysis.....	232
7.3	The influence of different catalysts on hydrogen production from gasification of sugarcane bagasse char at 950 °C	235
7.3.1	Product yield	235
7.3.2	The influence of different catalysts on gas composition and hydrogen production	237
7.4	The influence of temperature on char gasification.....	238
7.4.1	Product yield	238
7.4.2	The influence of temperature on gas composition and hydrogen production	240
7.5	The influence of water/steam injection rate on gasification of char	242
7.5.1	Product yield	242
7.5.2	The influence of water injection rate on gas composition	243
7.6	Conclusions	245
7.7	Chapter references.....	246
Chapter 8 CONCLUSIONS AND FUTURE WORK.....		248
8.1	Introduction.....	248
8.2	Conclusions	249

8.2.1 Pyrolysis of waste biomass: Investigation of fast pyrolysis and slow pyrolysis process conditions on product yield and gas composition	249
8.2.2 Characterization of rice husk, sugarcane bagasse and wheat straw using thermogravimetric analysis	250
8.2.3 Hydrogen production from ultra-high temperature pyrolysis, steam gasification and catalytic steam gasification of rice husk, sugarcane bagasse and wheat straw	251
8.2.4 The influence of various process conditions on ultra-high temperature catalytic steam gasification of rice husk using 10 wt.% Ni-dolomite catalyst at 950 °C	251
8.2.5 The influence of catalyst and other process conditions on ultra-high temperature catalytic steam gasification of sugarcane bagasse	252
8.2.6 Catalytic steam gasification of residual biomass char	254
8.3 Future work	255
APPENDIX - A GAS CALCULATIONS	257
APPENDIX - B CALCULATION OF KINETIC PARAMETERS	262
APPENDIX - C GLOSSARY OF COMMONLY USED TERMS.....	265

LIST OF TABLES

Table 1-1 “ Proved ^a ” world oil reserve estimates from selected sources [3]	2
Table 1-2 Biomass energy potentials and current use in different regions (EJ/a) (EJ=10 ¹⁸) [15]	9
Table 2-1 Different classes of tar compounds [9].....	20
Table 2-2 Chemical composition of various biomasses: based on proximate analysis (wt.% dry basis) and ultimate analysis (wt.% dry, ash-free basis) adapted from [16].	22
Table 2-3 Ash composition of biomass (parts per million weight of dry biomass) [19]	25
Table 2-4 Component analysis of biomass (wt.% db) [20].....	27
Table 2-5 Various zones in the fixed-bed reactors and the respective reactions adapted from [87]	43
Table 2-6 Comparison of fixed bed and fluidized bed reactors [79]	46
Table 3-1 Proximate and ultimate analysis of feedstock	70
Table 3-2 Proximate and ultimate analysis of biomass feedstock sourced from Pakistan	71
Table 3-3 Surface properties of fresh catalysts	94
Table 4-1 Product yield from the fast pyrolysis of wood, rice husks and forestry residue in relation to pyrolysis temperature	104
Table 4-2 Gas composition from the fast pyrolysis of wood, rice husks and forestry residue in relation to pyrolysis temperature.....	107
Table 4-3 Gas composition and hydrogen production from the steam gasification of wood	108
Table 5-1 Cellulose, hemicellulose and lignin contents of biomass samples [1].....	116
Table 5-2 The effect of particle size on weight loss of biomass samples	124
Table 5-3 Comparison of kinetic parameters with literature	127
Table 5-4 Kinetic parameters	128
Table 5-5 Results from Coats-Redfern method	129
Table 5-6 Surface properties of fresh catalysts	132
Table 5-7 Pyrolysis of different biomass samples	137
Table 5-8 Steam gasification of different biomass samples.....	141
Table 5-9 Dolomite catalytic steam gasification of different biomass samples.....	145
Table 5-10 10 wt.% Ni-dolomite catalytic steam gasification of different biomass samples	148

Table 5-11 The effect of gasification temperature on pyrolysis-gasification of rice husk	155
Table 5-12 The effect of temperature on BET surface area of reacted 10 wt.% Ni-dolomite	159
Table 5-13 The influence of water injection rate on pyrolysis /gasification of rice husk	163
Table 5-14 The effect of particle size on pyrolysis-gasification of rice husk	168
Table 5-15 The effect of catalyst to sample ratio on pyrolysis-gasification of rice husk	172
Table 5-16 The influence of carrier gas flow rate on pyrolysis-gasification of rice husk	175
Table 6-1 Surface properties of fresh catalysts	187
Table 6-2 Results of pyrolysis (950 °C) - gasification (950 °C) of sugarcane bagasse with or without different catalysts	191
Table 6-3 The influence of different catalysts on product yield from pyrolysis (950 °C) -gasification (1000 °C) of sugarcane bagasse.....	192
Table 6-4 Comparison of surface area of fresh and reacted catalyst	195
Table 6-5 The influence of gasification temperature on pyrolysis-gasification of sugarcane bagasse (pyrolysis temperature of 950 °C)	202
Table 6-6 The influence of gasification temperature on surface area of catalyst	205
Table 6-7 The effect of Ni-loading on pyrolysis (950 °C) - gasification (950 °C) of bagasse	208
Table 6-8 The influence of water injection rate on pyrolysis (950 °C) - gasification (1000 °C) of sugarcane bagasse.....	214
Table 6-9 Surface properties of fresh catalysts	218
Table 6-10 The effect of calcination temperature on pyrolysis (950 °C) - gasification (1000 °C) of sugarcane bagasse.....	219
Table 6-11 The effect of catalyst to sample ratio on pyrolysis (950 °C) - gasification (1000 °C) of sugarcane bagasse.....	223
Table 7-1 Elemental analysis of feedstock char.....	232
Table 7-2 XRF analysis of ash from different biomass samples (wt.%)	234
Table 7-3 Gasification of sugarcane bagasse char at 950 °C using various catalysts...	235
Table 7-4 The influence of temperature on gasification of bagasse char	239
Table 7-5 The influence of water injection rate on gasification of bagasse char.....	243

LIST OF FIGURES

Figure 1-1 World total primary energy supply by fuels in 2010 [1].....	1
Figure 1-2 Overview of renewable energy production from biomass [7].....	5
Figure 2-1 Schematic diagram of an up-draft reactor [87]	41
Figure 2-2 Schematic diagram of a down-draft reactor [78].....	42
Figure 2-3 Bubbling fluidised bed reactor (left) and circulating fluidised bed reactor (right) adapted from [79]	45
Figure 3-1 Photographs and SEM images of waste wood (a and b), rice husk (c and d) and forestry residue (e and f)	69
Figure 3-2 Photographs and SEM images of rice husk (a and b), bagasse (c and d) and wheat straw (e and f).....	72
Figure 3-3 Photograph of the ultra-high temperature up-draft reactor	75
Figure 3-4 Schematic diagram of the ultra-high temperature up-draft reactor	76
Figure 3-5 Repeatability test results for the up-draft ultra-high temperature reactor	79
Figure 3-6 Photograph of the ultra-high temperature down-draft reactor.....	80
Figure 3-7 Schematic diagram of the ultra-high temperature down-draft catalytic gasification reactor.....	81
Figure 3-8 Repeatability test results for down-draft ultra-high temperature reactor	84
Figure 3-9 Schematic diagram of slow pyrolysis reactor.....	85
Figure 3-10 Schematic diagram of a gas chromatography system	86
Figure 3-11 A schematic diagram of thermogravimetric analyser [5].....	88
Figure 3-12 Example graph of proximate analysis of biomass sample	89
Figure 3-13 Schematic diagram of a CHNS elemental analyser adapted from [6].....	90
Figure 3-14 TGA-TPO and DTG-TPO thermograms of different spent catalysts.....	91
Figure 3-15 LEO 1530 scanning electron microscope.....	92
Figure 3-16 Phillips CM200 transmission electron microscope	93
Figure 3-17 Bruker D8 X-ray diffraction (XRD) analyser [8].....	95
Figure 4-1 Comparison of product yield and gas composition from slow and fast pyrolysis of wood at 850 °C	99
Figure 4-2 Comparison of product yield and gas composition from slow and fast pyrolysis of rice husk at 850 °C.....	100
Figure 4-3 SEM images of residual char from slow and fast pyrolysis at 850 °C. Slow pyrolysis (a), and fast pyrolysis (b) of rice husk. Slow pyrolysis (c), and fast	

pyrolysis (d) of forestry residue. Slow pyrolysis (e) and fast pyrolysis (f) of wood biomass.	101
Figure 4-4 Comparison of product yield and gas composition from slow and fast pyrolysis of forestry residue at 850 °C	102
Figure 4-5 Broido model for the decomposition of cellulose [22].....	105
Figure 4-6 Thermal degradation of biomass in an inert atmosphere adapted from [3].	106
Figure 4-7 Percentage of the potential hydrogen production from various biomass samples	110
Figure 5-1 TGA and DTG thermograms of rice husk, sugarcane bagasse and wheat straw at 20 °C min ⁻¹ heating rate.	117
Figure 5-2 TGA and DTG thermograms of rice husk at 5, 20 and 40 °C min ⁻¹ heating rates.....	119
Figure 5-3 TGA and DTG thermograms of sugarcane bagasse at 5, 20 and 40 °C min ⁻¹ heating rates	120
Figure 5-4 TGA and DTG thermograms of wheat straw at 5, 20 and 40 °C min ⁻¹ heating rates.....	121
Figure 5-5 The influence of particle size on TGA and DTG thermograms of rice husk at 20 °C min ⁻¹ heating rate	122
Figure 5-6 The effect of particle size on TGA and DTG thermograms of bagasse at 20 °C min ⁻¹ heating rate	123
Figure 5-7 The influence of particle size on TGA and DTG thermograms of wheat straw at 20 °C min ⁻¹ heating rate	125
Figure 5-8 Pore size distribution (a), and N ₂ adsorption/desorption isotherms of the fresh catalysts (b).	133
Figure 5-9 SEM images of fresh catalysts (a) fresh dolomite non-calcined, (b) dolomite calcined at 1000 °C, (c) 10 wt.% Ni-dolomite calcined at 900 °C	134
Figure 5-10 TEM-EDX of fresh 10 wt.% Ni-dolomite catalysts calcined at 900 °C ...	135
Figure 5-11 XRD of fresh catalysts (a) fresh dolomite non-calcined, (b) fresh dolomite calcined at 1000 °C, (c) fresh 10 wt.% Ni-dolomite.....	136
Figure 5-12 Syngas composition from pyrolysis and steam gasification of rice husk (RH), sugarcane bagasse (BG), and wheat straw (WS).....	139
Figure 5-13 Syngas composition from dolomite catalytic steam gasification and 10 wt.% Ni-dolomite catalytic steam gasification of rice husk (RH), sugarcane bagasse (BG), and wheat straw (WS).	149
Figure 5-14 TGA-TPO and DTG-TPO results of reacted dolomite (Dol) and reacted 10 wt.% Ni-dolomite (Ni-Dol) catalysts during the catalytic steam gasification of rice husk (RH), bagasse (BG), and wheat straw (WS) at 950 °C.	151

Figure 5-15 TEM image of reacted 10 wt.% Ni-dolomite (Ni-Dol) catalysts	152
Figure 5-16 The effect of temperature on gas composition during the pyrolysis-gasification of rice husk	157
Figure 5-17 SEM images of fresh and reacted catalysts showing the effect of temperature (a) fresh 10 wt.% Ni-dolomite , (b) reacted 10 wt.% Ni-dolomite at 850 °C, (c) reacted at 900 °C, (d) reacted at 950 °C, (e) reacted at 1000 °C and (f) reacted at 1050 °C.....	160
Figure 5-18 TGA-TPO and DTG-TPO results showing the effect of temperature on reacted 10 wt.% Ni-dolomite catalyst during the pyrolysis-gasification of rice husk	161
Figure 5-19 The effect of water injection rate on gas composition during the pyrolysis-gasification of rice husk.....	165
Figure 5-20 TGA-TPO and DTG-TPO results showing the effect of water injection rate on reacted 10 wt.% Ni-dolomite catalyst during the pyrolysis-gasification of rice husk.....	166
Figure 5-21 SEM images of reacted catalysts showing the effect of water injection rate (a) reacted 10 wt.% Ni-dolomite at 2 ml hr ⁻¹ , (b) at 4 ml hr ⁻¹ , (c) at 6 ml hr ⁻¹ and (d) at 10 ml hr ⁻¹	167
Figure 5-22 The influence of particle size on gas composition during the pyrolysis-gasification of rice husk.....	170
Figure 5-23 The effect of catalyst to sample ratio on gas composition during the pyrolysis-gasification of rice husk.....	173
Figure 5-24 The effect of carrier gas flow rate on gas composition during the pyrolysis-gasification of rice husk.....	176
Figure 6-1 Pore size distribution (a), and N ₂ adsorption/desorption isotherms of the fresh catalysts (b).....	188
Figure 6-2 TGA results for mixture of bagasse and each produced catalyst	189
Figure 6-3 Composition of gases in the product mixture at 950 °C	193
Figure 6-4 Gas composition showing the influence of different catalyst at 1000 °C ...	194
Figure 6-5 TGA-TPO and DTG-TPO results of different coked catalyst during the pyrolysis-gasification of bagasse at 950 °C.....	196
Figure 6-6 TGA-TPO and DTG-TPO results of different coked catalyst during the pyrolysis-gasification of bagasse at 1000 °C.....	197
Figure 6-7 SEM images of fresh and reacted catalysts (a) fresh 10 wt.% Ni-dolomite , (b) reacted 10 wt.% Ni-dolomite at 950 °C, (c) fresh 10 % Ni-Al ₂ O ₃ , (d) reacted 10 % Ni-Al ₂ O ₃ , (e) fresh 10 wt.% Ni-MgO, and (f) reacted 10 wt.% Ni-MgO ...	199

Figure 6-8 SEM images of fresh and reacted catalysts (a) fresh 10 wt.%Ni-SiO ₂ , (b) reacted 10 wt.% Ni- SiO ₂ at 950 °C, (c) fresh 2 % Ce -10 % Ni-dolomite , (d) reacted 2 % Ce - 10 % Ni-dolomite, (e) fresh 5 % Ce - 10 wt.% Ni-dolomite and (f) reacted 5 % Ce - 10 wt.% Ni-dolomite.....	200
Figure 6-9 SEM of fresh and reacted catalysts (a) fresh 10 % Ce - 10wt.%Ni-dolomite and (b) reacted 10 % Ce - 10wt.%Ni-dolomite	201
Figure 6-10 The influence of gasification temperature on gas composition during the pyrolysis-gasification of sugarcane bagasse	204
Figure 6-11 TGA-TPO and DTG-TPO results showing the effect of temperature on reacted 10 wt.%Ni-Al ₂ O ₃ catalyst during the pyrolysis-gasification of sugarcane bagasse	206
Figure 6-12 SEM images of reacted 10 % Ni-Al ₂ O ₃ catalysts reacted at different temperatures (a) at 800 °C, (b) at 850 °C, (c) at 900 °C, (d) at 950 °C, (e) at 1000 °C, and (f) at 1050 °C	207
Figure 6-13 The influence of Ni loading on gas composition during the pyrolysis-gasification of bagasse	210
Figure 6-14 The influence of Ni-loading on surface area of fresh and reacted catalysts	211
Figure 6-15 TGA-TPO and DTG-TPO results showing the effect of Ni-loading on reacted Ni-alumina catalyst during the pyrolysis-gasification of bagasse.....	212
Figure 6-16 SEM images of fresh and reacted catalysts (a) fresh 5 wt.% Ni-Al ₂ O ₃ , (b) reacted 5 wt.% Ni-Al ₂ O ₃ , (c) fresh 20 wt.% Ni-Al ₂ O ₃ , (d) reacted 20 wt.% Ni-Al ₂ O ₃ , (e) fresh 40 wt.% Ni-Al ₂ O ₃ and (f) reacted 40 wt.% Ni-Al ₂ O ₃	213
Figure 6-17 The influence of water injection rate on gas composition	216
Figure 6-18 TGA-TPO and DTG-TPO results showing the effect of water injection rate on reacted 10 wt.% Ni-Al ₂ O ₃ catalyst during the pyrolysis-gasification of sugarcane bagasse	217
Figure 6-19 Pore size distribution (a), and N ₂ adsorption/desorption isotherms of the fresh catalysts (b).....	218
Figure 6-20 The influence of calcination temperature.....	221
Figure 6-21 The influence of calcination temperature on surface area of fresh and reacted catalysts	222
Figure 6-22 The influence of catalyst to sample ratio on gas composition	225
Figure 7-1 TGA and DTG thermograms of rice husk, sugarcane bagasse and wheat straw char at 25 °C min ⁻¹	233
Figure 7-2 Composition of gases in the product mixture (nitrogen free) from gasification of sugarcane bagasse char using different catalysts.....	237

Figure 7-3 The influence of temperature on gas composition during steam gasification of sugarcane bagasse char	241
Figure 7-4 The influence of water injection rate on gas composition during gasification of sugarcane bagasse char	244

ABBREVIATIONS

BET	Brauner, Emmett and Teller
BJH	Barrett, Joyner and Halenda
CHNS	Carbon, Hydrogen, Nitrogen and Sulphur
CHP	Combined heat and power
DTG	Derivative thermogravimetry
EDXS	Energy dispersive X-ray spectrometry
EIA	Energy Information Administration
GC-FID	Gas chromatography with flame ionization detector
GC-TCD	Gas chromatography with thermal conductivity detector
IEA	International Energy Agency
IGCC	Integrated gasification combined cycle
PEM	Proton exchange membrane
SEM	Scanning electron microscopy
SMR	Steam methane reforming reaction
SNG	Substitute natural gas
SOEC	Solid oxide electrolysis cell
TEM	Transmission electron microscopy
TGA	Thermogravimetric analysis
TPO	Temperature programmed oxidation
XRD	X-ray diffraction
XRF	X-ray fluorescence

NOMENCLATURE

A	Exponential factor
C/S	Catalyst to sample ratio
daf	Dry ash-free basis
db	Dry basis
Ea	Activation energy
EJ	10^{18} J
FC	Fuel conversion
Gb	Billion barrels (of oil)
m_{char}	Mass of char
m_{fuel}	Mass of biomass fuel
Mtoe	Million tonnes of oil equivalent
n	order of reaction
P	Absolute pressure
P°	Standard state pressure
PAH	Polycyclic aromatic hydrocarbons
PS	Particle size
R^2	Correlation coefficient
R	Universal gas constant
SBR	Steam to biomass ratio
T	Temperature
VM	Volatile matter

CHAPTER 1 INTRODUCTION

Energy is important for everyone's life. Energy is required to carry out a range of activities in our daily life. It is also required to keep our homes warm and to provide us hot water. It is the energy which runs our industries and transportation systems. Without the use of energy, it wouldn't be possible for us to achieve the present level of industrial, economic and military growth.

1.1 World energy demand and resources

In the new global economy, energy has become a central issue. Most of the world economies are dependent on fossil fuels to meet their energy demands. Fossil fuels constitute oil, gas and coal. Currently almost 80 % of world energy demand is met by fossil fuels (Figure 1-1). In 2010, among these fossil fuels, oil is adding a massive 32.4 % towards total world energy supply.

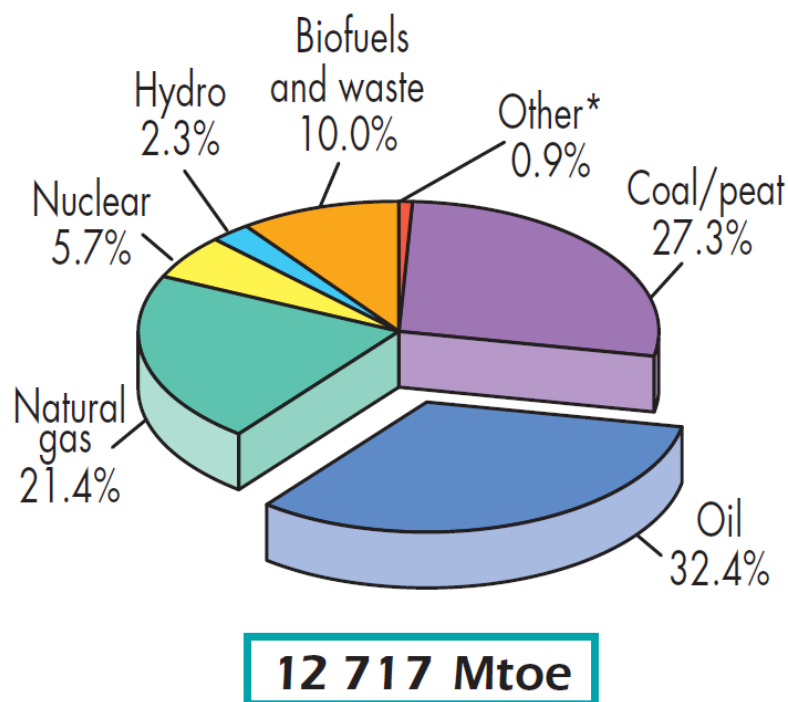


Figure 1-1 World total primary energy supply by fuels in 2010 [1]

According to the International Energy Agency (IEA) total world energy usage in 2007 was 12029 Million tonnes of oil equivalent (Mtoe) which is equivalent to 477.3 quadrillion Btu. A similar figure of 12483.41 Mtoe (495 Quadrillion Btu) is presented by US Energy Information Administration (EIA) for year 2007 [2]. For year 2010, a higher energy usage of 12717 Mtoe was reported by IEA [1]. EIA also projected the total world energy consumption till 2035, which comes out to be 18636.85 Mtoe (739 quadrillion Btu) per year in 2035. In their report, it is estimated that around one third of this total energy will come from oils. This shows that world energy demands heavily relies on the oil supply. It is well known that fossil fuels are non-renewable in nature. This non-renewable nature poses two big problems for our world. Firstly, sooner or later all the fossil fuels will be consumed. Secondly, combustion of fossil fuels releases huge quantities of carbon dioxide in our environment (just over 30,000 Million tonnes of CO₂ for year 2010) [1]. This extra carbon dioxide is creating an imbalance in nature's cycle and causing global warming.

It is interesting to investigate that how much oil reservoirs are left. As shown in Table 1-1, Owen et al. [3] reported that different sources have quoted different quantities of proven oil reservoirs.

Table 1-1 “Proved^a” world oil reserve estimates from selected sources [3]

	Oil & Gas Journal Jan 2009	World Oil Dec 2007	IEA World Energy Outlook 2008	BP Statistical Review June 2009	Independent authors
Billion barrels (Gb)	1342 ^b	1184 ^c	1241	1258 ^d	903

^a In this case ‘proved’ is defined as ‘reserves that can be recovered with reasonable certainty from known reservoirs under existing economic conditions’ (EIA 2009b). Correct reporting protocol also demands that the ‘proved’ reserves must be defined by a stipulated probability of achieving estimated volumes; hence the term ‘proved’ in this table is somewhat obscure.

^b Includes tar sands (172.2 Gb), crude oil, condensate.

^c Includes tar sands (4.9 Gb), crude oil, gas condensate and natural gas liquids.

^d BPSR figure includes tar sands (22 Gb), crude oil, gas condensate, natural gas liquids.

The highest figure in the table above (1342 Gb) translates into 196708.36 Mtoe (7800 Quadrillion Btu). If we assume an average annual energy consumption of 15131.41 Mtoe (600 Quadrillion Btu) for next few decades [1], and one third contribution of oil towards the total world energy supply, then the present oil reserves will last only for the next 39 years. This figure of 39 years closely resembles the findings given by Shafiee et al. [4]. In the light of their calculations, they suggested the life of another 35 years for current oil reserves [4]. As the oil is contributing almost one third towards the world total energy and it is available only for the next few decades, this indicates the need to find the alternate energy sources which can replace the oils and guarantee the sustainable growth in the future.

1.2 Biomass and organic waste

Ever increasing energy demands, emission of large quantities of greenhouse gases and uncertainty about the supplies of fossil fuels in the future, are the major concerns of today's world economies. These factors will make it difficult for most of the nations to cope with their energy requirements. There is an utmost need to explore the alternative sources of energy which must be cheap, renewable and environment friendly. Biomass is one of the major components in the world's energy system. It plays a very important role in the energy ecosystem of developing nations, accounting for approximately 38 % of total primary energy supply [5].

Biomass mainly consists of organic matter from living organisms like plants and animals. Global annual production of biomass is 220 billion tonnes by photosynthesis [6]. Cellulose, hemicelluloses and lignin are the main components of biomass. It is renewable in nature and in principle it does not add carbon dioxide to the atmosphere. It is cheap and readily available in various forms like energy crops, forestry waste, agricultural waste, organic food waste, sewage sludge and animal manure. Biomass has the potential to replace conventional fossil fuels with reduction in greenhouse gases emission.

The use of organic waste has double advantages. Not only it eliminates the environmental pollution but also it can provide clean energy and saves foreign exchange which otherwise would have spent on fossil fuel purchase. Waste food, organic waste from food processing plants and waste edible oil are amongst the promising and sustainable sources of biomass. Different countries around the world have exploited the locally available biomass resources and saved millions of dollars. Malaysia is one of the major producers of palm oil in the world. It provides more than 40 % of the world palm oil supplies. They have generated millions of tonnes of biomass from palm oil production which mainly consist of palm oil fibre, palm oil shell and palm oil empty fruit bunch. Similarly sugarcane producing countries have a huge potential of using bagasse. It is rich in starch and can be used for the production of energy. Animal dung is also a potential renewable source for energy production. Non-edible oils like castor oil are important for the production of biodiesel. Crops residue materials like cotton & wheat straws, rice husk and corn stalks are potential biomass sources for many agricultural developing nations.

Biomass can be used in various ways to produce renewable energy. Different processes can be used to extract energy from biomass depending upon the nature of the desired end product. Different forms of biomass like energy crops, residues from forest & crops, by products from industries and organic waste can be employed as starting material. Before conversion to energy, issues related to transportation, storage and pre-treatment of biomass must be addressed. A systematic approach is required to enhance the overall efficiency of conversion process.

Conversion processes can be broadly categorized as thermochemical, physicochemical and biochemical. The nature of output product mainly depends on the process employed and hence the operating parameters of that process. Solid, liquid and gaseous fuels can be produced from these processes. Thermochemical processes like pyrolysis and gasification can be used to produce solid, liquid or gaseous products. Flexibility to produce solid, liquid and gaseous fuels is a very important advantage of thermochemical conversion processes over the others. Liquid oils can be directly extracted from the seed of some plants like *Jatropha* (*Jatropha curcas*) using physical methods like pressing or extraction. In biochemical processes, different microorganisms are used to convert the raw feedstock into the useful products like ethanol or biogas. Fermentation and anaerobic digestion are the most popular biochemical methods used to produce liquid

and gaseous fuel from the raw feedstock. These processes are more suitable for feedstock containing higher moisture contents e.g. animal manure. The overview of the energy production from biomass is outlined in Figure 1-2 adapted from [7].

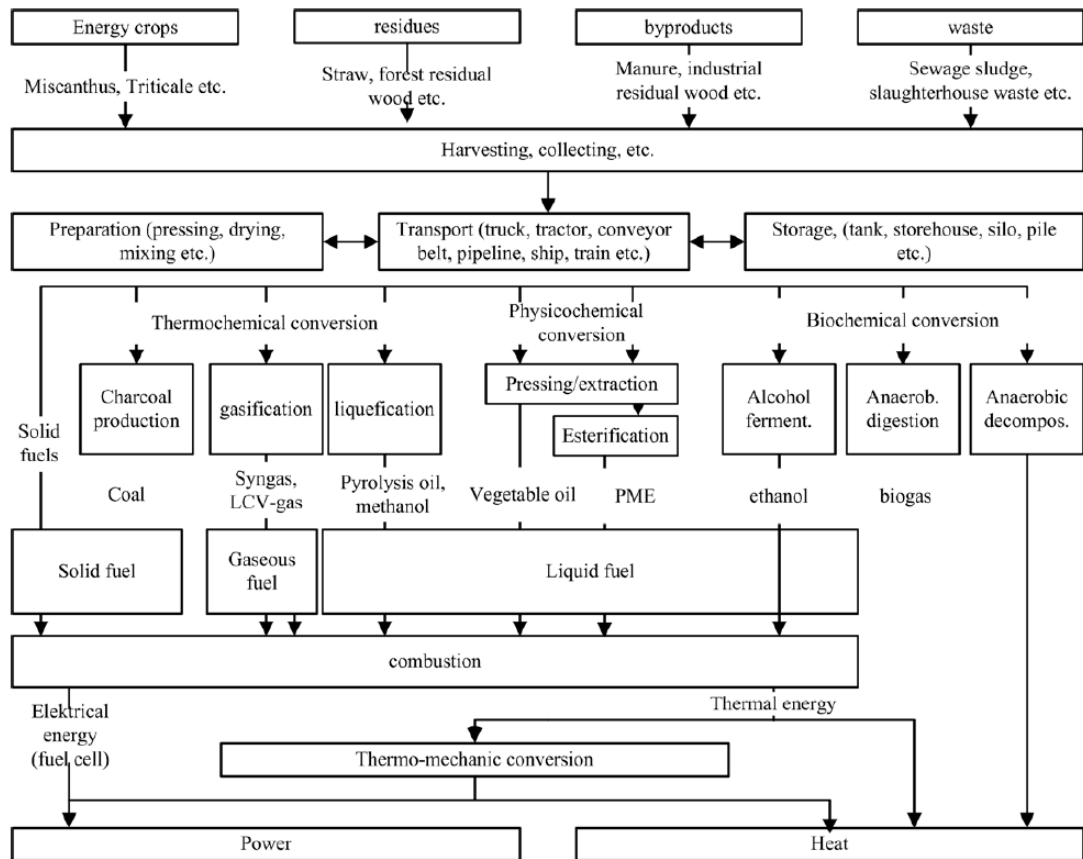


Figure 1-2 Overview of renewable energy production from biomass [7]

Most of industrial plants used combined heat and power (CHP) to further enhance the overall yield of the process and hence reduce the cost. Heat produced during the process is used either in pre-treatment/drying of biomass or to produce hot water for house/plant heating system or to produce steam that can produce even more electricity using a steam turbine.

1.3 Hydrogen

Hydrogen is the simplest of all the elements known. It has a potential to be a future fuel. It is abundantly available in our universe. Hydrogen is the cleanest fuel. It has the maximum energy per unit mass (142.31 kJ g^{-1}) and it does not produce any of the greenhouse gases on combustion. The only exhaust from the combustion of hydrogen is water.

1.3.1 Hydrogen economy

The phrase hydrogen economy was first time used by the Australian chemist John Bockris in the early 1970s [8]. The main idea of the hydrogen economy is to produce significant amount of energy using hydrogen as a fuel with the consequent reduction in greenhouse emissions. During the initial stages, fossil fuels along with nuclear energy will play a major role in the energy market. With the advancements in hydrogen production, storage and transportation technologies, eventually hydrogen will replace fossil fuels.

The main drivers of hydrogen economy are

- Reduction in greenhouse gases emissions
- Energy security against fossil fuel depletion
- Good local air quality
- Reduction in noise pollution in cosmopolitan cities
- International competitiveness and geo-political dominance

Hydrogen economy has its own benefits over the finite sources of fossil fuel but the cost of fuel cells and absence of sufficient refuelling infrastructure are the major challenges that must be overcome to make this dream come true. In order to make a fast and quick transition from fossil fuels to hydrogen economy, vital support is required from governments in terms of funding and policy making. Funds are required for infrastructure development and demonstration projects. Policies like tax credits & subsidies to encourage hydrogen use and carbon tax to discourage the use of fossil fuels are very essential. It is suggested in some studies [9] that the technological barriers in implementing hydrogen economy are already overcome or are readily solvable if governments support is available. Since governments in many countries around the

world are supporting R&D for hydrogen production, storage and transportation, prospects of hydrogen economy are promising.

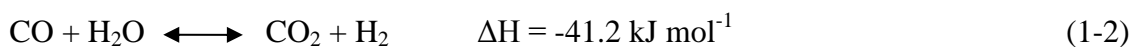
1.3.2 Hydrogen production

The current world demand of hydrogen is above 50 million metric tonnes per year [8]. It is mainly used in ammonia fertilizer, chemical industries and refineries. Due to the use of hydrogen as the cleanest fuel, its demand is expected to rise heavily in the next few years. The following are the main methods used to produce hydrogen.

- Steam methane reforming (SMR) of natural gas
- Coal gasification
- Biomass gasification
- Electrolysis (Direct/Wind/Solar)
- Nuclear thermochemical

1.3.2.1 Steam methane reforming (SMR) of natural gas

SMR is the cheapest and widely accepted method used to produce hydrogen gas from natural gas. This process consists of two steps.



The first reaction is the methane reforming reaction. It is endothermic in nature and optimally carried out between 700 - 950 °C. The second reaction is known as the water-gas shift (WGS) reaction. It is an exothermic reaction and production of hydrogen depends on the parameters of this reaction. This process is 80 % efficient [8] i.e. 20 % natural gas is used to provide heat for endothermic reaction. Use of natural gas makes this process unfavourable. Major drawback of this method are the dependence on fossil fuel and the emission of large quantities of greenhouse gases into the atmosphere [10].

1.3.2.2 Coal gasification

During gasification, coal is burnt under substoichiometric conditions in the presence of steam. This process of burning coal in a controlled environment produces a mixture of CO and H₂ known as synthesis gas or syngas. This syngas can be converted into hydrogen and carbon dioxide using water-gas shift reaction. The overall process is described below.



Coal gasification is an important process for the production of cheap hydrogen but release of massive amount of carbon dioxide into the atmosphere is a major issue. The other problem associated with coal gasification are, mining, grinding, transportation, disposal of residual ash and presence of other trace elements like sulphur. Release of sulphur compounds into the atmosphere is harmful and may cause acid rain. The co-firing of coal with the biomass is a promising option for the reduction of NO_x and SO₂ [11, 12].

1.3.2.3 Biomass gasification

The chemical formula of biomass is generally represented by C_xH_yO_z where the average value of x, y and z are 3.72, 5.49 and 2.61 respectively [13]. Besides carbon, hydrogen and oxygen, it also contains some traces of other elements. Large quantities of biomass are readily available all around the world in various forms like energy crops, forestry residues, industrial by-products and organic waste. Biomass is renewable in nature and in principle it does not add carbon dioxide into the atmosphere. Carbon dioxide produced during the gasification of biomass is consumed by plants during photosynthesis to produce more biomass.

Different studies have mentioned varying biomass potential. Berndes et al. [14] predicted the maximum potential of 400 EJ/a in 2050. An overview of the biomass resources available and its potential is shown in Table 1-2, reproduced from Parikka et al. [15].

Gasification of biomass is mainly carried out in a gasifier where biomass reacts with gasifying agent (normally steam) providing limited supply of oxygen. Synthesis gas

produced is cleaned and further upgraded to pure hydrogen. Various factors affect the quality and quantity of synthesis gas and hence the yield of final hydrogen gas production.

Table 1-2 Biomass energy potentials and current use in different regions (EJ/a) (EJ=10¹⁸) [15]

Biomass potential	North America	Latin America	Asia	Africa	Europe	Middle East	Former USSR	World
Woody biomass	12.8	5.9	7.7	5.4	4	0.4	5.4	41.6
Energy crops	4.1	12.1	1.1	13.9	2.6	0	3.6	37.4
Straw	2.2	1.7	9.9	0.9	1.6	0.2	0.7	17.2
Other	0.8	1.8	2.9	1.2	0.7	0.1	0.3	7.6
=Potential, Sum (EJ/a)	19.9	21.5	21.4	21.4	8.9	0.7	10	103.8
Use (EJ/a)	3.1	2.6	23.2	8.3	2	0	0.5	39.7
Use/potential (%)	16	12	108	39	22	7	5	38

The most important factors include reaction temperature, gasifier design, gasifying agent like steam/oxygen/air, particle size and residence time. Physical and chemical properties of biomass like moisture contents, ash contents are also very important. Flexibility of using various forms of available biomass and its renewable nature makes biomass gasification a favourable option for the production of hydrogen gas. Enhanced yield of hydrogen gas is reported after the use of catalyst [16].

1.3.2.4 Electrolysis (Direct/Wind/Solar)

Electrolysis involves direct breakdown of water into hydrogen and oxygen. Electrolysers are used to carry out the process using electricity. Commercially available low temperature electrolysers can achieve electrical efficiencies of 56 – 73 %. At standard temperature and pressure (25 °C & 1 atm) 70.1 - 53.5 KWh of electricity is required to produce one kilogram of hydrogen gas [10].

Different technologies are used for electrolysis. Most common technologies include alkaline electrolyser, proton exchange membrane (PEM) and solid oxide electrolysis cell (SOEC). All technologies have their own advantages and disadvantages in terms of cost, maintenance and efficiencies.

Net carbon dioxide emission from electrolytic hydrogen depends on the source of electricity used in electrolysis. If electricity was produced using fossil fuels, it will not only result in more carbon dioxide emission but will also make the whole process uneconomical. It is suggested that the combined electricity production from wind or solar energy with electrolysis to make the process economic and environment friendly but added cost and non-uniform distribution of solar & wind energy resources reduces the prospects of this technology to become first choice of hydrogen production.

1.3.2.5 Nuclear thermochemical

Direct heat can be used to split water into hydrogen and oxygen. But it is well established that it requires a very high temperature of ~ 2500 °C. The availability of materials which can withstand such high temperature and sources required to achieve this high temperature are very rare. These two major barriers limit the wide range adaptation of the process.

However energy released during atomic fission in a nuclear reaction can be used to carry out direct thermolysis of water molecules. As the nuclear technology is available only in a few countries, this process cannot be adopted worldwide. Despite of all these limitations, nuclear thermolysis cannot be regarded as a green technology. Drilling, processing and refining of nuclear fuel also results in carbon dioxide emission. Furthermore, disposal of nuclear waste is a risky and hazardous process.

Due to the greenhouse gases emissions and inherited limitations of different hydrogen production technologies, hydrogen production from biomass is a promising option for the sustainable economic growth of the world.

1.4 Energy from biomass

1.4.1 Biological methods

Energy can be produced from biomass and organic waste using microorganisms. Fermentation and anaerobic digestion are two important biological methods that can be used for energy production.

1.4.1.1 Fermentative hydrogen production

Bacteria species such as *Enterobacter*, *Bacillus* and *Clostridium* can produce hydrogen gas using enzymes on organic substrate. Dark fermentation bacteria do not require light to produce hydrogen while photo fermentation bacteria need light to carry out the process.

First step is hydrolysis of biomass/organic waste into carbohydrates using enzymes. These carbohydrates are used by dark fermentation bacteria to produce fatty acids and hydrogen gas. Light fermentation bacteria can use this fatty acid substrate to produce more hydrogen gas. This combination of dark and light fermentation has improved the overall yield of the process [17]. Overall low yield and large surface area required are the major limitation of the process.

1.4.1.2 Anaerobic digestion

Some bacteria in the absence of oxygen can produce combustible gas from organic substrate using enzymes. This is relatively an old process, largely used for the production of biogas from animal manure. Biogas is a mixture of methane and carbon dioxide. This process is feasible for agricultural places where agricultural waste/ animal manure is readily available on regular basis. Gas produced from the process can be used for combustion or upgraded for other applications. Slow reaction time, large digester size and feedstock availability are the major issues for the large scale application of this process.

1.4.2 Thermochemical methods

Energy can be generated from biomass using various thermochemical methods. Biomass is heated in the presence/absence of oxygen (depending on the process) to produce heat. This heat can be used for heating, cooking and for the production of electricity.

1.4.2.1 Combustion

Combustion is one of the oldest methods to generate heat from biomass. Biomass is burnt in open atmosphere in the presence of excess amount of oxygen to produce carbon dioxide, water and heat. Heat generated from combustion of biomass can be used in various ways especially for electricity generation. A maximum temperature of 1000 °C can be achieved during combustion [18]. Combustion is feasible for the biomass with less than 50 % moisture contents. Pre-treatment of biomass i.e. drying cutting, chopping and emission of carbon dioxide in large quantities into the atmosphere makes process unfavourable.

1.4.2.2 Pyrolysis

Pyrolysis is the process of conversion of biomass and waste materials into useful liquid, gaseous fuels and char. The process is carried out in the absence of oxygen. Thermal breakdown of biomass produces varying proportion of char, liquid oils and gaseous fuel, depending on the process conditions. Pyrolysis starts around 300 - 350 °C and it goes up to 700 °C. This process is more favourable for the production of solid char and liquid oils as compared to gaseous fuels. Different parameters like temperature, particle size, heating rate, reactor design, swap gas flow rate, reaction time and chemical composition of feedstock determine the yield of entire process.

Depending upon the heating rate pyrolysis can be categorized into slow, fast or flash pyrolysis.

Slow pyrolysis

During slow pyrolysis, heating rate varies from 5 - 7 °C min⁻¹. This slow heating rate produces more solid char and lesser amounts of liquid oils and gaseous fuels. Output of the process varies with the increase in reaction temperature. Increasing temperature

produces more oils up to 550 - 600 °C and less char. Further increase in temperature favours the gas yield and a decrease in oil and char yield is observed [19].

Fast pyrolysis

A higher heating rate of around 300 °C min⁻¹ is used in fast pyrolysis. It favours production of more oils and less char. Fast pyrolysis is more successful with fluidized bed reactor in producing more oil yield.

Flash pyrolysis

Flash pyrolysis employs very high heating rates ($> 100 \text{ }^\circ\text{C s}^{-1}$) and reaction time is only few seconds or even less. Entrained flow and fluidized bed reactors are more common in flash pyrolysis. Due to high heating rate and low reaction time, particle size is an important factor. Particle size from 105 - 250 μm is favourable for flash pyrolysis. Oil yield increases in flash pyrolysis but gas yield also increases during the process.

Oil produced during pyrolysis cannot be used directly as transportation fuel, because it contains water and oxygen contents in large proportions. This pyrolysis oil must be upgraded before it can be used as a transportation fuel. Pyrolysis oil mainly consists of acids, aldehydes, ketones, esters, phenols, furans, sugars and various nitrogen and oxygenated compounds. This oil can be used as a fuel in petrol and diesel engines after up gradation. It can also be used to produce syngas which can be used to produce a variety of industrial chemicals. It can also be used as combustion fuel and for the production of electricity. Char produced during the pyrolysis can be used to produce activated carbon or carbon nanotubes, as a solid fuel in boilers. Char can also be used as a feedstock in gasification to produce syngas.

Pyrolysis is more favourable for oil production from organic materials but gasification is more feasible for the production of gaseous fuel which can be further upgraded to produce pure hydrogen gas.

1.4.2.3 Gasification

Gasification is the process of conversion of biomass or organic waste feedstock into a combustible gas. This process is carried out at substoichiometric conditions typically at temperature varying from 500 - 850 °C. Combustible gas produced is called synthesis gas, commonly known as syngas. Syngas is a mixture of various gases. It comprises of

carbon monoxide, hydrogen, methane, carbon dioxide in varying proportion, depending on the process conditions.

Overall yield of the process depend on the following parameters.

- Reaction temperature
- Particle size
- Residence time
- Heating rate
- Catalyst
- Reactor design
- Steam to biomass ratio
- Gasifying agent such as air/steam/oxygen

Reaction temperature is the most influencing of all the parameters. Increase in reaction temperature evidenced increase in gas yield. Particle size and residence time are also important reaction parameters which are discussed in detail in the next chapter. Use of various catalysts also enhances the overall yield of the process.

Use of air as gasifying agent produces a syngas with lower heating contents due to higher percentage of nitrogen in air. Whereas use of oxygen produces syngas with higher heating value but cost associated with pure oxygen does not make the process economically viable. Steam gasification is the most favourable option for production of hydrogen. Steam reacts with different volatiles during the gasification process and contributes considerably to the overall hydrogen yield.

The process of gasification is flexible as it accepts a wide variety of input feedstock. Synthesis gas produced during the process can be used in a variety of applications ranging from transportation fuels to hydrogen gas for fuel cells.

1.5 Chapter references

- [1] I. E. Agency, "Key World Energy statistics," ed: International Energy Agency, 9, rue de federation, 75739 Paris Cedex 15 - France, 2012, p. 82.
- [2] H. Gruenspecht, "International energy Outlook 2010 with projections to 2035," C. f. S. a. I. Studies, Ed., ed. Washington DC: US Energy Information Administration, 2010, p. 21.
- [3] N. A. Owen, O. R. Inderwildi, and D. A. King, "The status of conventional world oil reserves--Hype or cause for concern?," *Energy Policy*, vol. 38, pp. 4743-4749, 2010.
- [4] S. Shafiee and E. Topal, "When will fossil fuel reserves be diminished?," *Energy Policy*, vol. 37, pp. 181-189, 2009.
- [5] Y. Kalinci, A. Hepbasli, and I. Dincer, "Biomass-based hydrogen production: A review and analysis," *International Journal of Hydrogen Energy*, vol. 34, pp. 8799-8817, 2009.
- [6] U. K. Mirza, N. Ahmad, and T. Majeed, "An overview of biomass energy utilization in Pakistan," *Renewable and Sustainable Energy Reviews*, vol. 12, pp. 1988-1996, 2008.
- [7] E. Iakovou, A. Karagiannidis, D. Vlachos, A. Toka, and A. Malamakis, "Waste biomass-to-energy supply chain management: A critical synthesis," *Waste Management*, vol. In Press, Corrected Proof, 2010.
- [8] W. C. Lattin and V. P. Utgikar, "Transition to hydrogen economy in the United States: A 2006 status report," *International Journal of Hydrogen Energy*, vol. 32, pp. 3230-3237, 2007.
- [9] W. McDowall and M. Eames, "Forecasts, scenarios, visions, backcasts and roadmaps to the hydrogen economy: A review of the hydrogen futures literature," *Energy Policy*, vol. 34, pp. 1236-1250, 2006.
- [10] J. D. Holladay, J. Hu, D. L. King, and Y. Wang, "An overview of hydrogen production technologies," *Catalysis Today*, vol. 139, pp. 244-260, 2009.
- [11] S. Munir, W. Nimmo, and B. M. Gibbs, "Co-combustion of Agricultural Residues with Coal: Turning Waste into Energy," *Energy & Fuels*, vol. 24, pp. 2146-2153, 2010/03/18 2010.
- [12] S. S. Daood, M. T. Javed, B. M. Gibbs, and W. Nimmo, "NOx control in coal combustion by combining biomass co-firing, oxygen enrichment and SNCR," *Fuel*, vol. 105, pp. 283-292, 3// 2013.
- [13] V. Kirubakaran, V. Sivaramakrishnan, R. Nalini, T. Sekar, M. Premalatha, and P. Subramanian, "A review on gasification of biomass," *Renewable and Sustainable Energy Reviews*, vol. 13, pp. 179-186, 2009.
- [14] G. Berndes, M. Hoogwijk, and R. van den Broek, "The contribution of biomass in the future global energy supply: a review of 17 studies," *Biomass and Bioenergy*, vol. 25, pp. 1-28, 2003.
- [15] M. Parikka, "Global biomass fuel resources," *Biomass and Bioenergy*, vol. 27, pp. 613-620, 2004.
- [16] J. F. González, S. Román, D. Bragado, and M. Calderón, "Investigation on the reactions influencing biomass air and air/steam gasification for hydrogen production," *Fuel Processing Technology*, vol. 89, pp. 764-772, 2008.
- [17] H. Argun, F. Kargi, I. K. Kapdan, and R. Oztekin, "Biohydrogen production by dark fermentation of wheat powder solution: Effects of C/N and C/P ratio on hydrogen yield and formation rate," *International Journal of Hydrogen Energy*, vol. 33, pp. 1813-1819, 2008.

- [18] R. C. Saxena, D. Seal, S. Kumar, and H. B. Goyal, "Thermo-chemical routes for hydrogen rich gas from biomass: A review," *Renewable and Sustainable Energy Reviews*, vol. 12, pp. 1909-1927, 2008.
- [19] H. B. Goyal, D. Seal, and R. C. Saxena, "Bio-fuels from thermochemical conversion of renewable resources: A review," *Renewable and Sustainable Energy Reviews*, vol. 12, pp. 504-517, 2008.

CHAPTER 2 LITERATURE REVIEW

Energy demand is increasing every year. Fear of fossil fuel depletion and heavy emissions of greenhouse gases from combustion of these fossil fuels has led to research to find clean and alternative sources to meet the future energy demands. Biomass is one of the clean and sustainable sources of energy. It is renewable in nature with net zero carbon dioxide emission into the atmosphere. It is available abundantly in various forms and it can be used to produce hydrogen gas which is a clean fuel.

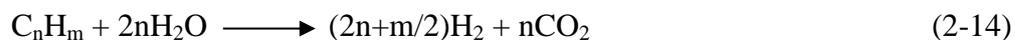
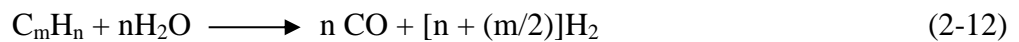
2.1 Biomass gasification

Gasification is the process of conversion of carbonaceous materials e.g. paper waste, woodchips, sawdust, wood residue, bark, shrubs and municipal solid waste into combustible gas. The gas produced commonly known as synthesis gas or syngas. It is a mixture of hydrogen, carbon monoxide, carbon dioxide and methane and lighter hydrocarbons including ethane, ethene, propane, propene, butane, butene and butadiene. Syngas is commonly used to generate electrical energy and heat. It is also used as a raw material for the production of many industrial chemicals, liquid and gaseous fuels such as hydrogen gas.

Gasification can be classified into air, steam or oxygen gasification depending upon the type of gasifying agent used. In every case, the amount of oxygen supplied is less than the total amount required for complete combustion. After gasification, syngas requires clean-up to remove undesirable substances including sulphur, tar and particles. When biomass is heated under a limited supply of oxygen, firstly it is pyrolysed and yields light hydrocarbons rich in hydrogen along with tar compounds & hydrocarbon gases. Feedstock is further decomposed thermally to produce carbon and syngas with higher hydrogen contents than the original feedstock. Steam gasification is more efficient than air gasification in terms of the amount of syngas produced per kilogram of feedstock. The effect of catalyst was also investigated by various researchers [1-6] at low temperature ($T < 500\text{ }^{\circ}\text{C}$) and medium temperature ($500\text{ }^{\circ}\text{C} < T < 900\text{ }^{\circ}\text{C}$) range. Catalysts have a net positive effect on syngas yield but cost and deactivation of catalyst are the major issues which still need to be addressed.

2.1.1 Gasification reactions

Depending upon the conditions in the gasifier, the following equations represent the major gasification reactions taking place inside the gasifier.



Oxygen is consumed in oxidation reactions (Eq. (2-1) – Eq. (2-3)). All these reactions are exothermic and the amount of heat produced is responsible for the rise in temperature and thermal breakdown of feedstock to drive the gasification process. The reactions in (Eq. (2-4) and Eq. (2-5)) are known as water gas reactions. These reactions are the principle gasification reactions and are endothermic in nature. Reaction in Equation (2-6) is known as the Boudourd reaction. This reaction is also endothermic in nature. This reaction is favourable at elevated gasification temperatures.

Reactions 2-7 and 2-8 are methane formation reactions. These reactions are very slow under normal gasification conditions and favoured by high pressure. Reaction 2-9 is known as the water-gas shift reaction. This reaction is very important for the production of hydrogen from gasification. Catalysts can be used to carry out this reaction even at lower temperatures. Increase in pressure has no effect on this reaction. Reactions 2-10 and 2-11 are steam reforming and dry reforming reactions respectively. Reactions 2-12 and 2-13 are hydrocarbon and tar reforming reaction respectively. Reaction 2-14 is overall gasification reaction.

2.1.2 Syngas clean-up systems

Syngas produced during the gasification process must be cleaned and filtered from toxic gases and particulates. If not trapped during cleaning and filtration, these gases and particulates may pose a threat to the environment. Type of application of syngas determines the level of cleaning and filtration required. Much cleaner gas is required for fuel cells as compared to boilers for steam production.

The syngas mainly consists of CO, CO₂, H₂, NH₃, N₂, CH₄, H₂S, HCl, HCN, elemental carbon and traces of heavier hydrocarbon gases. The syngas must be cleaned from different acid gases like SO₂ and HCl which otherwise may cause acid rain [7]. Depending upon the composition of feedstock, syngas is processed in a series of process units to remove particulate, heavy metals and inorganic acid gases. These processes may include gas cooling followed by venturi scrubbers, or wet electrostatic precipitators [8]. Some facilities may include fabric filters for particulate removal. Demisters are also employed to remove visual water vapours before the gas is emitted into the atmosphere.

2.1.3 Tar removal

Reforming of tar generated during the biomass gasification processes is also very important since it is a huge obstacle in the utilization of these processes for power generation or hydrogen production [9]. Tar compounds can be broadly classified into five different classes. The properties and description of various classes of tar compounds is shown in Table 2-1.

Tar derived from pyrolysis/gasification processes will be condensed as temperature is lower than its dew point (~300 °C), then block and foul process equipment like fuel lines, filters, engines and turbines. The current tar reduction or destruction methods can be broadly divided into five main groups: mechanical methods (such as scrubber, filter, cyclone, and electrostatic precipitators), self-modifiers (influence of the operating parameters during biomass gasification, including two stage gasification processes), thermal cracking, catalyst cracking and plasma methods. Various groups are researching catalytic cracking of tar at elevated temperatures over different catalysts [10-12].

Jordan et al. [13] researched the composition and dew point of tar produced during the gasification of fuel cane bagasse. It was found that the concentration of tar was 376 ± 27 mg m⁻³ of syngas collected. Further investigations on the collected tar samples revealed that majority of the tar compounds were of class 2 and class 5 although ~ 8 % of class 1 tar was also found in the mixture. In order to reduce the concentration of tar in the syngas mixture, Jordan et al. [14] investigated the influence of CaO on tar reduction and dew point depression during fuel cane bagasse gasification. It was reported that the tar concentration in the syngas was reduced 44 – 80 % with the increase in syngas yield between 17 – 37 %.

Table 2-1 Different classes of tar compounds [9]

Class	Description	Properties	Representative compounds
1	GC-undetectable	Very heavy tars; cannot be detected by GC	Determined by subtracting the GC-detectable tars from the total gravimetric tar
2	Heterocyclic aromatics	Tars containing hetero atoms; highly water soluble	Pyridine, phenol, quinoline, isoquinoline, dibenzophenol cresols
3	Light aromatic (1 ring)	Usually single ring light hydrocarbons; do not pose a problem regarding condensation or solubility	Toluene, ethylbenzene, xylenes, styrene
4	Light PAH compounds (2-3 rings)	2 and 3 ring compounds; condense at low temperatures even with low concentrations	Indene, naphthalene, methyl-naphthalene, biphenyl, acenaphthalene, fluorene, phenanthrene, anthracene
5	Heavy PAH compounds (4-7 rings)	Larger than 3 ring; condensation occurs at high temperatures even with low concentrations	Fluoranthene, pyrene, chrysene, perylene, coronene

2.2 Review of gasification conditions

Overall yield of the syngas from the gasification process mainly depends on following parameters.

- Feedstock composition
- Feedstock preparation (e.g. particle size, moisture level)
- Reaction temperature
- Heating rate
- Presence of catalyst
- Residence time
- Steam to biomass ratio
- Reactor design
- Gasifying agent

Depending upon the operating conditions, gasifier configuration and gasification agent, four types of syngas can be produced.

- i. Low heating value gas (3.5 to 10 MJ m⁻³)
- ii. Medium heating value gas (10 to 20 MJ m⁻³)
- iii. High heating value gas (20 to 35 MJ m⁻³)
- iv. Substitute natural gas (SNG) (over 35 MJ m⁻³)

Low heating value gas can be used as gas turbine fuel in an IGCC (Integrated gasification combined cycle), as a boiler fuel for steam production and as a smelting and reducing agent for iron ores. In addition to the above applications medium heating value gas can be used for hydrogen production, for fuel cells and for chemicals and fuel synthesis. High heating value gas can also be used in all the above mentioned applications but with less methanation reactions and with more ease. SNG can be used easily as a substitute for natural gas and hence can be used for the production of hydrogen gas and for chemical production and also as a feed for fuel cells.

2.2.1 Feedstock composition

Biomass is a natural substance which accumulates energy in the presence of sunlight using the process of photosynthesis. Biomass largely contains cellulose, hemi-cellulose and lignin. The physical and chemical characteristics of biomass resources vary widely. The variation can occur between the samples of the same resource or variation could occur from one region to another [15]. This is especially true for waste products.

Wood waste comes from different sources like soft or hard wood. There are significant differences between different samples in terms of physical, chemical characteristics and heating values. Moisture content in biomass is also an important factor. Higher moisture contents lower the efficiency of the gasification process. Typically 10 to 20 % moisture contents are desirable. Green biomass contains more moisture and hence need preheating. Table 2-2 presents the chemical composition of various biomass based on approximate and ultimate analysis [16]. Proximate analysis was carried out on dry basis and ultimate analysis was performed on dry, ash-free basis. Proximate analysis provides information regarding volatile matter (VM), fixed carbon (FC) and ash contents (A) while the ultimate analysis provides more accurate information about elemental composition.

Table 2-2 Chemical composition of various biomasses: based on proximate analysis (wt.% dry basis) and ultimate analysis (wt.% dry, ash-free basis) adapted from [16].

Biomass group, sub-group and variety	Proximate analysis (db) ^a				Ultimate analysis (daf) ^b					
	VM	FC	A	Sum	C	O	H	N	S	Sum
1. Eucalyptus bark	78	17.2	4.8	100	49	45	5.7	0.3	0.1	100
2. Forest residue	79.9	16.9	3.2	100	53	41	5.4	0.7	0.1	100
3. Land clearing wood	69.7	13.8	16.5	100	51	43	6	0.4	0.1	100
4. Oak sawdust	86.3	13.4	0.3	100	50	44	5.9	0.1	0	100
5. Pine bark	73.7	24.4	1.9	100	54	40	5.9	0.3	0.1	100
6. Pine chips	72.4	21.6	6	100	53	41	6.1	0.5	0.1	100
7. Pine sawdust	83.1	16.8	0.1	100	51	43	6	0.1	0	100
8. Poplar	85.6	12.3	2.1	100	52	42	6.1	0.6	0	100
9. Spruce bark	73.4	23.4	3.2	100	54	40	6.2	0.1	0.1	100
10. Spruce wood	81.2	18.3	0.5	100	52	41	6.1	0.3	0.1	100
11. Wood residue	78	16.6	5.4	100	51	42	6.1	0.5	0.1	100
12. Arundo grass	80.2	16.4	3.4	100	49	45	6.1	0.6	0.1	100

13. Bamboo whole	81.6	17.5	0.9	100	52	43	5.1	0.4	0	100
14. Reed canary grass	73.4	17.7	8.9	100	49	43	6.3	1.5	0.2	100
15. Sweet sorghum grass	77.2	18.1	4.7	100	50	44	6.1	0.4	0.1	100
16. Switch grass	80.4	14.5	5.1	100	50	43	6.1	0.7	0.1	100
17. Barley straw	76.2	18.5	5.3	100	49	44	6.2	0.7	0.1	100
18. Corn straw	73.1	19.2	7.7	100	49	44	6.4	0.7	0.1	100
19. Rape straw	77.4	17.9	4.7	100	49	45	6.4	0.5	0.1	100
20. Rice straw	64.3	15.6	20.1	100	50	43	5.7	1	0.2	100
21. Wheat straw	74.8	18.1	7.1	100	49	44	6.1	0.7	0.2	100
22. Almond hulls	73.8	20.1	6.1	100	51	42	6.4	1.2	0.1	100
23. Almond shells	74.9	21.8	3.3	100	50	43	6.2	1	0.1	100
24. Groundnut shells	73.9	22.7	3.4	100	51	40	7.5	1.2	0	100
25. Hazelnut shells	77.1	21.4	1.5	100	52	42	5.5	1.4	0	100
26. Olive husks	79	18.7	2.3	100	50	42	6.2	1.6	0.1	100
27. Olive pits	77	19.9	3.1	100	53	39	6.6	1.1	0.1	100
28. Olive residue	67.3	25.5	7.2	100	58	34	5.8	1.4	0.2	100
29. Palm kernels	77.3	17.5	5.2	100	51	40	6.5	2.7	0.3	100
30. Pistachio shells	81.6	17	1.4	100	51	42	6.4	0.7	0.2	100
31. Plum pits	80.8	17.8	1.4	100	50	42	6.7	0.9	0.1	100
32. Rice husks	62.8	19.2	18	100	49	44	6.1	0.8	0.1	100
33. Sugarcane bagasse	85.5	12.4	2.1	100	50	44	6	0.2	0.1	100
34. Sunflower husks	76	20.9	3.1	100	50	43	5.5	1.1	0	100
35. Walnut hulls	79.6	17.5	2.9	100	55	37	6.7	1.6	0.1	100
36. Walnut shells	59.3	37.9	2.8	100	50	42	6.2	1.4	0.1	100
37. Demolition wood	75.8	17.3	6.9	100	52	41	6.4	1.1	0.1	100
38. Furniture waste	83	13.4	3.6	100	52	42	6.1	0.3	0	100
39. Refuse-derived fuel	73.4	0.5	26.1	100	54	37	7.8	1.1	0.5	100
40. Sewage sludge	48	5.7	46.3	100	51	33	7.3	6.1	2.3	100
41. Wood yard waste	66	13.6	20.4	100	52	40	6	1.1	0.3	100
<i>Mean</i>	75.4	17.8	6.805	100	51	42	6.2	1	0.2	100
<i>Minimum</i>	48	0.5	0.1		49	33	5.1	0.1	0	
<i>Maximum</i>	86.3	37.9	46.3		58	45	7.8	6.1	2.3	

^a Dry basis

^b Dry, ash-free basis

Most of the biomass in Table 2-2 have a high percentage of volatile matter. Ash contents are lower in quantity but vary considerably from one biomass to another. Ultimate analysis shows that almost all the biomass contains lower quantities of nitrogen and sulphur. This low concentration of nitrogen and sulphur gives an advantage to biomass over conventional fossil fuels. Significant variations are observed in the values of both proximate and ultimate analysis. Volatile matter varies from 48 wt.% (minimum in sewage sludge) to 86.3 wt.% (maximum in oak dust). Similarly a

wide variation is observed in the values of fixed carbon and ash contents. Less variation is observed in the elemental composition of biomass from ultimate analysis. This is especially true for carbon, hydrogen and oxygen contents.

Most of the biomass has a higher content of volatile matter and low content of ash, nitrogen and sulphur, which is interesting with respect to its applications in gasification and pyrolysis processes. The low content of sulphur diminishes the possibility of acid species formation which can produce “acid rain” or corrode the metallic parts of the gasification installation. The low N content ensures that fuel NO_x formation during the gasification process is negligible.

Jordan et al. [17] researched the displacement of alkali and alkaline earth metals present in the fuel cane bagasse during gasification in a down draft gasifier. It was found that the 30 % of potassium was captured by aluminosilicate compounds and retained in the ash while 50 % of the alkali earth metals were realised into the syngas. Sodium, potassium, silica and calcium were responsible for the formation of clinkers and agglomerates.

Ash mainly consists of mineral matter. Major components of ash from thirteen different biomass are shown in Table 2-3. Biomass ash is mainly comprised of sodium (Na), potassium (K), Magnesium (Mg), Calcium (Ca), Phosphorus (P), Silica (Si), Iron (Fe) and Aluminium (Al). Other elements like Cobalt (Co), Chromium (Cr), Copper (Cu), Manganese (Mn), Nickel (Ni), Sulphur (S) and Zinc (Zn) are present in traces. High potassium, magnesium and calcium contents are present in the ash of bagasse, corn cob and corn stalk. Particularly high concentration of potassium is present in rice husk, groundnut shell, coir pith and wheat straw. Zn contents in rice husk ash are almost 100 times more than other biomass.

Dogru et al. [18] investigated the gasification of hazelnut shells in a down-draft gasifier. It was reported that the hazelnut shells were gasified easily and were a promising option for high energy production. It was found that the 4.06 to 4.48 kg hr^{-1} was the optimum feed rate for the gasifier. Syngas with a gross calorific value of $\sim 5 \text{ MJ m}^{-3}$ was obtained from the gasification of hazelnut shells. The volumetric flow rate of syngas was 8 – 9 $\text{Nm}^3 \text{ hr}^{-1}$.

Table 2-3 Ash composition of biomass (parts per million weight of dry biomass) [19]

Sr#	Biomass	Al	Ca	Fe	Mg	Na	K	P	Si	Co	Cr	Cu	Mn	Ni	S	Zn
1	Bagasse	–	1518	125	6261	93	2682	284	17340	–	–	18	9	16	60	16
2	Coconut coir	148	477	187	532	1758	2438	47	2990	0.6	2	68	4	2	64	25
3	Coconut shell	73	1501	115	389	1243	1965	94	256	0.5	0.3	5	1	13	35	9
4	Coir pith	1653	3126	837	8095	10564	26283	1170	13050	3.2	0.2	1239	27	22	476	40
5	Corn cob	–	182	24	1693	141	9366	445	9857	–	–	Trace	19	6	15	11
6	Corn stalks	1911	4686	518	5924	6463	32	2127	13400	8	11	32	12	13	564	32
7	Cotton gin waste	–	3737	746	4924	1298	7094	736	13000	–	–	Trace	38	10	58	22
8	Groundnut shell	3642	12970	1092	3547	467	17690	278	10960	2.3	6	11	44	11	299	52
9	Millet husk	–	6255	1020	11140	1427	3860	1267	200000	–	–	Trace	38	49	317	94
10	Rice husk	–	1793	533	1612	132	9061	337	200000	–	–	21	108	32	163	1244
11	Rice straw	–	4772	205	6283	5106	5402	752	200000	–	–	Trace	463	45	221	47
12	Subabul wood	–	6025	614	1170	92	614	100	195	–	–	1	2	1	66	40
13	Wheat straw	2455	7666	132	4329	7861	28930	214	44440	–	–	7	25	25	787	18

High contents of silica are observed in straw and rice husks (~95 wt.%) while high calcium (~70 wt.%), magnesium (~14 wt.%) and potassium (~7 wt.%) contents are present in wood biomass. Coconut coir has higher potassium contents (~36 wt.%) than sodium (~13 wt.%). Aluminium is absent in bagasse, corn cob, cotton gin waste, husks, rice straw and wood biomass. Although cobalt and chromium are among the minor elements in ash but these elements are also absent in straws, husks wood, bagasse, corn cob and cotton gin waste.

Cellulose, hemicellulose and lignin are major components of a typical biomass. Percentage by weight (wt.%) of each component in 13 different biomass is shown in Table 2-4 on a dry basis (adapted from [20]).

Thermogravimetric analysis (TGA) is used extensively to investigate the thermal decomposition of biomass. The system consists of an electrically heated furnace with a sample holder on a microbalance. The sample is placed in the sample holder is heated from room temperature to the final required temperature with known flow rate and heating rate. Accurate microbalance and thermocouples connected with a computer are used to record the sample weight loss against temperature and time. Weight loss data is plotted on screen in real time and finally all the data recorded on a file. Williams and Besler [21, 22] used rice husk and wood samples to investigate the thermal decomposition on various temperatures and heating rates. It was observed that for cellulose, hemicelluloses and lignin, maximum weight loss occurs only at one specific temperature for each but in the case of wood two temperatures are noticed for maximum weight loss; one close to the cellulose maximum weight loss temperature and the other closer to hemicellulose. Hemicellulose decomposes between 220 and 320 °C while thermal decomposition of cellulose starts around 250 °C and ends at 360 °C. Lignin decomposes gradually between 80 - 500 °C.

Daood et al. [23] studied the oxidation of char from bagasse, cotton stalk and coal under 1 % and 3 % oxygen concentration in a TGA. The char reactivity was increased when the oxygen concentration was increased from 1 % to 3 %. Biomass samples were found to be more reactive than the studied coal. Vassile et al. [24] compiled the organic and inorganic phase composition of 93 different biomass samples from different sources. Detailed analysis showed a wide variation in terms of organic matter, inorganic matter and fluid matter present in different biomass samples.

Table 2-4 Component analysis of biomass (wt.% db) [20]

	Ash	Holocellulose	Cellulose	Hemicellulose	Lignin	Extractives	Total (holo)	Total (hemi)
Bagasse	2.9	65	41.3	22.6	18.3	13.7	99.9	98.8
Coconut coir	0.8	67	47.7	25.9	17.8	6.8	111.7	99
Coconut shell	0.7	67	36.3	25.1	28.7	8.3	98.7	100.1
Coir pith	7.1	40.6	28.6	15.3	31.2	15.8	94.8	98.1
Corn cob	2.8	68.2	40.3	28.7	16.6	15.4	102.9	101.8
Corn stalks	6.8	63.5	42.7	23.6	17.5	9.8	97.6	100.5
Cotton gin waste	5.4	90.2	77.8	16	0	1.1	86.7	100.2
Groundnut shell	5.9	55.6	35.7	18.7	30.2	10.3	102	100.7
Millet husk	18.1	50.6	33.3	26.9	14	10.8	96.5	104.1
Rice husk	23.5	49.4	31.3	24.3	14.3	8.4	96.5	101.8
Rice straw	19.8	52.3	37	22.7	13.6	13.1	98.8	106.2
Subabul wood	0.9	65.9	39.8	24	24.7	9.7	101.2	99
Wheat straw	11.2	55.8	30.5	28.9	16.4	13.4	96.7	100.4

2.2.2 Biomass particle size

A considerable amount of literature has been published on biomass gasification [5, 25-37]. Particle size is one of the major factors affecting the yield and composition of synthesis gas. Several studies have investigated the influence of particle size on the gas yield, fuel conversion and synthesis gas composition [38-44].

As a general trend, the concentration of all the combustible gases (CO, H₂ and CH₄) increase with the decrease in particle size while there is a slight decrease in the concentration of CO₂. Fuel conversion also increases with the decrease in particle size. Similarly with the decrease in particle size, an incremental trend is observed in gas yield and heating value of synthesis gas.

Hernández et al. [39] investigated the influence of particle size on the gas yield, gas composition, fuel conversion (FC %), lower heating value and gas efficiency of biomass. A series of gasification experiments were carried out using dealcoholized marc of grape (solid residue of grapes) as a target biomass fuel. All the experiments were carried out at 1050 °C at a pressure of 3 bars with the relative fuel to air ratio (F_{rg}) ~ 4. Biomass flow rate (m_f) and air flow rate (m_a) were varied from 1.49 to 1.67 kg hr⁻¹ & 2.04 to 2.29 kg hr⁻¹ respectively. Fuel conversion FC(%) was calculated by altering the particle size from 0.5, 1, 2, 4 to 8 mm using the following formula [39].

$$FC(\%) = \left(1 - \frac{m_{char}}{m_f}\right) \cdot 100 \quad (2 - 15)$$

Where m_{char} and m_f are the mass of char-ash residue and mass of biomass fuel respectively.

An increase in the concentration of CO, H₂ and CH₄ was seen with the diminishing effect on the concentration of CO₂. Fuel conversion (FC) also increased from 57.5 % to 91.4 % when the particle size was decreased from 8 mm to 0.5 mm. Conversion efficiency was also improved with the decrease in particle size. This is perhaps due to the increase in heating value and near constant gas yield.

Many factors contribute towards the increased fuel conversion and enhanced yield of CO, H₂ and CH₄. It is well established that the decrease in particle size results in improved heat and mass transfer during the reaction. It also increases the surface area to volume ratio of fuel particles. This increased surface area to volume ratio makes it easier for most of volatiles to evolve, leaving behind a highly porous particle. This very porous nature of remaining char increases its reactivity by decreasing the temperature gradient and internal heat transfer conduction resistance within the char particle. Reaction takes place all over the particle instead of only at the surface. This resulted in the up gradation of the synthesis gas produced. In other words, by decreasing the particle size, diffusion coefficient resistance is lowered and heat and mass transferred is improved considerably. This results in the rate of reaction controlled by chemical kinetics and hence the rate of reaction increases exponentially with the increase in reaction temperature and surface area to volume ratio. This is in agreement with Babu et al. [45] who suggested that less time is required for reaction completion when the particle size is small.

Thermochemical analysis of char-ash residue also suggests that the decrease in particle size produces more volatiles during the reaction thus less volatiles and more ash contents are observed in the char-ash residue of lower particle size biomass. Hernández et al. [39] investigated the influence of biomass particle size during gasification of biomass in an entrained flow reactor. It was reported that for smaller particle size (< 1 mm) higher ash contents were obtained which in turn were related to increase in fuel conversion and decrease in fix carbon contents. They suggested that the gasification reaction takes place effectively for the particle size of less than 1 mm.

Li et al. [43] performed a series of experiments on palm oil waste in the presence of catalyst. Reactions were carried out at a constant gasifier temperature of 800 °C while the temperature of catalyst bed was maintained at 850 °C. Steam to biomass ratio was kept constant at a value of 1.33. Four groups of particle size 5 - 2, 2 - 1, 1 - 0.15 and <0.15 mm were investigated under the above mentioned conditions. Gas yield was increased from 2.16 m³ kg⁻¹ to 2.41 m³ kg⁻¹ when the particle size was decreased from 5 mm to less than 0.15 mm. A diminishing trend was noticed in the values of LHV of synthesis gas from 10.28 MJ/Nm³ to 8.99 MJ/Nm³ with the decrease in particle size. Effective heat and mass transfer along with the increased surface area to volume ratio

are the main factors for the increase in the concentration of CO, H₂ and other combustible species.

Xiao et al. [40] carried out steam gasification of biomass in a laboratory-scale fixed bed reactor. The effects of particle size on gas composition and carbon conversion efficiency were investigated. Five different groups of biomass sizes (below 0.075 mm, 0.075-0.15 mm, 0.15-0.3 mm, 0.3-0.6 mm and 0.6-1.2 mm) were used in this study. Temperature was varied from 600 - 900 °C while fuel flow rate and steam to biomass ratio were kept constant at the values of 5 g min⁻¹ and 1.2 respectively. It was noticed that at a constant temperature, decreasing particle size increased carbon conversion efficiency and gas yield. This effect was less evident at higher temperatures where the results tend to converge. This was partially due to the fact that increase in temperature increases the effective thermal conductivity which is the result of an increase in radiation contribution to heat transfer.

A decline in the amount of char and tar was observed with the decrease in particle size. The smallest particle size (below 0.075 mm) produced a negligible amount of char and tar (0.4 %) at 700 °C. This amount further decreased with the increase in temperature or with the decrease in particle size. More than 10 % char and tar was reported for the largest particle size (0.6-1.2 mm) even at 900 °C. As discussed in the literature [38-42, 44, 45], the reason for better conversion and less char and tar is primarily related to the surface area to volume ratio and better heat and mass transfer. For larger particles the reaction is controlled by heat and mass transfer while for the smallest particles, the reaction is controlled by chemical kinetics. Greater heat transfer resistance creates a temperature gradient inside the larger particles. This temperature gradient causes reactions to take place only at the particle surface which results in more char and tar and lower carbon conversion efficiencies.

A decrease in particle size supports the reactions which produce CO and H₂. Primarily increased surface area provides greater contact with steam and hence the concentration of hydrogen was increased by the water gas shift reaction along with carbon gasification. Secondary tar cracking and Boudouard reaction also favours H₂ and CO production.

A diminishing effect was observed in CO₂ concentration when the particle size was reduced. Perhaps it was related to the equilibrium between CO, CO₂ and H₂ in the water gas shift and other gasification reactions. CH₄ concentration increased with the decrease in particle size. This was supported by the fact that CH₄ concentration was not affected by the water gas shift reaction. An inverse relationship exists between the particle size and rate of reaction of the following reactions and this causes a minor increase in CH₄ concentration with the decrease in biomass particle size. Better heat transfer results in more volatiles. An increase in overall gas yield and conversion efficiency was also witnessed, when particle size was reduced.

Luo et al. [41] performed a series of pyrolysis and gasification experiments on a municipal solid waste (MSW) sample. Experiments were designed to study the effect of particle size on the yield of syngas. A laboratory-scale fixed bed reactor was used and temperature was varied from 600 to 900 °C. Three groups of particle size (below 5 mm, 5 - 10 mm and above 10 mm) were investigated. A decrease in particle size showed a positive effect on the concentration of CO, H₂ and other combustible species. When particle size was reduced, gas yield and carbon conversion efficiency were also improved while a decrease in the amount of char-ash residue was noticed.

Onay et al. [46] conducted fixed-bed pyrolysis of rapeseed. The effect of temperature, sweep gas flow rate and particle size were investigated on the yield of oil, gas and char. Six particle size groups (below 0.425 mm, 0.425 - 0.6 mm, 0.6 - 0.85 mm, 0.85 - 1.25 mm, 1.25 - 1.8 mm and above 1.8 mm) were used in this study to carry out slow pyrolysis; without any sweep gas. For the smallest particle size group (below 0.425 mm) a minor increase in char yield was observed while a decline was observed in gas and oil yield, when compared with the largest particle size group (1.25 - 1.8 mm). This increase in char yield might be the result of recondensation and repolymerization of various species in the absence of sweep gas. Interestingly neither the smallest particle size group nor the largest particle size group produced maximum oil and gas yield. Instead the intermediate particle size group (0.85 - 1.25 mm) produced maximum oil and gas yield.

Onay et al. [47] also performed fast pyrolysis of the same six particle size groups using the same biomass at 550 °C with sweep gas velocity of 100 cm³ min⁻¹. With the decrease in particle size, an increase in gas and char yield while a decrease in oil yield

was observed for the smallest particle size. Although the effect is not linear over the entire particle size range but again maximum oil yield was witnessed for the intermediate particle size (0.6 - 0.85 mm)

Wei et al. [48] performed fast pyrolysis of various biomass types in a free fall reactor. Decreasing particle size increased overall gas yield but the amount of char and tar was reduced. The concentration of CO, H₂ and other combustible gases was also increased with the decrease in particle size.

Wilk et al. [49] reported that with an increasing proportion of particles smaller than 1 mm, the product gas contained less H₂ and more CO and CH₄. Less product gas was generated and the concentration of tar increased.

2.2.3 The influence of gasification temperature

Temperature is the key parameter for steam gasification of biomass. Many researchers [5, 35, 37, 50-62] investigated the effect of temperature on gasification performance. From the literature, it can be inferred that hydrogen concentration increases with the increase in gasification temperature. Overall gas yield and carbon conversion efficiency are also enhanced with the increase in temperature. The gasification process is the result of combination of a series of complex and competing reactions shown below. Species are interlinked by chemical equilibrium. The major gasification reactions are outlined in Section 2.1.

Reactions 2-1 to 2-3 are oxidation reactions. These reactions are exothermic in nature and all the oxygen is consumed by these reactions. Water gas reactions are endothermic in nature and are favoured by the increase in temperature. 131 kJ of energy is required to convert one mole of carbon and steam into hydrogen and carbon monoxide. At higher temperatures CO produced by the water gas reaction is consumed by the water gas shift reaction. The Boudouard reaction is also endothermic (+172 kJ mol⁻¹) and the formation of CO is favoured by higher temperature. It is observed that for temperatures above 700 °C, formation of CO is favoured.

Water gas shift reaction is one of the two major reactions for the production of hydrogen during gasification. It is slightly exothermic in nature (-41 kJ mol⁻¹). Reaction is favoured for medium to high temperatures (~ 600 – 800 °C). The steam methane

reforming reaction is endothermic ($+206 \text{ kJ mol}^{-1}$) and it is favoured by higher temperatures ($\sim 700 - 1100 \text{ }^\circ\text{C}$). This is the main reaction used by industry to produce large quantities of hydrogen for hydrogenation of edible oils and for the production of ammonia. Carbon is mainly gasified in oxidation, Boudouard and water gas reactions. The overall reaction can be summarized by Equation 2-14 as presented by Yan et al. [50].

Yan et al. [50] investigated the effect of gasification temperature on the production of hydrogen gas from biomass char. Steam gasification was carried out in a fixed-bed reactor using nitrogen as a purge gas. Temperature was varied from 600 to 850 $^\circ\text{C}$ while the steam flow rate was kept constant at 0.165 g min^{-1} , per gram of sample. It was reported that the highest concentration of hydrogen was obtained at 850 $^\circ\text{C}$. Overall dry gas yield and carbon conversion efficiency also improved with the increase in temperature. This is mainly due to the fact that the higher temperatures favour more volatiles release, further reforming and cracking of volatiles and gasification of residual char. Increase in overall gas yield was mainly due to the water gas, Boudouard and steam methane reforming reactions. All these reaction are endothermic and favour the gasification of carbon with the increase in temperature. Further cracking and reforming of tar due to higher temperatures also contribute towards the increase in overall gas yield and improved carbon conversion efficiency. From 600 – 700 $^\circ\text{C}$, the concentration of H_2 and CO was lower as compared to the other species while the opposite was true for higher temperatures. This indicates that the water gas shift reaction was the dominant reaction during this temperature range. Decrease in heating value of the product gas was reported with the increase in temperature. This was mainly due to the higher percentage of CO and H_2 along with a decrease in the concentration of CH_4 in the product gas. From the temperature 800 – 850 $^\circ\text{C}$ sharp increase in CO concentration but a decline in H_2/CO concentration was observed. During the same temperature range, a decrease in the concentration of CO_2 and CH_4 was observed. This was again due to the water gas, Boudouard and steam methane reforming reactions. This argument was further supported by an increased ash percentage in the residue.

Luo et al. [51] also investigated the effect of temperature on the production of hydrogen gas from the steam gasification of pine sawdust. Temperature was varied from 600 to 900 $^\circ\text{C}$ with a fixed steam to biomass ratio of 1.43. A fixed-bed reactor used in this study was fitted with a screw feeding system and the fuel flow rate was kept constant at

the rate of 5 g min^{-1} . Increase in dry gas yield and carbon conversion efficiency was reported with the increase in temperature. More gaseous products (volatiles) evolved at higher temperatures. Endothermic reactions like Boudouard, water gas and steam methane reforming reaction were favoured by higher temperatures. Steam cracking and reforming of tar was also made possible due to higher temperatures. H_2 , CO and CO_2 were the major components in the product gas while small quantities of hydrocarbon gases such as CH_4 , C_2H_4 and C_2H_6 were observed. Increase in H_2 and CO_2 concentration was observed but a decline in the concentration of CO was noticed. This was probably interlinked with the dominance of the water gas shift reaction. Methane decomposition was favoured by the increase in temperature mainly due to the steam methane reforming reaction. A decline from 15.4 to 4.8 % was observed in the CH_4 concentration. C_2H_4 and C_2H_6 were present in small quantities and a decreasing trend in the concentration of these species was observed with the increase in temperature.

Franco et al. [52] studied the temperature effect on the steam gasification of biomass using a fluidised bed reactor. They studied three different biomass (Pine, Holm-oak and Eucalyptus) while the temperature was varied from 700 to 900 °C. Biomass samples were fed to the reactor using a screw feeding system. In order to investigate the effect of temperature, steam flow rate was 4.6 g min^{-1} while steam to biomass ratio was kept constant at 0.8. Moisture contents in the biomass samples were around 10 % and particle size was in the range of 1250 μm to 2000 μm . Gas yield increased with the increase in temperature. Further reforming and cracking decreased the amount of residual char. Higher gaseous products were obtained primarily due to the endothermic reactions favoured by higher temperatures. Further gasification of char and cracking of heavier hydrocarbon species and tar also contributed toward this increase in overall yield. For temperatures of 750 to 850 °C variation in gas yield was observed for different biomass but at 900 °C almost the same gas yield was observed for all the three biomass.

This difference in gas yield at lower temperatures might be related to the char reactivity of different biomass which in turn is related to the cellulose and lignin contents of the biomass. Char gasification with steam is also favoured by higher temperature as it is an endothermic reaction. In agreement with the literature, gas yield, energy to carbon conversion and carbon conversion efficiency increased with the increase in temperature. Gas heating value decreased with the increase in temperature. This effect is very

significant for temperatures higher than 850 °C. At these temperatures a sharp increase in H₂ concentration and a decline in hydrocarbon concentration was reported. Higher temperatures thermally cracked the heavier hydrocarbons and converted them into lighter species.

In the case of all three biomass, the hydrogen concentration increased with the increasing temperature. From 800 to 900 °C, a sharp decline was observed in the concentration of C_nH_m for eucalyptus and holm-oak biomass but its concentration was almost constant for pine. A gradual decrease in CO concentration was observed for all three biomass. This was mainly linked to the equilibrium of water gas, Boudouard and water-gas shift reactions. A slight decrease in the concentration of CO₂ and CH₄ was also noticed. At higher temperatures, Boudouard and steam methane reforming reaction favours the breakdown of CO₂ and CH₄ respectively.

Xiao et al. [53] performed the steam gasification of livestock manure in a fluidised bed. Biomass was fed at a constant rate of 0.6 kg hr⁻¹ into a two stage gasifier. Reactor temperature was varied from 540 to 639 °C and the reactions were carried out in a nitrogen environment. In agreement with other studies, increase in temperature improved the carbon conversion efficiency and gas yield. Hydrogen concentration and energy conversion also improved with the increase in temperature. This improved gasification performance was attributed to the further release of volatiles and thermal cracking and steam reforming of tar. According to the Le chatelier principle, higher temperatures favour the forward endothermic steam reforming reaction.

Gao et al. [54] investigate the influence of temperature on the steam gasification of pine sawdust. They used a fixed-bed gasifier connected with a porous ceramic reformer. Biomass was fed to the reactor using a screw feeder at a constant rate of 0.44 kg hr⁻¹. Steam flow rate and steam to biomass ratio were kept constant at 0.67 kg hr⁻¹ and 1.05 respectively. During this study, temperature was varied from 800 to 950 °C. Overall gas yield and hydrogen gas concentration increased with the increase in temperature while product gas heating value was decreased. They reported that higher temperature favours endothermic reactions which in turn resulted in higher concentration of hydrogen in product gas.

2.2.4 Steam to biomass ratio

Steam to biomass ratio is one of the major factors affecting the gas yield and hydrogen concentration. Among the other operating parameters, the influence of steam to biomass ratio has been widely studied [50, 62-68]. Optimal steam to biomass ratio is essential for maximum gas yield and enhanced hydrogen gas concentration. Little or no steam results in lower gas yield and less concentration of hydrogen because steam is required for all the major reactions for the production of hydrogen gas. These reactions include water gas, steam methane reforming and water gas shift reactions. Similarly if excess steam is injected into the reactor, it results in lower gas yield and less hydrogen concentration. There are two possible explanations for this behaviour, firstly injecting excess steam lowers reactor temperature and secondly increased concentration of steam disturb the equilibrium of the above mentioned interlinked reactions and results in lower gas yield and less hydrogen concentrations.

Li et al. [43] investigated the effect of steam to biomass ratio on the yield and the composition of gas produced during the steam gasification of palm oil waste. All the experiments were carried out at a constant reactor temperature of 800 °C. Steam to biomass ratio was varied from 0 to 2.67 while all other reaction parameters were kept constant. Steam to biomass ratio was varied by varying the steam rate from 0 to 0.8 kg hr⁻¹ while biomass feed was kept constant at 0.3 kg hr⁻¹. Initially with the introduction of steam, an increasing trend was observed in overall gas yield and hydrogen gas concentration while a decrease in LHV was noticed. This increasing trend in hydrogen concentration and overall gas yield was almost linear when the steam to biomass ratio (SBR) was increased from 0 to 1.33 but when SBR was varied from 1.33 to 2.67 a decreasing trend was observed for gas yield and hydrogen gas concentration. The increase was probably explained by the fact that the initial introduction of steam favoured the forward water gas and water gas shift reactions while the decrease in hydrogen concentration was probably the result of decrease in reaction temperature with the injection of excess steam. CO₂ concentration increased when SBR was increased from 0 to 2.67 whereas CO, CH₄ and other lighter hydrocarbons shows a decreasing trend. This might be due to the steam reforming reaction which was favoured by the increase in SBR from 0 to 2.67. Cracking of tar and lighter hydrocarbons was further favoured by the increase in residence time due to the use of catalyst.

Luo et al. [51] performed steam gasification of biomass in a fixed-bed reactor. The effect of steam to biomass ratio was investigated at a constant temperature of 900 °C. SBR was varied from 0 to 2.80. It was reported that when the SBR was varied from 0 to 0.73, tar contents decreased sharply from 4.7 to 0 %. This proved the initial effectiveness of steam injection into the reaction environment. When SBR was varied from 0.73 to 2.80 gas composition of H₂ and CO₂ was not monotonic. Initially there was an increase in H₂ and CO₂ concentration perhaps due to the decomposition of CH₄ and other lighter hydrocarbons. Water gas, thermal cracking of tar, water gas shift reaction and Boudouard reactions were favoured by the increased steam while the opposite was true when a decline in the concentration of H₂ and CO₂ was observed with the excess injection of steam. Increase in steam partial pressure favoured the above mentioned reactions in reverse direction.

Initial steam injection of steam favoured tar cracking and decomposition of hydrocarbons and resulted in enhanced gas yield and improved carbon conversion efficiencies. On the other hand, excess steam lowered the reactor temperature and decreased decomposition of steam. Considering the maximum overall gas yield and carbon conversion, an optimal value of 1.43 was suggested for SBR. At this SBR of 1.43 a maximum dry gas yield of 2.53 Nm³ kg⁻¹ and maximum carbon conversion efficiency of 92.59 % were achieved. Maximum concentration of hydrogen gas was obtained at SBR of 2.10.

Franco et al. [52] investigated the effect of steam to biomass ratio on steam gasification of biomass. Three different biomass; pine, eucalyptus and holm-oak were used in this study. SBR was varied from 0.4 to 0.85 w/w whereas reaction temperature was kept constant at 800 °C. Variation in SBR was achieved by varying the biomass feed rate while steam flow rate was kept constant. Maximum gaseous products were obtained for SBR ranging from 0.6 to 0.7. For pine wood, a decrease in CO concentration was observed for SBR of up to 0.6 while no significant change in concentration was observed for higher SBR values. With the increase in SBR, little or no influence was observed on lighter hydrocarbons concentration. No significant changes in the concentration of CO₂ were observed while H₂ formation was favoured by the introduction of steam and the maximum H₂ concentration was obtained for SBR values of 0.6 to 0.7. Similar trends were found for the other two biomass samples. Gas yield, carbon conversion efficiency and energy contents were increased with the increase in

SBR up to 0.7 while lowest HHV were observed for the same SBR range. When the SBR was lower than 0.6, less steam was available to complete the water gas and steam methane reforming reactions but when it was increased from 0.7, water gas reactions are favoured which resulted in enhanced H₂ and CO concentration. This increased H₂ concentration favoured the methanation reaction and hence formation of CH₄. Increased CO concentration was explained by the enhanced rate of reaction for the Boudouard reaction which is favoured by more steam being available. CO₂ concentration was almost constant for all values of SBR.

2.2.5 The influence of gasifying agent

Overall gas yield and the percentage of individual gases in a syngas heavily depend on the nature of the gasifying agent. Steam, air and oxygen are normally used as gasifying agents. In some literature [28, 69-71], it has been reported that a combination of air and steam was used to vary the amount of available oxygen for the gasification reaction. Steam and oxygen gasification have proved to be more effective in terms of amount of hydrogen gas production. The cost associated with the use of pure oxygen makes the overall process less economically feasible. In order to carry out steam gasification, a higher temperature is required to carry out gasification reactions to produce hydrogen from biomass and steam. Air gasification is cheap and cost effective for large scale industrial processes. Many researchers [72-76] have investigated the air gasification of different biomass materials but the low production of hydrogen gas makes it less attractive.

González et al. [28] performed a comparative study to investigate the effect of gasifying agents on the gasification of biomass. Olive oil waste was used in this study and a constant SBR of 1.2 w/w was used. Temperature was varied from 700 to 900 °C and ZnCl₂ and dolomite were used as a catalyst. Results showed that the less solid was produced for steam gasification as compared to air gasification. At 900 °C only 6.04 % solid was left unreacted but in case of air gasification 17.69 % solid was found at the end of the reaction at the same temperature. This showed that the presence of steam favoured the gasification of solid biomass. Water gas, water gas shift reaction and steam reforming reaction, all are favoured by the presence of steam in the gasification reactor. With steam gasification, the use of ZnCl₂ and dolomite as a catalyst further decrease the solid yield by enhancing the gasification of solid char. Solid yield was further decreased

from 6.04 % (in case of steam gasification) to 2.97 % for ZnCl_2 and 1.85 % for dolomite.

Similarly, use of steam as a gasifying agent also showed a positive impact on hydrogen gas yield. At 900 °C, when air was used as a gasifying agent, the concentration of hydrogen and CO produced were 4.73 and 6.95 moles kg^{-1} of biomass respectively. In contrast, when steam was used as a gasifying agent, concentration of both hydrogen and CO increased drastically to 32.59 and 10.4 moles kg^{-1} of biomass respectively. Use of dolomite and ZnCl_2 did not show any appreciable effect on the yield of hydrogen and carbon monoxide.

Lv et al. [71] performed air and oxygen/steam gasification of pine wood in a down draft gasifier. Char was used as a catalyst and the effect of gasifying agent was studied. It was noticed that the use of steam as a gasifying agent improved the overall gas yield and hydrogen concentration. Syngas with almost double the heating value was obtained when steam was used as a gasifying agent compared to air. Maximum heating value of 11.11 MJ Nm^{-3} was obtained for steam gasification. Maximum hydrogen yield (45.16 g kg^{-1} of biomass) was also obtained using steam as a gasifying agent.

Munir et al. [77] investigated the thermal analysis and devolatilization kinetics of cotton stalk, bagasse and shea meal under air and nitrogen environment in a TGA. It was noticed that a higher temperature was required during the pyrolysis as compared to the oxidative environment (51 °C for cotton stalk and bagasse). Furthermore, the weight loss ($\% \text{ s}^{-1}$) was 0.10 to 0.18 during pyrolysis as compared to 0.19 to 0.28 in an oxidative environment.

Lucas et al. [78] performed the air and steam gasification of densified biofuels. Preheated air and steam were used in this study to investigate the effect of various parameters in a fixed-bed up-draft gasifier. It was observed that the use of steam as a gasifying agent improved the hydrogen yield mainly because of water gas reaction, water gas shift reaction and steam reforming reaction. An increase in heating value was also observed. This increase was primarily due to the increase in the concentration of combustible species (CH_4 , H_2 , CO , C_2H_4 etc) in the syngas. As steam gasification is a highly endothermic process and a large amount of energy is required for thermal decomposition of steam, a sharp decrease in process temperature was observed. A similar trend was observed for bed temperature and syngas exiting the reactor. The use

of steam as a gasifying agent also improved thermal cracking of tar and resulted in a higher concentration of gaseous species and less amount of solids residue.

2.3 Gasification reactors

Design type of reactor is one of the major factors affecting the overall gasification process. Based on working principle, there are two main types of gasification reactors: fixed-bed and fluidised bed reactors. The two main types of fixed-bed reactors include updraft and down draft gasification reactors. While circulating fluidised bed and bubbling fluidised bed reactors are the two types of fluidised bed reactors. Many researchers [25-27, 79, 80] have investigated the effect of reactor type on gasification performance.

2.3.1 Fixed bed reactors

Fixed bed reactors are stationary reactors which are relatively easy to design and operate. These types of reactors are suitable for small to medium applications. Due to the absence of mixing medium, achieving a uniform temperature is difficult at large scale. In a fixed bed reactor the sample is normally introduced from the top of the reactor while the product gases leaves either from the top or from the bottom depending upon up draft or down draft configuration. The gasifying agent is introduced either from the bottom of the grate or from the sides of the reactor. Typically fixed bed reactors have high carbon conversion efficiency [81-83]. Biomass with higher ash contents can also be used for gasification in these reactors. Dry ash or molten slag is also possible to collect at the bottom of the reactor. Non-uniform temperature distribution at larger scales, long heating periods, strict requirements for the biomass size and limited scale-up potential are the major down sides of the fixed-bed reactors.

2.3.1.1 Up-draft fixed-bed reactors

In an up draft reactor biomass is introduced from the top of the reactor and it falls down due to gravity while the gasifying agent (air/steam/oxygen) is introduced from the bottom of the reactor. The synthesis gas produced during the process goes upward and leaves the reactor from the upper portion of the reactor.

As shown in Figure 2-1, biomass dropped from the top falls down due to gravity and passes through different zones. Biomass is dried and devolatilized in drying and devolatilization zones respectively. Char is formed due to drying and devolatilization resulting in an increase in the temperature of this zone. Hot gases flowing upward are reduced immediately above the oxidation zone. The oxidation zone is the bottom zone and it is hottest of all the zones. These hot gases while passing upward cause pyrolysis and drying of the biomass. This whole process cools the gases and product gases leave at the top at relatively lower temperature. Tar and volatiles are produced due to the pyrolysis of biomass. Some of the tar may leave along with the outgoing gases. Ash is swept downward along with the solid biomass opposite to the direction of flow of gases. Finally ash falls at the bottom through a grate. Therefore up draft reactors produce higher tar contents than the down draft reactors but due to the lower temperature of exiting gases overall thermal efficiency of the up-draft gasifier is better than the down draft counterpart [83-86].

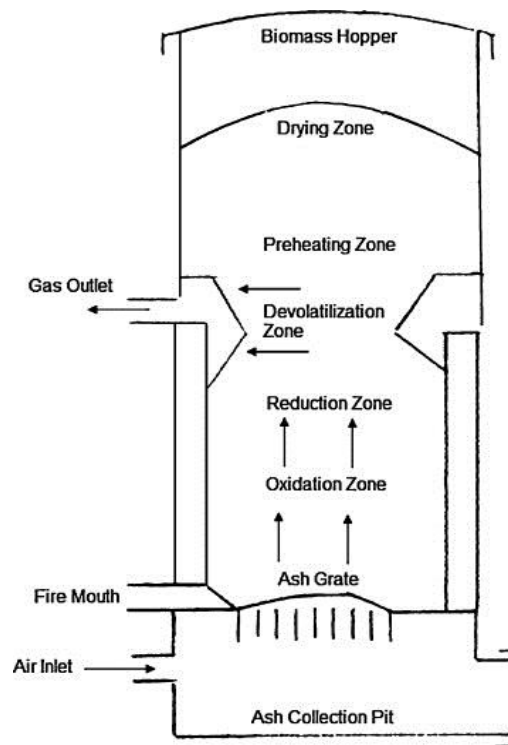


Figure 2-1 Schematic diagram of an up-draft reactor [87]

2.3.1.2 Down-draft fixed-bed reactors

In a down draft reactor, biomass is introduced from the top and the gasifying agent (air/steam/oxygen) is introduced from either from the sides of the reactor or from the top of the reactor. The product gases leave the reactor near the bottom.

Similar to the up draft reactor, biomass falls freely from the top and pass through different heating zones. Biomass is first dried and devolatilized in drying and devolatilization zones respectively. Due to this devolatilization, char is formed and this char formation increases the reaction temperature. As the char goes further down, oxidation and reduction reactions take place in their respective zones. Various reactions occurring in different zones are summarized in Table 2-5, adapted from Buragohain et al. [87].

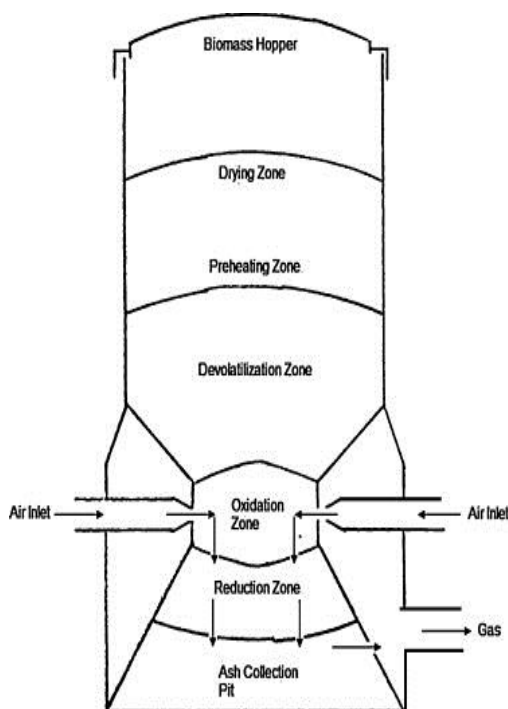


Figure 2-2 Schematic diagram of a down-draft reactor [78]

As the product gases leave the reactor from the bottom just after the oxidation zone, temperature of the exit gases is relatively higher hence the overall efficiency of the down draft reactor is low as compared to an updraft reactor. Just before leaving the reactor product gases pass through the hottest zone. This results in further cracking and decomposition of tar and hence less tar contents are observed in product gases leaving

the reactor. Many Researchers [71, 82] have used down draft fixed bed reactors for biomass gasification.

Akay et al. [88] studied the gasification of fuel cane bagasse in a down draft 50 KWe gasifier. The system consists of a batch type gasifier consisted of a tube with a throat at the base, gas cleaning system and air blower system. The syngas from gasifier was cleaned using two cyclones and a wet scrubber. The cleaned syngas was fed to a 30 KW engine.

Table 2-5 Various zones in the fixed-bed reactors and the respective reactions adapted from [87]

S. No.	Zone	Temperature range (°C)	Reactions
1.	Drying zone	30–65	$\text{H}_2\text{O}(\text{moisture}) \rightarrow \text{H}_2\text{O}(\text{steam})$
2.	Preheating zone	100–200	–
3.	Devolatilization (or pyrolysis) zone	200–600	$\text{C}_x\text{H}_y\text{O}_z \rightarrow \text{volatile gases and tar}$
4.	Oxidation zone	1000–1200	$\text{C} + 0.5\text{O}_2 \rightarrow \text{CO} + 268 \text{ kJ/gmol}$ $\text{C} + \text{O}_2 \rightarrow \text{CO}_2 + 406 \text{ kJ/gmol}$ $\text{H}_2 + 0.5\text{O}_2 \rightarrow \text{H}_2\text{O} + 242 \text{ kJ/gmol}$
5.	Reduction zone (primary)	800–1000	$\text{C} + \text{H}_2\text{O} \rightarrow \text{CO} + \text{H}_2 - 131.4 \text{ kJ/gmol}$ $\text{C} + 2\text{H}_2\text{O} \rightarrow \text{CO}_2 + 2\text{H}_2 - 78.7 \text{ kJ/gmol}$ $\text{C} + \text{CO}_2 \rightleftharpoons 2\text{CO} - 172.6 \text{ kJ/gmol}$ $\text{CO} + \text{H}_2\text{O} \rightleftharpoons \text{CO}_2 + \text{H}_2 + 42 \text{ kJ/gmol}$ $\text{CO} + 3\text{H}_2\text{O} \rightleftharpoons \text{CH}_4 + \text{H}_2\text{O} + 88 \text{ kJ/gmol}$
6.	Reduction zone (secondary)	800–1000	$\text{C} + \text{CO}_2 \rightleftharpoons 2\text{CO} - 172.6 \text{ kJ/gmol}$ $\text{CO}_2 + \text{H}_2 \rightarrow \text{CO} + \text{H}_2\text{O} - 41.2 \text{ kJ/gmol}$ $\text{C} + 2\text{H}_2 \rightarrow \text{CH}_4 + 75 \text{ kJ/gmol}$
7.	Ash collection pit	<500	–

2.3.2 Fluidised bed reactors

In contrast to fixed-bed reactors, fluidised bed reactors use a moving bed of inert material such as sand or silica. Feedstock is introduced from the bottom of the reactor and fluidised using air, nitrogen, steam, recycled product gases or a combination. Product gases leave the reactor from the upper part. Due to the fluidisation, heat transfer increases which in turn leads to better reaction rates and improved conversion efficiency. Fluidised bed reactors are suitable for medium to large applications and they

can be easily scaled to megawatt applications. These types of reactors are relatively suited for the applications where constant supply of product gas is required e.g. power plants. Major advantages of fluidised bed reactor include uniform temperature distribution, flexibility in terms of fuel type, excellent gas-solid mixing and hence uniform product gases. Due to the higher fluidisation velocity, product gas contains more particulates as compared to fixed-bed reactors [25, 42, 53, 63, 70, 73, 79, 80, 89, 90]. Bubbling fluidised reactor and circulating fluidised reactors are two major types of fluidised bed reactors.

2.3.2.1 Bubbling fluidised bed reactors

In a bubbling fluidised bed reactor inert material such as sand/silica or alumina is used as a bed material. These materials have high specific heat capacity and can withstand higher temperatures. Catalysts can also be used to enhance the carbon conversion efficiency and reduce the tar formation. However catalyst poisoning is more common in fluidised bed reactors. Finely grounded biomass is introduced from the bottom just above the distributor plates. These distributor plates could be perforated or porous. The main function of these plates is to hold the bed material along with the biomass and let the fluidising agent pass in. The velocity of the fluidising medium is almost five times higher than the minimum fluidisation velocity. Typical bed temperature is around 800 °C. Finely ground biomass particles undergo pyrolysis on the hot reactor bed. Gaseous products are released and char is formed due to devolatilization. Char particles lifted along with the fluidising medium undergoes gasification in relatively upper portion of the reactor [73, 91, 92].

Due to the higher bed temperature, higher molecular weight tar components cracked and net tar contents reduce considerably. A schematic diagram of a bubbling fluidised bed reactor is shown in Figure 2-3. Arrows at the bottom indicates the fluidising agent entering into the reactor and outward arrows on the top indicates the leaving product gases.

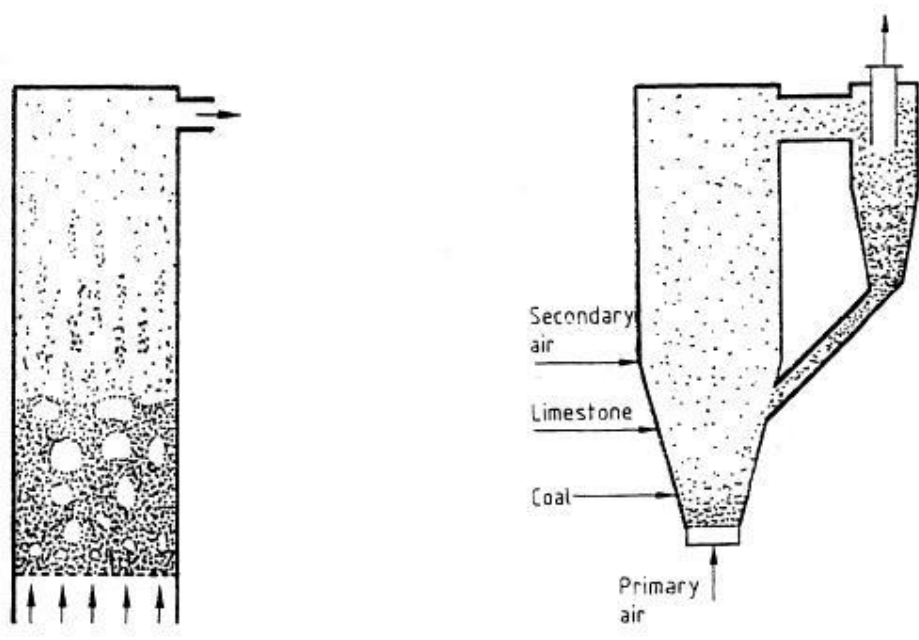


Figure 2-3 Bubbling fluidised bed reactor (left) and circulating fluidised bed reactor (right) adapted from [79]

2.3.2.2 Circulating fluidised bed reactors

The circulating fluidised bed reactor is an extension of bubbling fluidised reactor. The velocity of fluidisation material is much higher than the minimum fluidisation velocity therefore all the biomass and the bed material is lifted in the air. This higher flow rate of fluidisation medium increases the heat transfer and hence the carbon conversion efficiency. The product gases leaving the main reactor are a relatively lean mixture containing solid biomass and bed material particles.

In order to remove the particulates from the product gases, a cyclone separator is attached to the main reactor. This cyclone separator may be a single stage or multi stage, depending upon the biomass type, its size distribution and end application of product gases. This stream of output gases is fed into a cyclone separator. Solid particles separated from the gas are sent back to the main reactor through a pipe. Biomass particles continue circulating between the main reactor and the cyclone separator unless they are reduced in size due to combustion or gasification [55, 93, 94]. In this configuration, gasification can be performed even at high pressures [92]. A

circulating fluidised bed reactor is shown in Figure 2-3 indicating the entrance of fluidising air and exit of product gases from the top of the cyclone separator.

Gasification reactors can be categorized into direct or indirect heating reactors on the basis of the method of heat transfer or heat source. In a direct heating reactor, a fraction of biomass is combusted inside the reactor chamber which increases the reactor temperature and provides the heat required for endothermic gasification reactions. In the indirect method, biomass/char is combusted in a separate chamber and heat is transferred using heat exchangers from the combustion chamber to the gasification chamber. Various advantages and disadvantages of fixed bed reactors and fluidised bed reactors were reported by Warnecke et al. [79] A short list of advantages and disadvantages is shown in Table 2-6 adapted from [79].

Table 2-6 Comparison of fixed bed and fluidized bed reactors [79]

Reactor type	Fixed bed	Fluidized bed
Technology	Hot spots with exothermic reaction Possible ash fusion on grate Channelling possible Low specific capacity Long periods for heat-up	Best temperature distribution Conflicting temperature requirement Good gas solid contact and mixing High specific capacity Easily started and shut down Easy and fast heat-up
Use of material	Large pellets as uniform as possible needed High ash content feedstock possible Extensive gas clean up needed	Tolerates wide variations in fuel quality Broad particle-size distribution Relatively clean gas is produced High dust content in gas phase
Use of energy	High carbon conversion efficiency	High carbon conversion efficiency
Environmental	Molten slag possible	Ash not molten
Economy	High investment for high loads	Low investment

2.4 Catalytic gasification

Catalysts are widely used in biomass gasification to enhance the hydrogen yield and to reduce tar contents [12, 95-106]. These catalysts can be categorised as either primary or secondary catalysts. Primary catalysts are directly mixed with the biomass prior to gasification. These catalysts can be added by dry mixing with biomass or by wet impregnation. As these catalysts cannot be recovered, cheap catalysts are used for mixing. They have little reforming effect on gasification products but can effectively reduce tar contents in the product gas. Catalysts placed in a separate reactor downstream, are known as secondary catalysts. Temperature and other operating conditions in this separate reactor are similar to that of the main reactor. Gaseous products from the main reactor pass over the catalyst placed in this chamber. These types of catalysts can be recovered and reused. Conditions inside the chamber can be controlled independent of the main gasification reactor and steam or CO₂ can also be introduced to enhance the H₂ yield and reduce tar contents as shown in the reactions in Section 2.1 [107]. Secondary catalysts placed in a separate reactor play an active reforming role for hydrocarbons and methane.

Various types of catalysts are used for biomass gasification [2, 3, 28, 43, 53, 65, 89, 107-128]. Dolomite, olivine and metal catalysts are among the most commonly used catalysts. Sutton et al. [107] reviewed various catalysts used in biomass gasification. They grouped these catalysts in three major categories namely 1) Dolomite 2) Alkali metal catalysts and 3) Nickel based catalysts. Ni-based catalysts are effective for tar reduction and enhanced hydrogen production. Although the noble metals like Rh and Ru are more effective than Ni based catalysts, their high cost makes them less favourable.

Many researchers have used Ni-based catalysts for biomass gasification [65, 89, 107, 110-112, 117, 120, 124, 126]. Ni based catalysts are also commonly used in industry but the problems associated with the sintering, fouling and mechanical deactivation of these catalysts must be addressed. In many cases, various additives are added to enhance the catalytic activity of Ni-based catalysts. Different types of catalysts used in biomass gasification are discussed in the next section.

2.4.1 Mineral-based catalysts

Various minerals are used as catalyst for various chemical reactions. Mineral-based catalysts also play an important role in biomass gasification. Dolomite and olivine are the most widely used naturally occurring catalysts in biomass gasification. These catalysts help reducing the tar contents and enhance the overall gas yield.

2.4.1.1 Dolomite

Dolomite is a crystalline ore used as a catalyst in biomass gasification [2, 3, 89, 90, 107, 110, 115, 120, 124, 127]. It is a magnesium ore with a chemical formula of $\text{MgCO}_3 \cdot \text{CaCO}_3$. Exact composition depends on the mineral source. Pore size and surface area also varies from source to source. Typically it contains 30 wt.% CaO, 21 wt.% MgO and 45 wt.% CO_2 along with traces of Al_2O_3 , Fe_2O_3 and SiO_2 . Being one of naturally occurring minerals, it is cheap and widely used as a primary catalyst. It is dry mixed with biomass prior to gasification. It is also used in downstream reactors to reduce tar contents in product gases. In this case it helps in reducing coking of nickel based reforming catalysts.

Corujo et al. [110] carried out gasification of eucalyptus saligna in a laboratory scale reactor. The amount of dolomite catalyst was varied from 2 g to 20 g and its effect on product gas composition was investigated. The use of Ni-loaded calcined dolomite increased 30 % product gas volume. The maximum energy yield (21.50 MJ kg^{-1} on a dry-wood basis) was obtained with the least amount of Ni loading (0.4 wt.% Ni-dolomite). Ni loading also improved the catalytic ability of dolomite catalysts. Only 0.05 g carbon was formed after 5 hours of operation when dolomite was loaded with 1.6 wt.% Ni.

The performance of various catalysts has been evaluated by Miccio et al. [120] in a bubbling fluidised bed reactor. Dolomite, olivine, quartzite and alumina were investigated in this study. Use of dolomite as a catalyst resulted in enhanced overall gas yield and reduced tar formation. In comparison to the other catalysts used in this study, use of olivine showed a nominal gas yield (1.02 kg/kg while 1.14 for quartzite and 1.21 for alumina). Its performance in relation to tar reduction was also the same. The least amount of tar was released when alumina was used as a catalyst while the use of quartz

produced maximum tar. Dolomite and olivine were intermediate with 14 g m^{-3} and 12 g m^{-3} of tar respectively.

Tomishige et al. [127] performed gasification of cedar wood in a fluidised bed reactor. Performance of various catalysts has been compared in this study. Dolomite was compared with commercial steam reforming catalyst G-91 and $\text{Rh/CeO}_2/\text{SiO}_2$ at relatively lower temperatures (550 to 700 °C). Although the other catalysts like G-91 and $\text{Rh/CeO}_2/\text{SiO}_2$ out performed dolomite catalyst but its use as a catalyst reduced tar from 139 g m^{-3} (no catalyst) to 113 g m^{-3} . Similarly it improved H_2 concentration from 1.99 (no catalyst) to 3.22 vol.%.

Hu et al. [115] compared the performance of dolomite and olivine catalysts during the gasification of apricot stones in a fixed-bed reactor. Both catalysts were used downstream to enhance the hydrogen concentration in the product gas. Calcined dolomite produced more H_2 ($130.9 \text{ g H}_2 \text{ kg}^{-1}$ biomass daf.) as compared to the olivine catalyst ($67.7 \text{ g H}_2 \text{ kg}^{-1}$ biomass daf.) at 850 °C with steam to biomass ratio of 0.8 but calcined olivine kept its mechanical strength and dolomite appeared to be a friable substance.

2.4.1.2 Olivine

Olivine is also one of the minerals widely used as a catalyst in biomass gasification. Its chemical formula is $(\text{Mg, Fe})_2 \text{SiO}_4$ commonly known as magnesium iron silicate. Various groups have used it to research its catalytic activity on biomass gasification [90, 94, 111, 112, 115, 120, 123].

Catalytic activity of naturally occurring dolomite and olivine was investigated by Rapagná et al. [90] in a laboratory scale reactor. Almost similar results were reported for both catalysts under the same operating conditions but olivine exhibited better mechanical strength especially when used in a fluidised bed reactor. Both catalysts improved tar cracking and resulted in less tar content in the product gas. Courson et al. [112] optimised olivine based catalysts to enhance the hydrogen gas yield from biomass gasification. Catalyst was loaded with more than 5 % NiO and calcined at 1100 °C. When tested at 800 °C with a CH_4/CO_2 ratio of 1, hydrogen yield was more than 95 % after 80 hours. Very good stability of the catalyst was observed with little or no sintering or coking. In another study conducted by Courson et al. [111], a similar kind

of Ni/olivine catalyst was investigated at various calcination temperatures. Catalyst containing 2.8 wt.% Ni, calcined at 1100 °C out performed others with 95 % methane conversion in dry reforming and 88 % in steam-reforming. It produced 80 % CO during dry reforming and 75 % during steam reforming process. Characterisation after use of the catalyst showed little carbon deposition and no sintering of nickel particles. These results after 260 hours of operation at 800 °C suggest this catalyst as one of the most suitable candidates for fluidised bed reactors.

2.4.2 Nickel based and other metal catalysts

As nickel based catalysts have been used by industry for many years for steam reforming of hydrocarbons and methane, most of the literature available is based on commercially available nickel catalysts. Nickel based catalyst have various advantages over their other counterparts. Many supporter/promoter species can be added into these nickel based catalysts to enhance their catalytic capabilities. Being the most important element in group VIII metals, nickel is widely used in industries as a reforming catalyst for methane and hydrocarbons [65, 89, 107, 110-112, 117, 120, 124, 126]. Normally at temperatures around 800 °C or above, nickel based catalysts enhance over all gas yield (mainly CO and H₂ concentration) and reduce methane and hydrocarbons concentrations.

Various Ni-based catalysts are listed below.

- i. Ni/Al₂O₃ catalyst
- ii. Ni-Al catalyst
- iii. Ni-Al-Mg and Ni- Al-K catalysts
- iv. Ni/MgO catalyst
- v. Ni/CeO₂ catalyst
- vi. Ni/CeO₂/Al₂O₃ catalyst
- vii. Ni/Olivine
- viii. Ni/Dolomite
- ix. Ni/Zeolite and Ni/Ce/Zeolite
- x. Ni based commercial catalysts

Alumina is a good support for nickel catalysts. It enhances physical and chemical stability of catalyst and improves its mechanical resistance. Ni/Al₂O₃ catalyst has been used by many researchers [53, 120, 126] for biomass gasification. This catalyst showed high mechanical strength but it faces a deactivation problem.

In order to solve this problem other combinations of Ni and Al have been developed in the form of Ni-Al catalyst. It was prepared by co-precipitation and showed high catalytic activity due to its thermal stability and bigger surface area. Martínez et al. [119] developed and investigated the performance of Ni-Al catalyst after introducing La into the catalyst. It improved overall gas yield but H₂ concentration remain unchanged.

Alkali/Alkaline earth metals like K or Mg have been introduced into Ni-Al catalyst to improve its physical strength especially for its use in fluidised bed reactors. K is important and it is supposed to improve carbon gasification and reduce carbon deposition on catalysts. Addition of MgO to Ni produces a catalyst which is effective for reforming. Sato et al. [124] developed and tested the performance of Ni/MgO catalyst for biomass gasification. This catalyst when loaded with CaO from dolomite and doped with WO₃ as a promoter against sulphur showed improved reforming activity. They used naphthalene as a model tar compound in this study and catalyst showed improved resistance to coking and sulphur poisoning in comparison to various commercially available nickel catalysts.

CeO₂ is an effective promoter for Ni catalysts. It reduces coking on nickel based catalyst by promoting the reaction between carbon and steam. This promotion capability is due to the fact that CeO₂ has the capability to store oxygen. Despite acting as a promoter, it showed low activity for tar gasification. Park et al. [65] researched various Ni/CeO₂ catalysts for biomass gasification. ZrO₂ was added to this catalyst and various concentrations were investigated but 15 wt.% Ni/CeO₂ (75 %) – ZrO₂ (25 %) showed enhanced catalytic activity over the other commercial catalysts. The presence of CeO₂ stopped coking and the catalyst performed for 5 hours effectively. Similarly addition of CeO₂ to Ni/Al₂O₃ improved the performance and solved the problem of deactivation by stopping coke formation on the catalyst. This resulted in improved performance during biomass gasification and enhanced H₂ production and reduction in tar [114, 122].

Olivine and dolomite are minerals used as catalysts. Olivine helps to reduce tar concentration during gasification of biomass but Ni was added to improve its

performance. Dolomite is one of the most commonly used minerals as a catalyst for biomass gasification. It is soft in nature and need some support like Ni to improve its mechanical strength and hence catalytic activity. Details about olivine and dolomite catalysts have been discussed in previous section.

Another class of Ni based catalyst is Ni/Zeolite or Ni/Ce/zeolite. Increased surface area, adjustable acid sites and special pore size make this catalyst a very important candidate for biomass gasification. Addition of CeO₂ prevents the carbon deposition on catalyst. Many commercial nickel based catalysts have been researched by various groups for gasification of biomass. It is observed that catalysts designed for naphtha reforming are more suitable for tar reduction as compared to the ones used for hydrocarbon (methane and natural gas) reforming [129].

Alkali and other metal catalysts are also used in biomass gasification mainly to reduce tar and to upgrade the product gases. Typically these metals are used as primary catalysts and added in the biomass sample either by dry mixing or wet impregnation. Being used as a primary catalyst creates problems related to the recovery of these catalysts. As these catalysts are not very cheap and non-recovery of these catalysts renders the whole gasification process uneconomical. Due to the use of these catalysts, increase in ash concentration has also been reported [107] which poses another problem for the whole process.

Demirbas et al. [113] used various alkali metal catalysts to investigate their catalytic ability on pyrolysis of various biomass samples (cotton cocoon shell, tea factory waste and olive husk). Temperature was varied from 502 °C (775 K) to 752 °C (1025 K) with equal increments of 75 °C. When the amount of Na₂CO₃ was varied from 5 to 45 g for different temperatures mentioned above for cotton cocoon shell biomass, an increase in H₂ concentration was observed. Similar kind of behaviour was observed for K₂CO₃ where relatively higher concentration of 49 vol.% and 47 vol.% were produced for temperatures of 502 °C (775 K) and 577 °C (850 K) respectively.

Maroño et al. [118] used a Fe-Cr catalyst to accelerate the water gas shift reaction in a micro reactor. The catalyst performed well at lower temperatures 350 – 450 °C and an increase of 10 - 17 % in H₂ concentration was observed. Tasaka et al. [125] investigated the performance of Co/MgO catalyst in a fluidised bed reactor during steam gasification of radiata pine. Higher performance of MgO loaded with 12 wt.% Co was reported.

2.5 Ultra-high temperature gasification of biomass

Biomass gasification at ultra-high temperatures ($T > 900\text{ }^{\circ}\text{C}$) is a relatively new area for many researchers. Enhanced hydrogen yield, higher carbon conversion efficiency and low tar in the product gas make the process simple and attractive. No further cracking or reforming of product gas is required e.g. high temperature of the reactor eliminates the need of a separate reactor which is often required to further crack down the tar contents in the product gas. As this area of research is relatively new, the effect of various catalysts and other gasification variables must be investigated to better understand this biomass gasification at ultra-high temperatures.

Very few researchers have studied biomass gasification around $1000\text{ }^{\circ}\text{C}$ or above [78, 130-135]. Jangsawang et al. [131] studied the various factors of biomass gasification (temperature, steam/cellulose, air/steam) using the EQUIL (a part of Chemkin software) code. They used cellulose as a biomass model compound and compared the calculated results with the experimental results. During the simulation, temperature was varied from 400 K to 1800 K while experiments were carried out from $500\text{ }^{\circ}\text{C}$ to $1000\text{ }^{\circ}\text{C}$. It was established that the concentration of H_2 and CO increased with the increase in temperature in both cases. But the actual concentration was less than the theoretical result. Steam only gasification was found to be more effective than air-steam gasification.

In another study [130] Gupta et al. carried out gasification of different biomass at ultra-high temperature using a specially designed reactor. The reactor comprises of a combustion chamber surrounded by an electrically heated furnace. High temperature steam was obtained from the combustion of hydrogen and oxygen in this combustion chamber. The desired mass flow rate of steam was achieved by the flow rate of oxygen and hydrogen. Thermocouples were also used at different positions to measure the temperature. Before the product gas passed to any analysing equipment, it was passed through a filter to trap any particulates. The gas was analysed by a micro gas chromatograph. Paper, cardboard and wood pellets, cellulose and MSW (municipal solid waste) were used as target material and temperature was varied from $700\text{ }^{\circ}\text{C}$ to $1100\text{ }^{\circ}\text{C}$. Again the experimental results were compared with the calculated results using EQUIL; a part of Chemkin software. The results showed a strong influence of high-temperature on the overall gas yield in general and on hydrogen concentration in

particular. Paper waste produced the highest amount of hydrogen (~ 36 %) at 1000 °C. All other biomass produced ~ 25 % hydrogen at 1100 °C. Results produced by EQUIL were in agreement with the experimental results. Higher temperature resulted in low tar contents. Using the same gasification reactor, Kriengsak et al. [132] gasified paper waste, wood chips and coal up to 1200 °C. Results showed a 10 times decrease in tar with the increase in temperature. It was also observed that increasing the temperature up to 1200 °C also increase the hydrogen gas production especially in cellulose rich biomass like waste papers. An increase in CO concentration with a decrease in CO₂ concentration was observed.

Skoulou et al. [133, 134] investigated the gasification of olive kernel at high temperature using steam as gasifying agent. Temperature was varied from 750 °C to 1050 °C. A gas of medium heating value was obtained at 1050 °C. Almost 40 % hydrogen was produced at a maximum temperature of 1050 °C. Tar contents were decreased from 124.07 g/Nm³ to 25.26 g/Nm³; a reduction of 79.64 %. Similarly Zhou et al. [135] carried out gasification of three different biomass (Rice husk, sawdust and camphor wood) at high temperatures. Temperature was varied from 1000 °C to 1400 °C. Results indicated that the increase in temperature favour biomass gasification and enhance H₂ and CO yield.

2.6 Research aims and objectives

The overall aim of the project is to study the various process parameters of biomass gasification at ultra-high temperatures (T ~1000 °C) in order to enhance the yield of hydrogen gas.

Objectives of this research are as follows.

- Design of ultra-high temperature steam gasification reactor
- Investigate the influence of slow pyrolysis and flash pyrolysis on gas yield and hydrogen yield
- Comparative study of pyrolysis, two-stage pyrolysis/gasification and catalytic steam gasification of various biomass samples at ultra-high temperature

- Investigation of various process parameters including gasification temperature, presence of catalyst, steam injection rate, catalyst to sample ratio and carrier gas flow rate on hydrogen production from biomass using steam gasification
- Preparation of catalysts to investigate the influence of various catalysts on hydrogen production from the two-stage pyrolysis/gasification of biomass
- Investigation of various catalysts parameters including calcination temperature, Ni loading and addition of other metals on hydrogen yield
- Investigate the influence of various process parameters on ultra-high temperature steam gasification of biomass char

2.7 Conclusions

- Gasification is the process of conversion of solid carbonaceous materials into various combustible gases. Biomass mainly consists of cellulose, hemicellulose and lignin. The process of biomass gasification is a complex set of reactions interlinked with each other.
- Production of hydrogen gas from biomass depends on various factors. Physical properties of biomass such as its size, shape and physical structure or chemical properties such as amount of ash, fixed carbon or volatile matter effects the process. Smaller particle size favours the process and better surface to volume ratio results in enhanced hydrogen production. Pre-treatment of the biomass to bring it to the required size and shape is also an important obstacle for the large scale implementation of biomass gasification. Gasification temperature is the most influencing parameter for the whole process and increase in temperature results in an increase in overall gas yield. Use of steam as a gasifying agent has proved very useful. It plays a very important role in the whole process. A considerable increase in hydrogen concentration was reported when steam was used as a gasifying agent as compared to air. As the whole process of biomass gasification is the set of various reversible chemical reactions linked together, varying the steam to biomass ratio results in considerable change in gas composition. A nominal steam supply enhances the hydrogen yield.
- Design of the gasification reactor is also one of the major factors in determining the overall gas yield and efficiency of the whole process. Two most commonly used gasification reactors are fixed bed reactors and fluidised bed reactors. Both types have their own pros and cons but fixed bed reactors, being simple, are easy to design and operate especially for small scale applications like the usage in a laboratory. Up-draft and down-draft are the two types of fixed bed reactors while bubbling fluidised bed reactors and circulating fluidised bed reactors are the two sub categories of fluidised bed reactors.

- Use of catalyst to enhance the yield the hydrogen concentration and to reduce the tar in product gas has proved to be very effective. Various types of catalysts are in use to enhance hydrogen concentration either by cracking of the tar or by catalysing the steam reforming reactions. Various mineral based catalysts like dolomite/olivine or metal based catalysts like nickel/alkali metals are in use.
- Production of hydrogen gas at ultra-high temperature ($T > 900\text{ }^{\circ}\text{C}$) is relatively a new area of research and much work needs to be done in order to attain the in depth understanding of the whole gasification process.

2.8 Chapter references

- [1] J. Arauzo, D. Radlein, J. Piskorz, and D. S. Scott, "A New Catalyst for the Catalytic Gasification of Biomass," *Energy & Fuels*, vol. 8, pp. 1192-1196, 1994/11/01 1994.
- [2] M. Asadullah, T. Miyazawa, S.-i. Ito, K. Kunimori, S. Koyama, and K. Tomishige, "A comparison of Rh/CeO₂/SiO₂ catalysts with steam reforming catalysts, dolomite and inert materials as bed materials in low throughput fluidized bed gasification systems," *Biomass and Bioenergy*, vol. 26, pp. 269-279, 2004.
- [3] M. Asadullah, T. Miyazawa, S.-i. Ito, K. Kunimori, and K. Tomishige, "Demonstration of real biomass gasification drastically promoted by effective catalyst," *Applied Catalysis A: General*, vol. 246, pp. 103-116, 2003.
- [4] H. Chen, Y. Ding, N. T. Cong, B. Dou, V. Dupont, M. Ghadiri, *et al.*, "Progress in low temperature hydrogen production with simultaneous CO₂ abatement," *Chemical Engineering Research and Design*, vol. 89, pp. 1774-1782, 9// 2011.
- [5] K.-Y. Chiang, K.-L. Chien, and C.-H. Lu, "Hydrogen energy production from disposable chopsticks by a low temperature catalytic gasification," *International Journal of Hydrogen Energy*, vol. 37, pp. 15672-15680, 2012.
- [6] A. Corujo, L. Yermán, B. Arizaga, M. Brusoni, and J. Castiglioni, "Improved yield parameters in catalytic steam gasification of forestry residue; optimizing biomass feed rate and catalyst type," *Biomass and Bioenergy*, vol. 34, pp. 1695-1702, 2010.
- [7] P. Mondal, G. S. Dang, and M. O. Garg, "Syngas production through gasification and cleanup for downstream applications — Recent developments," *Fuel Processing Technology*, vol. 92, pp. 1395-1410, 8// 2011.
- [8] E. Furimsky, "Gasification in Petroleum Refinery of 21st Century," *Oil & Gas Science and Technology - Rev. IFP*, vol. 54, pp. 597-618, 1999.
- [9] P. J. Woolcock and R. C. Brown, "A review of cleaning technologies for biomass-derived syngas," *Biomass and Bioenergy*, vol. 52, pp. 54-84, 5// 2013.
- [10] B. Dou, J. Gao, X. Sha, and S. W. Baek, "Catalytic cracking of tar component from high-temperature fuel gas," *Applied Thermal Engineering*, vol. 23, pp. 2229-2239, 12// 2003.
- [11] D. Wang, W. Yuan, and W. Ji, "Char and char-supported nickel catalysts for secondary syngas cleanup and conditioning," *Applied Energy*, vol. 88, pp. 1656-1663, 5// 2011.
- [12] E. M. Grieco, C. Gervasio, and G. Baldi, "Lanthanum–chromium–nickel perovskites for the catalytic cracking of tar model compounds," *Fuel*, vol. 103, pp. 393-397, 1// 2013.
- [13] C. A. Jordan and G. Akay, "Occurrence, composition and dew point of tars produced during gasification of fuel cane bagasse in a downdraft gasifier," *Biomass and Bioenergy*, vol. 42, pp. 51-58, 7// 2012.
- [14] C. A. Jordan and G. Akay, "Effect of CaO on tar production and dew point depression during gasification of fuel cane bagasse in a novel downdraft gasifier," *Fuel Processing Technology*, vol. 106, pp. 654-660, 2// 2013.
- [15] E. M. Monono, P. E. Nyren, M. T. Berti, and S. W. Pryor, "Variability in biomass yield, chemical composition, and ethanol potential of individual and mixed herbaceous biomass species grown in North Dakota," *Industrial Crops and Products*, vol. 41, pp. 331-339, 1// 2013.

- [16] S. V. Vassilev, D. Baxter, L. K. Andersen, and C. G. Vassileva, "An overview of the chemical composition of biomass," *Fuel*, vol. 89, pp. 913-933.
- [17] C. Andrea Jordan and G. Akay, "Speciation and distribution of alkali, alkali earth metals and major ash forming elements during gasification of fuel cane bagasse," *Fuel*, vol. 91, pp. 253-263, 1// 2012.
- [18] M. Dogru, C. R. Howarth, G. Akay, B. Keskinler, and A. A. Malik, "Gasification of hazelnut shells in a downdraft gasifier," *Energy*, vol. 27, pp. 415-427, 5// 2002.
- [19] V. Kirubakaran, V. Sivaramakrishnan, R. Nalini, T. Sekar, M. Premalatha, and P. Subramanian, "A review on gasification of biomass," *Renewable and Sustainable Energy Reviews*, vol. 13, pp. 179-186, 2009.
- [20] K. Raveendran, A. Ganesh, and K. C. Khilar, "Influence of mineral matter on biomass pyrolysis characteristics," *Fuel*, vol. 74, pp. 1812-1822, 1995.
- [21] P. T. Williams and S. Besler, "The pyrolysis of rice husks in a thermogravimetric analyser and static batch reactor," *Fuel*, vol. 72, pp. 151-159, 1993.
- [22] P. T. Williams and S. Besler, "The influence of temperature and heating rate on the slow pyrolysis of biomass," *Renewable Energy*, vol. 7, pp. 233-250, 1996.
- [23] S. S. Daood, S. Munir, W. Nimmo, and B. M. Gibbs, "Char oxidation study of sugar cane bagasse, cotton stalk and Pakistani coal under 1% and 3% oxygen concentrations," *Biomass and Bioenergy*, vol. 34, pp. 263-271, 2010.
- [24] S. V. Vassilev, D. Baxter, L. K. Andersen, C. G. Vassileva, and T. J. Morgan, "An overview of the organic and inorganic phase composition of biomass," *Fuel*, vol. 94, pp. 1-33, 4// 2012.
- [25] Z. A. B. Z. Alauddin, P. Lahijani, M. Mohammadi, and A. R. Mohamed, "Gasification of lignocellulosic biomass in fluidized beds for renewable energy development: A review," *Renewable and Sustainable Energy Reviews*, vol. In Press, Corrected Proof.
- [26] M.-K. Bahng, C. Mukarakate, D. J. Robichaud, and M. R. Nimlos, "Current technologies for analysis of biomass thermochemical processing: A review," *Analytica Chimica Acta*, vol. 651, pp. 117-138, 2009.
- [27] A. V. Bridgwater, "The technical and economic feasibility of biomass gasification for power generation," *Fuel*, vol. 74, pp. 631-653, 1995.
- [28] J. F. González, S. Román, D. Bragado, and M. Calderón, "Investigation on the reactions influencing biomass air and air/steam gasification for hydrogen production," *Fuel Processing Technology*, vol. 89, pp. 764-772, 2008.
- [29] Y. Kalinci, A. Hepbasli, and I. Dincer, "Biomass-based hydrogen production: A review and analysis," *International Journal of Hydrogen Energy*, vol. 34, pp. 8799-8817, 2009.
- [30] R. C. Saxena, D. Seal, S. Kumar, and H. B. Goyal, "Thermo-chemical routes for hydrogen rich gas from biomass: A review," *Renewable and Sustainable Energy Reviews*, vol. 12, pp. 1909-1927, 2008.
- [31] A. Tanksale, J. N. Beltramini, and G. M. Lu, "A review of catalytic hydrogen production processes from biomass," *Renewable and Sustainable Energy Reviews*, vol. 14, pp. 166-182.
- [32] I. Ahmed, W. Jangsawang, and A. K. Gupta, "Energy recovery from pyrolysis and gasification of mangrove," *Applied Energy*, vol. 91, pp. 173-179, 2012.
- [33] I. I. Ahmed and A. K. Gupta, "Sugarcane bagasse gasification: Global reaction mechanism of syngas evolution," *Applied Energy*, vol. 91, pp. 75-81, 2012.

- [34] C. E. Efika, C. Wu, and P. T. Williams, "Syngas production from pyrolysis-catalytic steam reforming of waste biomass in a continuous screw kiln reactor," *Journal of Analytical and Applied Pyrolysis*, vol. 95, pp. 87-94, 5// 2012.
- [35] L. Emami Taba, M. F. Irfan, W. A. M. Wan Daud, and M. H. Chakrabarti, "The effect of temperature on various parameters in coal, biomass and CO-gasification: A review," *Renewable and Sustainable Energy Reviews*, vol. 16, pp. 5584-5596, 2012.
- [36] J. F. Pérez, A. Melgar, and P. N. Benjumea, "Effect of operating and design parameters on the gasification/combustion process of waste biomass in fixed bed downdraft reactors: An experimental study," *Fuel*, vol. 96, pp. 487-496, 2012.
- [37] K. Qin, W. Lin, P. A. Jensen, and A. D. Jensen, "High-temperature entrained flow gasification of biomass," *Fuel*, vol. 93, pp. 589-600, 2012.
- [38] J. M. Encinar, J. F. González, and J. González, "Steam gasification of *Cynara cardunculus* L.: influence of variables," *Fuel Processing Technology*, vol. 75, pp. 27-43, 2002.
- [39] J. J. Hernández, G. Aranda-Almansa, and A. Bula, "Gasification of biomass wastes in an entrained flow gasifier: Effect of the particle size and the residence time," *Fuel Processing Technology*, vol. 91, pp. 681-692, 2010.
- [40] S. Luo, B. Xiao, X. Guo, Z. Hu, S. Liu, and M. He, "Hydrogen-rich gas from catalytic steam gasification of biomass in a fixed bed reactor: Influence of particle size on gasification performance," *International Journal of Hydrogen Energy*, vol. 34, pp. 1260-1264, 2009.
- [41] S. Luo, B. Xiao, Z. Hu, S. Liu, Y. Guan, and L. Cai, "Influence of particle size on pyrolysis and gasification performance of municipal solid waste in a fixed bed reactor," *Bioresource Technology*, vol. 101, pp. 6517-6520, 2010.
- [42] S. Rapagnà and A. Latif, "Steam gasification of almond shells in a fluidised bed reactor: the influence of temperature and particle size on product yield and distribution," *Biomass and Bioenergy*, vol. 12, pp. 281-288, 1997.
- [43] J. Li, Y. Yin, X. Zhang, J. Liu, and R. Yan, "Hydrogen-rich gas production by steam gasification of palm oil wastes over supported tri-metallic catalyst," *International Journal of Hydrogen Energy*, vol. 34, pp. 9108-9115, 2009.
- [44] R. Yin, R. Liu, J. Wu, X. Wu, C. Sun, and C. Wu, "Influence of particle size on performance of a pilot-scale fixed-bed gasification system," *Bioresource Technology*, vol. 119, pp. 15-21, 2012.
- [45] B. V. Babu and A. S. Chaurasia, "Modeling for pyrolysis of solid particle: kinetics and heat transfer effects," *Energy Conversion and Management*, vol. 44, pp. 2251-2275, 2003.
- [46] O. Onay and O. Mete Koçkar, "Fixed-bed pyrolysis of rapeseed (*Brassica napus* L.)," *Biomass and Bioenergy*, vol. 26, pp. 289-299, 2004.
- [47] O. Onay and O. M. Kockar, "Slow, fast and flash pyrolysis of rapeseed," *Renewable Energy*, vol. 28, pp. 2417-2433, 2003.
- [48] L. Wei, S. Xu, L. Zhang, H. Zhang, C. Liu, H. Zhu, *et al.*, "Characteristics of fast pyrolysis of biomass in a free fall reactor," *Fuel Processing Technology*, vol. 87, pp. 863-871, 2006.
- [49] V. Wilk and H. Hofbauer, "Influence of fuel particle size on gasification in a dual fluidized bed steam gasifier," *Fuel Processing Technology*, vol. 115, pp. 139-151, 11// 2013.
- [50] F. Yan, S.-y. Luo, Z.-q. Hu, B. Xiao, and G. Cheng, "Hydrogen-rich gas production by steam gasification of char from biomass fast pyrolysis in a fixed-

- bed reactor: Influence of temperature and steam on hydrogen yield and syngas composition," *Bioresource Technology*, vol. 101, pp. 5633-5637, 2010.
- [51] S. Luo, B. Xiao, Z. Hu, S. Liu, X. Guo, and M. He, "Hydrogen-rich gas from catalytic steam gasification of biomass in a fixed bed reactor: Influence of temperature and steam on gasification performance," *International Journal of Hydrogen Energy*, vol. 34, pp. 2191-2194, 2009.
- [52] C. Franco, F. Pinto, I. Gulyurtlu, and I. Cabrita, "The study of reactions influencing the biomass steam gasification process," *Fuel*, vol. 82, pp. 835-842, 2003.
- [53] X. Xiao, D. D. Le, L. Li, X. Meng, J. Cao, K. Morishita, *et al.*, "Catalytic steam gasification of biomass in fluidized bed at low temperature: Conversion from livestock manure compost to hydrogen-rich syngas," *Biomass and Bioenergy*, vol. 34, pp. 1505-1512, 2010.
- [54] N. Gao, A. Li, and C. Quan, "A novel reforming method for hydrogen production from biomass steam gasification," *Bioresource Technology*, vol. 100, pp. 4271-4277, 2009.
- [55] G. Chen, J. Andries, H. Spliethoff, M. Fang, and P. J. van de Enden, "Biomass gasification integrated with pyrolysis in a circulating fluidised bed," *Solar Energy*, vol. 76, pp. 345-349.
- [56] I. F. Elbaba and P. T. Williams, "Two stage pyrolysis-catalytic gasification of waste tyres: Influence of process parameters," *Applied Catalysis B: Environmental*, vol. 125, pp. 136-143, 8/21/ 2012.
- [57] T. Imam and S. Capareda, "Characterization of bio-oil, syn-gas and bio-char from switchgrass pyrolysis at various temperatures," *Journal of Analytical and Applied Pyrolysis*, vol. 93, pp. 170-177, 2012.
- [58] S. Septien, S. Valin, C. Dupont, M. Peyrot, and S. Salvador, "Effect of particle size and temperature on woody biomass fast pyrolysis at high temperature (1000–1400°C)," *Fuel*, vol. 97, pp. 202-210, 2012.
- [59] Y. Chen, H. Yang, X. Wang, S. Zhang, and H. Chen, "Biomass-based pyrolytic polygeneration system on cotton stalk pyrolysis: Influence of temperature," *Bioresource Technology*, vol. 107, pp. 411-418, 2012.
- [60] P. Fu, S. Hu, J. Xiang, L. Sun, S. Su, and J. Wang, "Evaluation of the porous structure development of chars from pyrolysis of rice straw: Effects of pyrolysis temperature and heating rate," *Journal of Analytical and Applied Pyrolysis*, vol. 98, pp. 177-183, 2012.
- [61] K. Sasaki, X. Qiu, Y. Hosomomi, S. Moriyama, and T. Hirajima, "Effect of natural dolomite calcination temperature on sorption of borate onto calcined products," *Microporous and Mesoporous Materials*, vol. 171, pp. 1-8, 2013.
- [62] J. J. Hernández, R. Ballesteros, and G. Aranda, "Characterisation of tars from biomass gasification: Effect of the operating conditions," *Energy*, vol. 50, pp. 333-342, 2013.
- [63] A. Kumar, K. Eskridge, D. D. Jones, and M. A. Hanna, "Steam-air fluidized bed gasification of distillers grains: Effects of steam to biomass ratio, equivalence ratio and gasification temperature," *Bioresource Technology*, vol. 100, pp. 2062-2068, 2009.
- [64] A. Smolinski, K. Stanczyk, and N. Howaniec, "Steam gasification of selected energy crops in a fixed bed reactor," *Renewable Energy*, vol. 35, pp. 397-404, 2010.
- [65] H. J. Park, S. H. Park, J. M. Sohn, J. Park, J.-K. Jeon, S.-S. Kim, *et al.*, "Steam reforming of biomass gasification tar using benzene as a model compound over

- various Ni supported metal oxide catalysts," *Bioresource Technology*, vol. 101, pp. S101-S103, 2010.
- [66] D. Li, L. Wang, M. Koike, Y. Nakagawa, and K. Tomishige, "Steam reforming of tar from pyrolysis of biomass over Ni/Mg/Al catalysts prepared from hydrotalcite-like precursors," *Applied Catalysis B: Environmental*, vol. 102, pp. 528-538, 2011.
- [67] K. Umeki, T. Namioka, and K. Yoshikawa, "The effect of steam on pyrolysis and char reactions behavior during rice straw gasification," *Fuel Processing Technology*, vol. 94, pp. 53-60, 2012.
- [68] P. Nanou, H. E. Gutiérrez Murillo, W. P. M. van Swaaij, G. van Rossum, and S. R. A. Kersten, "Intrinsic reactivity of biomass-derived char under steam gasification conditions-potential of wood ash as catalyst," *Chemical Engineering Journal*, vol. 217, pp. 289-299, 2013.
- [69] A. Ponzio, S. Kalisz, and W. Blasiak, "Effect of operating conditions on tar and gas composition in high temperature air/steam gasification (HTAG) of plastic containing waste," *Fuel Processing Technology*, vol. 87, pp. 223-233, 2006.
- [70] P. M. Lv, Z. H. Xiong, J. Chang, C. Z. Wu, Y. Chen, and J. X. Zhu, "An experimental study on biomass air-steam gasification in a fluidized bed," *Bioresource Technology*, vol. 95, pp. 95-101, 2004.
- [71] P. Lv, Z. Yuan, L. Ma, C. Wu, Y. Chen, and J. Zhu, "Hydrogen-rich gas production from biomass air and oxygen/steam gasification in a downdraft gasifier," *Renewable Energy*, vol. 32, pp. 2173-2185, 2007.
- [72] T.-Y. Mun, J.-W. Kim, and J.-S. Kim, "Air gasification of dried sewage sludge in a two-stage gasifier: Part 1. The effects and reusability of additives on the removal of tar and hydrogen production," *International Journal of Hydrogen Energy*.
- [73] M. Campoy, A. Gómez-Barea, F. B. Vidal, and P. Ollero, "Air-steam gasification of biomass in a fluidised bed: Process optimisation by enriched air," *Fuel Processing Technology*, vol. 90, pp. 677-685, 2009.
- [74] J. D. Martínez, E. E. Silva Lora, R. V. Andrade, and R. L. Jaén, "Experimental study on biomass gasification in a double air stage downdraft reactor," *Biomass and Bioenergy*, vol. 35, pp. 3465-3480, 8// 2011.
- [75] M. A. A. Mohammed, A. Salmiaton, W. A. K. G. Wan Azlina, M. S. Mohammad Amran, and A. Fakhru'l-Razi, "Air gasification of empty fruit bunch for hydrogen-rich gas production in a fluidized-bed reactor," *Energy Conversion and Management*, vol. 52, pp. 1555-1561, 2011.
- [76] T.-Y. Mun, J.-W. Kim, and J.-S. Kim, "Air gasification of railroad wood ties treated with creosote: Effects of additives and their combination on the removal of tar in a two-stage gasifier," *Fuel*, vol. 102, pp. 326-332, 12// 2012.
- [77] S. Munir, S. S. Daood, W. Nimmo, A. M. Cunliffe, and B. M. Gibbs, "Thermal analysis and devolatilization kinetics of cotton stalk, sugar cane bagasse and shea meal under nitrogen and air atmospheres," *Bioresource Technology*, vol. 100, pp. 1413-1418, 2009.
- [78] C. Lucas, D. Szewczyk, W. Blasiak, and S. Mochida, "High-temperature air and steam gasification of densified biofuels," *Biomass and Bioenergy*, vol. 27, pp. 563-575, 2004.
- [79] R. Warnecke, "Gasification of biomass: comparison of fixed bed and fluidized bed gasifier," *Biomass and Bioenergy*, vol. 18, pp. 489-497, 2000.

- [80] E. Natarajan, A. Nordin, and A. N. Rao, "Overview of combustion and gasification of rice husk in fluidized bed reactors," *Biomass and Bioenergy*, vol. 14, pp. 533-546.
- [81] R. Kramreiter, M. Url, J. Kotik, and H. Hofbauer, "Experimental investigation of a 125 kW twin-fire fixed bed gasification pilot plant and comparison to the results of a 2 MW combined heat and power plant (CHP)," *Fuel Processing Technology*, vol. 89, pp. 90-102, 2008.
- [82] F. V. Tinaut, A. Melgar, J. F. Pérez, and A. Horrillo, "Effect of biomass particle size and air superficial velocity on the gasification process in a downdraft fixed bed gasifier. An experimental and modelling study," *Fuel Processing Technology*, vol. 89, pp. 1076-1089, 2008.
- [83] W. Yang, A. Ponzio, C. Lucas, and W. Blasiak, "Performance analysis of a fixed-bed biomass gasifier using high-temperature air," *Fuel Processing Technology*, vol. 87, pp. 235-245, 2006.
- [84] N. Gao, A. Li, C. Quan, and F. Gao, "Hydrogen-rich gas production from biomass steam gasification in an updraft fixed-bed gasifier combined with a porous ceramic reformer," *International Journal of Hydrogen Energy*, vol. 33, pp. 5430-5438, 2008.
- [85] E. Kurkela, P. Ståhlberg, P. Simell, and J. Leppälähti, "Updraft gasification of peat and biomass," *Biomass*, vol. 19, pp. 37-46, 1989.
- [86] G. Berndes, M. Hoogwijk, and R. van den Broek, "The contribution of biomass in the future global energy supply: a review of 17 studies," *Biomass and Bioenergy*, vol. 25, pp. 1-28, 2003.
- [87] B. Buragohain, P. Mahanta, and V. S. Moholkar, "Biomass gasification for decentralized power generation: The Indian perspective," *Renewable and Sustainable Energy Reviews*, vol. 14, pp. 73-92, 2010.
- [88] G. Akay and C. A. Jordan, "Gasification of Fuel Cane Bagasse in a Downdraft Gasifier: Influence of Lignocellulosic Composition and Fuel Particle Size on Syngas Composition and Yield," *Energy & Fuels*, vol. 25, pp. 2274-2283, 2011/05/19 2011.
- [89] L. Di Felice, C. Courson, N. Jand, K. Gallucci, P. U. Foscolo, and A. Kiennemann, "Catalytic biomass gasification: Simultaneous hydrocarbons steam reforming and CO₂ capture in a fluidised bed reactor," *Chemical Engineering Journal*, vol. 154, pp. 375-383, 2009.
- [90] S. Rapagnà, N. Jand, A. Kiennemann, and P. U. Foscolo, "Steam-gasification of biomass in a fluidised-bed of olivine particles," *Biomass and Bioenergy*, vol. 19, pp. 187-197, 2000.
- [91] S. Kaewluan and S. Pipatmanomai, "Potential of synthesis gas production from rubber wood chip gasification in a bubbling fluidised bed gasifier," *Energy Conversion and Management*, vol. In Press, Corrected Proof.
- [92] W. de Jong, J. Andries, and K. R. G. Hein, "Coal/biomass co-gasification in a pressurised fluidised bed reactor," *Renewable Energy*, vol. 16, pp. 1110-1113.
- [93] P. García-Ibañez, A. Cabanillas, and J. M. Sánchez, "Gasification of leached orujillo (olive oil waste) in a pilot plant circulating fluidised bed reactor. Preliminary results," *Biomass and Bioenergy*, vol. 27, pp. 183-194, 2004.
- [94] J. Pecho, T. J. Schildhauer, M. Sturzenegger, S. Biollaz, and A. Wokaun, "Reactive bed materials for improved biomass gasification in a circulating fluidised bed reactor," *Chemical Engineering Science*, vol. 63, pp. 2465-2476, 2008.

- [95] Y. Richardson, J. Blin, and A. Julbe, "A short overview on purification and conditioning of syngas produced by biomass gasification: Catalytic strategies, process intensification and new concepts," *Progress in Energy and Combustion Science*, vol. 38, pp. 765-781, 2012.
- [96] B.-S. Huang, H.-Y. Chen, K.-H. Chuang, R.-X. Yang, and M.-Y. Wey, "Hydrogen production by biomass gasification in a fluidized-bed reactor promoted by an Fe/CaO catalyst," *International Journal of Hydrogen Energy*, vol. 37, pp. 6511-6518, 2012.
- [97] R. Isha and P. T. Williams, "Hydrogen production from catalytic steam reforming of methane: influence of catalyst composition," *Journal of the Energy Institute*, vol. 85, pp. 29-37, 2012.
- [98] E. Salaices, H. de Lasa, and B. Serrano, "Steam gasification of a cellulose surrogate over a fluidizable Ni/ α -alumina catalyst: A kinetic model," *AIChE Journal*, vol. 58, pp. 1588-1599, 2012.
- [99] C. Yang, L. Jia, S. Su, Z. Tian, Q. Song, W. Fang, *et al.*, "Utilization of CO₂ and biomass char derived from pyrolysis of *Dunaliella salina*: The effects of steam and catalyst on CO and H₂ gas production," *Bioresource Technology*, vol. 110, pp. 676-681, 2012.
- [100] J. A. Onwudili and P. T. Williams, "Hydrogen and methane selectivity during alkaline supercritical water gasification of biomass with ruthenium-alumina catalyst," *Applied Catalysis B: Environmental*, vol. 132-133, pp. 70-79, 3/27/2013.
- [101] S. Singh, M. A. Nahil, X. Sun, C. Wu, J. Chen, B. Shen, *et al.*, "Novel application of cotton stalk as a waste derived catalyst in the low temperature SCR-deNO_x process," *Fuel*, vol. 105, pp. 585-594, 3// 2013.
- [102] C. Wu, Z. Wang, J. Huang, and P. T. Williams, "Pyrolysis/gasification of cellulose, hemicellulose and lignin for hydrogen production in the presence of various nickel-based catalysts," *Fuel*, vol. 106, pp. 697-706, 2013.
- [103] I. F. Elbaba and P. T. Williams, "High yield hydrogen from the pyrolysis-catalytic gasification of waste tyres with a nickel/dolomite catalyst," *Fuel*, vol. 106, pp. 528-536, 2013.
- [104] P. H. Blanco, C. Wu, J. A. Onwudili, and P. T. Williams, "Characterization and evaluation of Ni/SiO₂ catalysts for hydrogen production and tar reduction from catalytic steam pyrolysis-reforming of refuse derived fuel," *Applied Catalysis B: Environmental*, vol. 134-135, pp. 238-250, 2013.
- [105] C. Wang, B. Dou, H. Chen, Y. Song, Y. Xu, X. Du, *et al.*, "Renewable hydrogen production from steam reforming of glycerol by Ni-Cu-Al, Ni-Cu-Mg, Ni-Mg catalysts," *International Journal of Hydrogen Energy*, vol. 38, pp. 3562-3571, 2013.
- [106] L.-x. Zhang, S. Kudo, N. Tsubouchi, J.-i. Hayashi, Y. Ohtsuka, and K. Norinaga, "Catalytic effects of Na and Ca from inexpensive materials on in-situ steam gasification of char from rapid pyrolysis of low rank coal in a drop-tube reactor," *Fuel Processing Technology*, vol. 113, pp. 1-7, 2013.
- [107] D. Sutton, B. Kelleher, and J. R. H. Ross, "Review of literature on catalysts for biomass gasification," *Fuel Processing Technology*, vol. 73, pp. 155-173, 2001.
- [108] M. Asadullah, T. Miyazawa, S.-i. Ito, K. Kunitomi, M. Yamada, and K. Tomishige, "Gasification of different biomasses in a dual-bed gasifier system combined with novel catalysts with high energy efficiency," *Applied Catalysis A: General*, vol. 267, pp. 95-102, 2004.

- [109] M. Asadullah, T. Miyazawa, S.-i. Ito, K. Kunimori, M. Yamada, and K. Tomishige, "Catalyst development for the gasification of biomass in the dual-bed gasifier," *Applied Catalysis A: General*, vol. 255, pp. 169-180, 2003.
- [110] A. Corujo, L. Yermán, B. Arizaga, M. Brusoni, and J. Castiglioni, "Improved yield parameters in catalytic steam gasification of forestry residue; optimizing biomass feed rate and catalyst type," *Biomass and Bioenergy*, vol. In Press, Corrected Proof.
- [111] C. Courson, E. Makaga, C. Petit, and A. Kiennemann, "Development of Ni catalysts for gas production from biomass gasification. Reactivity in steam- and dry-reforming," *Catalysis Today*, vol. 63, pp. 427-437, 2000.
- [112] C. Courson, L. Udrón, D. Swierczynski, C. Petit, and A. Kiennemann, "Hydrogen production from biomass gasification on nickel catalysts: Tests for dry reforming of methane," *Catalysis Today*, vol. 76, pp. 75-86, 2002.
- [113] A. Demirbas, "Gaseous products from biomass by pyrolysis and gasification: effects of catalyst on hydrogen yield," *Energy Conversion and Management*, vol. 43, pp. 897-909, 2002.
- [114] A. Haryanto, S. Fernando, and S. Adhikari, "Ultrahigh temperature water gas shift catalysts to increase hydrogen yield from biomass gasification," *Catalysis Today*, vol. 129, pp. 269-274, 2007.
- [115] G. Hu, S. Xu, S. Li, C. Xiao, and S. Liu, "Steam gasification of apricot stones with olivine and dolomite as downstream catalysts," *Fuel Processing Technology*, vol. 87, pp. 375-382, 2006.
- [116] S. Hurley, H. Li, and C. Xu, "Effects of impregnated metal ions on air/CO₂-gasification of woody biomass," *Bioresource Technology*, vol. 101, pp. 9301-9307, 2010.
- [117] B. Dou, G. L. Rickett, V. Dupont, P. T. Williams, H. Chen, Y. Ding, *et al.*, "Steam reforming of crude glycerol with in situ CO₂ sorption," *Bioresource Technology*, vol. 101, pp. 2436-2442, 4// 2010.
- [118] M. Maroño, J. M. Sánchez, and E. Ruiz, "Hydrogen-rich gas production from oxygen pressurized gasification of biomass using a Fe-Cr Water Gas Shift catalyst," *International Journal of Hydrogen Energy*, vol. 35, pp. 37-45, 2010.
- [119] R. Martínez, E. Romero, L. García, and R. Bilbao, "The effect of lanthanum on Ni-Al catalyst for catalytic steam gasification of pine sawdust," *Fuel Processing Technology*, vol. 85, pp. 201-214, 2004.
- [120] F. Miccio, B. Piriou, G. Ruoppolo, and R. Chirone, "Biomass gasification in a catalytic fluidized reactor with beds of different materials," *Chemical Engineering Journal*, vol. 154, pp. 369-374, 2009.
- [121] M. Ni, D. Y. C. Leung, and M. K. H. Leung, "A review on reforming bio-ethanol for hydrogen production," *International Journal of Hydrogen Energy*, vol. 32, pp. 3238-3247, 2007.
- [122] J. Nishikawa, T. Miyazawa, K. Nakamura, M. Asadullah, K. Kunimori, and K. Tomishige, "Promoting effect of Pt addition to Ni/CeO₂/Al₂O₃ catalyst for steam gasification of biomass," *Catalysis Communications*, vol. 9, pp. 195-201, 2008.
- [123] S. Rapagná, H. Provendier, C. Petit, A. Kiennemann, and P. U. Foscolo, "Development of catalysts suitable for hydrogen or syn-gas production from biomass gasification," *Biomass and Bioenergy*, vol. 22, pp. 377-388, 2002.
- [124] K. Sato and K. Fujimoto, "Development of new nickel based catalyst for tar reforming with superior resistance to sulfur poisoning and coking in biomass gasification," *Catalysis Communications*, vol. 8, pp. 1697-1701, 2007.

- [125] K. Tasaka, T. Furusawa, and A. Tsutsumi, "Biomass gasification in fluidized bed reactor with Co catalyst," *Chemical Engineering Science*, vol. 62, pp. 5558-5563.
- [126] A. D. Taylor, G. J. DiLeo, and K. Sun, "Hydrogen production and performance of nickel based catalysts synthesized using supercritical fluids for the gasification of biomass," *Applied Catalysis B: Environmental*, vol. 93, pp. 126-133, 2009.
- [127] K. Tomishige, M. Asadullah, and K. Kunimori, "Syngas production by biomass gasification using Rh/CeO₂/SiO₂ catalysts and fluidized bed reactor," *Catalysis Today*, vol. 89, pp. 389-403, 2004.
- [128] X. Xiao, X. Meng, D. D. Le, and T. Takarada, "Two-stage steam gasification of waste biomass in fluidized bed at low temperature: Parametric investigations and performance optimization," *Bioresource Technology*, vol. In Press, Accepted Manuscript.
- [129] M. P. Aznar, M. A. Caballero, J. Gil, J. A. Martín, and J. Corella, "Commercial Steam Reforming Catalysts To Improve Biomass Gasification with Steam–Oxygen Mixtures. 2. Catalytic Tar Removal," *Industrial & Engineering Chemistry Research*, vol. 37, pp. 2668-2680, 1998/07/01 1998.
- [130] A. K. Gupta and W. Cichonski, "Ultrahigh temperature steam gasification of biomass and solid wastes," *Environmental Engineering Science*, vol. 24, pp. 1179-1189, 2007.
- [131] W. Jangsawang, A. Klimanek, and A. K. Gupta, "Enhanced yield of hydrogen from wastes using high temperature steam gasification," *Journal of Energy Resources Technology-Transactions of the Asme*, vol. 128, pp. 179-185, 2006.
- [132] S. N. Kriengsak, R. Buczynski, J. Gmurczyk, and A. K. Gupta, "Hydrogen Production by High-Temperature Steam Gasification of Biomass and Coal," *Environmental Engineering Science*, vol. 26, pp. 739-744, 2009.
- [133] V. Skoulou, E. Kantarelis, S. Arvelakis, W. Yang, and A. Zabaniotou, "Effect of biomass leaching on H₂ production, ash and tar behavior during high temperature steam gasification (HTSG) process," *International Journal of Hydrogen Energy*, vol. 34, pp. 5666-5673, 2009.
- [134] V. Skoulou, A. Swiderski, W. Yang, and A. Zabaniotou, "Process characteristics and products of olive kernel high temperature steam gasification (HTSG)," *Bioresource Technology*, vol. 100, pp. 2444-2451, 2009.
- [135] J. Zhou, Q. Chen, H. Zhao, X. Cao, Q. Mei, Z. Luo, *et al.*, "Biomass-oxygen gasification in a high-temperature entrained-flow gasifier," *Biotechnology Advances*, vol. 27, pp. 606-611.

CHAPTER 3 RESEARCH METHODOLOGY

3.1 Introduction

This chapter describes different methods and techniques used to carry out the high temperature pyrolysis/gasification of biomass samples with the aim to obtain high hydrogen yield. Initially, three different biomass samples: rice husk, waste wood, and forestry residue were characterised using proximate and ultimate analysis (results are shown in section 3.2.1). A two-stage, ultra-high temperature reactor (maximum furnace temperature of 1200 °C and reactor temperature of 1050 °C) was designed in CAD software. At first, the reactor was built in an up-draft configuration with a special water-cooled sample holding chamber at the top of the reactor (explained in section 3.3.1). The suitability of the reactor was validated by performing repeatability tests under identical conditions. Flash pyrolysis and flash gasification experiments (results shown in chapter 4) were performed in this reactor. These results were compared with that of conventional slow pyrolysis performed in a separate one-stage fixed bed reactor detailed in section 3.3.3.

After initial investigations, the reactor was modified to accommodate the catalyst (explained in section 3.3.2). The reactor was altered to a down-draft configuration to take advantage of the hottest bottom zone for cracking and reforming of various hydrocarbons. The biomass sample was pyrolysed in the first stage (top reactor). Gases, volatiles and liquids evolved from the pyrolysis were made to react with the catalyst and steam in the second stage (bottom reactor) already at a higher temperature of 950 - 1000 °C. This modified reactor was again validated for further research by performing repeatability experiments. From this point onwards, three other biomass samples: wheat straw, rice husk and sugarcane bagasse were researched in this two-stage pyrolysis/gasification reactor. As mentioned in section 3.2.1, long term sustainable supply of these biomass materials and the higher volatiles and lower ash contents in these biomass samples; especially in wheat straw and sugarcane bagasse make them favourable for higher hydrogen yield. Various characterisation techniques used to characterise the biomass samples, residual char, fresh and reacted catalysts are explained in section 3.4.

3.2 Materials

3.2.1 Biomass

Waste wood, rice husk, and forestry residue were used for flash pyrolysis and flash gasification experiments. Waste wood used in this study was sourced from Brites (www.brites.eu) in the form of wood pellets. These wood pellets were made up of saw dust produced during the processing of spruce or pine wood. Rice husk and forestry residue samples were sourced from Malaysia. Forestry residue was a mixture of Meranti (*Shorea acuminata*) and Karas (*Aquilaria malaccensis*) tropical trees typically found in Malaysia. Photographs and scanning electron microscope (SEM) images of these three biomass samples are shown in Figure 3-1. Proximate and ultimate analyses of waste wood, rice husk and forestry residue were carried out using a thermogravimetric analyser (TGA) and a CHNS elemental analyser. Both proximate and ultimate analysis results are presented on an ash-free basis in Table 3-1. It can be indicated from the results that wood biomass contains the highest percentage of volatiles (80.6 wt.%) with the lowest percentage of fixed carbon (13.4 wt.%). For rice husk, fixed carbon was highest (17.8 wt.%) among the three biomass samples however the percentage of volatiles was found to be the lowest (75.9 wt.%) among all. Ultimate analysis results showed that all three biomass samples contain a similar percentage of carbon. Hydrogen percentage in wood biomass was slightly higher than other samples. Similarly slightly higher nitrogen was observed in rice husk. Oxygen concentration was calculated by difference.

Photographs of three biomass samples along with the low resolution scanning electron microscope (SEM) images are shown in Figure 3-1. It is evident that wood and forestry residue samples showed similar anatomical features under the microscope. For forestry residue, woody structure was clearly visible. Similar structure was observed for waste wood sample. Rice husk, on the other hand showed markedly different anatomical structure. Its 2D sheet like structure was more like the combination of different linear strings each made up of beads like structure.

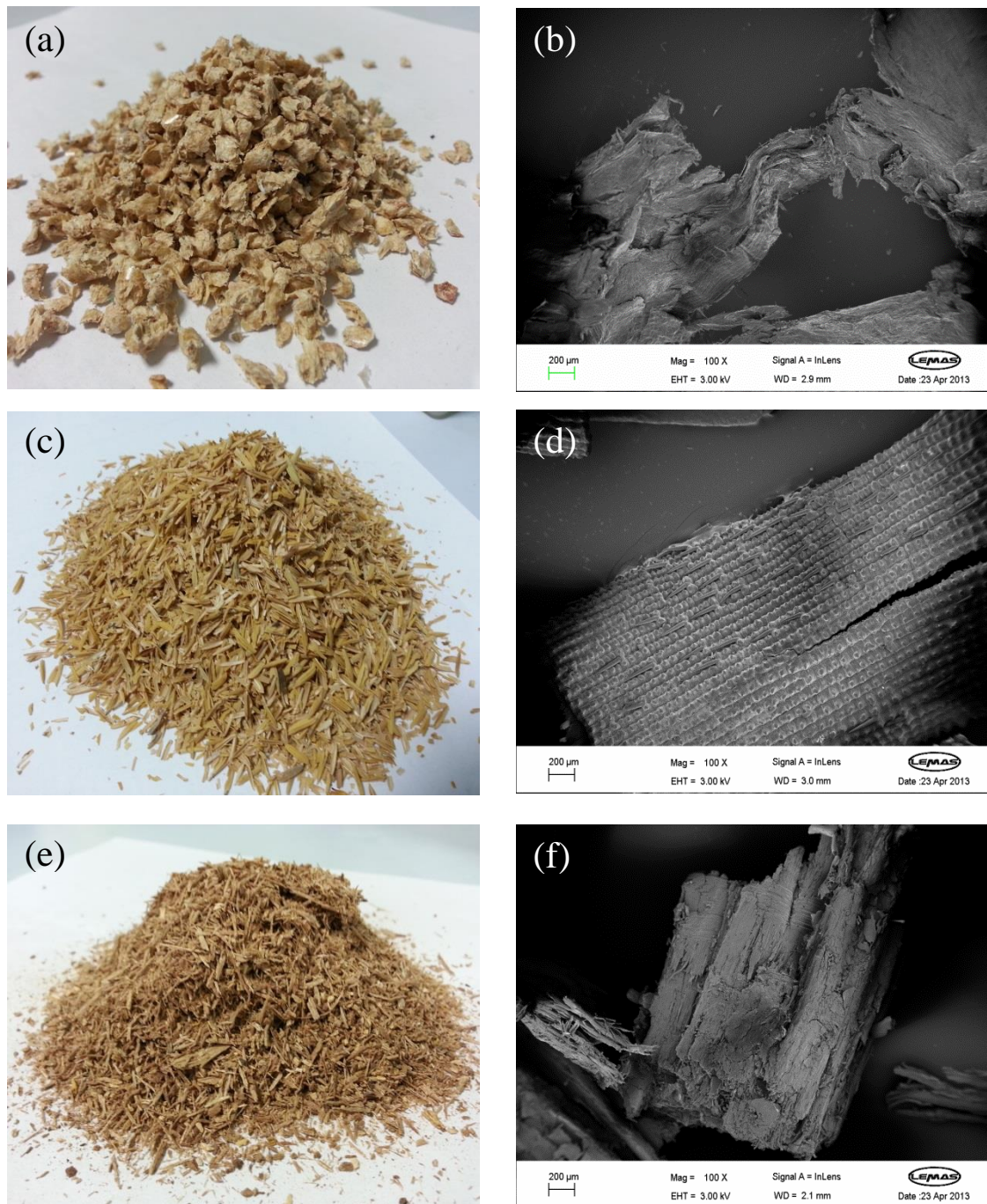


Figure 3-1 Photographs and SEM images of waste wood (a and b), rice husk (c and d) and forestry residue (e and f)

After initial investigation of flash pyrolysis and flash gasification (chapter 4), the ultra-high temperature reactor was modified from up-draft to down-draft configuration with the provision of catalyst in the second stage. Sugar cane (*saccharum officinarum*) bagasse, Rice (*Oryza sativa*) husk and wheat (*Triticum aestivum*) straw samples

(sourced from Pakistan) were used for further research (chapters 5 and 6). Wheat straw and rice husk samples were collected from known fields near Faisalabad city, Pakistan (coordinates 31 21 N, 72 59 E) while sugarcane bagasse samples were obtained from known fields near Samundri (coordinates 30 48 N, 71 52 E). These fields supply sugarcane to Gojra Samundri Sugar Mills Limited. When received, samples were bagged in plastic bags and transported to the UK. After receiving in the UK, samples were grounded and sieved to 1.4-2.8 mm particle size and kept in air tight containers to ensure the consistent composition until final usage. As shown in Table 3-2, these samples were chosen due to the larger proportion of volatiles with lower contents of ash especially in the sugarcane bagasse.

Table 3-1 Proximate and ultimate analysis of feedstock

Proximate Analysis (ash-free basis)				
Feedstock	Volatile matter (wt.%)	Fixed carbon (wt.%)	Moisture (wt.%)	
Waste wood	80.6	13.4	6.0	
Rice husk	75.9	17.8	6.3	
Forestry residue	77.9	15.3	6.8	
Ultimate analysis (ash-free basis)				
Feed stock	C (wt.%)	H (wt.%)	N (wt.%)	O ^a (wt.%)
Waste wood	48.5	6.2	0.8	44.5
Rice husk	49.0	5.9	1.1	44.1
Forestry residue	49.4	5.8	0.9	43.9

^a Calculated by difference

Being an agricultural country, Pakistan is one of the main producers of wheat, rice and sugarcane. Pakistan is the fifth largest sugarcane producer in the world. It is estimated that 49,373 thousand metric tonnes of sugarcane is produced annually with 16,293.09 thousand metric tonnes of bagasse is available in the form of residue from sugar industry. Furthermore, 1376.6 thousand metric tonnes of rice husk and 35,796 thousand metric tonnes of wheat straw is available annually from 6883 thousand metric tonnes of rice and 23,864 thousand metric tonnes of wheat respectively [1]. In 2011-2012 fiscal

year more than 24 million tonnes of wheat was produced in Pakistan [2]. This indicates that these biomass samples have huge potential in terms of long term sustainable supply. Results of proximate and ultimate analysis of rice husk, sugarcane bagasse and wheat straw samples are shown in Table 3-2. From the proximate analysis results shown in Table 3-2, it can be indicated that relatively higher volatiles were present in the bagasse and wheat straw samples. The highest volatiles in bagasse, presented on ash-free basis, accounted for around 83 % of the total weight. 78.4 wt.% of volatiles were found in wheat straw sample while slightly lesser 77 wt.% were present in rice husk. The amount of fixed carbon in wheat straw was 18.8 wt.%. For rice husk and bagasse it was found to be 15.7 wt.% and 11.1 wt.% respectively.

Table 3-2 Proximate and ultimate analysis of biomass feedstock sourced from Pakistan

Proximate Analysis (ash-free basis)				
Feedstock	Volatile matter (wt.%)	Fixed carbon (wt.%)	Moisture (wt.%)	
Bagasse	82.9	11.1	6.0	
Rice husk	77	15.7	7.4	
Wheat Straw	78.4	18.8	2.8	

Ultimate analysis (ash-free basis)				
Feed stock	C (wt.%)	H (wt.%)	N (wt.%)	O ^a (wt.%)
Bagasse	46.3	5.7	0.8	47.2
Rice husk	48.1	6.5	1.5	43.8
Wheat Straw	47.6	5.8	0.8	45.8

^a Calculated by difference

Relatively higher ash was present in rice husk sample. The amount of residual ash found was 1.6 wt.% for bagasse, 6.9 wt.% for wheat straw and 17.2 wt.% for rice husk. Higher ash contents in rice husk were also reported by other authors [3]. In-depth investigation of chemical composition of ash from 86 different biomass samples were collected and presented by Vassilev et al. [4]. They reported that ash from rice husk contains 94.48 wt.% of SiO₂ as compared to 46.79 wt.% for bagasse and 50.35 wt.% for wheat straw. Other species found in ash were CaO, MgO, K₂O, P₂O₅, Al₂O₃, Fe₂O₃ and Na₂O.

In order to compare the morphological structure, photographs and SEM images of three biomass samples are shown in Figure 3-2. All SEM images were taken at low resolution of 500X. From results it is evident that the bagasse and wheat straw possess fibrous structure while for rice husk, it was a sheet like structure comprising of regularly shaped crests and troughs.



Figure 3-2 Photographs and SEM images of rice husk (a and b), bagasse (c and d) and wheat straw (e and f)

3.2.2 Catalyst

During an initial study, cost effective and naturally abundant dolomite and 10 wt.% Ni-dolomite catalysts were used during the two-stage pyrolysis/gasification of rice husk biomass (chapter 5). Dolomite was calcined at 1000 °C and then grounded and sieved to attain a particle size between 50-212 µm. In order to increase the hydrogen yield, 10 wt.% Ni-dolomite catalyst was prepared by a wet impregnation method. Aqueous solution of $\text{Ni}(\text{NO}_3)_2 \cdot 6\text{H}_2\text{O}$ (received from Sigma Aldrich UK) was obtained by dissolving it in deionised water. Calcined dolomite was mixed in this aqueous solution and stirred for four hours. The left over paste was dried at 105 °C overnight followed by calcination in an air atmosphere at 900 °C. Catalyst was finally ground and sieved to achieve the particle size of 50 - 212 µm.

In order to investigate the influence of different metal oxide supports on hydrogen yield from pyrolysis/gasification of biomass, seven different Ni-based catalysts; 10 wt.% Ni-dolomite, 10 wt.% Ni-MgO, 10 wt.% Ni-SiO₂, 10 wt.% Ni-Al₂O₃, 2 wt.% Ce-10 wt.% Ni-dolomite, 5 wt.% Ce-10 wt.% Ni-dolomite and 10 wt.% Ce-10 wt.% Ni-dolomite were compared with silica sand in terms of hydrogen yield (chapter 6). All metal oxides and $\text{Ce}(\text{NO}_3)_3 \cdot 6\text{H}_2\text{O}$ were received from Sigma Aldrich UK. For the preparation of 2 wt.% Ce – 10 wt.% Ni-dolomite, 5 wt.% Ce – 10 wt.% Ni-dolomite and 10 wt.% Ce – 10 wt.% Ni-dolomite catalysts, dolomite was mixed and stirred into the aqueous solution of $\text{Ni}(\text{NO}_3)_2 \cdot 6\text{H}_2\text{O}$ and $\text{Ce}(\text{NO}_3)_3 \cdot 6\text{H}_2\text{O}$ followed by overnight drying at 105 °C and calcination at 900 °C. All the catalysts were calcined at 900 °C and grinded and sieved to achieve a particle size range between 50-212 µm.

The influence of calcination temperature on 10 wt.% Ni-Al₂O₃ catalyst was also researched. The 10 wt.% Ni-Al₂O₃ catalyst was prepared by a wet impregnation method. After overnight drying at 105 °C, the catalyst was divided in four different samples of around 5g each. Each sample was calcined in an air atmosphere at calcination temperatures of 700, 800, 900 and 1000 °C. During the investigation of nickel loading on the Ni-Al₂O₃ catalyst, four different Ni loadings of 5 wt.%, 10 wt.%, 20 wt.% and 40 wt.% on the alumina support were prepared separately using wet impregnation method. After drying and calcination at 900 °C, all the catalysts were tested for hydrogen production during pyrolysis/gasification of sugarcane bagasse biomass.

3.3 Pyrolysis/gasification reactors

Two different reactors (ultra-high temperature two-stage reactor and single-stage fixed-bed reactor) were used in this research work. The ultra-high temperature reactor was initially built in an up-draft configuration for flash pyrolysis studies (chapter 4) and later modified to a down-draft configuration for catalytic steam gasification research (chapters 5 and 6). The single stage fixed-bed reactor was employed to investigate the pyrolysis of biomass samples under slow heating rate conditions ($10\text{ }^{\circ}\text{C min}^{-1}$) and results were compared with flash pyrolysis results in chapter 4. Details of each individual reactor configuration are explained in the following sections.

3.3.1 Up-draft ultra-high temperature fixed-bed reactor

3.3.1.1 Up-draft flash pyrolysis reactor

In order to study the flash pyrolysis of biomass at ultra-high temperature, a special rig needs to be designed. A novel fixed bed up-draft reactor was designed in Solid Works; a CAD software developed by Dassault systems. A photograph of the reactor is shown in Figure 3-3. The main objective was to design a reactor which must be capable of attaining ultra-high temperatures ($950 - 1050\text{ }^{\circ}\text{C}$) and can hold the sample around room temperature while the main reactor is reaching that desired high temperature in an air-tight environment. This involves various material challenges as the normal stainless steel used to build conventional reactors cannot withstand such high furnace temperatures of up to $1200\text{ }^{\circ}\text{C}$. Inconel was chosen as a target material for this high temperature application. It is an alloy of various metals including Ni, Cr, Fe, Mo, Nb, Co, Mn, Cu, Al and Ti. The reactor was made up of 60.96 cm long inconel tube with 2.54 cm internal diameter. From the top, it is connected to a specially designed sample holding chamber to hold the sample before pyrolysis. The reactor was heated using two furnaces (slightly different in size) manufactured by Elite Thermal Systems limited. Each furnace is provided with a controller unit (Eurotherm model # 2416) to control the final temperature, heating rate, hold time etc.

The lower furnace (model # TSV12/38/200) was used to generate steam from the water injected into the reactor using a syringe pump manufactured by Cole Parmer Instruments Ltd UK. It is 900 watts furnace with a maximum rated temperature of $1200\text{ }^{\circ}\text{C}$. The main furnace was used to heat the main reactor zone. Maximum power rating

for this furnace was 1 KW, a maximum rated temperature for this furnace also was 1200 °C. The schematic diagram of reactor system is shown in Figure 3-4.



Figure 3-3 Photograph of the ultra-high temperature up-draft reactor

Two condensers were connected to the output of the reactor to capture any condensable liquids in the gas stream. The first condenser was directly attached to the reactor was water-cooled and its temperature was around 15 °C. The second condenser was filled with dry-ice with a temperature of around -80 °C. Glass wool was used in this second condenser to capture any oil vapours or mist. SKC sample bags (part # 231-15) were used to collect the gas samples. Nitrogen was used as a purge gas in the reactor. Two nitrogen streams were injected into the reactor; one from the bottom to the main reactor zone while the other stream was injected into the sample holding chamber (SHC) to keep an inert atmosphere in the chamber. In order to measure the flow of nitrogen and hence the total volume, two flow meters (model # Brooks GT1355/D1F2D1B5A000) were used. The range of these flow meters was 48- 480 mL min⁻¹.

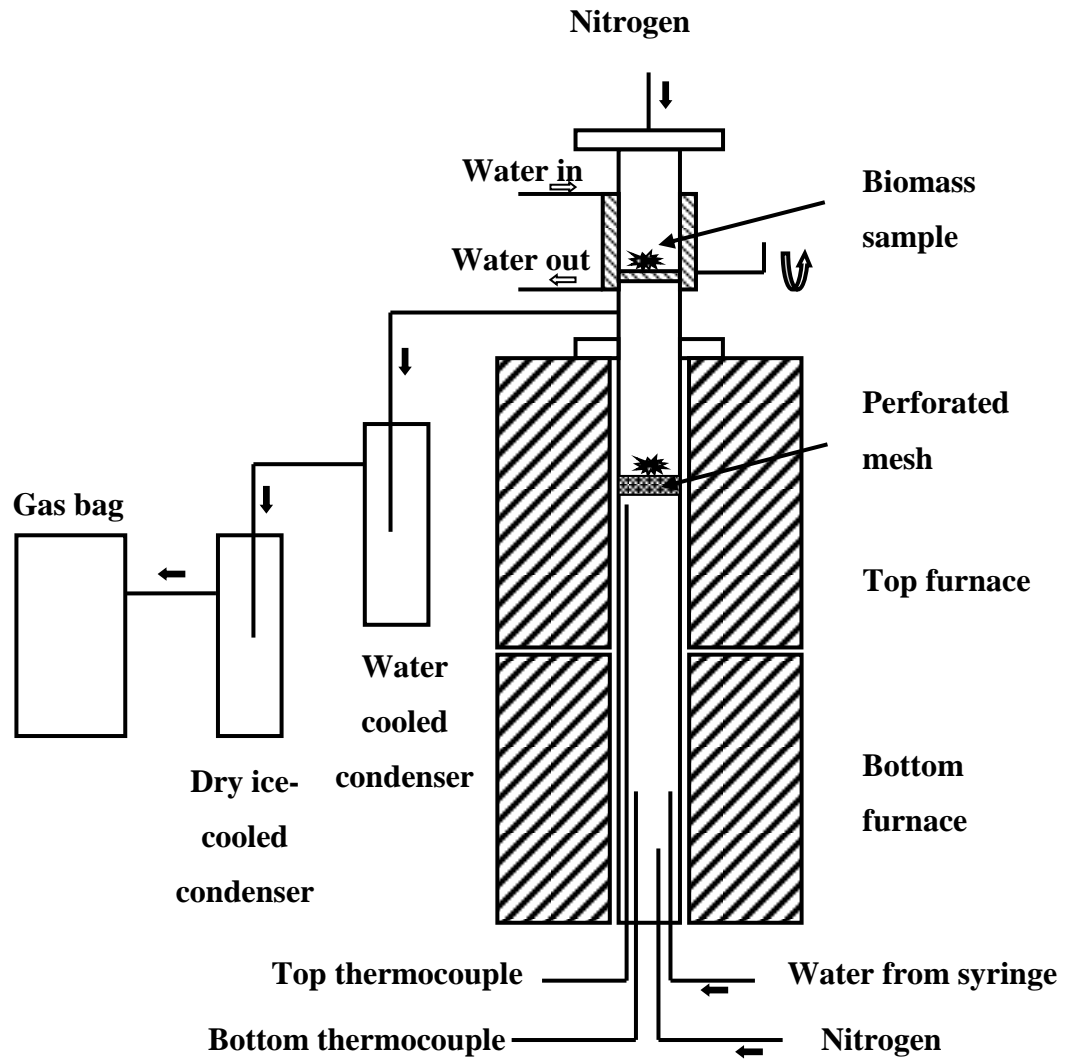


Figure 3-4 Schematic diagram of the ultra-high temperature up-draft reactor

Two N-type thermocouples were installed inside the reactor from the bottom. The placement of these thermocouples was adjusted to measure the temperature near the central zone of both furnaces. Maximum temperature range for these N type thermocouples supplied by RS components was 1250 °C. Each thermocouple was 500 mm long with a 3 mm diameter (RS catalogue # 611-292). Fuji temperature controller (model # PXR4 TAY1 1V000) was used to display the temperature readings for both thermocouples. As shown in Figure 3-4, four inputs were provided from the bottom of the reactor. Two inputs were used to install the thermocouples. The other two inputs were used to inject the nitrogen and steam. Nitrogen gas comes from the flow meter which is connected to gas cylinder. For gasification experiments, water was injected

using a syringe pump. Flow rate and total volume of the water injected can be precisely measured and controlled by this Cole Parmer syringe pump. This water enters into the lower part of the reactor and is immediately converted into steam and moves upward into the main reactor. The total weight of the steam injected into the system was calculated by weighing the syringe before and after each experiment. In the centre of the main reactor, a perforated sample plate or mesh was placed from the top. The purpose of this plate was to provide the base for the biomass sample coming down and to pass the steam and nitrogen gas coming from the bottom of the reactor. The sample when dropped from the sample holding chamber at the top falls directly on this plate where it is then completely pyrolysed. Any remaining char and ash at the end of the experiment can be collected from this plate as this plate can be brought out of the reactor using a vertical rod connected to it.

A special chamber was designed to hold the sample before it was dropped down into the main reactor. The main function of this sample holding chamber was to keep the sample around room temperature in an inert atmosphere. This was achieved using a hollow disc as a floor of this chamber connected with metallic pipes on both ends so that water keeps flowing through the inside of this disc while the sample is placed at the top of this plate. This constant flow of water through the disc stops the rapid increase in temperature. This cooling effect was further supplemented by a water cooled jacket around this sample-holding chamber. The height of whole chamber was 12.70 cm with inner diameter of 2.54 cm. The chamber was made up of steel and connected with the main reactor using flanges. A nitrogen bleed was injected into the chamber to ensure the inert atmosphere. The flow rate of this nitrogen bleed can be adjusted using a flow meter installed in the main control panel of the reactor (shown in Figure 3-3). Before the start of the pyrolysis, the sample was introduced into the chamber stays at the top of the hollow disc. When the furnaces attain the required temperature, this hollow disc was rotated 90 degree about its centre axis and the sample was dropped down onto the sample plate in the main reactor. During the testing phase, a K type thermocouple was installed in this sample-holding chamber to monitor the variations in temperature inside the chamber while main reactor was reaching to 1050 °C. The process was repeated three times. It was noticed that the highest temperature of this sample holding chamber was 76 °C which indicates the effectiveness of this chamber for keeping the sample cool.

3.3.1.2 Standard operating procedure for up-draft flash pyrolysis reactor

A standard operating procedure was devised to carryout flash pyrolysis and flash gasification experiments. Before the start of the experiment, reactor and its components were checked for any visible damages such as insulation of electric cables and any cracks on glassware. The condenser system (two flasks and connecting pipes), and sample plate were weighed and then connected to the reactor. The syringe was also weighed and required steam flow rate (for gasification experiments) was set on syringe pump. A clean sample gas bag was connected to the outlet pipe of the condenser system to collect the gases. Sample holding chamber was also connected to the reactor. Five grams of biomass sample was placed on hollow disc in sample holding chamber and the chamber was closed from the top. Nitrogen supply connections were made and both flow meters were set to the required flow rate of 100 ml min^{-1} . Finally both furnaces were start heating to the desired temperature of $950 \text{ }^{\circ}\text{C}$. Once the required temperature was achieved, the biomass sample was dropped from the sample holding chamber into the reactor. All the gases were collected into the gas sample bag for 40 minutes. All the condensable liquids in the gas stream were captured in condenser system using dry ice.

Once the gas collection time was over, gas sample bag was disconnected and gas was analysed offline using gas chromatography. The condenser system was disconnected from the reactor and was weighed and subtracted the initial weight to find the amount of liquid collected. Syringe was disconnected from the reactor and weighed. The amount of injected steam was calculated by the difference of initial and final weight of the syringe. Once the reactor was cooled down to the room temperature, the sample plate was removed from the reactor and was weighed to find the weight of the solid residue.

3.3.1.3 Repeatability test for up-draft flash pyrolysis reactor

In order to establish the suitability of the up-draft reactor for further research, repeatability tests were performed. All the experiments were performed under identical conditions. Waste wood samples were used for these repeatability experiments. The results of these experiments are presented in Figure 3-5.

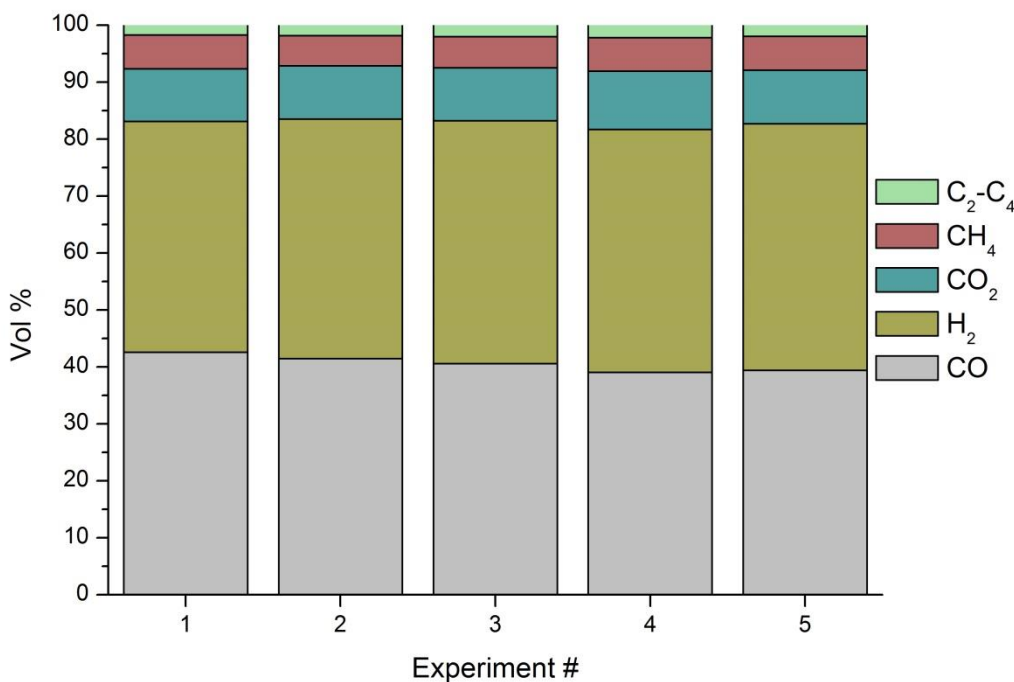


Figure 3-5 Repeatability test results for the up-draft ultra-high temperature reactor

All the experiments were performed using the standard operating procedure. The reactor was heated to 950 °C temperature with steam flow rate of 6 mL hr⁻¹. The flow of nitrogen gas kept constant at 200 mL min⁻¹ and product gases were collected for 40 minutes after dropping the sample in the main reactor. The weight of flasks, sample plate and water syringe was measured before and after every experiment to get a good mass balance. The product gases collected in the gas bag were analysed using Varian GCs CP-3800 and CP-3380. The results obtained from analysis were converted into gas percentage, mass in grams and number of moles using a Microsoft Excel formula-sheet. As shown in Figure 3-5, the reactor showed a good repeatability in terms of percentage of product gases. Near constant gas composition was obtained under the same conditions. The mean values of individual gases were found to be 40.61 vol.% for CO, 42.24 vol.% for H₂, 9.44 vol.% for CO₂, 5.71 vol.% for CH₄ and 1.94 vol.% for C₂-C₄ hydrocarbons. The standard deviation values were also calculated for each individual gas for all five experiments. The standard deviation value for CO was 1.31. For H₂, it

was 0.94 and for CO₂ it was 0.37. The standard deviation value for CH₄ and C₂-C₄ hydrocarbons was found to be 0.26 and 0.14. These mean values and standard deviation values clearly indicate that these results are repeatable.

3.3.2 Down-draft ultra-high temperature fixed bed reactor

3.3.2.1 Down-draft catalytic steam gasification reactor

After flash pyrolysis and flash gasification research using the up-draft configuration (Chapter 4), this ultra-high temperature fixed-bed reactor was modified to a down-draft configuration. One of the major advantages of down-draft configuration was the higher thermal cracking and reforming of hydrocarbons and tars as all the volatiles, liquids and gases pass through the hottest reactor zone before leaving the reactor. The photograph of the modified down-draft reactor is shown in Figure 3-6 while the schematic diagram of the entire system is shown in Figure 3-7.



Figure 3-6 Photograph of the ultra-high temperature down-draft reactor

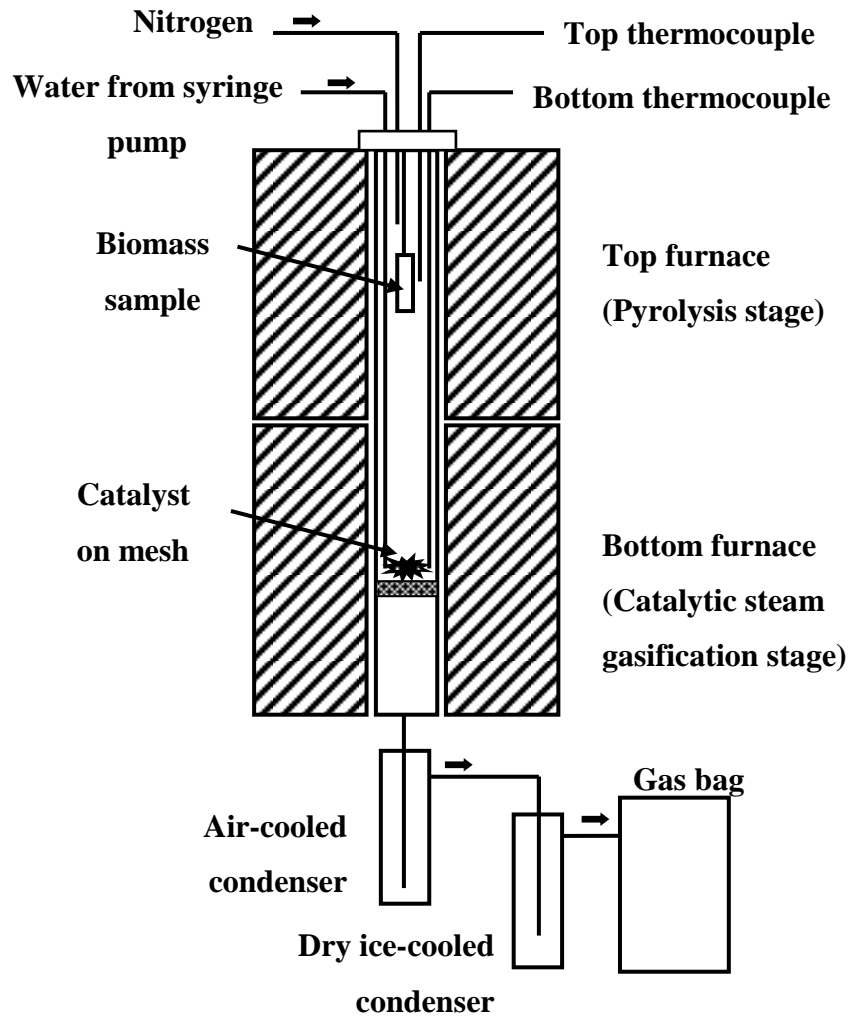


Figure 3-7 Schematic diagram of the ultra-high temperature down-draft catalytic gasification reactor

As compared to the previous up-draft design detailed in Section 3.3.1, the following changes/improvements were made in this new reactor design.

- As the name suggests, in down-draft reactor, the flow of materials e.g. gases was from top to bottom.
- Only one nitrogen feed was introduced from top to bottom as there was no special sample holding chamber.
- Biomass sample was placed inside the sample crucible which was hanging to the top cover by means of a hook in top pyrolysis stage.
- Two N-type thermocouples were installed from the top instead from the bottom.
- Steam was injected from the top by means of a syringe pump.

- A ring was welded inside the reactor tube at the middle point of the bottom reactor so that the perforated mesh can be placed on the top of it. This mesh was used as a physical support to place the catalyst on quartz wool.
- Analogue nitrogen flow meter was replaced with the digital mass flow rate controller to precisely control the nitrogen flow.

3.3.2.2 Standard operating procedure for down-draft gasification reactor

A standard operating procedure was developed to perform ultra-high temperature pyrolysis and gasification of biomass in a modified reactor. Before the start of the experiment, empty and cleaned sample pot/crucible was weighed and 4 grams of biomass sample was placed in it. The reactor tube, catalyst mesh and condenser system (two condensers and connecting pipes) were weighed separately before the start of each experiment. Before placing the reactor tube inside the furnace heaters, 2 grams of catalyst (for catalytic steam gasification experiments) was placed on quartz wool on a perforated mesh (catalyst to sample ratio of 0.5). The water syringe was weighed and connected to the reactor using a syringe pump. Steam to biomass ratio was 1.37 for gasification experiments as steam was introduced at 0.1 g min^{-1} for 55 minutes (5.5 g) for 4 grams of biomass. An empty and cleaned gas bag was connected to the output of the condenser system. Once all the connections were made, the desired temperature of $950 \text{ }^{\circ}\text{C}$ was set for both pyrolysis and gasification reactors. The flow rate of nitrogen was set to 100 ml min^{-1} . Initially, gasification stage was heated from room temperature to $950 \text{ }^{\circ}\text{C}$ at $20 \text{ }^{\circ}\text{C min}^{-1}$. Once the desired temperature for gasification stage was achieved, steam injection into the gasification stage was started along with the heat up of the pyrolysis stage from ambient temperature to $950 \text{ }^{\circ}\text{C}$ at $20 \text{ }^{\circ}\text{C min}^{-1}$. All the volatiles, liquids and gases evolving from the pyrolysis stage were made to react with the steam in the presence of catalyst in the gasification stage. All the condensable liquids and unreacted steam were collected in condenser system using glass wool trap and dry ice. The synthesis gas was collected in a gas sample bag.

For pyrolysis experiments in the absence of catalyst, the biomass sample was placed in the pyrolysis reactor stage and both stages were heated simultaneously at $20 \text{ }^{\circ}\text{C min}^{-1}$ for ~50 minutes to achieve the final temperature of $950 \text{ }^{\circ}\text{C}$. The gases were collected for another 40 minutes to ensure good material balance. For pyrolysis experiments, the total gas collection time was 90 minutes. For gasification experiments, the gasification

stage was heated first from ambient to 950 °C in ~50 minutes. Then the pyrolysis stage was also heated to 950 °C in ~50 minutes. The gases were collected for another 40 minutes to ensure good material balance. The total gas collection time for gasification experiments was 140 minutes.

Once the gas collection time was over, gas bag was disconnected from the condenser system and gases were analysed offline using gas chromatography. The condenser system, syringe and the sample pot/crucible were weighed after the experiment. The amount of liquids obtained was calculated by the difference in the weight of the condenser system before and after the experiment. The amount of residual char was calculated by the difference in the weight of the sample pot/crucible. The amount of injected water was calculated by the difference in the weight of the syringe before and after the experiment.

3.3.2.3 Repeatability test for down-draft catalytic steam gasification reactor

Repeatability tests were performed on the down-draft reactor to ensure the suitability of this reactor for further research. Waste wood biomass sample was used for these experiments. The waste wood sample was placed inside the crucible and the reactor was heated up to the final reactor temperature of 950 °C. Nitrogen flow rate was kept constant at 100 ml min⁻¹. Five experiments were performed under identical conditions and results are shown in Figure 3-8. These results indicate that the gas composition was near constant and confirm the suitability of this reactor for further research work.

The mean values of individual gases were found to be 31.78 vol.% for CO, 29.80 vol.% for H₂, 25.85 vol.% for CO₂, 10.11 vol.% for CH₄ and 2.43 vol.% for C₂-C₄ hydrocarbons. The standard deviation values were also calculated for each individual gas for all five experiments. The standard deviation value for CO was 0.65. For H₂, it was 1.62 and for CO₂ it was 1.71. The standard deviation value for CH₄ and C₂-C₄ hydrocarbons was found to be 0.95 and 0.17. These mean values and standard deviation values clearly indicate that these results are repeatable.

Furthermore, in terms of mass balance, a good agreement in the values of all five experiments was found. The mass balance values for all five experiments were 100.50, 101, 98.75, 99.75 and 99.50 (wt.%).

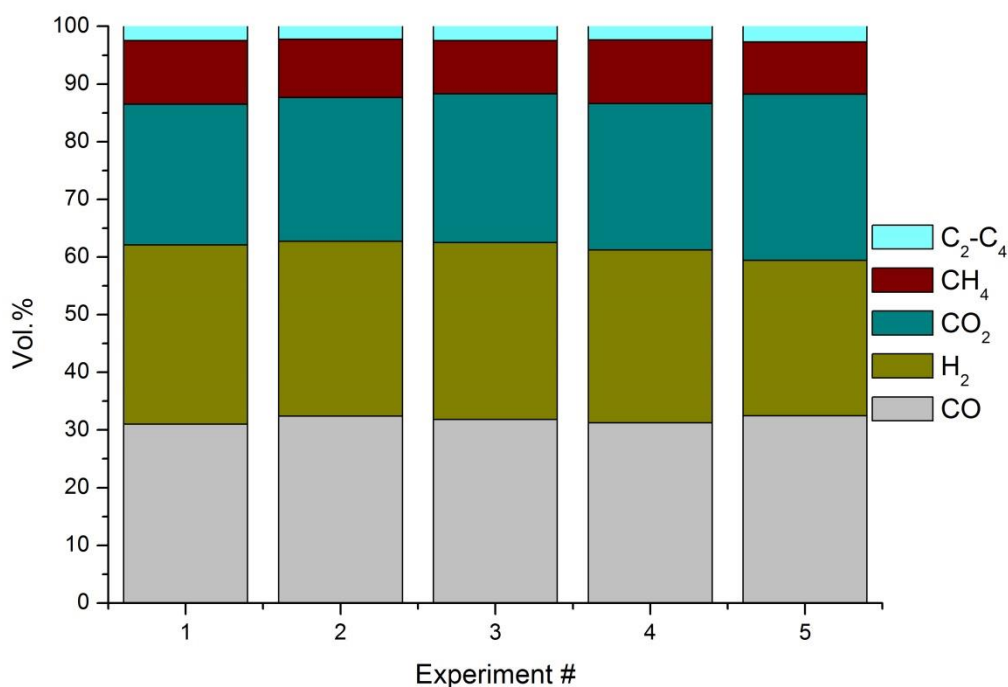


Figure 3-8 Repeatability test results for down-draft ultra-high temperature reactor

3.3.3 Single-stage fixed bed reactor

The slow pyrolysis experiments were performed on single stage, down-draft fixed-bed reactor. The slow pyrolysis reactor was constructed of steel and was 250 mm long with 30 mm inner diameter and continually purged with nitrogen. The reactor was heated using a tube furnace of 1.2 KW. This reactor was capable of attaining the maximum temperature of 900 °C. Heating rate, final temperature and hold time was controlled by an electronic controller (Eurotherm model #2210e) using a K type thermocouple placed inside the reactor. A sample crucible held the biomass sample in the reactor. The reactor was heated to the final temperature of 850 °C at a heating rate of 10 °C min⁻¹. Final temperature was maintained for 30 min. Condensers were used to condense the oils and condensable liquids consisting of water-cooled and dry-ice condensers. Gases were collected in a gas bag and were analysed off-line using gas chromatography technique. A schematic diagram of the slow pyrolysis reactor system is shown in Figure 3-9. Before the start of the actual research work, repeatability of the reactor system was investigated at 800 °C. Three experiments were performed under identical conditions. Product yield and mass balance results were compared. Results were found to be very

close and confirm the reliability and reproducibility of the reactor system. For three repeatability experiments the mass balance was found to be 99.97, 100.14 and 99.92 wt.%. The standard deviation values of gas, oil and char yield were found to be 0.20, 0.06, and 0.04 respectively. The mean (average) yield for gas, oil and char was 6.95, 42, 51.06 wt.% respectively.

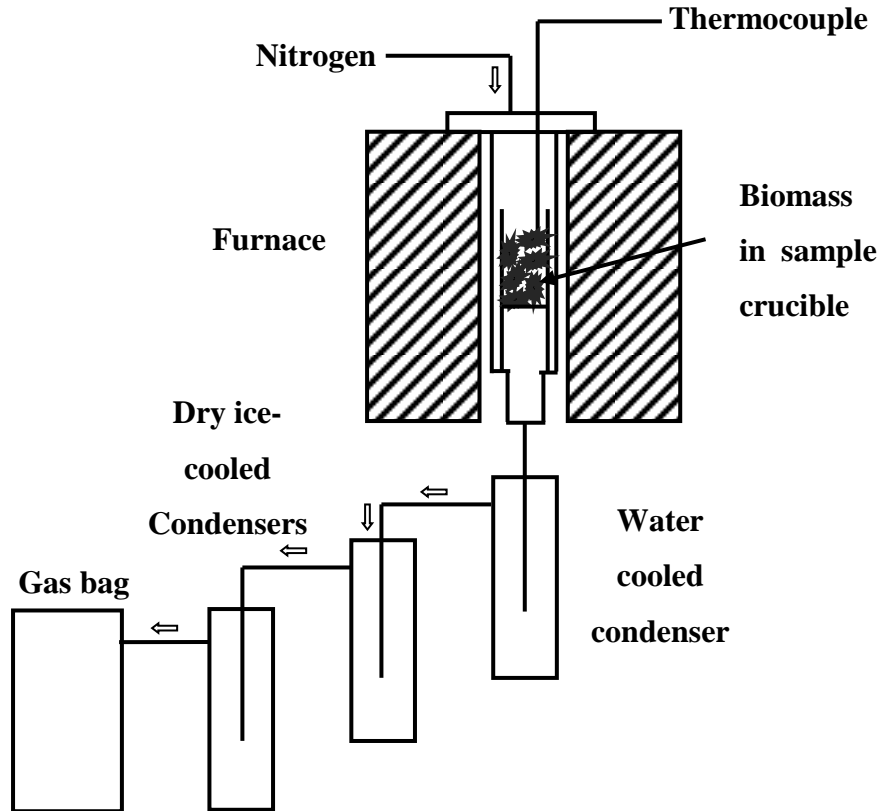


Figure 3-9 Schematic diagram of slow pyrolysis reactor

During slow pyrolysis experiments, 5 g of biomass was weighed into the sample crucible and was placed inside the reactor. Then reactor was heated from ambient temperature to 850 °C at a heating rate of 10 °C min⁻¹. Nitrogen as a carrier gas was used at a flow rate of 200 ml min⁻¹ with a residence time of 0.9 min. Oils produced during slow pyrolysis were collected using a condenser system and gas was collected in gas bag. Weight of char and liquid oils was calculated from the weight of sample crucible and condenser system before and after every experiment.

3.4 Analysis and characterisation

3.4.1 Gaseous products analysis

3.4.1.1 Gas analysis

Gases produced during the pyrolysis/gasification of biomass were analysed using an established gas chromatography technique. The mixture of gases was analysed for hydrocarbons (C_1 - C_4), and permanent gases (H_2 , O_2 , N_2 , CO , CO_2). A simplified schematic diagram of a gas chromatography system is shown in Figure 3-10.

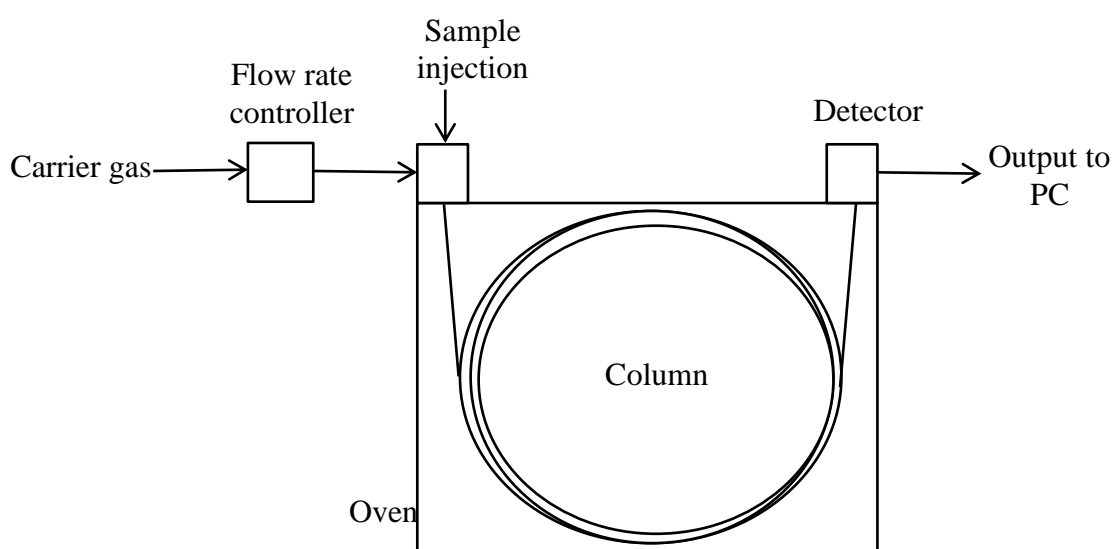


Figure 3-10 Schematic diagram of a gas chromatography system

A typical GC system consists of an inert carrier gas (also known as mobile phase), a metallic column inside the temperature controlled oven and a detector connected to a computer. The sample was injected into the injector using a one ml glass syringe. The inner lining of the column is coated with a microscopic layer of liquid or polymer known as stationary phase. Gases injected into the column react with the stationary phase differently and hence the time required to reach the detector is different for different gases. The detector detects the gas and presents the signal on a computer in volts or millivolts depending upon the volume of the gas. Typically TCD (thermal conductivity detector) or FID (flame ionization detector) is used in GCs.

The gases collected in the gas sample bag were analysed for hydrocarbons (C₁-C₄) using a Varian CP-3380 gas chromatograph with a column packed with an 80 - 100 mesh Hysep packing with a flame ionization detector (GC/FID). The column was 2 meters long and 2 mm in diameter. Nitrogen was used as a carrier gas. The temperature of the oven was initially set at 60 °C for 3 min, and then increased at 10 °C min⁻¹ heating rate up to 100 °C with a hold time of 3 min. Finally, the temperature was increased from 100 to 120 °C at 20 °C min⁻¹ with a hold time of 10 min.

Permanent gases (H₂, CO, N₂, O₂, CO₂) were analysed using a second Varian CP-3380 chromatograph comprised of two columns with two thermal conductivity detectors (GC/TCD). One column packed with a 60-80 mesh molecular sieve, was used to separate hydrogen, carbon monoxide, nitrogen, and oxygen. The other column packed with 80-100 mesh Hysep was used to analyse carbon dioxide. Argon was used as a carrier gas. Both columns were 2 meters long and 2 mm in diameter. The GC oven for CO₂ was set at 40 °C and held for 7 min. The GC oven for H₂, CO, N₂, O₂ was kept constant at 30 °C while injector and detector were set at 120 °C. Concentration of all individual gases and hence the mass balance was calculated using the method explained in Appendix A.

3.4.2 Biomass and char characterization

3.4.2.1 Proximate analysis

Proximate analysis was performed using a Shimadzu TGA-50H thermogravimetric analyser. The system consists of an electrically heated furnace with a sample holder on a microbalance. The sample is placed in the sample holder is heated from room temperature to the final required temperature with known flow rate and heating rate. Accurate microbalance and thermocouples connected with a computer are used to record the sample weight loss against temperature and time. Weight loss data is plotted on screen in real time and finally all the data recorded on a file. The system has a provision of providing different atmospheres such as air or nitrogen. An automatic valve switching system is connected to the device and thermal degradation environment can be changed in runtime. A simplified schematic diagram of the TGA is shown in Figure 3-11.

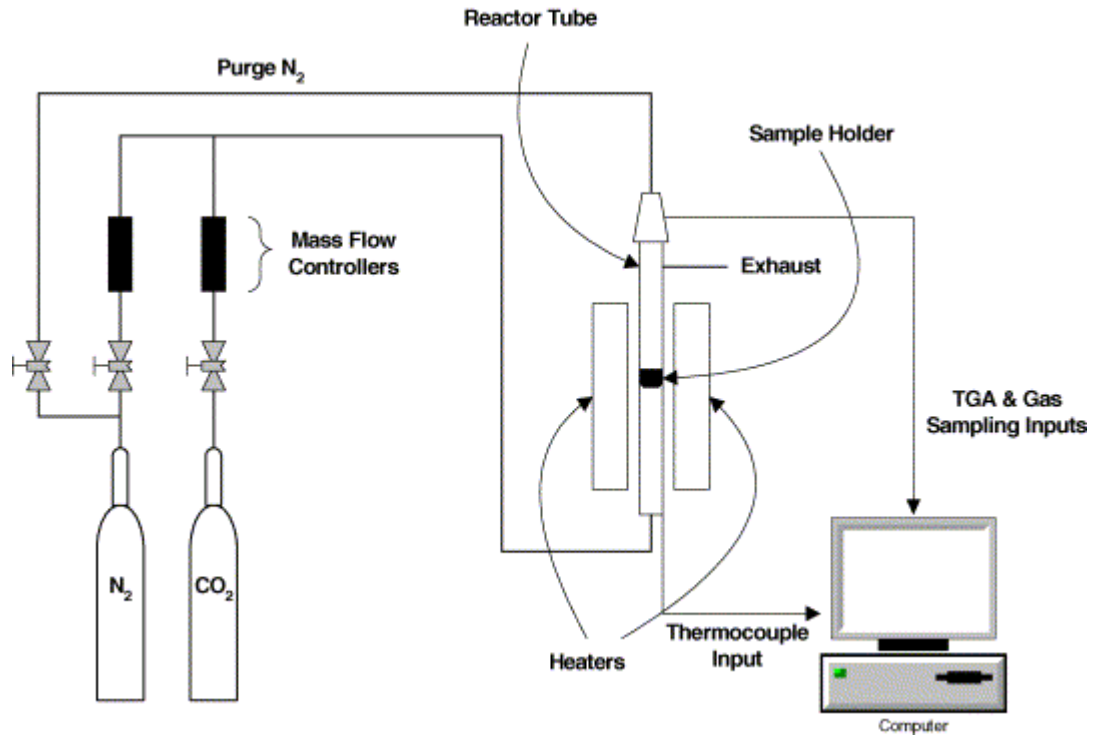


Figure 3-11 A schematic diagram of thermogravimetric analyser [5]

Proximate analysis is used to investigate the moisture, ash and fixed carbon contents in the sample. It is a three stage process. As a first step, sample is heated up to 110 °C in nitrogen environment with a heating rate of 25 °C min⁻¹. When the final temperature is achieved, the sample is held at that temperature for 10 minutes so that the constant weight is attained.

The weight loss in this first step represents the moisture content in the sample. In the second stage volatile matter in the sample is measured by the weight loss when the sample is heated up to 925 °C in a nitrogen environment with a hold time of 10 minutes. Finally fixed carbon is measured by the weight loss when the sample is combusted in an air atmosphere at temperature of up to 935 °C. Any residual material in the sample holder is ash. A typical graph obtained from the proximate analysis of the biomass samples is shown in Figure 3-12.

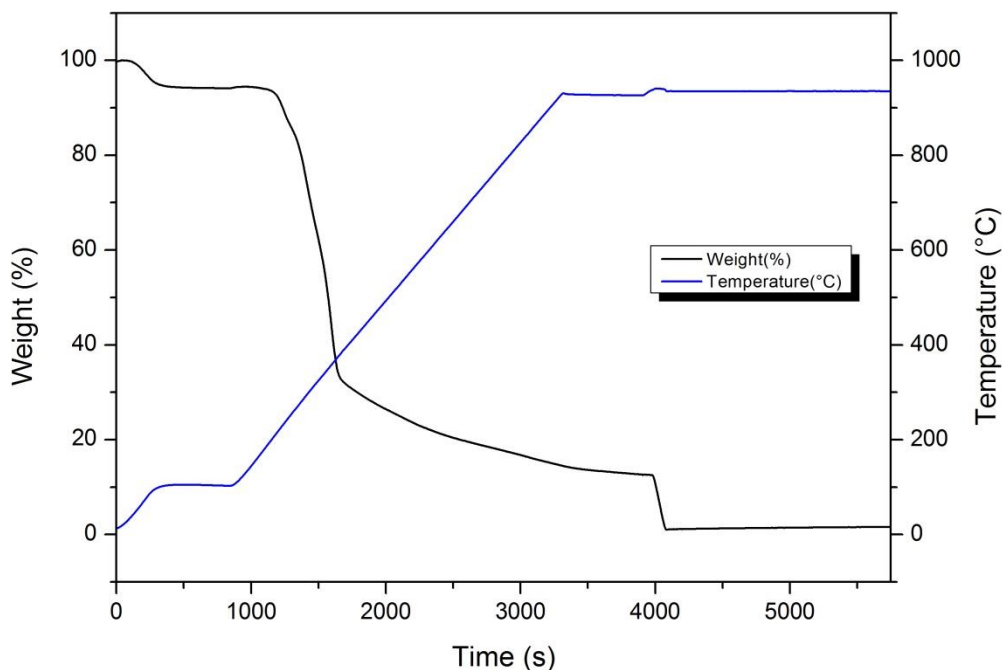


Figure 3-12 Example graph of proximate analysis of biomass sample

3.4.2.2 Ultimate analysis

The Carlo Erba Flash EA 11112 elemental analyser was used to determine the elemental composition (C, H, N, and S) of biomass sample. The sample is combusted into gases without being diluted or decomposed using a dynamic flash combustion technique in this analyser. The schematic diagram of the analyser is shown in Figure 3-13.

Around 3 mg of dried sample sealed in a tin capsule is inserted into the combustion chamber using auto sampler. Typically the combustion chamber maintains its 1000 °C temperature in helium environment but introduction of known quantity of oxygen to the chamber causes complete oxidation of the sample. This raises the temperature of the reaction chamber up to 1800 °C for a few seconds. Nitrogen oxides and SO₃ are reduced to SO₂ and elemental nitrogen when these combustion gases pass through the reduction chamber. Gases from the reduction chamber are separated by GC column and detected by TCD (Thermal conductivity detector). Elemental data is obtained in computer software using this TCD output. Each sample is analysed twice and mean value is used to determine the elemental composition of the sample.

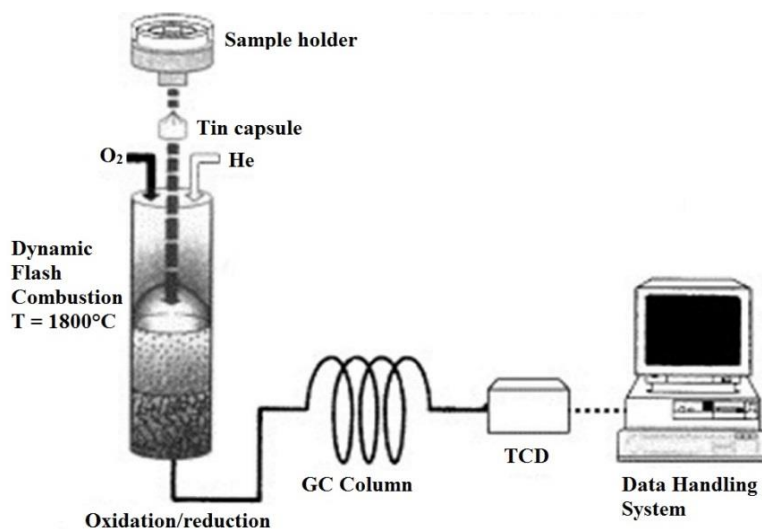


Figure 3-13 Schematic diagram of a CHNS elemental analyser adapted from [6]

3.4.2.3 X-ray fluorescence (XRF) analysis of ash

The residual ash from the biomass samples was analysed using an Olympus Innovex X-5000 X-ray Fluorescence (XRF). This device is equipped with a Rh source and is capable of analysing powders and solids. It is a non-destructive characterisation technique and samples can be analysed in less than 5 minutes. During XRF analysis, the sample is exposed to intense beam of X-rays which illuminated the sample. Some of this incident X-ray energy is absorbed by the sample to remove the electrons from the lower electronic shells like K and L shells. Once electrons are removed by this high energy incident X-rays from these shells, vacancies are created. The electrons from the upper shell jump to fill up vacancies in these low energy shells and release energy in the form of radiations. Because these radiations are characteristic of each individual element, these elements can be identified by these radiations. All the data from the device sent to the software which can recognise the elements present in a sample.

3.4.3 Catalyst characterization

3.4.3.1 Temperature programmed oxidation (TPO)

The temperature programmed oxidation (TPO) technique was used to characterise the reacted catalysts using a thermogravimetric analyser (TGA). This technique is used to

investigate the amount of coke deposited on the spent catalyst from the process of pyrolysis/gasification.

Around 15 mg of reacted catalyst was placed inside the crucible of the TGA and heated from room temperature to 800 °C at a heating rate of 15 °C min⁻¹ in an air atmosphere (50 ml min⁻¹). The weight loss of the sample was recorded in relation to time and temperature. TGA-TPO and DTG-TPO curves of various catalysts are shown in Figure 3-14. The amount of coke deposited on the catalyst was calculated using the following equation [7].

$$w = \frac{w_1 - w_2}{w_1} \times 100 \text{ (wt. \%)} \quad (3 - 1)$$

Where w is the amount of deposited carbon on catalyst in wt.%, w_1 is the initial catalyst weight after moisture loss and w_2 is the final catalyst weight after oxidation.

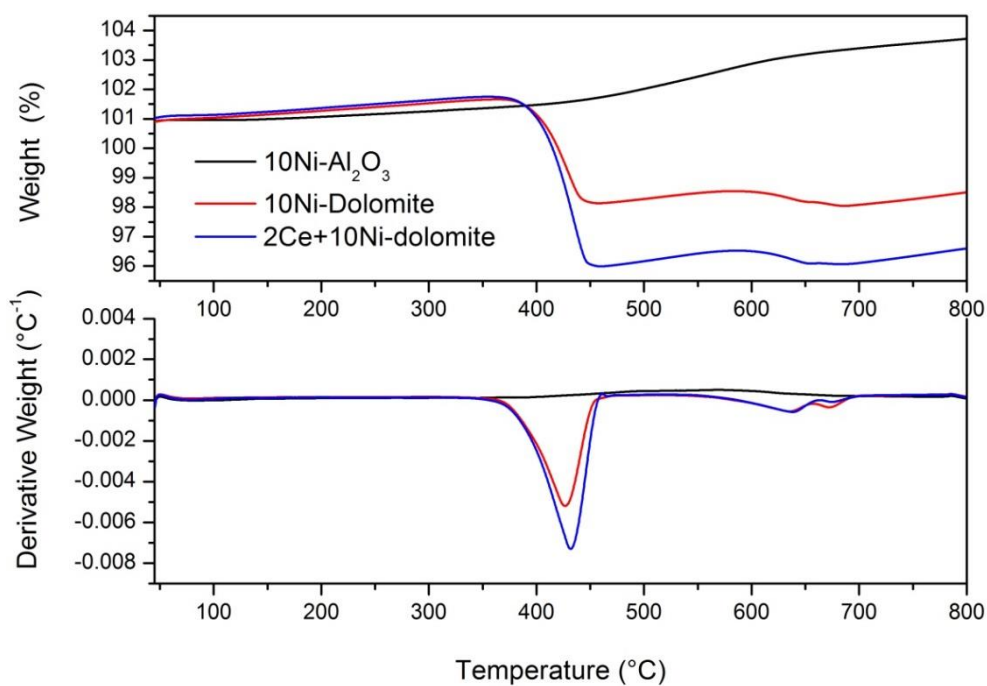


Figure 3-14 TGA-TPO and DTG-TPO thermograms of different spent catalysts

3.4.3.2 Scanning electron microscopy (SEM)

A Field Emission Gun Scanning Electron Microscope (FEGSEM) LEO 1530 equipped with an 80 mm X-Max SDD detector was used to analyse the microscopic structure of fresh and reacted catalysts. The system was also equipped with energy dispersive X-ray spectroscopy (EDXS). A photograph of LEO 1530 SEM is shown in Figure 3-15.

In a scanning electron microscope, a high energy electron beam is generated using an electron gun. The electron beam is then focused using two sets of condenser lenses. Once the beam is focused, it passes through a deflector coil which deflects the beam onto the desired area of the specimen. The deflected electrons are detected by electron detectors to form the image of the sample. This high energy electron beam scans the area line by line to produce a high resolution image.

Each specimen was prepared in the form of powder. A double sided adhesive carbon disc was used to fix the sample on aluminium studs. The excess sample on the disc was removed by pressurised air. The sample was then coated with a 5 nm platinum layer in a coater. The high resolution electron microscopy was carried out under vacuum conditions at 2.5 - 3 mm working distance with a supply voltage of 3 KV.



Figure 3-15 LEO 1530 scanning electron microscope

The EDXS system was used to qualitatively analyse the elemental composition of the sample. The X-ray beam was focused on to the sample and the amount of energy release from the sample was measured using detector. The results were compared with the existing elemental library to identify the different elements present in the specimen.

3.4.3.3 Transmission electron microscopy (TEM)

A Phillips CM-200 Field Emission Gun Transmission Electron Microscope (FEG-TEM) coupled with an energy dispersive X-ray spectrometer (EDXS) was also used to further investigate the morphology of some of the fresh and reacted catalysts. A photograph of complete Phillips CM-200 TEM system is shown in Figure 3-16. In contrast to SEM (where deflected or scattered electrons from the sample form the image), in the transmission electron microscope, electrons are transmitted through a thin layer of the sample and collected behind the plate to form the image.

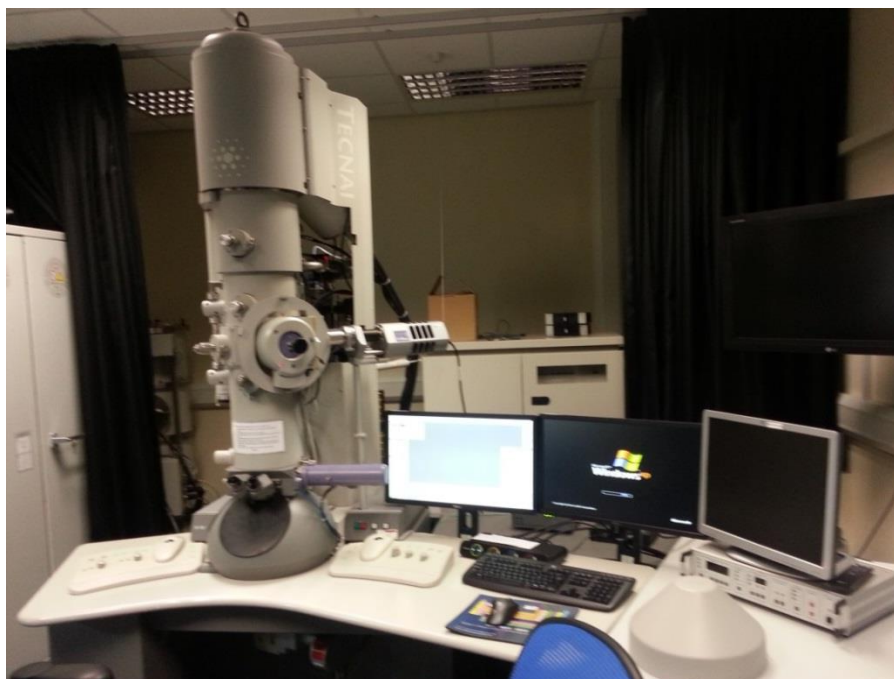


Figure 3-16 Phillips CM200 transmission electron microscope

Fine powders of catalysts were prepared by grinding and sieving to study by TEM. Samples were first dispersed in acetone and then spread on a Cu grid supported by a perforated carbon membrane. A high energy electron beam of up to 200 KV was used to analyse the prepared samples. High resolution images of fresh and reacted catalysts

were obtained to compare the morphological differences in fresh and reacted catalysts. The nature of deposited carbon on the reacted catalysts was also studied using this technique.

3.4.3.4 Brunauer–Emmett–Teller (BET) surface area analysis

The BET (Brunauer, Emmett and Teller) surface area, pore volume, and pore size distribution of fresh catalysts were measured using a Nova-2200e surface area and pore size analyser from Quantachrome instruments USA. In order to analyse the surface properties of different catalysts, 0.1 gram of each sample was outgassed in a vacuum environment at 200 °C for 2 hours using sample cells.

After outgassing, samples were placed in the analysis chamber with filler rods in sample cells. The sample is then cooled to 77 K using a liquid nitrogen container. The partial pressure of nitrogen in the sample cell was increased from 0 to 1 and then (after allowing some time for equilibrium to be achieved) the amount of nitrogen adsorbed or desorbed from the sample surface was measured by static volumetric method. For full isotherm analysis, 21 points were taken for each adsorption and desorption curve while for BET surface area analysis only six points were taken. Density function theory (DFT) equilibrium model was used to calculate the pore size distribution. Example surface properties of some fresh catalysts are shown in Table 3-3.

Table 3-3 Surface properties of fresh catalysts

Fresh Catalyst	BET surface area	BJH pore volume	Average pore size
	$\text{m}^2 \text{g}^{-1}$	$\text{cm}^3 \text{g}^{-1}$	nm
10% Ni- Al_2O_3	76.82	0.2792	5.64
10% Ni-dolomite	5.56	0.0308	3.78
2%Ce-10% Ni-dolomite	7.37	0.0229	2.96
10% Ni-MgO	53.90	0.3939	36.08
10% Ni- SiO_2	8.16	0.0253	2.17

3.4.3.5 X-ray diffraction (XRD) analysis

X-ray diffraction analysis of the catalysts was carried out using a D8 Focus from Bruker Corporation to examine the crystal structure and crystallite size using Cu α_1 radiations. Powdered sample was loaded to an acrylic sample holder. The sample was pushed into the holder to form a flat surface. The angle 2θ between the X-ray source and detector was varied from 10 to 80 degrees. DIFFRACPlus software was used to collect the data from the D8 analyser. Eva software along with the ICDD PDF2 (International Centre for Diffraction Data Powder Diffraction Files) database was used for phase identification.



Figure 3-17 Bruker D8 X-ray diffraction (XRD) analyser [8]

3.5 Chapter references

- [1] A. W. Bhutto, A. A. Bazmi, and G. Zahedi, "Greener energy: Issues and challenges for Pakistan—Biomass energy prospective," *Renewable and Sustainable Energy Reviews*, vol. 15, pp. 3207-3219, 2011.
- [2] *Wheat output for FY12 expected below target*. Available: <http://dawn.com/2012/04/18/wheat-output-for-fy12-expected-below-target/> Accessed on (2012, 08/11/12).
- [3] M. S. Abu Bakar and J. O. Titiloye, "Catalytic pyrolysis of rice husk for bio-oil production," *Journal of Analytical and Applied Pyrolysis*.
- [4] S. V. Vassilev, D. Baxter, L. K. Andersen, and C. G. Vassileva, "An overview of the chemical composition of biomass," *Fuel*, vol. 89, pp. 913-933, 2010.
- [5] C. Salvador, D. Lu, E. J. Anthony, and J. C. Abanades, "Enhancement of CaO for CO₂ capture in an FBC environment," *Chemical Engineering Journal*, vol. 96, pp. 187-195, 12/15/ 2003.
- [6] C.-J. Ma, M. Kasahara, S. Tohno, and K.-C. Hwang, "Characterization of the winter atmospheric aerosols in Kyoto and Seoul using PIXE, EAS and IC," *Atmospheric Environment*, vol. 35, pp. 747-752, 2001.
- [7] I. F. Elbaba and P. T. Williams, "Two stage pyrolysis-catalytic gasification of waste tyres: Influence of process parameters," *Applied Catalysis B: Environmental*, vol. 125, pp. 136-143, 8/21/ 2012.
- [8] *Bruker d8 Advance X-ray Diffractometer*. Available: <http://xraysrv.wustl.edu/web/xrd/brukerd8.html>, P. Carpenter. Accessed on (14/10/2013).

CHAPTER 4 FAST AND SLOW PYROLYSIS

OF BIOMASS

4.1 Introduction

Biomass plays a very important role in the world energy system, especially for developing nations, accounting for approximately 38 % of their primary energy supply [1]. Annual global production of biomass is estimated at 220 billion tonnes [2]. In this study, three different biomass samples; waste wood, rice husk and forestry residue were used to study the pyrolysis. The proximate and ultimate analysis results of these biomass samples are reported in chapter 3.

In this chapter, the comparison of product yield and gas composition obtained from the slow and fast pyrolysis (carried out at 850 °C) of these three different biomass samples was performed. Two different laboratory-scale fixed-bed reactors were used in this study. For fast pyrolysis experiments, biomass sample was exposed to the 850 °C temperature by dropping from a water-cooled chamber into the reactor's hot central zone. For slow pyrolysis experiments, biomass containing crucible was placed inside the reactor. Then the reactor was heated from room temperature to 850 °C at a constant heating rate of 10 °C min⁻¹. The detailed reactor diagrams and experimental procedures are explained in chapter 3.

It is well established that the proportion of the end products from the pyrolysis is highly dependent on the process conditions, particularly temperature and heating rate [3-7]. In this study, slow heating rate of 10 °C min⁻¹ was employed during slow pyrolysis experiments while a very high heating rate of more than 100 °C/s was used during fast pyrolysis experiments.

For three biomass samples, fast pyrolysis was also carried out at high temperatures of 750 – 1050 °C, to determine the influence of temperature on gas yield and composition. Steam gasification of the wood biomass sample was also carried out to further enhance the gas yield, particularly hydrogen yield.

4.2 Fast and slow pyrolysis of biomass at 850 °C

4.2.1 Product yield

Figure 4-1, Figure 4-2 and Figure 4-4 show the comparison of product yield and gas composition from the fast and slow pyrolysis of biomass in relation to the wood, rice husks and forestry residue respectively. The product yield from slow pyrolysis of biomass samples (5 grams each) at 850 °C was drastically different from that of fast pyrolysis. As shown in Figure 4-1, for the wood, only 24.7 wt.% gas yield was obtained from slow pyrolysis as compared to 78.63 wt.% from fast pyrolysis. For rice husk only 18.94 wt.% gas yield from slow pyrolysis was obtained in contrast of 66.61 wt.% from fast pyrolysis as shown in Figure 4-2. For forestry residue (Figure 4-4), only 24.01 wt.% of biomass was recovered as gas from slow pyrolysis while 73.91 wt.% of biomass was converted into gas from fast pyrolysis. The product yield from pyrolysis of biomass mainly depends on the process conditions such as temperature and heating rate and the residence time for which the volatiles stay at that final temperature. Zanzi et al. [8] investigated the fast pyrolysis of wood and agricultural residues using a free-fall reactor to determine the effects of heating rate, temperature, particle size and residence time on the product distribution and gas composition. They reported that higher heating rates favoured the cracking of tar and hydrocarbons into gaseous products. Also, higher heating rates lead to lower char and higher gas yield during fast pyrolysis. In contrast, during slow pyrolysis, longer residence time favours increased secondary reactions of recondensation and re-polymerization of volatiles and hydrocarbons present in the reactor which increases the formation of char [8]. Ahmed et al. [9] investigated the pyrolysis and gasification of mangrove biomass from 600 °C to 900 °C. Their results indicated the higher yield of syngas and hydrogen at higher temperature. During pyrolysis they achieved around 72 wt.% conversion efficiency which was significantly higher than their previous study [10].

The majority of the products obtained from slow pyrolysis of the three biomass samples were volatiles and tars which were collected in the form of liquid oils and an aqueous phase. The yield of liquids from slow pyrolysis was 59.4, 40, and 50.4 wt.% as compared to 12.31, 10.22 and 16.98 wt.% from fast pyrolysis for wood, rice husk and forestry residue respectively.

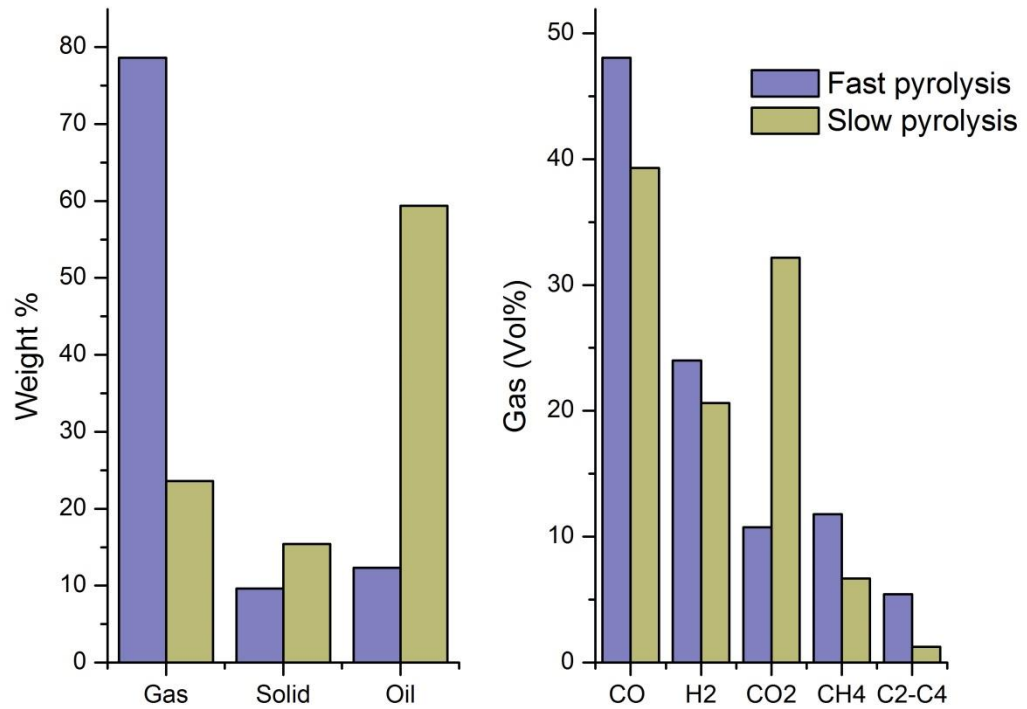


Figure 4-1 Comparison of product yield and gas composition from slow and fast pyrolysis of wood at 850 °C

Low char yields were obtained during fast pyrolysis when compared with the results of slow pyrolysis. For fast pyrolysis char yield from wood was 9.63 wt.% compared with 15.4 wt.% for slow pyrolysis. Rice husks have a high ash content which contributes, together with the char, to a high solids yield, which was 16.21 wt.% for fast pyrolysis and 37.2 wt.% for slow pyrolysis. Forestry residue char yield was similarly higher for slow pyrolysis (23.6 wt.%) compared to fast pyrolysis (7.69 wt.%). Onay et al. [11] performed a comparative study of slow and fast pyrolysis of rapeseed biomass and also reported that for slow pyrolysis experiments 18.3 wt.% of char was produced.

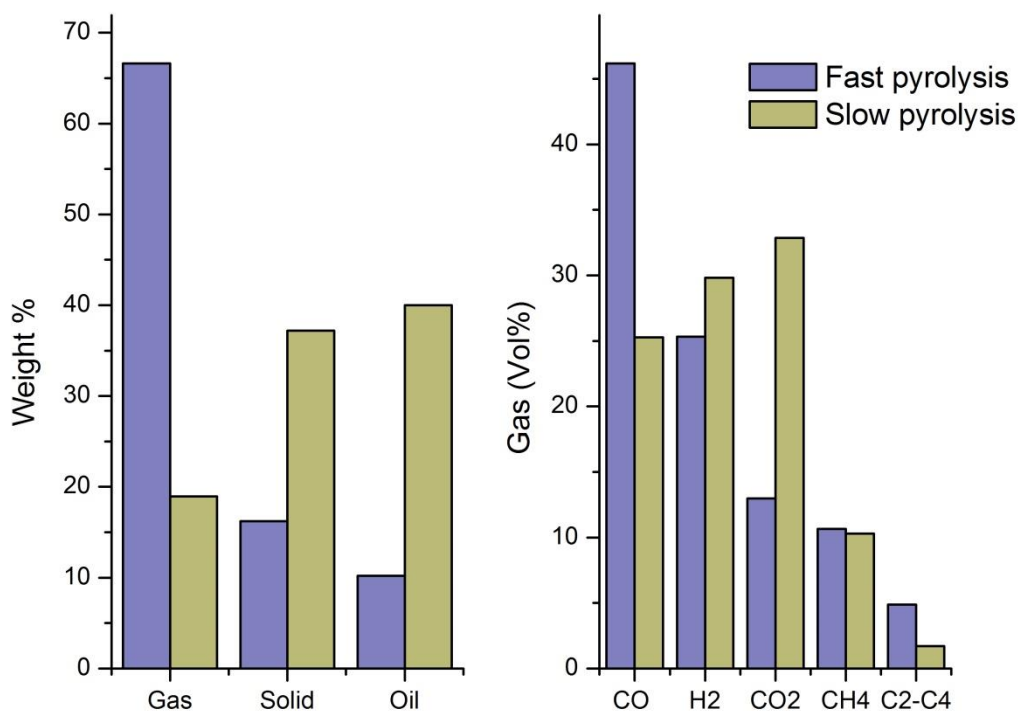


Figure 4-2 Comparison of product yield and gas composition from slow and fast pyrolysis of rice husk at 850 °C

When the solid yields in Figure 4-1, Figure 4-2 and Figure 4-4 were compared with the proximate analysis results in Chapter 3, there is a difference which is primarily due to the method of calculation as the results presented in chapter 3 are on ash-free basis while the results presented here are on actual basis. Furthermore, proximate analysis was carried out at 25 °C min⁻¹ up to a final temperature of 935 °C as compared to 850 °C at 10 °C min⁻¹. The difference in other factors including the design of reactor and other process conditions like residence time may also have affected the solid yield. Scanning electron microscope images of residual char from slow and fast pyrolysis of all three biomass samples are shown in Figure 4-3. Results presented here indicate that the char produced from fast pyrolysis was more porous and damaged. This effect was more pronounced for rice husk and forestry residue biomass samples. The porosity in biomass samples was mainly due to the sudden exposure of biomass samples to the higher heating rates and final temperature which caused the evolution of volatiles and gases from the biomass [12, 13].

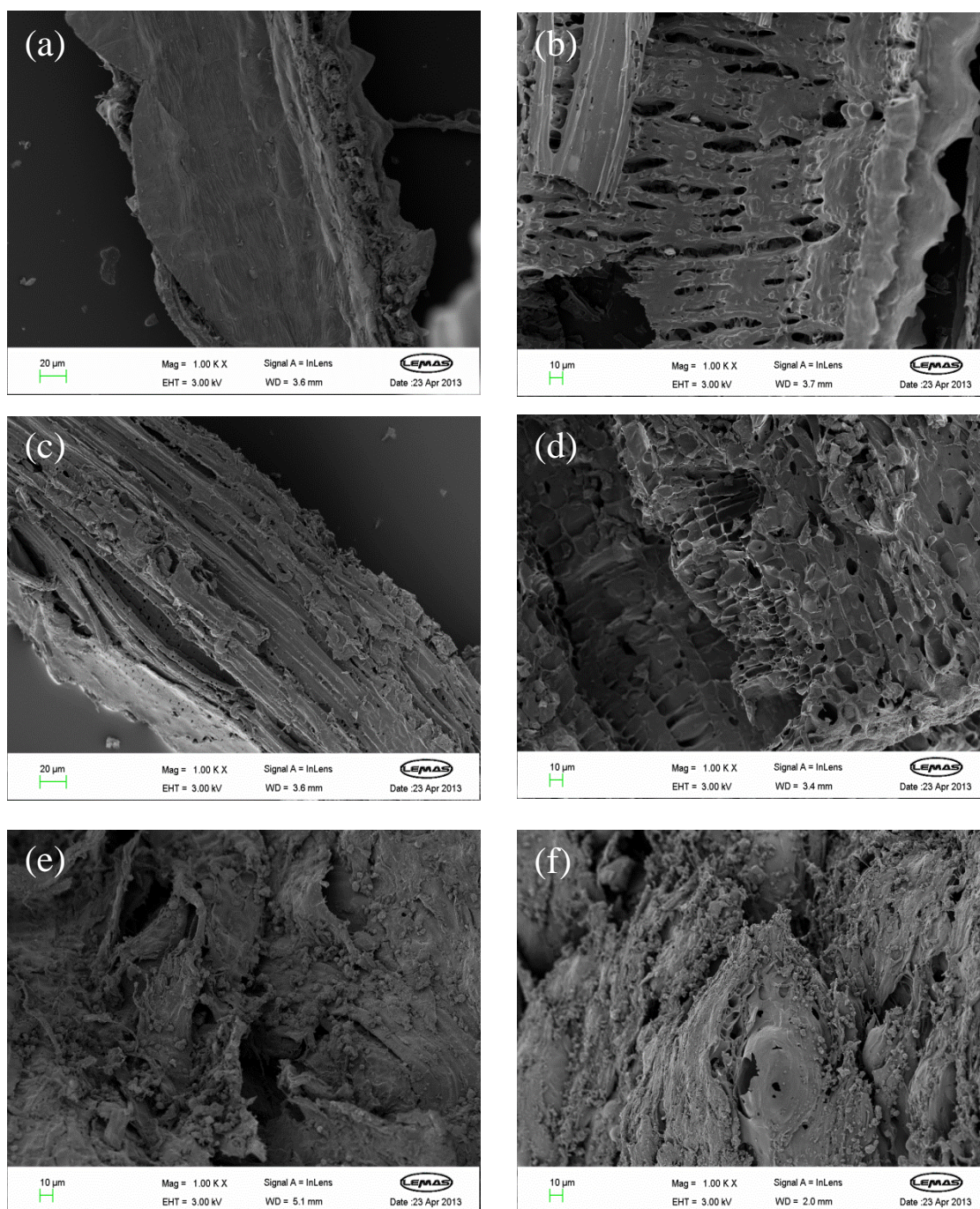


Figure 4-3 SEM images of residual char from slow and fast pyrolysis at 850 °C. Slow pyrolysis (a), and fast pyrolysis (b) of rice husk. Slow pyrolysis (c), and fast pyrolysis (d) of forestry residue. Slow pyrolysis (e) and fast pyrolysis (f) of wood biomass.

4.2.2 Gas composition from fast pyrolysis and slow pyrolysis of biomass at 850 °C

In terms of gas composition, Figure 4-1, Figure 4-2 and Figure 4-4 show that the main gases produced during both fast and slow pyrolysis were CO, CO₂, H₂, CH₄ and C₂-C₄ hydrocarbons. The figures also show that during fast pyrolysis, higher ratios of CO:CO₂ were found with fast pyrolysis compared to slow pyrolysis. During the fast pyrolysis of various agriculture residues, gas composition reported by Zanzi et al. [14] also showed a high CO:CO₂ ratio for fast pyrolysis of the biomass. In all thermochemical processes, thermal decomposition of biomass is the primary step while cracking, gas to gas and gas to solid interaction takes place during secondary reaction [15]. Secondary reactions occur due to the interaction among the volatiles and between the volatiles and solid residue [16]. The conditions of slow pyrolysis allowing for increased secondary char forming reactions.

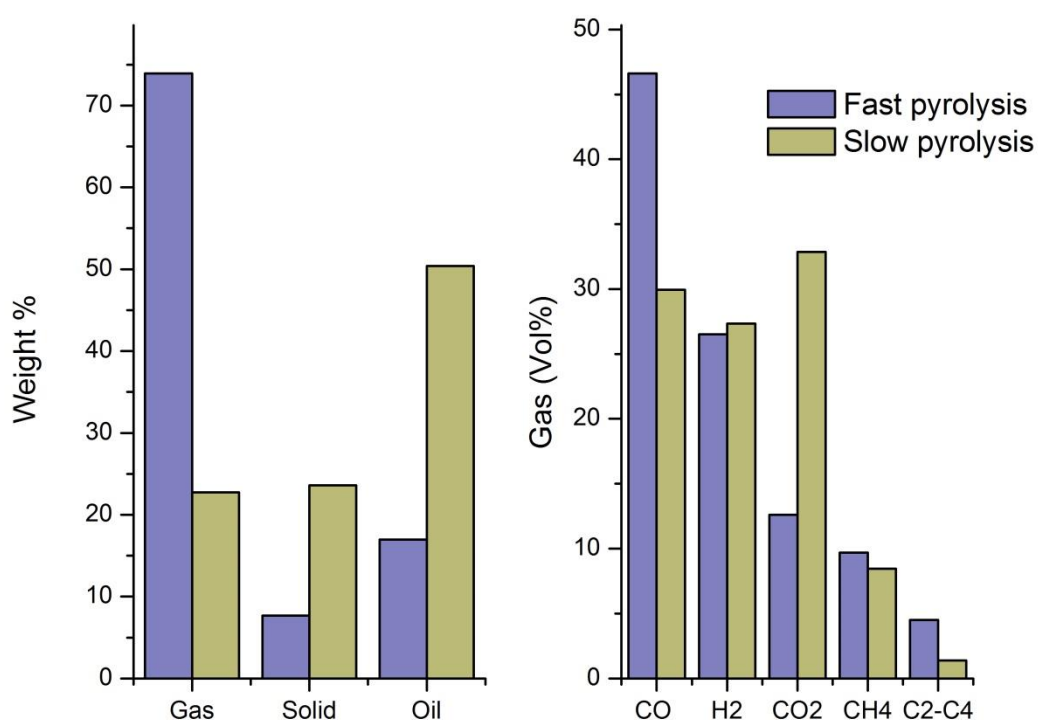


Figure 4-4 Comparison of product yield and gas composition from slow and fast pyrolysis of forestry residue at 850 °C

4.3 The influence of temperature on product yield from fast pyrolysis

4.3.1 Product yield

The influence of temperature over the range of 750 – 1050 °C on product yield was investigated using the fast pyrolysis reactor and the results are shown in Table 4-1. The gas yield increased with the rise in temperature for all of the biomass samples under fast pyrolysis conditions with a corresponding decreasing trend in char and oil yield. For example, gas yield was increased from 79.36 wt.% to 91.71 wt.% for wood, from 76.77 wt.% to 98.36 wt.% for rice husk and for forestry residue, the overall gas yield increased from 63.56 wt.% to 90.80 wt.% when the fast pyrolysis temperature was increased from 750 °C to 1050 °C. In terms of the highest gas yield on an ash-free basis (Table 4-1), 98.36 wt.% gas was obtained from rice husk, followed by 91.71 wt.% from wood. The gas yield from forestry residue was 90.80 wt.%, slightly less than the gas yield obtained from wood at 1050 °C.

The results obtained clearly indicate that the gas yield increased with the rise in temperature. In addition, the very high pyrolysis temperature not only leads to the instantaneous decomposition of oils into gaseous products but also the secondary char forming reactions are reduced at high temperature. As suggested by Shuangning et al. [17], yield of gaseous products from fast pyrolysis of biomass depends on the heating rate, final temperature as well as the time interval for which biomass sample is exposed to that higher temperature. They performed the flash pyrolysis of wheat straw, coconut shell, rice husk and cotton stalk. Investigated temperature range was from 750 – 900 K with 50 K interval. The flash heating rate was increased from 1.3 to 2.1 (10^4 K/s). Higher volatiles were recovered from all biomass samples at higher pyrolysis temperature of 900 K. However in terms of highest volatiles obtained during flash pyrolysis, the order of biomass samples was reported as: wheat straw > cotton stalk > coconut shell > rice husk.

Dupont et al. [16] used an entrained flow drop reactor to investigate the effect of temperature on fast pyrolysis of commercial beech wood. They investigated the fast pyrolysis at high temperature and reported that more than 75 wt.% of biomass was converted into gas at 1000 °C. Sun et al. [18] investigated the effect of temperature on

fast pyrolysis of rice husk and saw dust in an entrained flow reactor. Their investigated temperature range was from 700 °C to 1000 °C. They reported that 89.2 wt.% of sawdust was converted into gaseous products at 1000 °C. It was reported that the temperature had a profound effect on the gas yield. With the increase in temperature, an increase in gas yield along with the decrease in liquid and char yield was observed. It was noticed that the release of CO and CH₄ was dominant at lower pyrolysis temperatures while CO and H₂ were released at higher pyrolysis temperatures.

Table 4-1 Product yield from the fast pyrolysis of wood, rice husks and forestry residue in relation to pyrolysis temperature

	Temperature (°C)			
	750	850	950	1050
Wood (wt.%)				
Gas	75.81	78.63	81.87	87.61
Gas (ash-free)	79.36	82.31	85.70	91.71
Solid	10.39	9.63	6.26	4.32
Oil	16.41	12.31	10.00	8.40
Mass balance (wt.%)	102.61	100.57	98.13	100.33
Rice husk (wt.%)				
Gas	60.43	66.61	74.55	77.43
Gas yield (ash-free)	76.77	84.62	94.70	98.36
Solid	20.60	16.21	15.86	13.21
Oil	12.01	10.22	8.13	6.19
Mass balance (wt.%)	93.04	93.04	98.54	96.83
Forestry residue (wt.%)				
Gas	60.13	73.91	79.27	85.91
Gas yield (ash-free)	63.56	78.12	83.79	90.80
Solid	14.37	7.69	5.44	3.21
Oil	20.11	16.98	12.21	10.31
Mass balance (wt.%)	94.61	98.58	96.92	99.43

Zanzi et al. [14] investigated the fast pyrolysis of various biomass samples in a free fall reactor at 800 °C and 1000 °C. They reported that the 86 wt.%, 85.5 wt.%, 75.3 wt.% and 87 wt.% of straw, straw pellets, olive waste and birch wood were converted into gas at 1000 °C respectively. It was suggested that the higher ash contents in biomass

samples enhanced the reactivity of the char. The higher char yield was found in olive waste was primarily due to the higher lignin contents in this biomass samples. It was concluded that not only conditions of the pyrolysis process but also the composition and properties of the biomass sample influence the product yield, gas composition and char reactivity.

During fast pyrolysis experiments, samples were instantaneously exposed to the higher temperature (750 °C – 1050 °C). This leads to very high heating rates and short residence time as the products of pyrolysis are quickly swept from the reactor by the nitrogen purge gas. Due to the rapid heat transfer, instantaneous devolatilization of biomass particles takes place inside the reactor. Tar and volatiles evolved from the biomass particles released into the surrounding gas phase while the surrounding gases diffuse into the biomass particles [16]. Although the exact mechanism of biomass pyrolysis is not clear, several kinetic models of varying complexity have been developed [15, 16, 18-20]. However the overall process can be explained using empirical models, such as presented by Kilzer and Broido et al. [21]. According to their model, lignocellulosic materials follow one of two available pathways. At higher temperature, tar formation is favoured by the low activation energy of the reaction while at low temperatures, cellulose in the biomass sample converts into dehydro-cellulose which is converted into char and syngas.

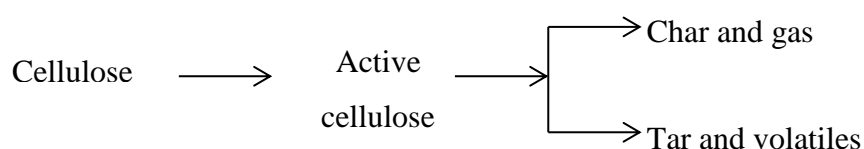


Figure 4-5 Broido model for the decomposition of cellulose [22]

However in another kinetic model [22], Broido explain the conversion of cellulose into “active-cellulose” which subsequently decomposes to either tar or char and gases. After initial devolatilization, secondary gas phase reactions between the permanent gases and tar add towards the overall gas yield. Furthermore, thermal cracking of these hydrocarbons and tar contribute significantly towards the increase in gas yield. Neves et al. [3] graphically explained the thermal degradation of biomass as a three step process. In first step, biomass gets dried after the evolution of moisture. In second step primary pyrolysis takes place where tar, char, permanent gases and water molecules formed.

During the third step, secondary pyrolysis takes place between these components from primary pyrolysis which result in various reactions like reforming, cracking, polymerization, oxidation and gasification.

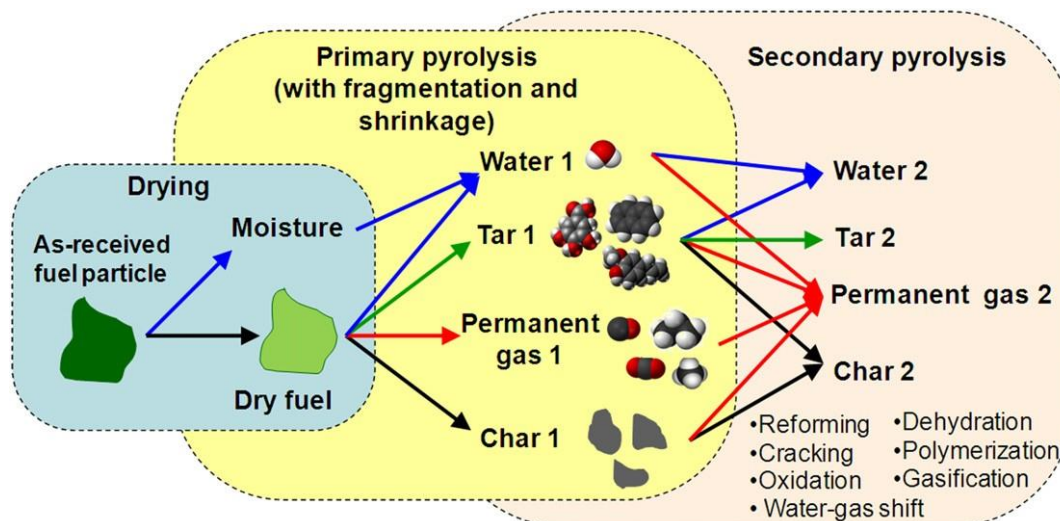


Figure 4-6 Thermal degradation of biomass in an inert atmosphere adapted from [3]

4.3.2 The effect of fast pyrolysis temperature on gas composition

The gas composition for the fast pyrolysis of the biomass samples in relation to temperature of pyrolysis from 750 - 1050 °C are shown in Table 4-2. The results show that there was small increase in CO and a decrease in CO₂ with increased pyrolysis temperature. The hydrogen yield was significantly increased with temperature and there was a consequent decrease in methane and C₂-C₄ hydrocarbons. Dupont et al. [12] investigated the fast pyrolysis of pine and spruce wood in an entrained flow reactor. They reported around 55 vol.% CO along with 23 vol.% H₂ at 950 °C. Also around 5 vol.% CO₂ and 15 vol.% CH₄ along with less than 10 vol.% lighter hydrocarbons were observed in the gas mixture.

Chen et al. [4] performed the fast pyrolysis of cotton stalks in a fixed bed reactor. They reported the increase in hydrogen concentration with the rise in temperature, from 27.74 vol.% H₂ at 750 °C and 36.66 vol.% of H₂ at 950 °C. Zanzi et al. [14] performed the rapid pyrolysis of straw, straw pellets, olive waste and birch wood at 800 °C and 1000 °C. Higher hydrogen and CO concentrations were reported with the rise in temperature.

However a decrease in concentrations of CO₂, CH₄ and other hydrocarbons was reported.

Table 4-2 Gas composition from the fast pyrolysis of wood, rice husks and forestry residue in relation to pyrolysis temperature

Feedstock	Gas	Temperature (°C)			
		vol.%	750	850	950
Wood	CO	45.12	47.10	45.94	48.74
	H ₂	26.91	27.46	29.21	31.01
	CO ₂	11.35	9.69	9.34	7.81
	CH ₄	11.29	10.89	11.24	9.33
	C ₂ -C ₄	5.33	4.86	4.28	3.11
Rice Husk	CO	45.01	46.17	48.31	49.40
	H ₂	21.84	25.32	27.83	30.30
	CO ₂	15.06	12.98	11.33	8.65
	CH ₄	11.92	10.65	8.94	8.67
	C ₂ -C ₄	6.17	4.88	3.59	2.99
Forestry residue	CO	43.8	46.6	48.07	46.61
	H ₂	23.7	26.5	29.05	30.53
	CO ₂	15.6	12.6	10.45	9.48
	CH ₄	11.62	9.7	9.14	9.62
	C ₂ -C ₄	6.1	4.5	3.29	3.76

Increase in CO concentration with the simultaneous decrease in CO₂ concentration and char at higher temperature indicate the increase in forward Boudouard reaction. As reported by Yang et al. [23] this reaction is favoured at higher temperatures. In their study of pyrolysis of palm oil waste, they had pointed out that not only the Boudouard reaction accounts for the increase in CO concentration but thermal breakdown of tar also leads to the formation of methane, hydrogen, water and lighter hydrocarbons. Furthermore, reaction between CO₂ and CH₄ is also favoured at low pressure and high temperature. This might be one of the possible explanations for the decrease in CO₂ and CH₄ concentration with the increase in temperature during the pyrolysis. During pyrolysis, water comes from both initial biomass moisture and gas phase reactions [24]. This water can react with the char, resulting in the water gas reaction. This water can

also react with other gases such as methane to perform the steam reforming reaction and also water gas shift reaction. However the concentration of water molecules was not high enough to bring about large changes in gas composition.

4.4 The influence of steam on the fast pyrolysis of biomass

The pyrolysis/gasification of one of the biomass sample (wood) was carried out in the presence of steam at temperatures of 750 °C, 850 °C, 950 °C and 1050 °C to determine the influence of steam on product gas yield, but in particular on hydrogen gas yield. The results are shown in Table 4-3. The presence of steam would increase the gasification type reactions of the biomass sample. It is evident that the increase in temperature showed an increase in hydrogen production. Comparison of the H₂ gas composition for wood pyrolysis in Table 4-2 and in the presence of steam (Table 4-3) shows that the hydrogen in the gas increased from, for example, 26.91 vol.% in the absence of steam to 44.13 vol.% in the presence of steam at the reaction temperature of 750 °C. As the temperature was increased in the presence of steam, there was a small but significant decrease in H₂. It is suggested that the addition of steam into the reaction system had a positive effect in terms of hydrogen production. In terms of CO gas yield, there was a decrease in the presence of steam compared to the fast pyrolysis results shown in Table 4-2.

Table 4-3 Gas composition and hydrogen production from the steam gasification of wood

Feedstock	Gas vol.%	Temperature (°C)			
		750	850	950	1050
Wood	CO	33.27	36.61	39.42	43.11
	H ₂	44.13	45.96	43.28	40.04
	CO ₂	13.29	9.26	9.44	8.57
	CH ₄	6.93	6.10	5.93	6.53
	C ₂ -C ₄	2.38	2.07	1.94	1.76

It can be assumed that the addition of steam has enhanced the water gas shift reaction. This is evident from the increase in hydrogen concentration and corresponding decrease in CO concentration. It is clear from the decreased methane concentration that the endothermic methane reforming reaction was also favoured by the presence of steam. This also contributed towards the enhanced CO and H₂ concentration at higher temperatures.

Steam reforming of hydrocarbons also takes place at higher temperature; this statement can be supported by the decrease in C₂-C₄ hydrocarbons concentrations when the fast pyrolysis results were compared with steam gasification results at any given temperature. Yan et al. [25] performed the steam gasification of char produced from pyrolysis of sawdust produced at 500 °C. They investigated the effect of temperature on gas composition of char from 600 °C to 850 °C. With steam flow rate of 0.165 g min⁻¹ g⁻¹ of biomass char, they received 52.41 vol.% H₂, 14.03 vol.% CO, 27.60 vol.% of CO₂, 1.74 vol.% CH₄ and less than 5 vol.% C₂-C₄ hydrocarbons at 850 °C. They also suggested that at higher temperature, water gas reaction, Boudouard reaction and steam methane reforming reaction has a significant influence on gas composition.

The hydrogen gas yield can be expressed in terms of millimoles of hydrogen per gram of biomass sample. For wood pyrolysis in the absence of steam, hydrogen yield increased from 4.66 mmoles g⁻¹ of biomass at 750 °C to 8.77 mmoles g⁻¹ at 850 °C. The highest hydrogen yield of 11.44 mmoles g⁻¹ was obtained at 950 °C, however further increase in temperature from 950 °C to 1050 °C led to a slight decrease in hydrogen yield with a determined value of 10.01 mmoles g⁻¹ of biomass. In the presence of steam, hydrogen yield increased from 14.58 mmoles of H₂ g⁻¹ of biomass at 750 °C to 21.35 mmoles of H₂ g⁻¹ at 850 °C however, with the further increased in temperature to 950 °C and 1050 °C, hydrogen yield slightly decreased. The slight decrease in hydrogen yield at higher temperature suggests that the forward water gas shift reaction is favourable at lower temperatures. Higher temperature may lead to the reverse water gas shift reaction which leads to an increase in CO concentration and decrease in hydrogen concentration.

4.5 Potential hydrogen production for fast pyrolysis

Potential hydrogen production is an indicator of how much of the percentage of the elemental hydrogen from the biomass is converted into the gaseous hydrogen in the syngas. Potential hydrogen production for all three biomass samples was calculated on an ash-free basis for fast pyrolysis of biomass in the absence of steam (Figure 4-7). Theoretical maximum hydrogen available in the 5 grams of biomass was 0.28 g for wood biomass, 0.18 for rice husk and 0.26 for forestry residue respectively. As shown in Figure 4-7, it is clear that the temperature has a positive effect on potential hydrogen production. For example, in the case of wood, it increased from 16.68 % at 750 °C to 34.87 % at 1050 °C. For rice husk, potential hydrogen production increased from 17.72 % at 750 °C, to 30.63 %, 40.41 % and to 36.18 % with the rise in temperature.

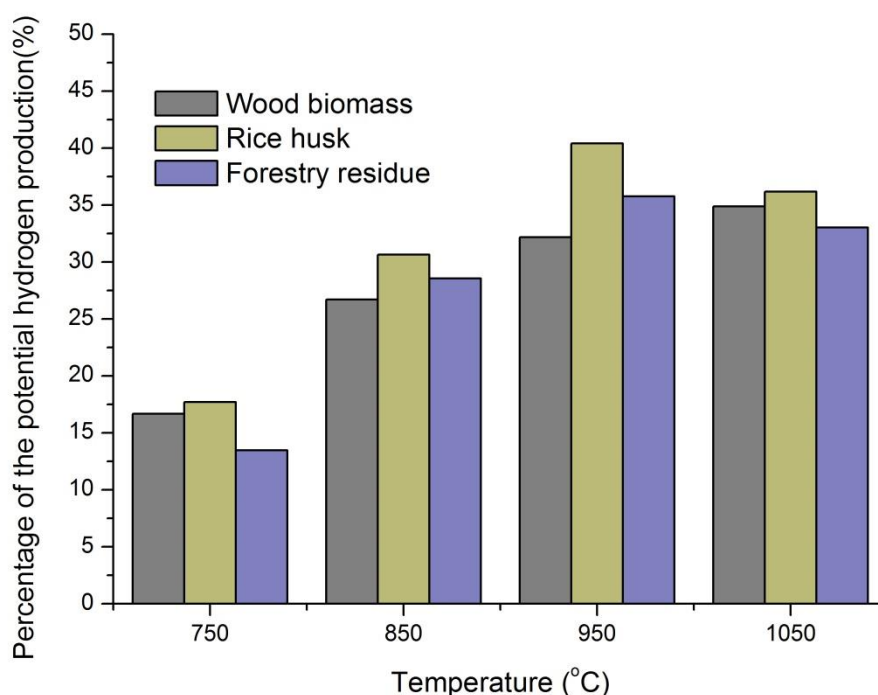


Figure 4-7 Percentage of the potential hydrogen production from various biomass samples

For forestry residue, the percentage of the potential hydrogen production increased from 13.47 % at 750 °C, to 28.56 % at 850 °C, to 35.76 % at 950 °C. However it decreased slightly to 33.02 % at 1050 °C. Higher potential hydrogen production at high

temperature can be explained on the basis of enhanced overall yield of syngas. This enhanced yield of syngas is mainly due to the secondary reaction taking place inside the reaction chamber and the thermal cracking of tar and other hydrocarbon leads to the higher syngas yield and in turn higher conversion of the hydrogen in the biomass to higher hydrogen yield. Rice husk showed the highest potential hydrogen production of 40.41 % at 950 °C while pyrolysis of forestry residue resulted in 35.76 % of potential hydrogen production at 950 °C.

4.6 Conclusions

The influence of process parameters on the yield and composition of products and gases from the fast and slow pyrolysis of waste biomass has been investigated. In addition, the influence of temperature and the presence of steam on the yield of products and gas composition from fast pyrolysis were investigated. The following conclusions can be drawn from this study.

- Slow pyrolysis of the wood, rice husks and forestry residue was markedly different from that of fast pyrolysis. For wood, only 24.7 wt.% gas yield was obtained from slow pyrolysis as compared to 78.63 wt.% from fast pyrolysis. For rice husk 18.94 wt.% gas was obtained, for forestry residue 24.01 wt.% gas was obtained compared to 66.61 wt.% and 73.91 wt.% from fast pyrolysis respectively. There were correspondingly lower yields of oil and char from fast pyrolysis whereas for slow pyrolysis oil and char yields were higher.
- The composition of the product gases was also influenced by the heating rate. The main gases produced during both fast and slow pyrolysis were CO, CO₂, H₂, CH₄ and C₂-C₄ hydrocarbons. However, for fast pyrolysis, higher ratios of CO:CO₂ were found compared to slow pyrolysis.
- The influence of increasing fast pyrolysis temperature between 750 – 1050 °C showed that gas yield increased with a corresponding decreasing trend in char and oil yield. Maximum gas yields, on an ash-free basis were 91.71 wt.% for wood, 98.36 wt.% for rice husk and 90.80 wt.% for forestry residue.

- Addition of steam to the fast pyrolysis of wood produced increased yields of hydrogen. For example, hydrogen concentration was 26.91 vol.% in the absence of steam increasing to 44.13 vol.% in the presence of steam at the reaction temperature of 750 °C.

4.7 Chapter references

- [1] Y. Kalinci, A. Hepbasli, and I. Dincer, "Biomass-based hydrogen production: A review and analysis," *International Journal of Hydrogen Energy*, vol. 34, pp. 8799-8817, 2009.
- [2] U. K. Mirza, N. Ahmad, and T. Majeed, "An overview of biomass energy utilization in Pakistan," *Renewable and Sustainable Energy Reviews*, vol. 12, pp. 1988-1996, 2008.
- [3] D. Neves, H. Thunman, A. Matos, L. Tarelho, and A. Gómez-Barea, "Characterization and prediction of biomass pyrolysis products," *Progress in Energy and Combustion Science*, vol. 37, pp. 611-630, 2011.
- [4] Y. Chen, H. Yang, X. Wang, S. Zhang, and H. Chen, "Biomass-based pyrolytic polygeneration system on cotton stalk pyrolysis: Influence of temperature," *Bioresource Technology*, vol. 107, pp. 411-418, 2012.
- [5] R. Isha and P. T. Williams, "Pyrolysis-gasification of agriculture biomass wastes for hydrogen production," *Journal of the Energy Institute*, vol. 84, pp. 80-87, 2011.
- [6] P. T. Williams, and Besler S., "The Pyrolysis of municipal solid waste," *Journal of the Institute of Energy*, vol. 65, pp. 192-200, 1992.
- [7] N. Miskolczi, F. Buyong, and P. T. Williams, "Thermogravimetric analysis and pyrolysis kinetic study of Malaysian refuse derived fuels," *Journal of the Energy Institute*, vol. 83, pp. 125-132, 2010.
- [8] R. Zanzi, K. Sjöström, and E. Björnbom, "Rapid high-temperature pyrolysis of biomass in a free-fall reactor," *Fuel*, vol. 75, pp. 545-550, 1996.
- [9] I. Ahmed, W. Jangsawang, and A. K. Gupta, "Energy recovery from pyrolysis and gasification of mangrove," *Applied Energy*, vol. 91, pp. 173-179, 2012.
- [10] I. Ahmed and A. K. Gupta, "Syngas yield during pyrolysis and steam gasification of paper," *Applied Energy*, vol. 86, pp. 1813-1821, 2009.
- [11] O. Onay and O. M. Kockar, "Slow, fast and flash pyrolysis of rapeseed," *Renewable Energy*, vol. 28, pp. 2417-2433, 2003.
- [12] C. Dupont, J.-M. Commandré, P. Gauthier, G. Boissonnet, S. Salvador, and D. Schweich, "Biomass pyrolysis experiments in an analytical entrained flow reactor between 1073K and 1273K," *Fuel*, vol. 87, pp. 1155-1164, 2008.
- [13] L. Tognotti and E. Biagini, "Characterization of biomass chars : reactivity and morphology of chars obtained in different conditions," *International Journal of Energy for a Clean Environment*, vol. 6, pp. 439-457, 2006-06-06.
- [14] R. Zanzi, K. Sjöström, and E. Björnbom, "Rapid pyrolysis of agricultural residues at high temperature," *Biomass and Bioenergy*, vol. 23, pp. 357-366, 2002.
- [15] J. Lédé, "Cellulose pyrolysis kinetics: An historical review on the existence and role of intermediate active cellulose," *Journal of Analytical and Applied Pyrolysis*, vol. 94, pp. 17-32, 2012.
- [16] C. Dupont, L. Chen, J. Cances, J.-M. Commandre, A. Cuoci, S. Pierucci, *et al.*, "Biomass pyrolysis: Kinetic modelling and experimental validation under high temperature and flash heating rate conditions," *Journal of Analytical and Applied Pyrolysis*, vol. 85, pp. 260-267, 2009.
- [17] X. Shuangning, L. Zhihe, L. Baoming, Y. Weiming, and B. Xueyuan, "Devolatilization characteristics of biomass at flash heating rate," *Fuel*, vol. 85, pp. 664-670, 2006.

- [18] S. Sun, H. Tian, Y. Zhao, R. Sun, and H. Zhou, "Experimental and numerical study of biomass flash pyrolysis in an entrained flow reactor," *Bioresource Technology*, vol. 101, pp. 3678-3684, 2010.
- [19] B. V. Babu and A. S. Chaurasia, "Modeling for pyrolysis of solid particle: kinetics and heat transfer effects," *Energy Conversion and Management*, vol. 44, pp. 2251-2275, 2003.
- [20] C. Di Blasi, "Modeling chemical and physical processes of wood and biomass pyrolysis," *Progress in Energy and Combustion Science*, vol. 34, pp. 47-90, 2008.
- [21] F. J. K. a. A. Broido, "Speculations on the nature of cellulose pyrolysis," *Pyro-dynamics*, vol. 2, pp. 151-163, 1965.
- [22] F. S. A. Broido, *Thermal Uses and Properties of Carbohydrates and Lignins*. New York: Academic Press, 1976.
- [23] H. Yang, R. Yan, H. Chen, D. H. Lee, D. T. Liang, and C. Zheng, "Pyrolysis of palm oil wastes for enhanced production of hydrogen rich gases," *Fuel Processing Technology*, vol. 87, pp. 935-942, 2006.
- [24] S. Septien, S. Valin, C. Dupont, M. Peyrot, and S. Salvador, "Effect of particle size and temperature on woody biomass fast pyrolysis at high temperature (1000–1400°C)," *Fuel*, vol. 97, pp. 202-210, 2012.
- [25] F. Yan, S.-y. Luo, Z.-q. Hu, B. Xiao, and G. Cheng, "Hydrogen-rich gas production by steam gasification of char from biomass fast pyrolysis in a fixed-bed reactor: Influence of temperature and steam on hydrogen yield and syngas composition," *Bioresource Technology*, vol. 101, pp. 5633-5637, 2010.

CHAPTER 5 TWO-STAGE PYROLYSIS

GASIFICATION OF RICE HUSK, BAGASSE

AND WHEAT STRAW

5.1 Introduction

In order to select the most suitable biomass samples for further research on hydrogen production, three different biomass samples: rice husk, sugarcane bagasse and wheat straw were initially characterized using thermogravimetric analysis (TGA) in chapter 3. In this chapter, a scanning electron microscope (SEM) was also used to characterize the structural and morphological differences among these biomass samples. In section 5.2, the influence of different parameters such as heating rate and particle size was investigated using TGA. Kinetic parameters of these biomasses were also calculated using the Coats-Redfern method.

In section 5.3, pyrolysis, steam gasification and catalytic steam gasification (using calcined dolomite and 10 wt.% Ni-dolomite) of all three biomass samples were performed. The purpose of this study was to select the best suited process and biomass sample to produce high hydrogen yield from two-stage pyrolysis/gasification reactor. In section 5.4, investigation of various process conditions such as temperature, water injection rate, catalysts to sample ratio, particle size and carrier gas flow rate were carried out using two-stage catalytic steam gasification.

5.2 Characterization of rice husk, sugarcane bagasse and wheat straw using thermogravimetric analysis

In order to design efficient thermochemical conversion systems, it is important to investigate the thermal degradation and kinetic behaviour of biomass samples. TGA is a very popular technique which is extensively used to investigate the devolatilization characteristics and thermal degradation behaviour of different biomass samples. In this section, comparison of three different biomass samples is outlined in section 5.2.1. The influence of heating rate on devolatilization of rice husk, bagasse and wheat straw is described in section 5.2.2. The effect of particle size on rice husk, bagasse and wheat

straw on pyrolysis/gasification is investigated in section 5.2.3. Furthermore, the Coats-Redfern method is used to investigate the kinetic parameters of the above mentioned three biomass samples in section 5.2.4.

5.2.1 Comparison of biomass samples

In this section, rice husk, bagasse and wheat straw are compared. Results of proximate and ultimate analysis of rice husk, sugarcane bagasse and wheat straw samples are shown in chapter 3. From the proximate analysis results shown in Section 3.1.1, it can be indicated that relatively higher volatiles were present in bagasse and wheat straw samples. The volatiles in bagasse, presented on an ash-free basis, accounted for around 83 wt.% of the total weight. 78.41 wt.% of volatiles were found in the wheat straw sample while 76.95 wt.% were present in rice husk. The amount of fixed carbon in wheat straw was 18.76 wt.%. For rice husk and bagasse it was found to be 15.68 wt.% and 11.09 wt.% respectively.

Biomass are essentially composed of three different components namely cellulose, hemicellulose and lignin. A small amount of ash and extractives were also found in biomass samples in varying proportion. Cellulose, hemicellulose and lignin components of rice husk, bagasse and wheat straw are presented in Table 5-1. Cellulose is a long chain linear homopolymer molecule with a degree of polymerization of up to 10,000 units. It consists of D-glucose monomers connected with each other using β (1-4) glycosidic linkage. Each six carbon monomer has hydroxyl groups at C₂, C₃ and C₆ positions making it capable of reacting like primary and secondary alcohols. It is different from starch which is another glucose polymer in which monomers are connected using α (1-4) glycosidic linkage.

Table 5-1 Cellulose, hemicellulose and lignin contents of biomass samples [1]

	Ash (wt.%)	Cellulose (wt.%)	Hemicellulose (wt.%)	Lignin (wt.%)	Extractives (wt.%)
Bagasse	2.9	41.3	22.6	18.3	13.7
Rice husk	23.5	31.3	24.3	14.3	8.4
Wheat straw	11.2	30.5	28.9	16.4	13.4

Hemicellulose on the other hand is a heteropolymer of various 5 ring sugars (xylose, arabinose) and 6 ring sugars (glucose, mannose, and galactose) connected with each other using acetic acid. It has a lower degree of polymerization with connected side chain molecules. Lignin is a complex heterogeneous racemic macromolecule consisting of three different C₉ alcohol monomers with varying degree of methoxylation.

From the results in Table 5-1, it is clear that the highest cellulose contents along with the lowest ash were present in bagasse. The highest ash and the lowest lignin contents were present in rice husk. The lowest cellulose and the highest hemicellulose were present in wheat straw.

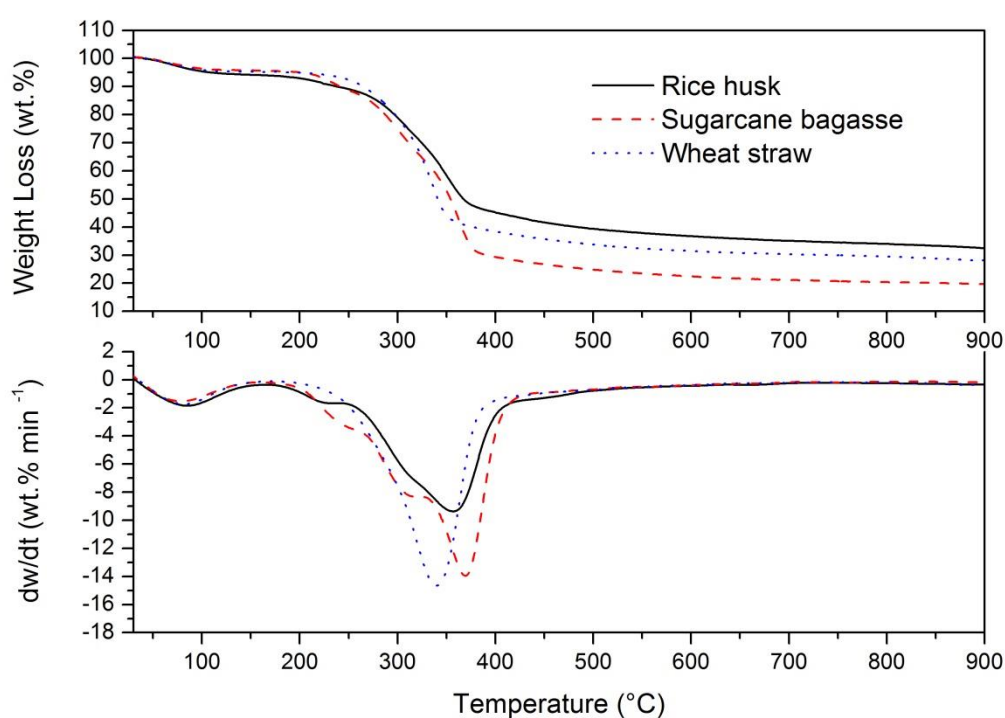


Figure 5-1 TGA and DTG thermograms of rice husk, sugarcane bagasse and wheat straw at 20 °C min⁻¹ heating rate.

Various researchers [2-4] have studied the thermal decomposition of cellulose, hemicellulose and lignin using TGA in an attempt to relate it to the thermal decomposition behaviour of different biomass. It is widely accepted that the decomposition of hemicellulose takes place before the decomposition of cellulose. It was reported [4] that a major weight loss peak was recorded between temperature of

220 °C – 315 °C. The decomposition of cellulose on the other hand starts around 315 °C up to a final temperature of 400 °C. One major weight loss peak is clearly observed between these two temperatures. Lignin decomposition takes place slowly over the entire temperature range.

Comparison of TGA and DTG thermograms of rice husk, bagasse and wheat straw is shown in Figure 5-1, it can be indicated that after the initial moisture loss around 100 °C, the highest weight loss for bagasse was mainly due the higher cellulose and hemicellulose contents which in turn produced more volatiles. This was further complemented by the highest cellulose contents results in Table 5-1. In the DTG thermogram of bagasse, the two shoulders on the left side of the main peak (around 300 °C) were most likely due to the decomposition of hemicellulose components in the biomass sample. The main weight loss peak around 375 °C can be assigned to the thermal decomposition of the cellulose component in biomass. Finally the slow decomposition of the sample over the entire temperature range can be assigned to lignin. For wheat straw, no separate decomposition peak or shoulder was visible before the main weight loss curve around 340 °C.

For rice husk, after the initial moisture loss, a slight shoulder visible around 225 °C indicate the decomposition of hemicellulose. Afterwards, major weight loss peak from 250 °C to 420 °C indicate the overlapping decomposition of hemicellulose and cellulose. In contrast to bagasse and wheat straw, it is evident from Figure 5-1, that the rice husk sample contains the lowest volatiles and the highest solid residue. These results were further supported by the lower volatiles reported in chapter 3.

5.2.2 The effect of heating rate

The effect of heating rate on the devolatilization behaviour of rice husk, bagasse and wheat straw were investigated using TGA. Three different heating rates of at 5, 20 and 40 °C min⁻¹ were employed during this investigation. TGA and DTG thermograms for rice husk, bagasse and wheat straw were shown in Figure 5-2, Figure 5-3, and Figure 5-4 respectively.

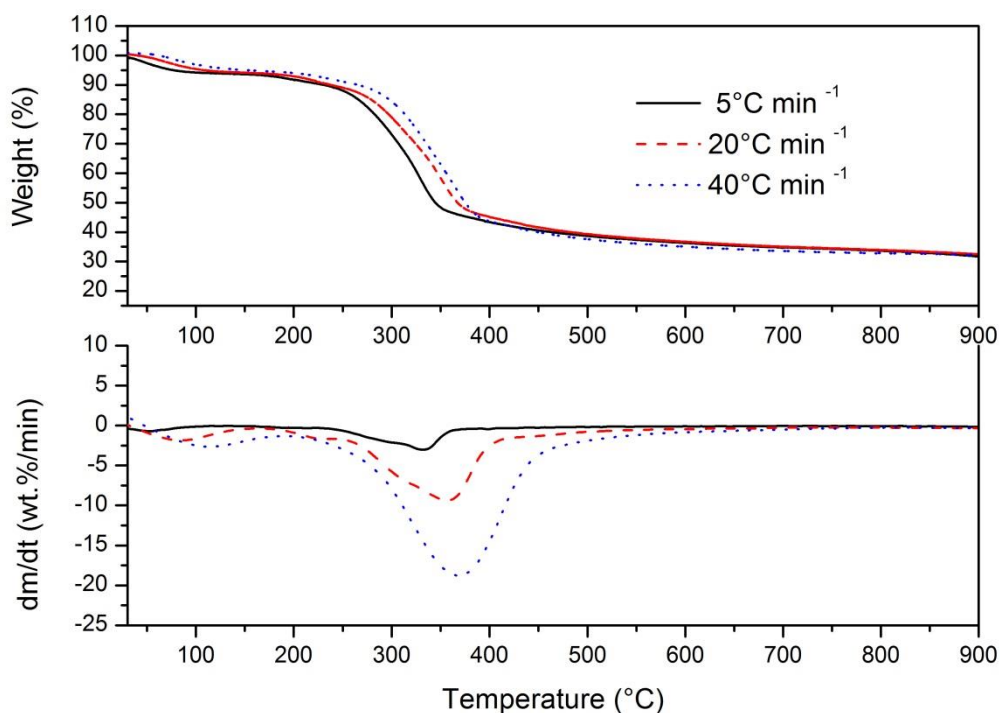


Figure 5-2 TGA and DTG thermograms of rice husk at 5, 20 and 40 °C min⁻¹ heating rates

The effect of heating rate on TGA and DTG rice husk is shown in Figure 5-2. From the TGA thermogram it is clear that the increase in heating rate shifted the release of volatiles to the slightly higher temperature. It was suggested in the literature [5, 6] that this lateral shift was primarily due to the heat transfer limitations at higher heating rates. Due to short reaction time at higher heating rates, higher temperature was required for the evolution of volatiles from biomass samples while at slow heating rates, large instantaneous energy along with longer residence time was available for the volatiles to evolve from biomass. DTG thermogram showed initial weight loss attributed to the moisture loss while the major weight loss observed between 250 °C to 450 °C was due to the thermal decomposition and release of volatiles from rice husk.

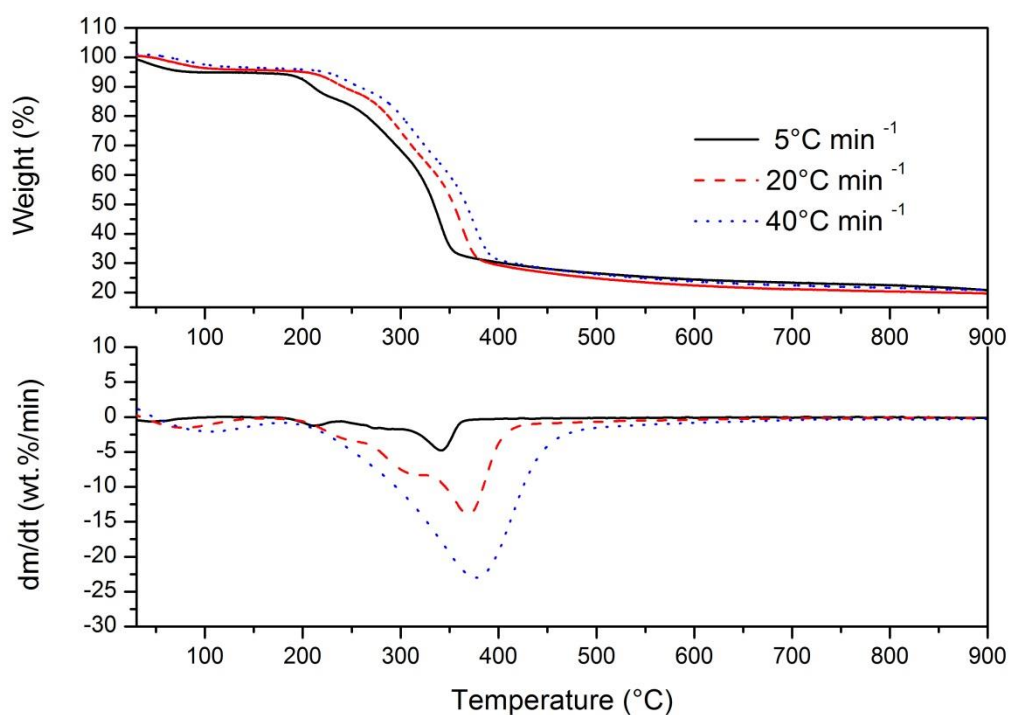


Figure 5-3 TGA and DTG thermograms of sugarcane bagasse at 5, 20 and 40 °C min⁻¹ heating rates

TGA and DTG thermograms of sugarcane bagasse sample shown in Figure 5-3 represent the effect of heating rate. It is observed by the DTG thermogram that at 5 °C min⁻¹ heating rate, a small weight loss peak was observed around 300 °C before the main weight loss peak. The effect is more pronounced at 20 °C min⁻¹ heating rate. Further increase in heating rate to 40 °C min⁻¹ caused the two peaks to merge together. Similar behaviour was reported by Ounas et al. [7]. This gradual weight loss behaviour at lower heating rates which was not evident in the DTG thermograms of rice husk and wheat straw, can be correlated to the variation in the amount of cellulose and hemicellulose contents in the sugarcane sample. As reported previously, the smaller peak around 300 °C can be correlated to the decomposition of hemicellulose present in bagasse and the major weight loss peak was attributed to the decomposition of cellulose. It is suggested that the later shift caused by the increase in heating rate merged the two peaks. Similar behaviour was also reported by Slopiecka et al. [5]. However with the increase in temperature, the opposite trend of separation of different

peaks was reported by Biagini et al. [8]. TGA and DTG thermograms of wheat straw shown in Figure 5-4 showed similar behaviour to rice husk.

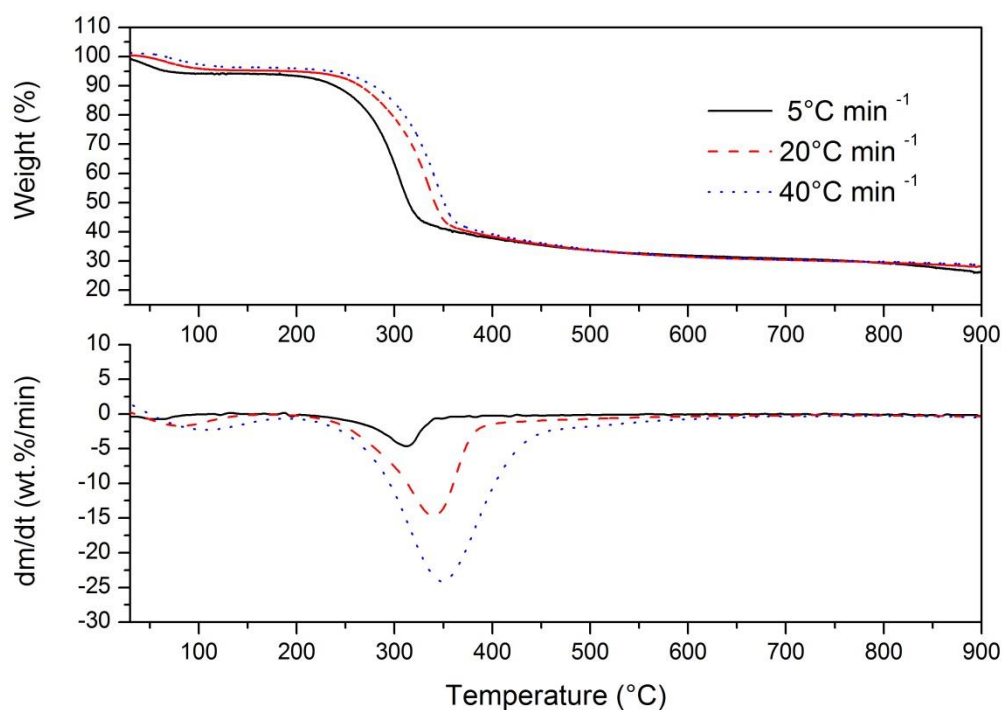


Figure 5-4 TGA and DTG thermograms of wheat straw at 5, 20 and 40 °C min⁻¹ heating rates

5.2.3 The effect of particle size

The effect of particle size on devolatilization of biomass was studied using TGA. Four different particle size ranges were studied at a constant heating rate of 20 °C min⁻¹. Each sample was volatilized in nitrogen atmosphere from room temperature to 930 °C with a dwell time of 10 min. TGA and DTG thermograms for rice husk, bagasse, and wheat straw are shown in Figure 5-5, Figure 5-6, and Figure 5-7 respectively.

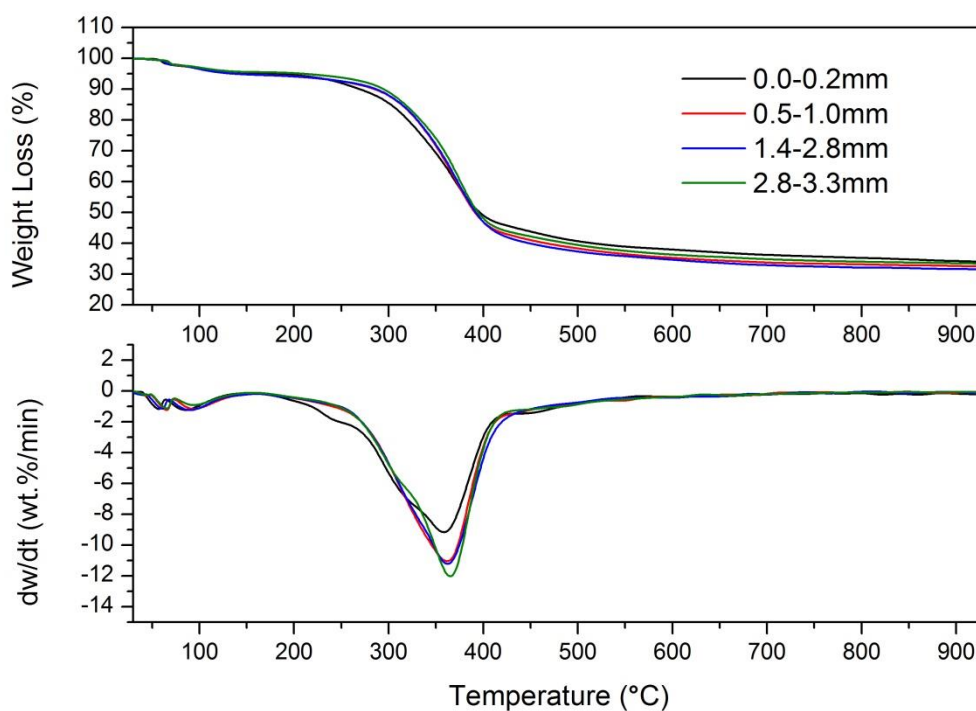


Figure 5-5 The influence of particle size on TGA and DTG thermograms of rice husk at $20\text{ }^{\circ}\text{C min}^{-1}$ heating rate

TGA and DTG thermograms of rice husk showing the effect of particle size are outlined in Figure 5-5. From the results shown, it is indicated that the TGA and DTG thermograms of particle size range 0.5 - 1.0 mm and 1.4 - 2.8 mm were similar and were overlapping each other over the entire temperature range. However the TGA and DTG thermograms of particle size 0.0 - 0.2 mm and 2.8 - 3.3 mm were markedly different. After initial moisture loss, for lowest particle size range, two peaks were visible in DTG thermogram while for the largest particle size range; only one main weight loss peak was observed. This can be explained by the fact that increase in particle diameter hinders the efficient heat transfer from the particle surface to the centre. Velden et al. [9] suggested that the internal heat conduction resistance is larger for larger particles, hence leading to a temperature gradient between the surface and centre of the biomass particle. The effect is minimal for smaller particle size but for the larger particles more time is required for complete conversion.

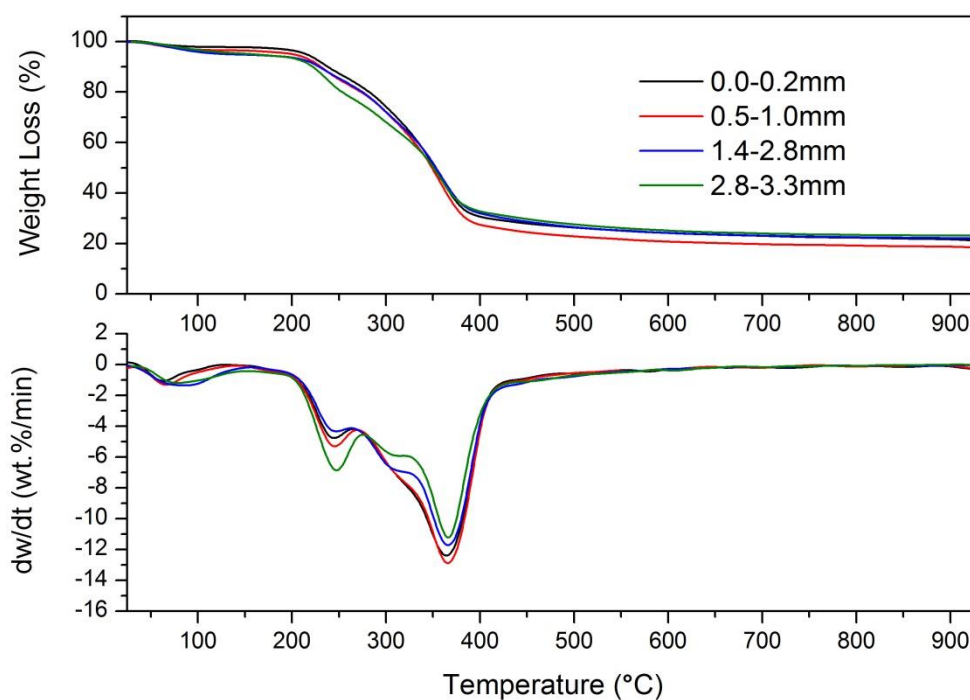


Figure 5-6 The effect of particle size on TGA and DTG thermograms of bagasse at 20 °C min⁻¹ heating rate

The effect of particle size on the devolatilization behaviour of sugarcane bagasse is presented in Figure 5-6. Lesser details were available from the TGA thermogram; indicating that slightly higher weight loss was observed from the highest particle size around 300 °C. However, the DTG thermogram evidenced two peaks in the range of 160 °C to 460 °C. Interestingly, the largest particle size range (2.8 - 3.3 mm) showed the highest weight loss for first peak around 250 °C with the lowest weight loss for second peak around 370 °C. Similar two peaks in DTG thermograms from the thermal decomposition of bagasse were reported in the literature [10, 11]. Shanmukharadhy et al. [12] studied the thermal degradation of bagasse using TGA. They reported that the energy required carrying out the endothermic pyrolysis reaction increases with the increase in particle size.

Table 5-2 The effect of particle size on weight loss of biomass samples

Biomass	Particle size (mm)	Weight loss (wt.%) in temperature range (°C)			Residue	Total
		20-160	160-460	460-930		
Rice husk	0-0.2	5.16	51.66	11.52	31.66	99.99
	0.5-1.0	5.67	54.42	8.96	31.15	100.20
	1.4-2.8	5.65	55.17	9.13	30.02	99.96
	2.8-3.3	4.69	54.16	9.20	32.04	100.10
Bagasse	0-0.2	2.26	69.52	9.68	18.54	100.00
	0.5-1.0	3.76	71.52	8.50	16.22	100.00
	1.4-2.8	5.24	65.72	7.80	21.25	100.00
	2.8-3.3	5.22	65.06	7.22	22.54	100.03
Wheat straw	0-0.2	4.76	38.57	11.96	44.72	100.00
	0.5-1.0	6.09	57.07	10.84	26.21	100.20
	1.4-2.8	5.45	57.64	12.04	24.87	100.00
	2.8-3.3	5.44	60.86	8.84	24.85	99.99

The effect of particle size on the weight loss behaviour of different biomass samples is shown in Table 5-2. Three different temperature ranges; ambient to 160 °C, 160 °C to 460 °C and 460 °C to 930 °C were chosen to compare the weight loss in three different regions of the thermograms. From results shown in Table 5-2, it is evident that during the thermal degradation of rice husk, no significant difference was observed. However for the smallest particle size, slightly lesser weight loss (51.66 wt.% instead of ~55 wt.%) was observed from 160 - 460 °C along with the slightly higher weight loss (11.52 wt.% as compared to ~9 wt.%) from 460 - 930 °C. Similar behaviour was observed for bagasse and wheat straw. This trend was most likely due to the effective heat and mass transfer to and from the surface of the smallest particle size as in smaller particles; surface area-to-volume ratio is high. In addition to this, the amount of residue left was also slightly increased with the increased particle size. This can be explained by the existence of temperature gradient in larger particles and hinder the heat and mass transfer to the particle centre leading to incomplete and ineffective conversion. Lu et al. [13] reported decrease in volatile yield with the increase in particle size.

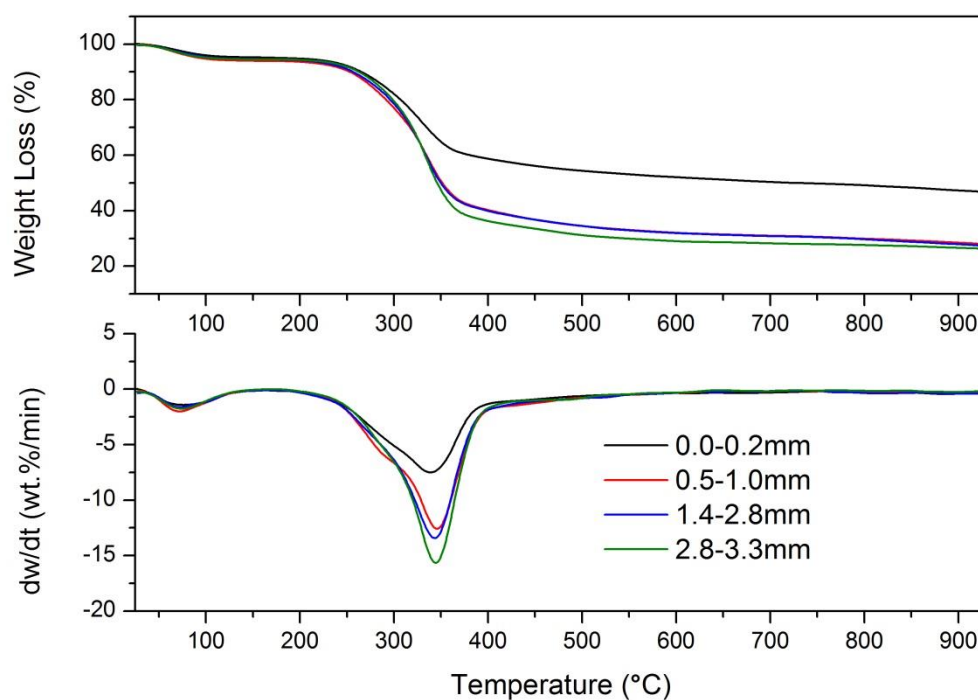


Figure 5-7 The influence of particle size on TGA and DTG thermograms of wheat straw at $20\text{ }^{\circ}\text{C min}^{-1}$ heating rate

Similar results were presented by Mani et al. [14] who studied the effect of particle size of wheat straw using TGA. Six different particle size ranges were investigated. DTG thermogram showed that the largest particle size exhibit the highest weight loss around $375\text{ }^{\circ}\text{C}$ while the smallest particle sizes showed the lowest weight loss in the same region.

5.2.4 Kinetic parameters

Pyrolysis of biomass is a complex process comprising of various competing parallel and series reactions. The use of TGA data to calculate kinetic parameters, i.e. activation energy, pre-exponential factor and order of reaction provides the general information about the overall reaction kinetics rather than individual reactions. However these kinetic parameters calculated from the TGA data are useful when comparing the reaction parameters such as reaction temperature and heating rates. Activation energy varies reaction rate with respect to temperature while pre-exponential factor is related to the material structure.

Non-isothermal technique is a simple and better way of finding the kinetic parameters of the biomass samples. In this study, Coats-Redfern method was used to calculate the kinetic parameters using non-isothermal kinetic data from TGA. A detailed description of processing non-isothermal kinetic data by using a modified Coats-Redfern method has been reported and discussed by Eftimie and Sayed [15]. Procedure to calculate the kinetic parameter from raw data using Coats-Redfern method was outlined by Ahmed et al. [16]. Three different heating rates were employed to obtain consistent and more reliable results. As mentioned in the previous section, three distinct reaction zones were observed during the thermogravimetric analysis. Major weight loss was observed during the second zone around 400 °C. At lower heating rate of 5 °C min⁻¹, the sugarcane bagasse sample showed a clearly separate weight loss peak separate from the main peak (Figure 5-6). Hence the two set of kinetic parameters were calculated for sugarcane bagasse at 5 °C min⁻¹ heating rate. Only one set of kinetic parameters was calculated because both peaks merged and appeared as one at higher heating rates. For rice husk and wheat straw samples only one set of kinetic parameters were calculated at each heating rate as shown in Table 5-4.

The results from the Coats-Redfern method are shown in Table 5-5. For a single reaction, activation energy is a single constant value but biomass thermal degradation is a complex process with several competing reactions. The activation energy reported here is a global activation energy or apparent activation energy of the entire process. The activation energy from rice husk was found to be varied from 25.05 kJ mol⁻¹ to 30.42 kJ mol⁻¹ with the certainty of more than 97 %. For wheat straw, it was found to be from 38.39 kJ mol⁻¹ to 70.22 kJ mol⁻¹. The certainty of results for wheat straw was more than 96 %. For bagasse energy of activation was from 28.27 kJ mol⁻¹ to 31.98 kJ mol⁻¹ with the certainty of more than 97 %.

The order of reaction of 0.5 was established at all heating rates for rice husk. For wheat straw the order of reaction was also found to be 0.5 for 5 °C min⁻¹ and 20 °C min⁻¹ but at 40 °C min⁻¹ heating rate, the order of reaction was found to be 2.0. For sugarcane bagasse, at 5 °C min⁻¹ heating rate showed the order of reaction of 2.0 while the main peak at 5 °C min⁻¹ showed the order of reaction of 0.5. Other higher heating rates also showed the 0.5 order of reaction for sugarcane bagasse.

The value of pre-exponential factor was found to be varied from 12.77 - 111.08 min⁻¹, 117.92 - 1.17x10⁶ min⁻¹ and 21.45 - 5.92x10⁴ min⁻¹ for rice husk, wheat straw and sugarcane bagasse respectively.

5.2.5 Comparison of activation energy from literature

Numerous studies [7, 10, 17-22] have attempted to explain the kinetic parameter from TGA data but there is a wide variation in kinetic parameters values. As shown in Table 5-3, these variations are mainly due to the type of method applied to calculate the kinetic parameters, heating rate, type of biomass and whether the experiment was carried out in an inert atmosphere or in oxygen atmosphere.

Table 5-3 Comparison of kinetic parameters with literature

Feedstock	E _a (kJ mol ⁻¹)		ref
	During Pyrolysis	During Combustion	
Rice Husk	25.05 - 30.42	-	This study
Wheat Straw	38.39 - 70.22	-	-do-
Bagasse	28.27 - 31.98	-	-do-
Rice husk	-	142.7- 188.5	[20]
Corn straw	76.30		[9]
Cotton stalk	-	50.10	[23]
Pakistani coal	-	89.83	-do-
Olive husk	-	83.20	[24]
Grape residue	-	71.42	-do-
Pine wood	-	100.40	-do-
Thai lignite	-	89.12	[25]
Corn stalk skin	126	-	[26]
Corn stalk core	101	-	-do-
Wheat straw	70.51	-	[27]
Wood chips	85.39	-	-do-

Table 5-4 Kinetic parameters

Reaction order	Feedstock	Heating rate 5 °C min ⁻¹				Heating rate 20 °C min ⁻¹				Heating rate 40 °C min ⁻¹			
		Temp (°C)	E _a (kJ mol ⁻¹)	A (min ⁻¹)	R ²	Temp (°C)	E _a (kJ mol ⁻¹)	A (min ⁻¹)	R ²	Temp (°C)	E _a (kJ mol ⁻¹)	A (min ⁻¹)	R ²
n=0.5	Bagasse	190-230	25.56	8.11	0.992	200-380	29.89	56.56	0.988	200-450	31.98	145.02	0.988
	Bagasse	240-360	28.27	59247.25	0.974								
	Rice Husk	230-360	27.96	12.77	0.982	220-390	25.05	19.59	0.972	240-430	30.42	111.08	0.976
	Wheat Straw	230-330	38.39	177.92	0.974	230-350	38.42	433.91	0.968	260-430	39.88	873.12	0.939
n=1.0	Bagasse	190-230	26.57	11.12	0.992	200-380	33.77	162.24	0.973	200-450	37.64	640.92	0.983
	Bagasse	240-360	34.51	47232.91	0.952								
	Rice Husk	230-360	33.15	51.00	0.972	220-390	29.38	63.61	0.960	240-430	36.76	556.79	0.972
	Wheat Straw	230-330	44.74	915.27	0.962	230-350	43.20	1476.96	0.953	260-430	48.29	6709.64	0.950
n=1.5	Bagasse	190-230	27.61	15.38	0.993	200-380	38.23	534.25	0.953	200-450	44.56	3793.50	0.970
	Bagasse	240-360	42.01	32903.24	0.926								
	Rice Husk	230-360	39.23	249.00	0.958	220-390	34.44	243.36	0.945	240-430	44.41	3711.53	0.964
	Wheat Straw	230-330	52.06	5885.45	0.948	230-350	48.60	5772.42	0.935	260-430	58.41	74143.5	0.957
n=2.0	Bagasse	190-230	28.68	21.45	0.993	200-380	43.29	2019.65	0.929	200-450	52.74	29846.7	0.952
	Bagasse	240-360	50.79	16208.39	0.900								
	Rice Husk	230-360	46.24	1492.30	0.943	220-390	40.24	1099.42	0.928	240-430	53.39	32852.3	0.953
	Wheat Straw	230-330	60.39	47436.34	0.932	230-350	54.61	25925.24	0.916	260-430	70.22	1170293	0.961

5.2.6 Conclusions for section 5.2

In this section, thermal degradation behaviour of three different biomass samples; rice husk, sugarcane bagasse and wheat straw was investigated using thermogravimetric analysis. The aim of this study was to investigate the effect of heating rate and particle size on the devolatilization characteristics of the above mentioned biomass samples. In addition, kinetic parameters were also calculated using Coats-Redfern method. The following conclusions can be made from this study.

- The effect of heating rate was investigated on all three biomass samples. It was indicated that the increase in heating rates caused the lateral shift in the TGA thermograms. It is suggested that this behaviour was due to short reaction time at higher heating rates; therefore higher temperature was required for the evolution of volatiles from biomass samples.
- Four different ranges of particles sizes were pyrolysed in TGA under identical conditions. It was found that the increase in particle size resulted in an increase in residual char yield. This was most likely due to the existence of temperature gradient in larger particles which hinders the heat and mass transfer to the particle centre leading to incomplete and ineffective conversion.
- Kinetic parameters i.e. activation energy, pre-exponential factor and order of reaction were calculated using Coats-Redfern method. For rice husk, the order of reaction was found to be 0.5 for all heating rates. For wheat straw it was 0.5 for 5 °C min⁻¹ and 20 °C min⁻¹ but for 40 °C min⁻¹ heating rate, order of reaction was changed to 2.0. For bagasse the first peak exhibited 2nd order while 0.5 order of reaction was calculated for second peak. In addition to that, activation energy results were compared with the various other biomasses in the literature and showed that the results presented in this study were comparable with the existing literature.

5.3 Hydrogen production from ultra-high temperature pyrolysis, steam gasification and catalytic steam gasification of rice husk, sugarcane bagasse and wheat straw

In this section, hydrogen production from pyrolysis, steam gasification and catalytic steam gasification of sugarcane bagasse, wheat straw and rice husk were investigated using a two stage pyrolysis-gasification system. Biomass samples were pyrolysed in the first stage, and the volatiles and liquids were gasified in the second stage. Unreacted steam and condensable liquids were collected in condenser system. A hydrogen-rich gas produced was collected in a gas sample bag and analysed offline using gas chromatography. Detailed explanation and procedure along with a schematic diagram of two stage pyrolysis-gasification system is given in chapter 3.

For pyrolysis experiments, both stages were heated simultaneously up to a final temperature of 950 °C while for steam gasification, the second stage was heated first up to 950 °C and then the biomass sample was pyrolysed in the first stage up to a final temperature of 950 °C. Volatiles and oils produced from pyrolysis were gasified in the second stage in the presence of steam. A silica sand bed was used in the second stage during steam gasification. Heating rate for both stages was kept constant at 20 °C min⁻¹. Water injection rate was 6 ml hr⁻¹ during gasification experiments. Nitrogen was used as a carrier gas at a flow rate of 100 ml min⁻¹. Dolomite and 10 wt.% Ni-dolomite were used during the catalytic steam gasification of biomass samples. Two grams of catalyst was placed in the second stage and heated up to 950 °C. Volatiles released from pyrolysis of biomass in the first stage reacts with the catalyst in the second stage, in the presence of steam producing more hydrogen.

Characterization results from different analytical techniques such as scanning electron microscopy (SEM), transmission electron microscopy (TEM) coupled with energy dispersive X-ray spectroscopy (EDX), and X-ray diffraction (XRD) of freshly prepared catalyst are presented in section 5.3.1. Pyrolysis and steam gasification results are discussed in section 5.3.2 and 5.3.3 respectively. Influence of dolomite and 10 wt.% Ni-dolomite on catalytic steam gasification of rice husk, sugarcane bagasse and wheat straw are outlined in section 5.3.4 and 5.3.5. Results from characterization of reacted catalyst are discussed in section 5.3.6.

5.3.1 Characterization of fresh catalysts

Two Different catalysts: dolomite and 10 wt.% Ni-dolomite were employed in this study to investigate the influence of catalyst on hydrogen production during the two-stage pyrolysis-gasification of biomass. Naturally occurring dolomite calcined at 1000 °C and 10 wt.% Ni-dolomite calcined at 900 °C prepared by wet impregnation method were ground and sieved to achieve the particle size between 50 - 212 µm. Both catalysts were calcined in an air atmosphere for 3 hours. Surface properties of dolomite and 10 wt.% Ni-dolomite are outlined in Table 5-6. Results of naturally occurring dolomite are also presented for reference and comparison. Details of catalyst preparation and characterization techniques are presented in chapter 3.

Table 5-6 Surface properties of fresh catalysts

Catalyst	BET surface area	BJH pore volume	Average pore size
	m ² g ⁻¹	cm ³ g ⁻¹	nm
Dolomite non-calcined	2.0290	0.0083	2.2220
Dolomite calcined at 1000 °C	4.6950	0.0110	2.8400
10%Ni-dolomite calcined at 900 °C	5.5590	0.0308	2.2120

It is evident from Table 5-6 that calcination of naturally occurring dolomite resulted in an increase in BET surface area from 2.0 m² g⁻¹ to 4.7 m² g⁻¹. BJH pore volume and average pore size also increased slightly from 0.0083 cm³ g⁻¹ to 0.0110 cm³ g⁻¹ and from 2.2 nm to 2.8 nm respectively. Addition of Ni into dolomite slightly increased the BET surface area to 5.6 m² g⁻¹, while a significant increase (almost three times) in BJH pore volume was observed. Addition of Ni, however, resulted in slight decrease in average pore size. Sasaki et al. [28] investigated the effect of temperature on calcination of naturally occurring dolomite. They reported the strong influence of calcination temperature on pore size distribution. Two distinct stages of decarbonation of CaMg(CO₃)₂ were identified: during the first stage, MgO was formed between 600 °C to 700 °C and then CaO was formed from 700 °C to 900 °C during the second stage.

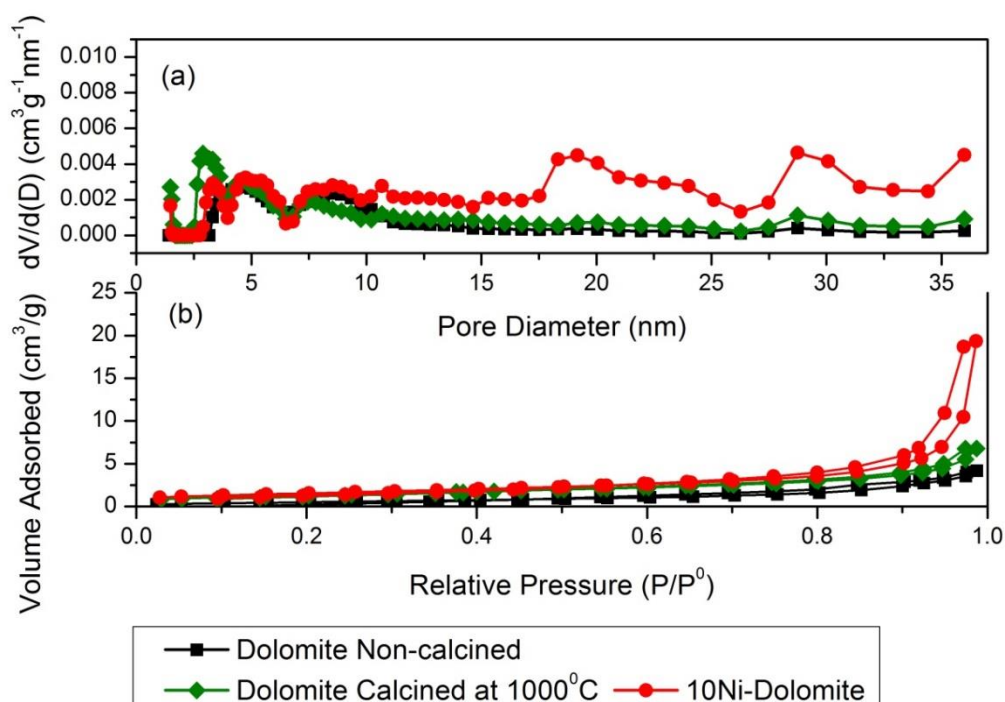


Figure 5-8 Pore size distribution (a), and N_2 adsorption/desorption isotherms of the fresh catalysts (b).

Results of pore size distribution are shown in Figure 5-8. From these results it can be indicated that the mesopores are predominant. Naturally occurring dolomite and calcined dolomite showed the presence of pores of smaller diameter range (<10 nm). Additional pores in the range of 18 - 25 nm were observed in 10 wt.% Ni-dolomite. Similar pore size distribution of naturally occurring dolomite and calcined dolomite were reported in [28].

The N_2 adsorption-desorption isotherms of naturally occurring dolomite and freshly prepared catalysts are shown in Figure 5-8. Dolomite non-calcined showed a feature of a type III isotherm in the IUPAC classification of adsorption isotherm. The Type III isotherms are observed in materials having strong adsorbate-adsorbate interaction and weak adsorbent-adsorbate interaction. These materials are characterised by the multilayer formation as heats of adsorption is less than the adsorbate heat of liquification. Adsorption proceeds as the adsorbate interaction with an adsorbed layer is greater than the interaction with the adsorbent surface [29]. The type of isotherm was

changed into type V for calcined dolomite and 10 wt.% Ni-dolomite (hysteresis loop was observed). It has been reported that the type V isotherm was related to type III and was due to the weak interaction between adsorbent and adsorbate [30]. Furthermore, the hysteresis loop present at higher P/P^0 for 10 wt.% Ni-dolomite was identified as type H3. This type of hysteresis loop was observed due to the aggregation of plate like particles which give rise to slit-shape pores [30].

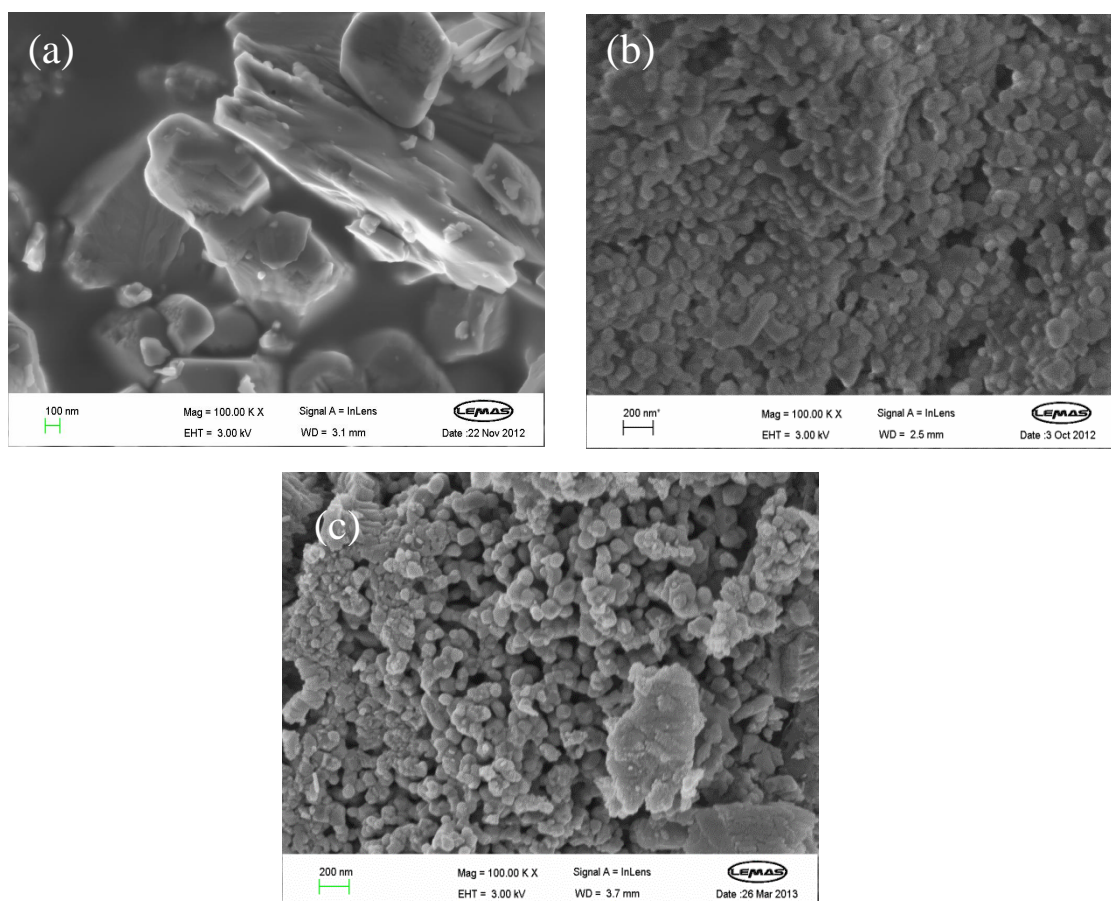


Figure 5-9 SEM images of fresh catalysts (a) fresh dolomite non-calcined, (b) dolomite calcined at 1000 °C, (c) 10 wt.% Ni-dolomite calcined at 900 °C

Scanning electron microscope (SEM) characterisation of the fresh catalysts are shown in Figure 5-9. Calcination of dolomite (Figure 5-9-b) resulted in a granular morphology due to the breakdown of the larger grains. Yoosuk et al. [31] researched the calcination of dolomite and suggested a two-step mechanism. During the first step $\text{CaMg}(\text{CO}_3)_2$ breakdown into MgO and $\text{Ca}(\text{CO}_3)_2$. Later on, in the second step $\text{Ca}(\text{CO}_3)_2$ further breaks down into CaO leaving CO_2 . Sasaki et al. [28] proposed that the Mg in dolomite

moves to the surface, showing external growth and CaCO_3 showed inward growth. SEM of the 10 wt.% Ni-dolomite shown in Figure 5-9-c indicate the presence of granular hexagonal plate-like morphology.

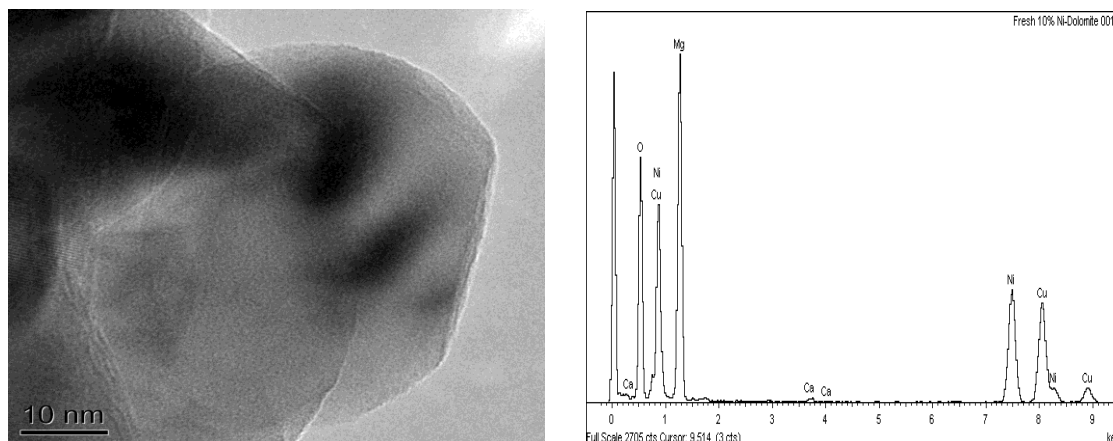


Figure 5-10 TEM-EDX of fresh 10 wt.% Ni-dolomite catalysts calcined at 900 °C

TEM-EDX results of the freshly prepared 10 wt.% Ni-dolomite catalyst are shown in Figure 5-10. Characteristic plate-shape morphology of dolomite was visible in the TEM image. Similar morphology was observed by Sasaki et al. [28]. During EDX analysis, Ni was also present along with the Ca and Mg in the sample.

The X-ray diffraction analysis of naturally occurring raw dolomite, calcined dolomite and 10 wt.% Ni-dolomite are presented in Figure 5-11. From these results shown in Figure 5-11(a), it can be inferred that the raw dolomite primarily consists of $\text{MgCa}(\text{CO}_3)_2$ however the presence of CaCO_3 was also reported [28]. Calcination of dolomite resulted in complete breakdown of $\text{MgCa}(\text{CO}_3)_2$ into CaO and MgO as shown in Figure 5-11(b) [32]. Addition of Ni into the dolomite resulted in the formation of NiO, NiMgO_2 along with CaO and MgO (shown in Figure 5-11(c)). Srinakruang et al. [33] investigated the effect of calcination temperature and Ni-loading on the tar gasification of Ni-dolomite catalyst. It was reported that the NiO phase was only present at a calcination temperature of 500 °C. At higher temperature a more stable form of NiMgO_2 was observed. In another study [34], it was suggested that there was a strong interaction between Ni species and dolomite, which resulted in fine dispersion of Ni particles on the dolomite surface.

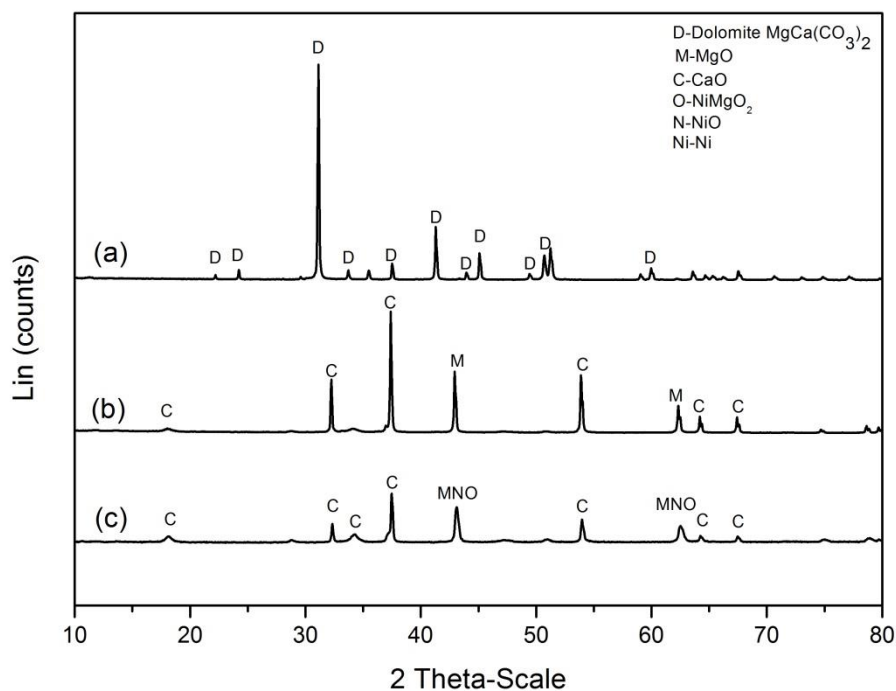


Figure 5-11 XRD of fresh catalysts (a) fresh dolomite non-calcined, (b) fresh dolomite calcined at 1000 °C, (c) fresh 10 wt.% Ni-dolomite

5.3.2 Pyrolysis of rice husk, sugarcane bagasse and wheat straw

5.3.2.1 Product yield from pyrolysis

Table 5-7 shows the results for the pyrolysis of rice husk, sugarcane bagasse and wheat straw performed at a heating rate of 20 °C min⁻¹ to a final temperature of 950 °C. During all experiments, 4 grams of biomass sample was placed in the sample holder in the upper pyrolysis stage and both stages were heated simultaneously. During pyrolysis of rice husk, 22.29 wt.% of biomass was converted into gas with the hydrogen production of 2.12 mmol g⁻¹ of rice husk. 30 wt.% of biomass was recovered as solid residue after the experiment. A relatively larger fraction of 42.25 wt.% was found in the form of liquid oil. The rice husk sample exhibited the lowest gas and oil yield resulting in the lowest feedstock to volatile conversion. This lowest conversion and highest solid yield from rice husk was primarily due to the higher ash contents in rice husk [35].

For sugarcane bagasse, gas yield in relation to biomass was 22.53 wt.% along with 20.25 wt.% solid and 54.25 wt.% liquid oil. Hydrogen production from pyrolysis of

bagasse was found to be 2.07 mmol g⁻¹. During the pyrolysis of wheat straw, 24.19 wt.% of gas, 24.75 wt.% solid and 50 wt.% liquid oil was recovered. Slightly higher yield of 2.22 mmol g⁻¹ of hydrogen was obtained from the pyrolysis of wheat straw. Similar results were reported by Sun et al. [36] who researched the two stage pyrolysis of wood sawdust. More than 50 wt.% liquid fraction was obtained at temperatures above 600 °C. This liquid fraction was the combination of non-evaporated tar and the evaporated liquid. The solid fraction was found to be around 21 wt.%. Burhenne et al. [37] performed the pyrolysis of wheat straw in a fixed bed pyrolysis reactor at 500 °C, they reported 20 wt.% gas yield with 47 wt.% liquid and 33 wt.% solid yield. It is also interesting to note that compared to rice husk, relatively higher oil yield was obtained from sugarcane bagasse and wheat straw. This is in agreement with the TGA and DTG results shown in Figure 5-1, indicating the presence of larger quantity of volatile matter in these biomass samples.

Table 5-7 Pyrolysis of different biomass samples

	Rice husk	Sugarcane bagasse	Wheat straw
Temperature (°C)	950	950	950
Particle size (mm)	1.4-2.8	1.4-2.8	1.4-2.8
Nitrogen flow rate (ml min ⁻¹)	100	100	100
H ₂ (mmol g ⁻¹ of biomass)	2.12	2.07	2.22
Mass balance			
Gas/(biomass) (wt.%)	22.29	22.53	24.19
Solid/(biomass) (wt.%)	30.00	20.25	24.75
Oil/(biomass) (wt.%)	42.25	54.25	50.00
Mass balance (wt.%)	94.54	97.03	96.44

The product yield from pyrolysis of biomass mainly depends on the final temperature, heating rate and the residence time [38]. The low gas yield and high liquid yield obtained from all three biomass samples was most likely due to the sweeping gas preventing thermal cracking, secondary re-condensation and re-polymerization reactions caused by the solid-vapour interaction. It should also be noted that although a high final pyrolysis temperature of 950 °C was used, the pyrolysis of the biomass would mostly be

completed by ~600 °C. At higher temperatures the release of volatiles is attributed to the further thermal degradation of high molecular weight pyrolysis products. In addition, the carrier gas removed the products from the hot reaction zone, thereby enhancing the liquid yield [39]. Results presented by Onay et al. [40] from the pyrolysis of rapeseed in a fixed bed reactor indicated that the presence of carrier gas enhanced the liquid yield by more than 5 wt.% with the corresponding decrease in gas and solid yield.

5.3.2.2 Gas composition and hydrogen production

The gas composition derived from the pyrolysis and steam gasification of rice husk (RH), sugarcane bagasse (BG) and wheat straw (WS) is shown in Figure 5-12. Pyrolysis of wheat straw produced almost equal concentrations of H₂ and CO; around 25 vol.% each were produced. Higher concentration of CO₂ of 38.31 vol.% was observed in the syngas mixture while the concentration of CH₄ was found to be 9.18 vol.%. C₂-C₄ hydrocarbons which include ethane, ethene, propane, propene, butane, butene and butadiene were found to be 2.34 vol.%. For rice husk, 26.5 vol.% of CO and 24.97 vol.% of H₂ was obtained from pyrolysis. Slightly lower concentration of CO₂ of 35.63 vol.% was recovered. The concentration of CH₄ and C₂-C₄ were 10.15 vol.% and 2.74 vol.% respectively. Similar concentration of CO 24.80 vol.%; H₂ 24.45 vol.%; and 38.34 vol.% of CO₂ were produced during the pyrolysis of sugarcane bagasse. The concentrations of CH₄ and C₂-C₄ were found to be 10.54 vol.% and 1.87 vol.% respectively. Similar results were presented by Burhenne et al. for wheat straw [37]. They performed the pyrolysis of wheat straw in a fixed bed pyrolysis reactor reporting less than 10 vol.% of H₂ and CH₄ each. However, 40 vol.% CO₂ and 20 vol.% CO were present in the gas mixture. García-Pérez et al. [41] investigated the pyrolysis of sugarcane bagasse and reported a similar gas composition. Around 46 vol.% CO₂ was found along with 29 vol.% of CO. However slightly lower yield of H₂ at 3 vol.% along with 7 vol.% CH₄ was reported. Xu et al. [42] researched the two stage pyrolysis of rice husk. First stage was a pyrolysis reactor at 500 °C connected with a continuous screw feeder. In their research, they used γ -Al₂O₃ and Fe₂O₃/ γ -Al₂O₃ catalysts in second stage to crack the volatiles and tars coming from the first stage. Both catalysts were calcined at 550 °C while the temperature in the second stage was kept at 700 °C. Compared to pyrolysis of rice husk in the absence of catalyst, it was found that the addition of γ -Al₂O₃ in the second stage resulted in a slight increase in H₂ concentration from 6.13 vol.% to 6.32 vol.%. However, addition of Fe₂O₃ in γ -Al₂O₃ in second stage

dramatically increased H₂ concentration from 6.32 vol.% to 31.19 vol.%. Significant decrease in CO concentration from 37.62 vol.% to 12.24 vol.% was also observed.

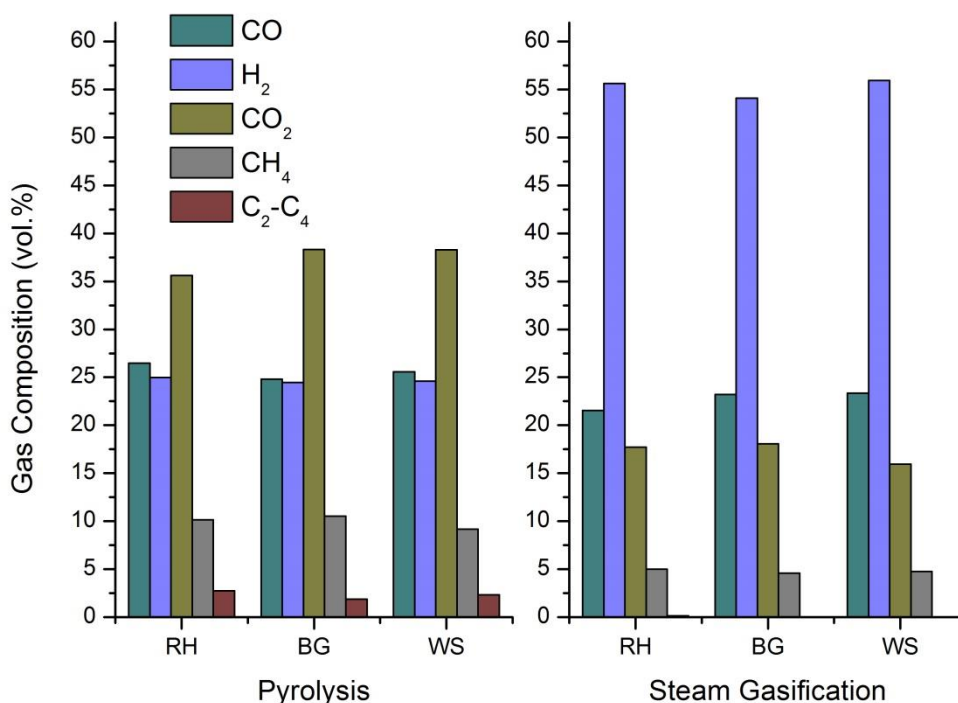


Figure 5-12 Syngas composition from pyrolysis and steam gasification of rice husk (RH), sugarcane bagasse (BG), and wheat straw (WS)

Neves et al. [43] explained the pyrolysis of biomass as a three step process. In the first step, as-received biomass released moisture and is converted into dry biomass. In the second step, this dry biomass undergoes primary pyrolysis, in which feedstock is converted into char with the evolution of volatiles, permanent gases, moisture and tar. During the last step, the complex interaction between these species results in reforming, cracking, oxidation, polymerization and other gasification reactions. It has been reported [44] that during the pyrolysis of cellulose and hemicellulose components present in biomass, CO and CO₂ were the major gas components from the decarboxylation of biomass at lower temperatures (< 400 °C). Further release of CO above 550 °C along with the release of hydrogen was also observed. This was most likely due to the thermal cracking and decarbonylation of aromatic compounds [44]. Similar observations are reported by Becidan et al. [45] who indicated the early release

of CO and CO₂ from biomass and later release of hydrogen at relatively higher temperature. Cellulose is the main component of biomass and it is found in large proportions in biomass materials. Various researchers [46-51] have studied the mechanism for the pyrolysis of cellulose. Empirical models, such as presented by Kilzer and Broido et al. [52] suggested that the lignocellulosic materials follow one of two available pathways. At higher temperature, tar formation is favoured by the low activation energy of the reaction while at low temperatures, cellulose in the biomass sample converts into dehydro-cellulose which is converted into char and syngas. Shin et al. [51] studied the kinetics of levoglucosan using molecular beam mass spectrometry (MBMS). According to their model, three types of compounds; primary, secondary and tertiary compounds were present during pyrolysis. With the increase in temperature, the concentration of primary compound (levoglucosan) decreased while the concentration of secondary compounds (methanol, acetaldehyde, acrolein and furans) increased to a certain temperature and decreased with the further increase in temperature. The concentration of tertiary compounds (carbon monoxide, permanent gases and other lighter hydrocarbons) was increased with the increase in temperature up to a higher temperature of 700 °C.

Diebold et al. [47] developed a model for the pyrolysis of cellulose using seven different pyrolysis reaction rate equations. The product composition of pyrolysis of cellulose was predicted as a function of time, temperature and heating rate. It was reported that the low heating rates coupled with the low final temperature produced more char while high heating rate coupled with higher final temperature produced higher gas yield. They suggested that the pyrolysis of cellulose initially produced char and active cellulose. This active cellulose gets converted into char, water, gases and condensable vapours.

Banyasz et al. [48] investigated the real time evolution of different species from the pyrolysis of cellulose using fast evolved gas-FTIR apparatus. The evolution of formaldehyde, hydroxyacetaldehyde, CO, and CO₂, was studied in details. They reported that the cellulose initially pyrolysed into anhydrocellulose (which lead to char formation) and lower degree of polymerised active cellulose which further converted into tar, CO₂ and char or produce different intermediates. These intermediates converted into hydroxyacetaldehyde or formaldehyde and CO.

Lin et al. [49] investigated the pyrolysis of cellulose using pyroprobe reactor and TGA-MS. It was reported that the first step was the depolymerization of cellulose to form

levoglucosan. Dehydration and isomerization of levoglucosan can produce other anhydrosugars such as levoglucosenone and furans. Other compounds such as glycolaldehyde and glyceraldehyde were also formed by fragmentation and retroaldol condensation. CO and CO₂ were produced from decarbonylation and decarboxylation reactions. Polymerization of pyrolysis products resulted in the formation of char. During their investigations on the mechanism of rapid cellulose pyrolysis, Luo et al. [46] also mentioned the formation of active cellulose and then the formation of levoglucosan.

5.3.3 Steam gasification of rice husk, bagasse and wheat straw

5.3.3.1 Product yield from steam gasification

The product and hydrogen yields from the two stage pyrolysis/steam gasification of rice husk, sugarcane bagasse and wheat straw using a sand bed are presented in Table 5-8. When compared with the pyrolysis results shown in Table 5-7, gas yield dramatically increased almost three fold. Gas yield in relation to biomass (corrected for no input water), was found to be 67.40 wt.% for rice husk, 63.72 wt.% for bagasse and 59.63 wt.% for wheat straw. However, gas yield in relation to biomass + water was 29.92 wt.% for rice husk, 27.38 wt.% for bagasse and 26.07 wt.% for wheat straw respectively.

Table 5-8 Steam gasification of different biomass samples

	Rice husk	Sugarcane bagasse	Wheat straw
Temperature (°C)	950	950	950
Nitrogen flow rate (ml min ⁻¹)	100	100	100
Particle size (mm)	1.4-2.8	1.4-2.8	1.4-2.8
Steam injection (ml hr ⁻¹)	6	6	6
H ₂ (mmoles g ⁻¹ of biomass)	23.71	21.18	21.59
Mass balance			
Gas/(biomass+water) (wt.%)	29.92	27.38	26.07
Solid/(biomass+water) (wt.%)	13.98	9.67	11.58
Mass balance (wt.%)	94.63	95.91	90.00
Gas/(biomass) (wt.%)	67.40	63.72	59.63
Solid/(biomass) (wt.%)	31.50	22.50	26.50

Higher hydrogen yield was attained from the steam gasification of volatiles and tars evolving from the pyrolysis of biomass sample in the first stage. Rice husk produced 23.71 mmoles of hydrogen per gram of biomass while 21.18 and 21.59 mmoles of hydrogen were recovered per gram of bagasse and wheat straw respectively. The significantly higher hydrogen yield indicates the effectiveness of two stage pyrolysis and gasification system over the single stage pyrolysis process. Several researchers [53-57] have employed two staged pyrolysis-gasification systems and reported low tar contents and higher gas and hydrogen yield.

5.3.3.2 Gas composition from steam gasification

The gas composition derived from the pyrolysis and steam gasification of rice husk (RH), sugarcane bagasse (BG) and wheat straw (WS) are detailed in Figure 5-12. In contrast to the pyrolysis results, during steam gasification, gas composition changed substantially. Carbon monoxide concentration slightly reduced from 25 vol.% during pyrolysis to around 23 vol.% during steam gasification. The concentration of CH₄ was also reduced from 10 vol.% during pyrolysis to less than 5 vol.% during gasification. Only trace amounts (0.14 vol.% for rice husk; 0.004 vol.% for wheat straw) of C₂-C₄ hydrocarbons were found in gas mixture during the steam gasification, however no C₂-C₄ hydrocarbons were detected during gasification of sugarcane bagasse. Previously during pyrolysis; around 2 vol.% of C₂-C₄ hydrocarbons were present in the gas mixture.

The hydrogen concentration in the product gaseous mixture was enhanced from around 25 vol.% during pyrolysis to 55 vol.% during two stage steam gasification. Hydrogen concentration of 55.62 vol.% for rice husk, 54.12 vol.% for bagasse and 55.94 vol.% for wheat straw were achieved.

The concentration of CO₂ reduced to almost half from 38 vol.% during pyrolysis to 17 vol.% during gasification. This decrease in CO₂ concentration at higher temperature indicates the increase in forward Boudouard reaction. As reported by Yang et al. [58] this reaction is favoured at higher temperatures. The endothermic reaction between CO₂ and CH₄ was also supported at high temperature contributing towards the decrease in CO₂ and CH₄ concentrations.

The injected steam also boosted the hydrogen concentration by reacting with CH₄, C, and CO. Water gas reaction, and steam methane reforming reaction, are favoured at

high temperature due to their endothermic nature. Water gas shift reaction, on the other hand is slightly exothermic but the equilibrium can be shifted towards the products at higher steam to biomass ratios. Herguido et al. [59] reported an increase in hydrogen concentration (up to 60 vol.%) with a corresponding decrease in CO concentration when they increased steam to biomass ratio (S/B) from 0.5 to 2.5. A sharp reduction in tar concentration was also noticed.

The decrease in C₂-C₄ hydrocarbons concentration was most likely due to the thermal cracking of larger hydrocarbon molecules into the smaller molecules. Thermal cracking of tar components, is one of the major advantages of the high temperature (> 900 °C) two-stage pyrolysis/gasification system over the other configuration as it require little or no syngas upgrading equipment for final use [60].

Wu et al. [2] investigated the effect of two different catalysts on pyrolysis/gasification of biomass components like cellulose, xylan and lignin using two-stage pyrolysis/gasification system in a down-draft configuration. Samples were pyrolysed in the first stage at 500 °C while all the derived products were gasified in the second stage at a higher temperature of 800 °C. The highest hydrogen yield of 55.1 vol.% was obtained from lignin sample in the presence of steam and Ni-Mg-Al catalyst. When compared with the results of the current study, it is evident that the two-stage high-temperature pyrolysis/gasification system used in this study was very effective as similar hydrogen concentration of (~55 vol.%) was obtained without catalyst.

Various researchers [61, 62] have studied the global mechanism of gasification. Ahmed et al.[61] proposed a detailed global mechanism of biomass gasification. It was reported that the initial heating of biomass produced active precursor compounds. For slow heating rate to final low gasification temperature, these precursor compounds produce char, gases and water. Further gasification of char can produce syngas consisting of CO, CO₂ and hydrogen.

For higher heating rate up to medium final temperature lead to the depolymerization of these precursor compounds forming aromatic cyclic and heterocyclic compounds. Repolymerization of these compounds can produced some char while the oligomerization of these single ring and multi-ring compounds can produce oligomer tar compounds with the evolution of CO₂. Further heating to a higher temperature can open the rings of these aromatic cyclic and heterocyclic compounds and form

aldehydes, ketones, carboxylic acids and other gases by fragmentation, decarbonylation and decarboxylation reaction. The tertiary reactions on these aldehydes, ketones, carboxylic acids compounds can produce syngas.

For higher heating rates coupled with higher final temperature can produce aldehydes, ketones, carboxylic acids and other gases from precursor compounds by fragmentation, decarbonylation and decarboxylation reaction. Aromatization and repolymerization can produce char from these compounds. Further tertiary reactions on these aldehydes, ketones, carboxylic acids can produce light hydrocarbons and CO. Final reforming of these hydrocarbons can also produce syngas consisting of CO, CO₂, and hydrogen.

5.3.4 Dolomite catalytic steam gasification of rice husk, bagasse and wheat straw

5.3.4.1 Product yield from dolomite catalytic steam gasification

In this set of experiments, the second stage containing dolomite (calcined at 1000 °C) was heated first to 950 °C. Once the desired temperature was achieved, the biomass sample was pyrolysed in the first stage up to a final temperature of 950 °C. Volatiles, gases and tar evolving from the pyrolysis of biomass were made to react with steam in the presence of calcined dolomite. The product and hydrogen yield derived from the dolomite catalytic steam gasification of the three biomass samples are shown in Table 5-9

As shown in Table 5-9, in relation to biomass (corrected for no input water), more than 60 wt.% of the biomass samples was converted into gas, however the gas yield in relation to biomass + water was found to be 24.63 wt.% for rice husk, 25.55 wt.% for bagasse and 25.63 wt.% for wheat straw respectively. As compared to the two-stage steam gasification results shown in Table 5-8, the solid yield was similar as the conditions in the pyrolysis stage were identical. Hydrogen yield was slightly improved to 22.55 mmoles g⁻¹ for rice husk, 22.30 mmoles g⁻¹ for bagasse and 21.97 mmoles g⁻¹ for wheat straw.

Table 5-9 Dolomite catalytic steam gasification of different biomass samples

	Rice husk	Sugarcane bagasse	Wheat straw
Catalyst	Dolomite	Dolomite	Dolomite
Catalyst weight (g)	2	2	2
Particle size (mm)	1.4-2.8	1.4-2.8	1.4-2.8
Nitrogen flow rate (ml min ⁻¹)	100	100	100
Water injection (ml hr ⁻¹)	6	6	6
Temperature (°C)	950	950	950
H ₂ (mmoles g ⁻¹ of biomass)	22.55	22.30	21.97
Mass balance			
Gas/(biomass+water) (wt.%)	24.63	25.55	25.63
Solid/(biomass+water) (wt.%)	12.45	9.87	11.16
Mass balance (wt.%)	94.69	92.78	95.71
Gas/(biomass) (wt.%)	62.31	60.82	61.46
Solid/(biomass) (wt.%)	31.50	23.50	26.75

It has been reported that the use of calcined dolomite (CaO-MgO) minimized tar production in the product gas mixture [63]. The better activity of calcined dolomite as compared to non calcined dolomite was due to the higher surface area and higher CaO and MgO contents. Simell et al. [64] suggested that the CaO is more reactive than dolomite. González et al. [54] investigated the two-stage gasification of olive cake using dolomite. They reported an improvement on hydrocarbon and tar cracking reactions. Wang et al. [65] used a two-stage gasification and catalytic system to enhance the hydrogen yield from pig compost. The gasification and catalytic stages were kept at constant temperature of 800 °C and 900 °C respectively. It was reported that the presence of calcined modified dolomite enhanced the hydrogen yield but this effect was more evident at lower temperature of 800 °C. Their results showed that hydrogen yield was increased from 10.62 mmoles g⁻¹ of sample to 18.76 mmoles g⁻¹ of sample. In this study, although the presence of naturally abundant and cost-effective dolomite did not improve hydrogen yield significantly, it was reported that addition of Ni in to dolomite was a promising option for enhanced hydrogen yield.

5.3.4.2 Gas composition from dolomite catalytic steam gasification

Gas composition results from catalytic two stage gasification of biomass samples using calcined dolomite are presented in Figure 5-13. Compared to the steam gasification results shown in Figure 5-12, a slight increase in hydrogen concentration, for example, for rice husk, increasing from 55 vol.% to 57 vol.% with a corresponding decrease in CO concentration from 21.53 vol.% to 19.97 vol.%. A slight increase in CO₂ concentration (from 17.70 vol.% to 19.59 vol.% for rice husk) along with some decrease in CH₄ concentration (4.99 vol.% to 3.02 vol.% for rice husk) was also observed. However no C₂-C₄ hydrocarbons were detected during the catalytic steam gasification of all three biomass samples.

Similar results are reported by González et al. [54], suggesting that the presence of dolomite improved the water gas shift reaction as was evidenced by higher hydrogen concentration with the reduction in CO concentration in the gas mixture. Other authors [66-68] also reported the effectiveness of dolomite as catalyst. Dolomite was found to be very effective for reduction of tar compounds. As reported by Olivares et al. [67] the tar cracking capability of dolomite was mainly due to the steam reforming and dry reforming reactions. Elbaba et al. [69] carried out two stage pyrolysis-gasification of waste tyres. During their investigation, pyrolysis temperature was kept constant at 500 °C while gasification in the presence of steam and calcined dolomite was carried out at 800 °C. 49.10 vol.% hydrogen was achieved using calcined dolomite catalyst.

5.3.5 10 wt.% Ni-dolomite catalytic steam gasification of rice husk, bagasse and wheat straw

5.3.5.1 Product yield from 10 wt.% Ni-dolomite catalytic steam gasification

Product yield and hydrogen production from the two-stage pyrolysis/gasification of the biomass samples using 10 wt.% Ni-dolomite are presented in Table 5-10. By introducing 10 wt.% Ni into the calcined catalyst increased the gas yield as well as hydrogen yield. When compared with the dolomite results presented in Table 5-9, Gas yield in relation to biomass + water increased marginally from 24.63 wt.% to 26.30 wt.% for rice husk, from 25.55 wt.% to 28.04 wt.% for bagasse and from 25.63 wt.% to 26.20 wt.% for wheat straw respectively. The presence of Ni in the dolomite also enhanced the hydrogen yield for all three biomass samples. Compared to the dolomite

results, hydrogen yield was enhanced from 22.55 mmol g⁻¹ to 25.44 mmol g⁻¹ for rice husk, from 22.30 mmol g⁻¹ to 25.41 mmol g⁻¹ for sugarcane bagasse and from 21.79 mmol g⁻¹ to 24.47 mmol g⁻¹ for wheat straw.

Significant increase in gas yield and hydrogen yield was also reported by Wang et al. [65]. They used a two-stage gasification system to enhance the hydrogen yield from pig compost. In the first stage, the sample was gasified in the presence of steam at 800 °C, while in the second stage, gases, volatiles and liquids were made to react with the catalyst at higher gasification temperature of 900 °C. The modified dolomite used in this study was prepared by mixing naturally occurring dolomite (calcined in an air atmosphere at 900 °C for 4 hours) with calcium aluminate and calcium citrate at a mass ratio of 7:2:1. The introduction of Ni into the modified dolomite catalyst increased the gas yield from 0.97 Nm³ kg⁻¹ to 1.33 Nm³ kg⁻¹ and hydrogen production was also enhanced from 18.76 mmol g⁻¹ to 32.45 mmol g⁻¹ of the sample. Ni-dolomite was also reported to be very effective in tar reduction. Only 0.24 g/Nm³ of tar was found with the use of Ni-dolomite catalyst.

Corujo et al. [70] investigated the influence of calcined dolomite and Ni-dolomite on the product yield from the steam gasification of forestry residue at 900 °C. Dolomite and different compositions of Ni-dolomite (prepared by incipient wetness method) were calcined at 900 °C in an argon atmosphere. With the introduction of Ni-dolomite, there was a significant increase in gas yield along with a decrease in tar and char formation reported.

Various researchers have reported the effectiveness of Ni for lower tar production and higher hydrogen production from gasification [69, 71-74]. However the deactivation of Ni based catalysts was reported mainly due to carbon deposition [72]. Due to the two-stage configuration and high temperature employed in this study, very little to no carbon was observed on the catalyst after reaction. From the results shown in Table 5-10, it is evident that the combination of high temperature steam gasification and the tar cracking capabilities of 10 wt.% Ni-dolomite is a promising option for the production of hydrogen from biomass.

Table 5-10 10 wt.% Ni-dolomite catalytic steam gasification of different biomass samples

	Rice husk	Sugarcane bagasse	Wheat straw
Catalyst	10%Ni-Dolomite	10%Ni-Dolomite	10%Ni-Dolomite
Catalyst weight (g)	2	2	2
Particle size (mm)	1.4-2.8	1.4-2.8	1.4-2.8
Nitrogen flow rate (ml min ⁻¹)	100	100	100
Water injection (ml hr ⁻¹)	6	6	6
Temperature (°C)	950	950	950
H ₂ (mmoles g ⁻¹ of biomass)	25.44	25.41	24.47
Mass balance			
Gas/(biomass+water) (wt.%)	26.30	28.04	26.20
Solid/(biomass+water) (wt.%)	13.02	8.98	10.80
Mass balance (wt.%)	96.65	96.80	97.23
Gas/(biomass) (wt.%)	63.64	70.24	64.90
Solid/(biomass) (wt.%)	31.50	22.50	26.75

5.3.5.2 Gas composition and hydrogen production

The gas composition derived from the pyrolysis-gasification of the biomass samples using 10 wt.% Ni-dolomite are compared with dolomite gasification results in Figure 5-13. For rice husk, the CO concentration slightly increased from 19.97 vol.% to 22.84 vol.% along with an increase in H₂ concentration from 57.40 vol.% to 59.13 vol.%. CO₂ concentration was reduced from 19.59 vol.% to 16.23 vol.% and CH₄ concentration reduced from 3.02 vol.% to 1.77 vol.%. Similar trends were observed for bagasse and wheat straw respectively. The increase in hydrogen concentration can be partly attributed due to the further cracking of tar components in the gas stream by the 10 wt.% Ni-dolomite catalyst.

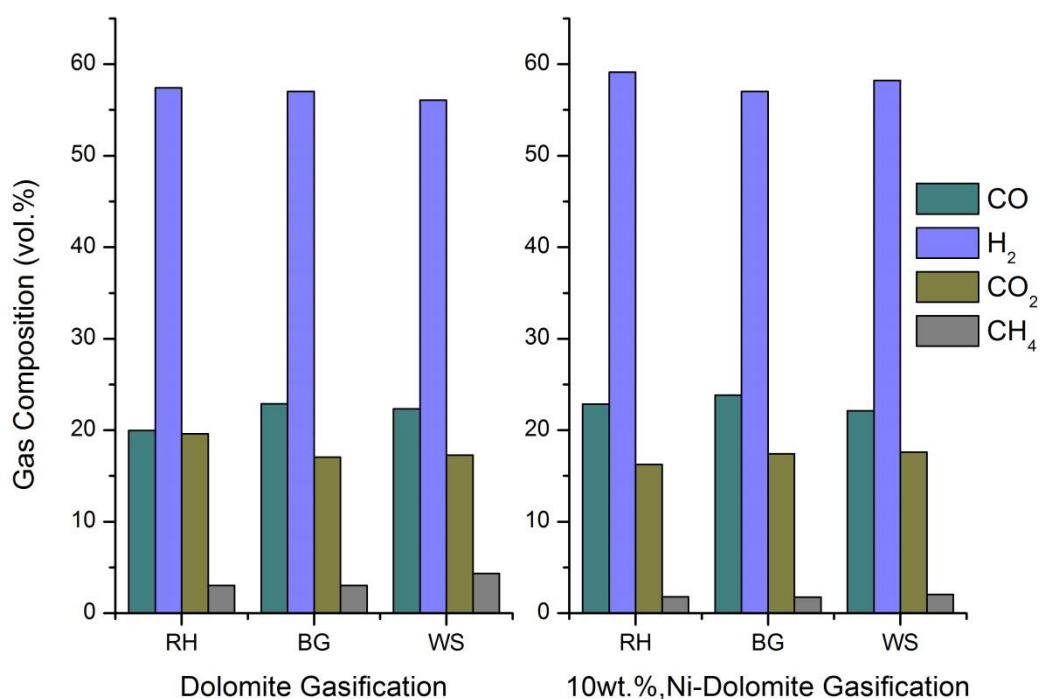


Figure 5-13 Syngas composition from dolomite catalytic steam gasification and 10 wt.% Ni-dolomite catalytic steam gasification of rice husk (RH), sugarcane bagasse (BG), and wheat straw (WS).

Corujo et al. [70] have also suggested that the increase in hydrogen concentration was due to the increase in overall gas yield due to thermal cracking of tar. Increase in CO concentration along with the decrease in CO₂ concentration might be due to the reverse water gas shift reaction. At high temperature, the equilibrium of the water gas shift reaction change towards the reactants. The reduction in CH₄ concentration can be explained due to the enhanced steam reforming reaction. Wang et al. [65] also reported a positive effect of addition of Ni onto modified dolomite. They reported that hydrogen concentration was enhanced from 36.60 vol.% for no catalyst to 43.32 vol.% for modified calcined dolomite and finally to 54.49 vol.% for 10 wt.% Ni impregnated onto calcined modified dolomite.

During steam gasification of forestry residue at 900 °C, Corujo et al. [70] indicated that addition of Ni into dolomite increased the hydrogen concentration in the gas mixture. The highest hydrogen concentration of 55.4 % was obtained using 1.6 wt.% Ni-

dolomite as compared to 46.2 % recovered from dolomite steam gasification. With the use of 1.6 wt.% Ni-dolomite, CO concentration was reduced from 33.2 % (for dolomite) to 17.8 %. Concentration of CO₂ was increased from 16.1 % for dolomite to 22.1 % for 1.6 wt.% Ni-dolomite. However the concentrations of CH₄ and other hydrocarbons remain unchanged. It was suggested that the increase in hydrogen concentration was due to the increase in total gas volume.

5.3.6 Characterization of reacted catalysts

Different characterization techniques such as temperature programmed oxidation (TPO), scanning electron microscopy (SEM), and transmission electron microscopy (TEM) were employed to characterize the reacted calcined dolomite and 10 wt.% Ni-dolomite for carbon deposition and other morphological changes.

The amount of carbon deposited on the catalyst was calculated using Equation (5-1).

$$w = \frac{(w_1 - w_2)}{w_1} \times 100 \text{ (wt. \%)} \quad (5-1)$$

Where w is the amount of deposited carbon on catalyst in wt.%, w_1 is the initial catalyst weight after moisture loss and w_2 is the final catalyst weight after oxidation.

For rice husk gasification, the amount of carbon deposited decreased from 5.66 wt.% to 1.33 wt.% when the catalyst was changed from dolomite to 10 wt.% Ni-dolomite. For bagasse, 10.13 wt.% carbon deposits were found on dolomite and 5.55 wt.% carbon was found on 10 wt.% Ni-dolomite. Similarly for wheat straw, 9.74 wt.% and 5.84 wt.% carbon deposits were found on dolomite and 10 wt.% Ni-dolomite respectively. It is evident from these results the addition of Ni in dolomite enhanced the catalytic activity at high temperature resulting in lower carbon deposition. TGA-TPO and DTG-TPO thermograms for reacted dolomite and 10 wt.% Ni-dolomite are shown in Figure 5-14. Two distinct peaks were observed from TGA-TPO profiles of both catalysts. The first peak around 425 °C can be assigned to the amorphous carbon [75] while the second peak found around 650 °C was most likely due to the presence of graphite carbon [76]. The presence of graphite carbon on the reacted 10 wt.% Ni-dolomite catalysts were evidenced from the TEM image shown in Figure 5-15. Similar graphite carbon patterns have been reported by Sehested et al. and Wang et al. [77, 78].

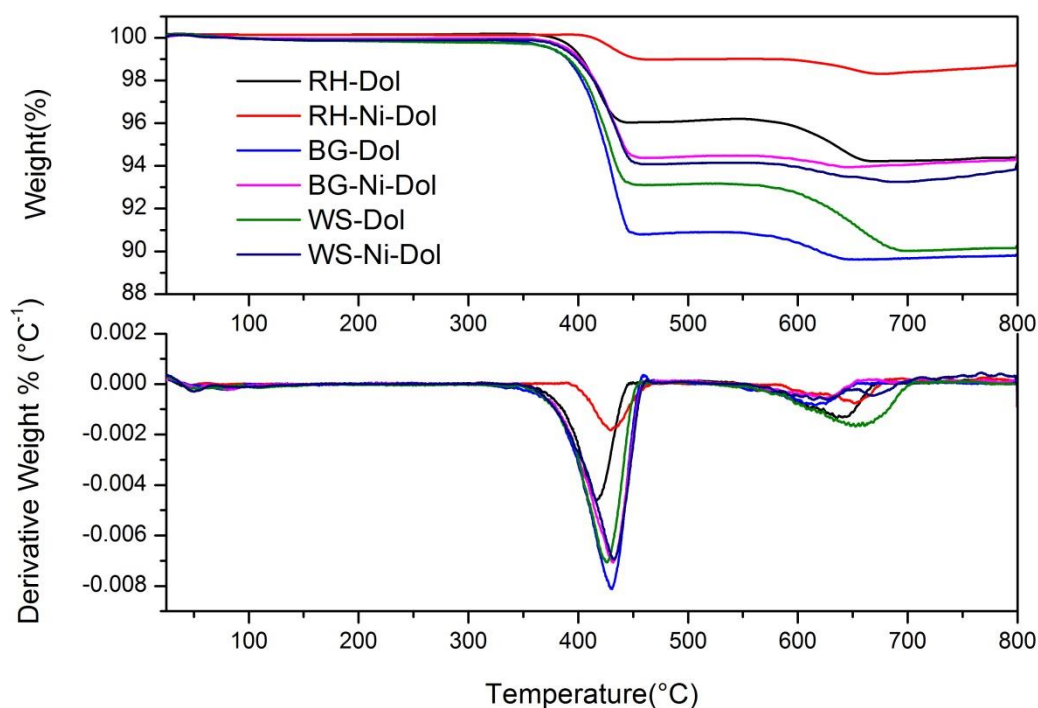


Figure 5-14 TGA-TPO and DTG-TPO results of reacted dolomite (DoI) and reacted 10 wt.% Ni-dolomite (Ni-DoI) catalysts during the catalytic steam gasification of rice husk (RH), bagasse (BG), and wheat straw (WS) at 950 °C.

Various researchers [79-81] have investigated the formation and morphology of deposited carbon on catalyst. It has been reported by Trimm et al. [82] that the deposition of carbon on the catalyst surface initiate with the dissociation of hydrocarbons derived from the pyrolysis/gasification of biomass; leading to the formation of highly reactive monoatomic carbon. This highly reactive carbon if not converted into CO can react with the Ni phase (produced from the in situ reduction of NiO phase) to form carbides which results in the formation of carbon whiskers by further dissolving and diffusing of reactive layered carbon into the Ni particles [83]. This process of deposition of layered carbon at the rear of the Ni particle results in the formation of filamentous carbon [81]. Further investigation of filamentous carbon formed were performed by Wang et al. [78]. It was suggested that filamentous carbon were consist of graphite sheets piled up in the shape of hollow cones. Similar findings have been reported [79, 81], showing the presence of Ni particles on the tip of the filamentous carbon.

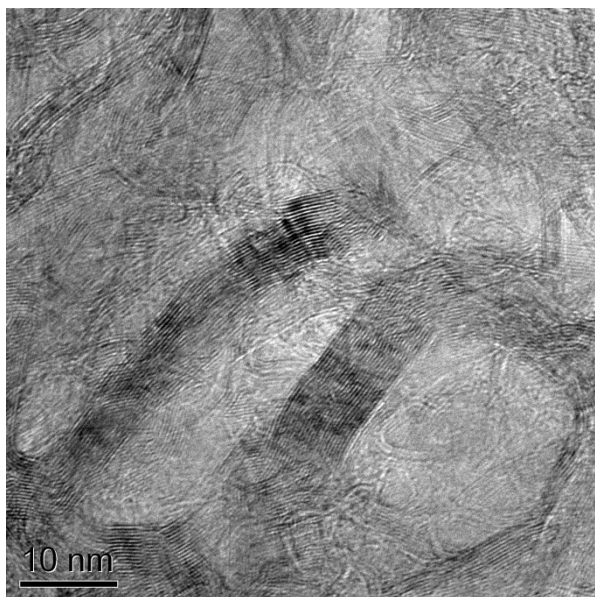


Figure 5-15 TEM image of reacted 10 wt.% Ni-dolomite (Ni-Dol) catalysts

5.3.7 Conclusions for section 5.3

In order to obtain high hydrogen yield, high temperature pyrolysis, steam gasification and catalytic steam gasification of rice husk, bagasse and wheat straw were performed in a two-stage fixed-bed reactor system. The following conclusions can be made from this study.

- Hydrogen yield increased dramatically from ~ 2 mmol g^{-1} for pyrolysis to ~ 21 mmol g^{-1} of biomass during two-stage pyrolysis/gasification in the presence of steam. This showed that the high temperature (950 °C) employed in this study was very promising as compared to conventional pyrolysis and gasification performed at lower temperatures.
- Use of calcined dolomite and 10 wt.% Ni-dolomite catalysts in the second stage further boosted gas yield and hydrogen yield. The highest hydrogen yield of 25.44 mmol g^{-1} of biomass was obtained from the pyrolysis/gasification of rice husk using 10 wt.% Ni-dolomite. The highest hydrogen concentration in the gas mixture was found to be 59.14 vol.%.
- The higher gas yield obtained in this study was primarily due to the higher temperature employed, leading to the thermal cracking of tar components and effective reforming of methane and other hydrocarbons thereby enhancing the hydrogen yield.
- Inexpensive and naturally abundant dolomite catalyst used in this study was characterized using TGA-TPO, SEM and TEM techniques. Significantly lower carbon deposits found on reacted 10 wt.% Ni-dolomite suggest that the high temperatures of pyrolysis/gasification has the potential to maintain the initial higher catalytic activity by suppressing the carbon formation and deposition on the catalyst.

5.4 The influence of process conditions on ultra-high temperature catalytic steam gasification of rice husk using 10 wt.% Ni-dolomite catalyst.

In the previous section, pyrolysis, steam gasification and catalytic steam gasification of rice husk, bagasse and wheat straw was performed to select the best suited process and biomass sample to produce hydrogen. It was found that the highest hydrogen yield was obtained from catalytic steam gasification of rice husk using 10 wt.% Ni-dolomite. In this section, the influence of various process conditions on two-stage catalytic pyrolysis/gasification of rice husk is investigated using 10 wt.% Ni-dolomite. Influence of temperature is investigated in section 5.4.1 while water injection rate is studied in section 5.4.2. Results from the effect of biomass particle size and catalyst to sample ratio are outlined in section 5.4.3 and 5.4.4 respectively. Finally the influence of carrier gas flow rate is reported in section 5.4.5.

5.4.1 The influence of gasification temperature

5.4.1.1 Product yield

Temperature is one of the most influential parameters affecting not only the gas yield but also the gas composition during pyrolysis and gasification [84]. In this study, the influence of temperature on product yield and gas composition during the two stage pyrolysis/gasification of rice husk was investigated. The temperature of the pyrolysis stage (top reactor) was kept constant at 950 °C while the temperature of the gasification stage (bottom reactor) was varied from 850 °C to 1050 °C with an increment of 50 °C. The gasification stage was first heated to the desired temperature and then the rice husk was pyrolysed in the first stage. In order to maximize the hydrogen yield; volatiles, liquids and tar evolving from the first stage were gasified in the second stage in the presence of steam using 10 wt.% Ni-dolomite as catalyst. The two-stage configuration was found to be very effective for high hydrogen yield with lower tar contents [54, 55]. Results from the influence of gasification temperature on product yield and hydrogen production are shown in Table 5-11.

Table 5-11 The effect of gasification temperature on pyrolysis-gasification of rice husk

	Temperature (°C)				
	850	900	950	1000	1050
Catalyst	10%Ni-Dolomite	10%Ni-Dolomite	10%Ni-Dolomite	10%Ni-Dolomite	10%Ni-Dolomite
Catalyst weight (g)	2	2	2	2	2
Particle size (mm)	1.4-2.8	1.4-2.8	1.4-2.8	1.4-2.8	1.4-2.8
Water injection (ml hr ⁻¹)	6	6	6	6	6
Nitrogen flow rate (ml min ⁻¹)	100	100	100	100	100
H ₂ (mmoles g ⁻¹ of biomass)	20.03	21.47	25.05	29.02	30.62
Mass balance (wt.%)					
Gas/(biomass+water)	23.29	24.83	26.30	27.99	26.62
Solid/(biomass+water)	12.13	12.96	13.02	13.34	13.56
Mass balance	98.75	96.02	96.65	95.62	92.93
Gas/(biomass)	60.49	60.33	63.64	67.66	61.84
Solid/(biomass)	31.50	31.50	31.50	32.25	31.50

From the results it is evident that with the increase in temperature, gas yield in relation to biomass + water increased from 23.29 wt.% at 850 °C to 26.62 wt.% at 1050 °C. However this increase in gas yield was not linear. Gas yield initially increased from 24.83 wt.% at 900 °C to 26.30 wt.% at 950 °C and to 27.99 wt.% at 1000 °C. However when the temperature was raised from 1000 °C to 1050 °C, the gas yield slightly decreased from 27.99 to 26.62 wt.%. Wang et al. [65] investigated the two-stage catalytic gasification of pig compost from 750 °C to 900 °C using Ni-modified dolomite. Gas yield linearly increased from 0.98 Nm³ kg⁻¹ at 750 °C to 1.33 Nm³ kg⁻¹ of feedstock at 900 °C. The increase in the gas yield with the increase in gasification temperature was primarily due to the thermal cracking of volatiles, liquids and steam reforming of higher hydrocarbons [85]. At higher temperature, the endothermic Boudouard reaction and water gas reaction also contributed towards the higher gas yield. Decarboxylation, depolymerization and thermal cracking reactions are also favoured with the increase in temperature [53].

The slight decrease in gas yield at the highest studied temperature of 1050 °C was most likely due to the series of complex repolymerization and condensation reactions favourable at temperature above 1000 °C [86, 87]. These condensation and repolymerization reactions lead to the formation of soot as considerable amount of soot was observed in the condenser system. The TGA-TPO and DTG-TPO results shown in Figure 5-18 indicate that the highest carbon deposits of 3.89 wt.% were found on the catalyst at 1050 °C. It has been suggested that above 1000 °C, the tertiary tars (PAHs), (even present in very small quantities) acted as a precursor for the formation of soot [88]. These polyaromatic hydrocarbon molecules grow into bigger aromatic complexes until they reach a critical weight, forming soot particles [86].

One of the major advantages of high temperature catalytic steam gasification used in this study was the enhanced gas and hydrogen yield with lower tar contents. It was reported [89] that as compared to olivine, the use of dolomite at higher temperature was more effective leading to a substantial decrease in all categories of tar compounds. Skoulou et al. [90] found a significant decrease in tar from 124.07g/Nm³ at 750 °C to 25.26 g/Nm³ at 1050 °C during the high temperature steam gasification of olive kernel. Although the concentration of tar reduced with the rise in temperature, it was noticed that at 1050 °C tar was mainly composed of light aromatic hydrocarbons with fraction

of polyaromatic hydrocarbons and heterocyclic compounds as compared to heavy tars found at 750 °C.

5.4.1.2 The influence of temperature on gas composition and hydrogen production

Hydrogen yield and concentration in the gaseous mixture increased with the rise in temperature. As shown in Table 5-11, hydrogen yield was enhanced linearly from 20.03 mmol g⁻¹ of rice husk at 850 °C to 30.62 mmol g⁻¹ at 1050 °C, however the major part of this increase was observed when the temperature was increased from 900 °C to 950 °C (21.47 to 25.05 mmol g⁻¹) and then from 950 °C to 1000 °C (25.05 to 29.02 mmol g⁻¹). González et al. [54] gasified olive cake biomass in a first reactor at 900 °C in the presence of steam. Volatiles, liquids and tar components were further gasified in a second reactor at 900 °C in the presence of dolomite. They reported 27.63 moles of hydrogen per kilogram of biomass.

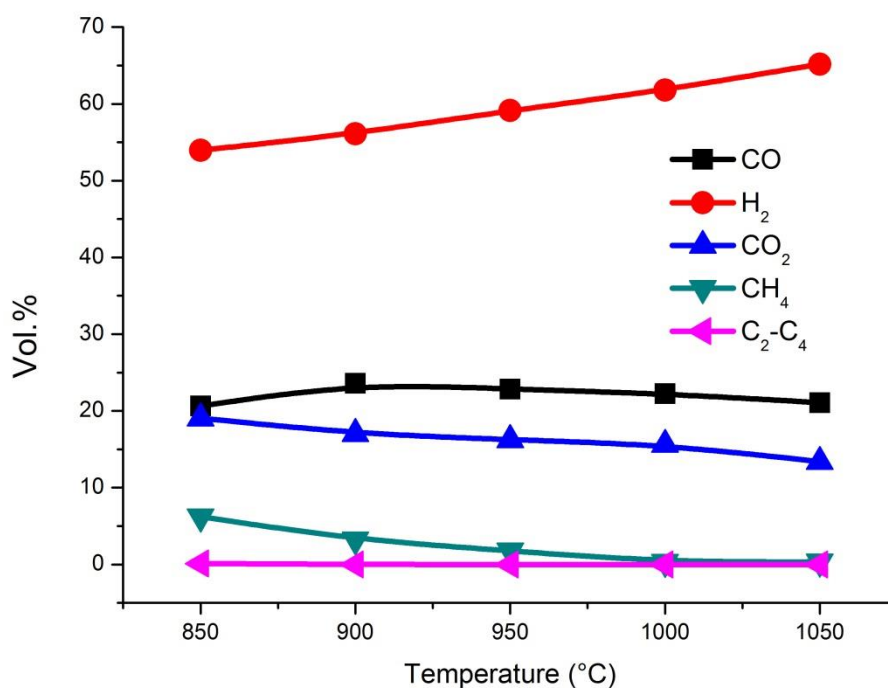


Figure 5-16 The effect of temperature on gas composition during the pyrolysis-gasification of rice husk

Hydrogen concentration in the gaseous mixture was also found to increase with temperature. It increased from 53.95 vol.% at 850 °C to 56.10 vol.% at 900 °C. Further increase in temperature leads to enhanced hydrogen concentration. At 950 °C, 59.14 vol.% while at 1000 °C, 61.80 vol.% and finally at 1050 °C, 65.18 vol.% of hydrogen was obtained. Results presented here are in agreement with the findings of González et al. [54], they reported around 52 vol.% of hydrogen from the two-stage gasification of olive cake at 900 °C. Skoulou et al. [90] performed steam gasification of olive kernel in a fixed bed gasifier. They also reported an increase in hydrogen gas concentration from less than 10 vol.% at 750 °C to ~42 vol.% at 1050 °C. Increase in hydrogen concentration with the rise in temperature can be explained by the fact that the higher temperature favours endothermic reactions (e.g. water gas reaction and Boudouard reaction) [84]. Steam reforming and dry reforming of methane and other higher hydrocarbons also contribute towards the higher hydrogen concentration. Thermal cracking of various tar components also lead to enhanced hydrogen yield at higher gasification temperatures [91].

As shown in Figure 5-16, the concentration of CO slightly increased from 20.64 vol.% at 850 °C to 21.08 vol.% at 1050 °C. A slight increase in CO concentration with the rise in temperature from 750 °C to 1050 °C was also reported by Skoulou et al. [90]. This increase was most likely due to the endothermic water gas, Boudouard reaction, steam methane reforming and thermal cracking of heavy tar components at elevated temperatures. It is also worth mentioning that the a major portion of produced CO was most likely to be consumed by the water gas shift reaction to produce hydrogen, however the extent of equilibrium of each reaction depends on many factors as various competing parallel reactions are taking place simultaneously in the gasifier. CO₂ concentration in the gaseous mixture gradually reduced from 19.06 vol.% at 850 °C to 13.38 vol.% at 1050 °C. This decrease in CO₂ concentration can be attributed to the endothermic Boudouard and dry reforming reactions favourable at higher temperatures [91]. CH₄ concentration also decreased from 6.22 vol.% at 850 °C to 0.35 vol.% at 1050 °C. This decrease was mainly due to the endothermic methane steam reforming reaction leading to the enhanced hydrogen and CO production. Only 0.12 vol.% lighter hydrocarbons (C₂-C₄) were detected at 850 °C. No C₂-C₄ hydrocarbons were detected at 900 °C or above. Similarly with the rise in temperature, a decrease in concentrations of

CH₄ and lighter hydrocarbons during the steam gasification of wood biomass was reported by Franco et al. [92].

The reacted 10 wt.% Ni-dolomite was characterized using TGA-TPO and SEM. In addition, BET surface area of fresh and reacted catalysts was also calculated. As shown in Table 5-12, compared to the surface area of fresh catalyst calcined at 900 °C, a gradual reduction in surface area with the increase in temperature was observed. Surface area was slightly reduced from 5.56 m² g⁻¹ for fresh calcined catalyst to 4.33 m² g⁻¹ at 850 °C. However, a loss of surface area to 1.94 m² g⁻¹ was observed at the gasification temperature of 1050 °C. This decrease in surface area was most likely due to the sintering of Ni particles on dolomite support. This effect was also evident from the comparison of SEM images (shown in Figure 5-17) of fresh and reacted catalysts at different gasification temperatures. Similar findings were reported by Sehested et al. [93] who investigated the sintering of 9.5 wt.% Ni-Al₂O₃ catalyst from 500 – 825 °C. They reported a decrease in surface area from 122 m² g⁻¹ at 500 °C to 84.8 m² g⁻¹ at 825 °C. Loss of surface area with the rise in temperature due to sintering was also reported in [94].

Table 5-12 The effect of temperature on BET surface area of reacted 10 wt.% Ni-dolomite

Catalyst	Reaction	BET surface
	Temperature	area
	(°C)	m ² g ⁻¹
Fresh 10% Ni-dolomite	-	5.56
Reacted 10% Ni-dolomite	850	4.33
Reacted 10% Ni-dolomite	1000	2.80
Reacted 10% Ni-dolomite	1050	1.94

Sintering is a complex process depending on various factors like temperature, time and atmosphere, nickel-support interaction. It has been reported [95] that the higher temperature and higher partial pressure of steam tend to promote sintering while increase in partial pressure of hydrogen showed an inhibitory effect on sintering of nickel [93]. It is widely accepted that the sintering of Ni particles follow one of the two

mechanisms namely particle migration and coalescence (PMC) and Ostwald ripening (OR) [77].

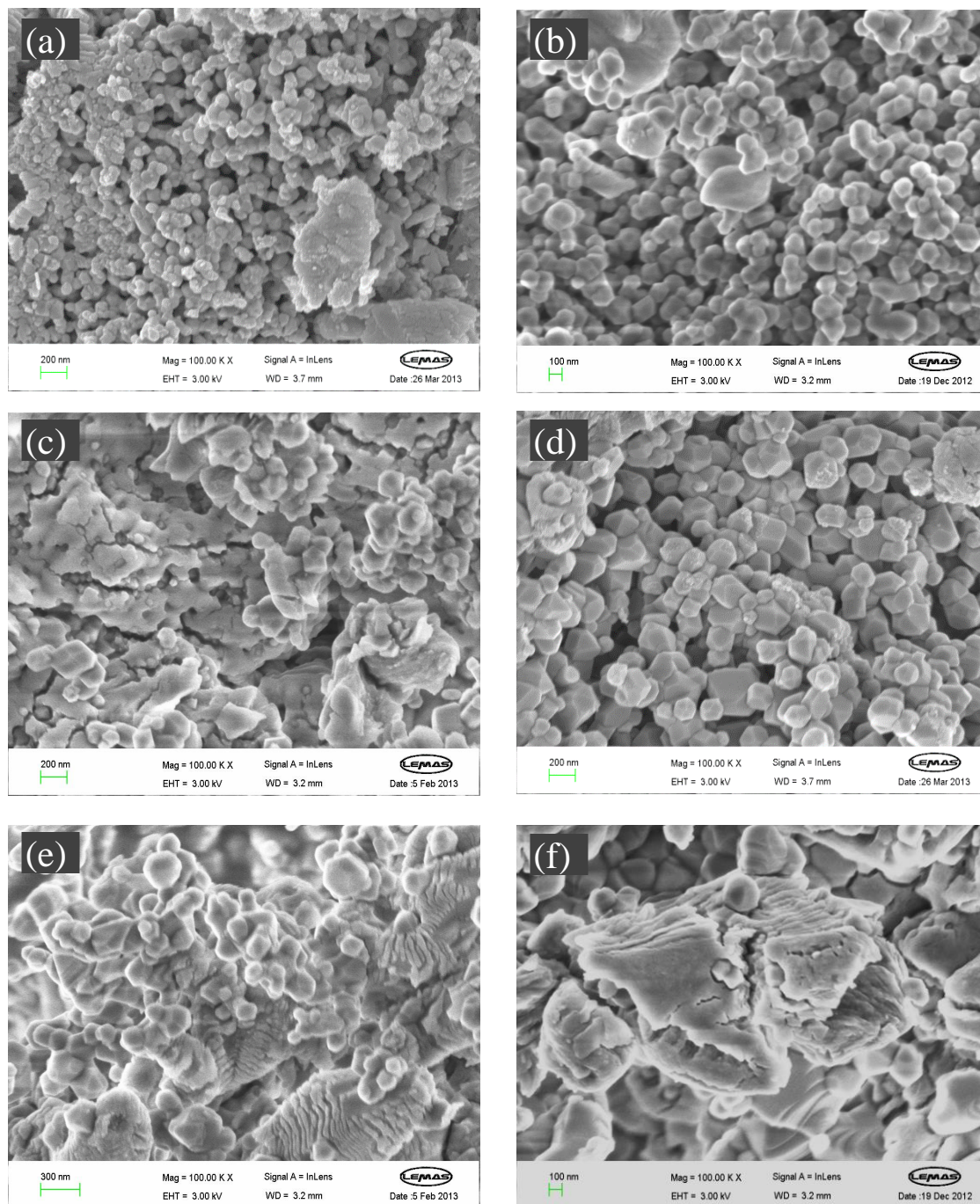


Figure 5-17 SEM images of fresh and reacted catalysts showing the effect of temperature (a) fresh 10 wt.% Ni-dolomite , (b) reacted 10 wt.% Ni-dolomite at 850 °C, (c) reacted at 900 °C, (d) reacted at 950 °C, (e) reacted at 1000 °C and (f) reacted at 1050 °C

During particle migration and coalescence, a Ni crystallite migrates over the support followed by coalescence whereas during Ostwald ripening (also known as atomic migration or vapour transport) is characterized by the absence of any translatory motion of Ni particles. Instead metal species emitted from one crystallite are captured by other crystallites via gas phase.

It has been suggested by Sehested et al. [77] that the increase in the rate of sintering at higher temperature was due to the change of sintering mechanism from particle migration to Ostwald ripening. Hansen et al. [96] used an in-situ TEM technique to investigate the mechanism of sintering of nanoparticles. They suggested the presence of three phases of sintering. During phase I, the catalyst rapidly lost its catalytic activity due to the Ostwald ripening mechanism. During phase II, slowdown of sintering was observed. They reported the combination of particle migration and Ostwald ripening was observed in this phase. During phase III, stable catalytic activity was observed after particle growth and support restructuring.

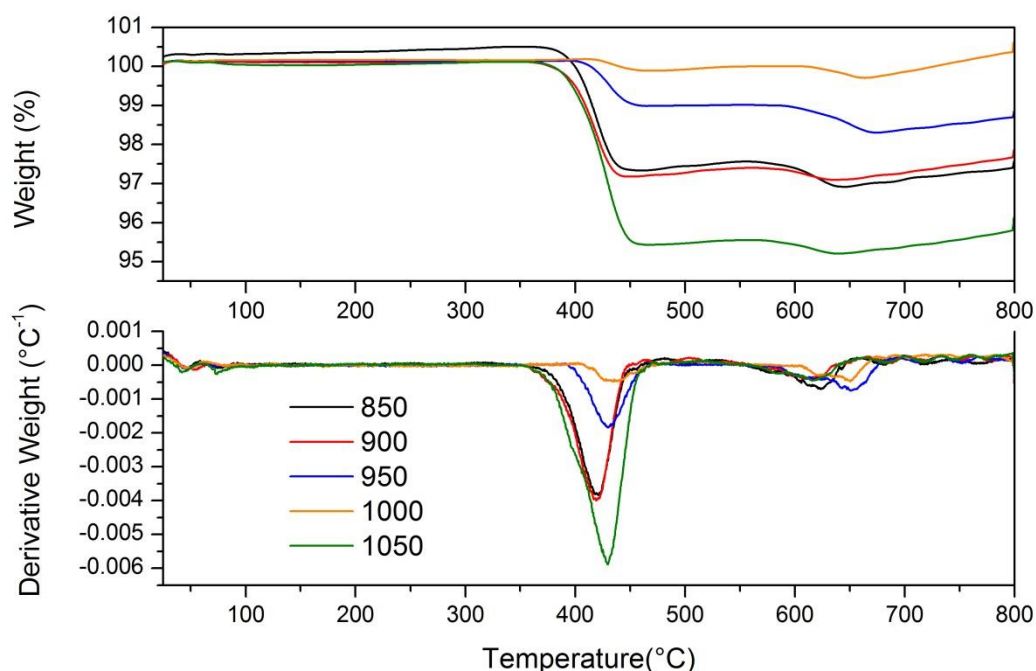


Figure 5-18 TGA-TPO and DTG-TPO results showing the effect of temperature on reacted 10 wt.% Ni-dolomite catalyst during the pyrolysis-gasification of rice husk

Reacted catalysts were characterized using TGA-TPO to investigate the amount of carbon deposition. It is evident from Figure 5-18, that the two-stage pyrolysis/gasification at high temperature was effective against coking of the catalyst. As indicated in Figure 5-18, maximum carbon deposition was only 3.89 wt.% at 1050 °C, compared to other studies where more than 30 wt.% of carbon deposition on catalyst was reported [97]. Except for 1050 °C, a gradual decrease in carbon deposition was noticed with the increase in temperature; from 2.46 wt.% at 850 °C to 2.16 wt.% at 900 °C, and finally to 1.17 wt.% at 950 °C. While no carbon deposits were detected for catalyst used at 1000 °C. This decrease in carbon deposition was most likely due to the enhanced endothermic Boudouard and water gas reactions at elevated temperature converting the carbon into gaseous species like carbon monoxide and carbon dioxide. The highest carbon deposition at 1050 °C was due to the recondensation and repolymerization reactions leading to the formation of soot. As shown in Figure 5-18, all catalyst showed two weight loss peaks; first peak around 430 °C while second higher temperature peak around 640 °C. It was suggested that the first peak was due to amorphous carbon [75] while the second peak was due to the presence of graphite carbon [76].

5.4.2 The effect of water/steam injection rate

5.4.2.1 Product yield

In this section, the influence of water injection rate on gas yield and hydrogen production was investigated using the two-stage pyrolysis/gasification reactor. Gasification stage was heated first. Once the desired temperature of 950 °C was achieved, then the rice husk sample was pyrolysed in the first stage along with the injection of steam into the second stage. During each experiment, 4 grams of biomass sample was pyrolysed while steam injection rate was varied from 2 ml hr⁻¹ to 10 ml hr⁻¹. Results of the influence of steam injection rate on product yield and hydrogen production are shown in Table 5-13.

Table 5-13 The influence of water injection rate on pyrolysis /gasification of rice husk

Sample	Water injection (ml hr ⁻¹)			
	2	4	6	10
Catalyst	Rice husk 10%Ni-Dolomite	Rice husk 10%Ni-Dolomite	Rice husk 10%Ni-Dolomite	Rice husk 10%Ni-Dolomite
Catalyst weight (g)	2	2	2	2
Particle size (mm)	1.4-2.8	1.4-2.8	1.4-2.8	1.4-2.8
Temperature (°C)	950	950	950	950
Nitrogen flow rate (ml min ⁻¹)	100	100	100	100
H ₂ (mmoles g ⁻¹ of biomass)	22.31	25.90	25.44	27.86
Mass balance (wt.%)				
Gas/(biomass+water)	42.49	33.40	26.30	18.62
Solid/(biomass+water)	22.41	16.54	13.02	9.06
Mass balance	96.63	91.41	96.65	95.64
Gas/(biomass)	61.61	63.63	63.64	64.23
Solid/(biomass)	32.50	31.50	31.50	31.25

From these results, it is evident that the gas yield in relation to biomass slightly increased with the increase in water injection rate. Gas yield increased from 61.61 wt.% for 2 ml hr⁻¹ to 64.23 wt.% for 10 ml hr⁻¹ water injection rate. Contrary to that, gas yield in relation to biomass + water reduced with the increase in water injection rate as more steam was available for the same quantity of biomass at higher water injection rates. Results presented here are in agreement with the findings of Xiao et al. [57] who performed the two-stage gasification of wood chips and pig compost in a fluidized bed reactor. They also reported an increase in gas yield with the increase in steam to carbon ratio. The decrease in tar contents was also reported in the literature as the steam to feedstock ratio was increased [98]. Meng et al. [99] also reported a declining trend for all classes of tar with the increase in steam to carbon ratio.

Higher gas yield with the increase in water injection rate was obtained as the higher water injection rates promote steam reforming of tar and other hydrocarbons leading to the higher gas yield [33, 57]. The water gas reaction was also thought to have played a role in enhancing gas yield. Hu et al. [100] investigated the influence of steam to biomass ratio (S/B) on gas yield from two stage gasification of apricot stones at 800 °C.

It was found that the hydrogen yield and hydrogen potential increased from S/B ratio of 0.4 - 0.8 however it decreased slightly with the increase in S/B ratio from 0.8 - 1.2. González et al. [54] also reported an increase in gas yield with the increase in steam flow rate during the two-stage gasification of olive cake.

5.4.2.2 The influence of water injection rate on gas composition and hydrogen production

The influence of water injection rate on gas composition is shown in Figure 5-19. It is clear that hydrogen concentration in the gas mixture increased with the increase in water injection rate. It increased from 56.29 vol.% to 61.88 vol.% with the increase in water injection rate from 2 ml hr⁻¹ to 10 ml hr⁻¹. Similarly the hydrogen yield shown in Table 5-13, significantly increased from 22.31 mmoles g⁻¹ of rice husk for 2 ml hr⁻¹ water injection rate to 27.86 mmoles g⁻¹ of rice husk for 10 ml hr⁻¹ water injection rate. Similar trends were reported in [57, 98]. This increase in hydrogen yield was most likely due to the water gas reaction, the water gas shift reaction, methane steam reforming reaction and steam reforming of tar components [101]. The concentration of CO decreased from 28.84 vol.% to 19.66 vol.% with the increase in water injection rate from 2 ml hr⁻¹ to 10 ml hr⁻¹, however, the concentration of CO₂ was enhanced slightly from 14.13 vol.% to 16.26 vol.%. This decrease in CO concentration along with the increase in CO₂ concentration was most likely due to the water gas shift reaction [54]. It is well known that the water gas shift reaction is slightly exothermic and production of hydrogen is not favoured at higher temperature, however according to the Le Chatelier's principle, the equilibrium can be shifted to favour hydrogen production by increasing the concentration of one of the reactants; in this case water injection rate. Karmakar et al. [102] investigated the effect of steam to biomass ratio on the steam gasification of rice husk at 750 °C. They reported an increase in hydrogen and CO₂ concentration along with the decrease in CO and CH₄ concentration when the steam to biomass ratio was varied from 0.6 to 1.70. Hydrogen concentration was found to be enhanced from 47.81 vol.% to 51.89 vol.% while CO concentration was reduced from 27.48 vol.% to 17.38 vol.%.

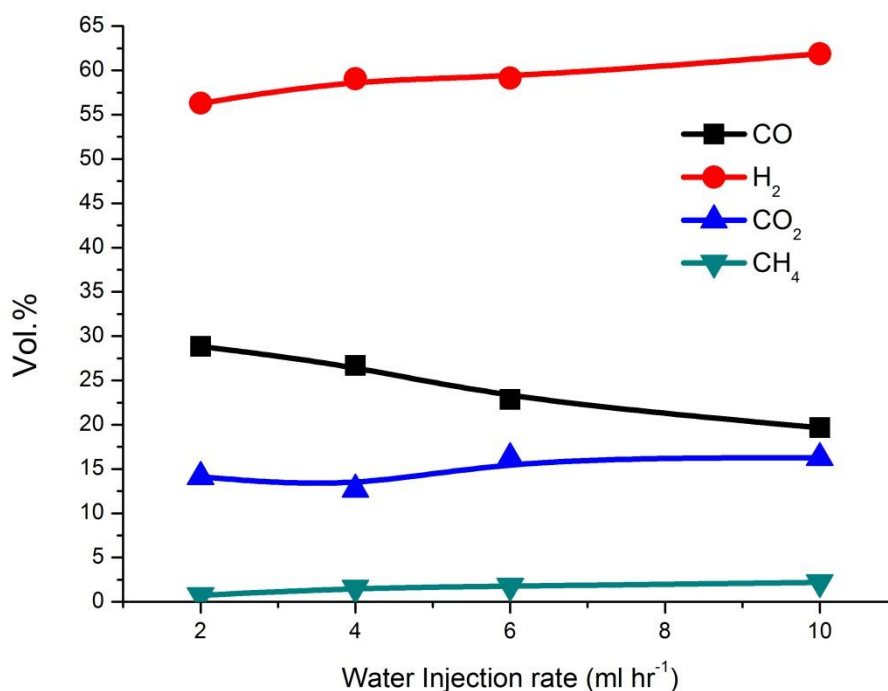


Figure 5-19 The effect of water injection rate on gas composition during the pyrolysis-gasification of rice husk

Contrary to the trends mentioned by some authors [57, 98], methane concentration was slightly increased from 0.74 vol.% to 2.20 vol.% when the water injection rate was increased from 2 ml hr⁻¹ to 10 ml hr⁻¹. This was most likely due to the methanation reaction forming methane from hydrogen available in the gaseous mixture [54, 92]. As the high temperature was employed in this study, no other hydrocarbons were detected. Franco et al. [92] studied the influence of steam to biomass ratio on gas yield and gas composition from the gasification of soft wood and hard wood. For their investigation, a bench scale fluidized bed was used at 800 °C. It was found that hydrogen yield was initially increased when the S/B ratio was increased from 0.5 to 0.7, however further increase in S/B ratio led to a slight reduction in hydrogen concentration. It was suggested that at lower S/B ratios, there was not enough steam to react with the biomass and hence to attain the equilibrium in gas mixture while at higher S/B ratios, it was speculated that the secondary water gas reaction might have resulted in the formation of hydrogen along with the CO₂.

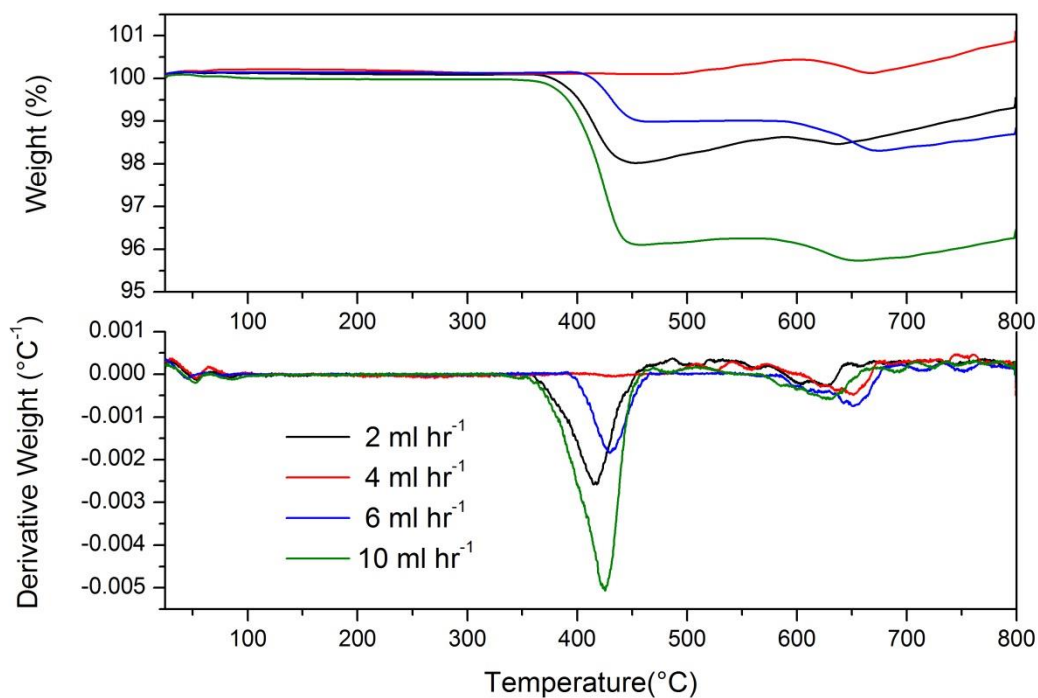


Figure 5-20 TGA-TPO and DTG-TPO results showing the effect of water injection rate on reacted 10 wt.% Ni-dolomite catalyst during the pyrolysis-gasification of rice husk

TGA-TPO and DTG-TPO curves showing the influence of water injection rate on reacted 10 wt.% Ni-dolomite are shown in Figure 5-20. From these results, it is evident that, in contrast to conventional gasification performed at relatively lower temperature, very little carbon deposits were found on the 10 wt.% Ni-dolomite catalyst [72]. As the amount of deposited carbon was very small, no deposits were visually observed from the SEM results shown in Figure 5-21. The amount of deposited coke was 0.46 wt.%, 0 wt.%, 1.17 wt.% and 3.54 wt.% for 2, 4, 6 and 10 ml hr⁻¹ respectively. It was noted that no carbon deposits were observed for 4 ml hr⁻¹ water injection rate however the amount of deposited carbon increased with the further increase in water injection rate. It was suggested that this coke formation at higher water injection rates was due to the lower residence time available to hydrocarbons [103].

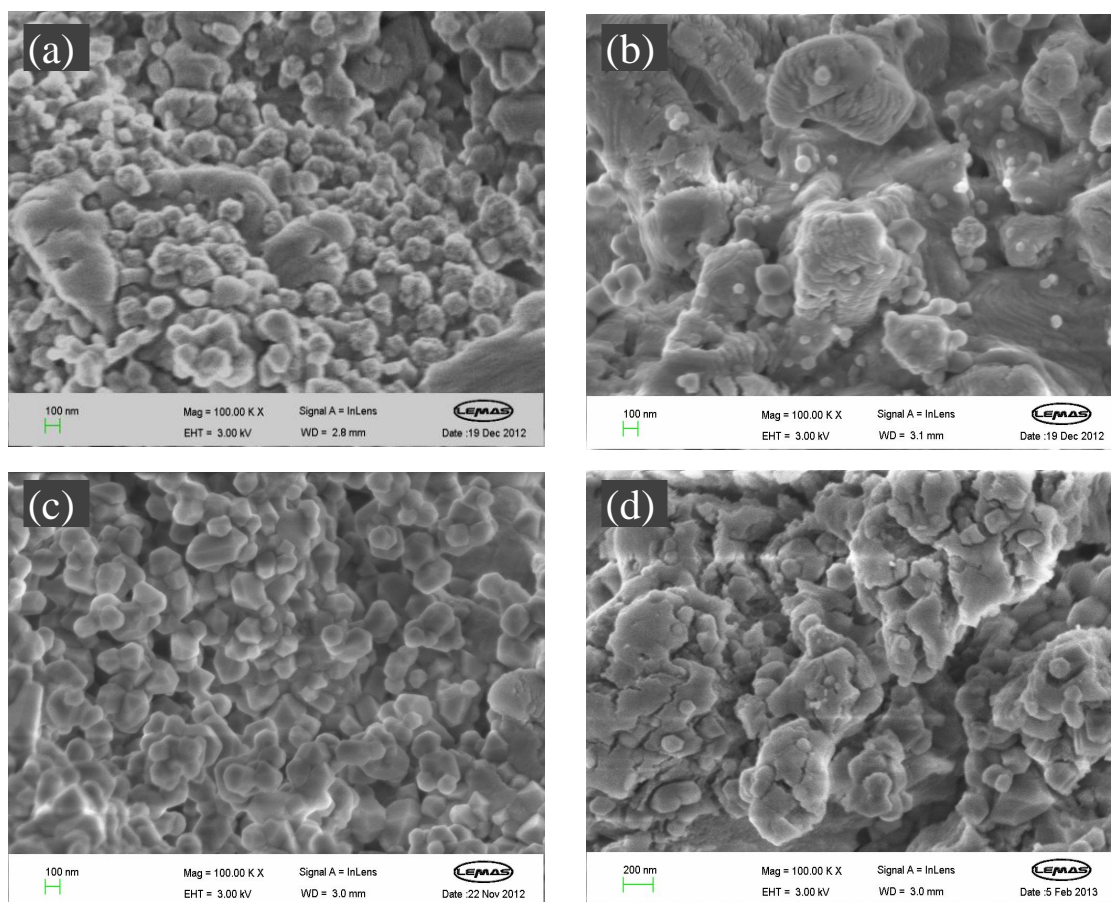


Figure 5-21 SEM images of reacted catalysts showing the effect of water injection rate (a) reacted 10 wt.% Ni-dolomite at 2 ml hr^{-1} , (b) at 4 ml hr^{-1} , (c) at 6 ml hr^{-1} and (d) at 10 ml hr^{-1}

From the DTG-TPO results shown in Figure 5-20, two oxidation peaks were observed. The second oxidation peak around $630 \text{ }^\circ\text{C}$ (most likely due to graphite carbon) was not affected by the water injection rate [104]. However the first oxidation peak observed around $430 \text{ }^\circ\text{C}$ (most likely due to amorphous carbon) was initially decreased at 2 ml hr^{-1} water injection rate to 4 ml hr^{-1} however with the further increase in water injection rate, higher carbon deposits were observed. It has been reported that compared to the aliphatic hydrocarbons, aromatic compounds have extremely higher tendency to form coke [105].

5.4.3 The influence of biomass particle size

5.4.3.1 Product yield

In this section, the influence of rice husk particle size on hydrogen production from two-stage pyrolysis/gasification was investigated. Four different particle size ranges; 212 - 500, 500 - 1000, 1405 - 2800 and 2800 - 3350 μm were obtained for this study. Results from the influence of particle size on product yield are shown in Table 5-14.

Table 5-14 The effect of particle size on pyrolysis-gasification of rice husk

Sample	Particle size (μm)			
	212-500	500-1000	1405-2800	2800-3350
	Rice husk	Rice husk	Rice husk	Rice husk
Catalyst	10%Ni-Dolomite	10%Ni-Dolomite	10%Ni-Dolomite	10%Ni-Dolomite
Catalyst weight (g)	2	2	2	2
Water injection rate (ml hr^{-1})	6	6	6	6
Temperature ($^{\circ}\text{C}$)	950	950	950	950
Nitrogen flow rate (ml min^{-1})	100	100	100	100
H_2 (mmoles g^{-1} of biomass)	29.13	26.74	25.44	25.05
Mass balance (wt.%)				
Gas/(biomass+water)	27.09	27.44	26.30	26.13
Solid/(biomass+water)	14.11	13.32	13.02	13.00
Mass balance	93.14	92.34	96.65	94.81
Gas/(biomass)	66.24	64.89	63.64	63.83
Solid/(biomass)	34.50	31.50	31.50	31.75

From the results shown in Table 5-14, it is evident that the gas yield in relation to biomass increased with the decrease in particle size. It enhanced from 63.83 wt.% for largest particle size range (2800 - 3350 μm) to 66.24 wt.% for smallest particle size range (212 - 500 μm). Similar findings are reported in the literature [106-108]. It was suggested [107] that this higher gas yield was due to the better mass and heat transfer which resulted from smaller particle diameter and larger surface area to volume ratio. The relatively larger surface area to volume ratio makes it easier for most volatiles to evolve, leaving behind very porous char particles. Due to this porous nature of char particles, gasification reactions take place throughout the particle instead of only at the

surface, hence the rate of reaction are controlled by chemical kinetic instead of heat and mass transfer [107]. It was mentioned by Babu et al. [109] that less time is required for the complete conversion of smaller particles. Li et al. [110] investigated the influence of particle size in a two-stage system. Gasification temperature was 800 °C while temperature of the catalyst bed was maintained at 850 °C. A steam to biomass ratio of 1.33 was used in their study. Four different groups of particle sizes; 5 - 2, 2 - 1, 1 - 0.15 and < 0.15 mm were investigated. It was reported that the gas yield increased from 2.16 to 2.41 m³ kg⁻¹ when the particle size was reduced from 5 mm to < 0.15 mm.

For larger particle sizes, gasification reactions are controlled by heat and mass transfer [111]. Greater heat resistance on these large particles creates a temperature gradient [112]. This temperature gradient causes the reactions to takes place only at the surface of the particle which results in more char and tar with lower carbon conversion efficiency. Hernández et al. [106] investigated the influence of particle size on gas yield and carbon conversion of marc (solid remains) of grapes using an entrained flow reactor. They reported higher fuel conversion for smaller particles. Fuel conversion was increased from 57.5 % for 8 mm particle size to 91.4 % for 0.5 mm particle size. It was suggested that the smaller particle size leads to the higher release of volatiles along with the better conversion of fixed carbon. Proximate analysis of char-ash residue indicated that the higher volatiles and fixed carbon contents were present in larger particle sizes of 8 mm while higher ash with the lowest fixed carbon and volatiles were obtained from the smallest particle size of 0.5 mm.

Luo et al. [107] investigated the effect of particle size and temperature on the steam gasification of pine sawdust in a laboratory-scale fixed bed reactor. They indicated that with the decrease in particle size, gas yield and carbon conversion efficiency increased. A decrease in tar and char contents was also reported. In their study, they plotted the influence of temperature on gas yield for each particle size. It was interesting to notice that for different particle sizes, the difference in gas yield was evident at lower temperature of 600 °C while these curves tended to merge at the higher temperature of 900 °C. It was suggested that this convergence was due to the increase in effective thermal conductivity at higher temperatures.

5.4.3.2 The influence of particle size on gas composition and hydrogen production

The results of gas composition from the influence of particle size on pyrolysis/gasification of rice husk are plotted in Figure 5-22. As shown in Figure 5-22, hydrogen concentration in the gas mixture was slightly improved from 59.45 vol.% for 2800 – 3350 μm particle size to 63.12 vol.% for 212 – 500 μm particle size, however hydrogen concentration increased from 60.44 vol.% for 500 – 1000 μm to 63.12 vol.% for 212 – 500 μm particle size range.

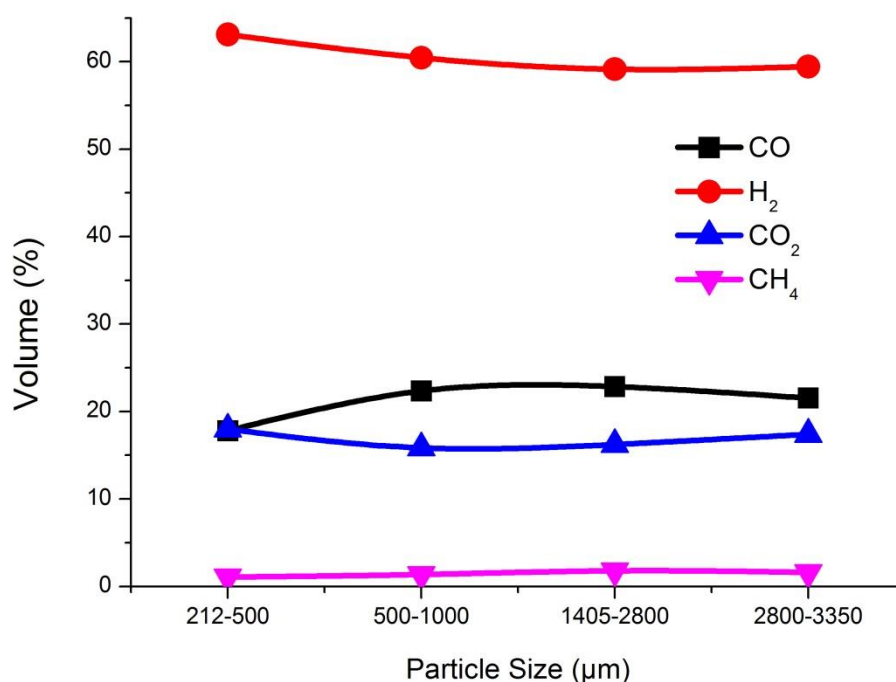


Figure 5-22 The influence of particle size on gas composition during the pyrolysis-gasification of rice husk

Hydrogen yield shown in Table 5-14, also followed the similar trend. Hydrogen yield was increased from 25.05 mmoles g^{-1} for largest particle size range (2800 - 3350 μm) to 29.13 mmoles g^{-1} for the smallest particle size range (212 - 500 μm). These results are in agreement with the findings of Luo et al. [107] and Hernández et al. [106]. Rapagnà et al. [113] performed the steam gasification of almond shell in a fluidized bed reactor. They also reported an increase in hydrogen concentration with the decrease in particle size. Luo et al. [107] reported an increase in hydrogen concentration with the decrease

in particle size. It was suggested that this increase in hydrogen concentration was due to the enhanced gas phase reaction due to the larger surface area to volume ratio of smaller particles. Other reactions such as the water gas shift reaction and water gas reaction also had played a significant role in improving hydrogen yield. It was suggested that the smaller biomass particles pyrolysed sufficiently and more volatiles were released [111].

Due to the higher temperature used in the current study, the influence of particle size on hydrogen production was not very evident. Zou et al. [114] also reported that during their investigations, particle size did not show a significant influence on a two stage pyrolysis gasification system.

When the particle size was reduced from 2800 - 3350 μm to 212 - 500 μm , the concentration of CO and CH₄ slightly reduced from 21.53 vol.% to 17.81 vol.% and from 1.62 vol.% to 1.08 vol.% respectively. Li et al. [110] also investigated the influence of particle size on gas composition during the two-stage pyrolysis/gasification of palm oil waste. They reported a slight decrease in CO and CH₄ concentrations with the decrease in particle size. The lower CO concentration of 17.81 vol.% along with the increase in hydrogen and CO₂ concentration for the smallest particle size range indicates the effectiveness of the water gas shift reaction. While the slight reduction in CH₄ concentration at higher temperature was most likely due to the methane steam reforming reaction [115].

5.4.4 The influence of catalyst to sample ratio

5.4.4.1 Product yield

In this section, the influence of catalyst to sample ratio (C/S) on hydrogen production and gas yield during two-stage pyrolysis/gasification of rice husk was investigated. Four catalysts to biomass ratios, 0.25, 0.5, 1.0 and 2.0 were researched in this study. During each experiment, 4 grams of rice husk was pyrolysed in the top reactor; heating up from ambient temperature to 950 °C at a constant heating rate of 20 °C min⁻¹. All the volatiles and gases evolved were gasified in the presence of steam and 10 wt.% Ni-dolomite catalyst, in the bottom stage reactor already at constant temperature of 950 °C. In order to investigate the effect of catalyst to biomass ratio, the mass of biomass sample was kept constant (4 grams) while the weight of catalyst present in the bottom stage was varied from 1 g, to 2 g, 4 g and to 8 g to obtain C/S ratios of 0.25, 0.5, 1.0 and 2.0

respectively. The product yield in relation to different catalyst to sample ratios is shown in Table 5-15. From the results shown in Table 5-15, it is noticed that the increase in catalyst to sample ratio from 0.25 to 2.0 does not have any appreciable influence on gas yield. For example, the gas yield in relation to biomass and water varied from 27.35 wt.% to 26.30 wt.% and to 26.47 wt.% and to 28.47 wt.%, when catalyst to sample ratio was increased from 0.25 to 0.5 and to 1.0 and to 2.0 respectively. Gas yield in relation to biomass also follow the similar trend. The gas yield in relation to biomass only, slightly varied from 66.20 wt.% for 0.25 C/S to 63.64 wt.% for C/S ratio of 0.5, to 63.53 wt.% for C/S ratio of 1.0 and to 67.69 wt.% for C/S ratio of 2.0.

Table 5-15 The effect of catalyst to sample ratio on pyrolysis-gasification of rice husk

	Catalyst to sample ratio (C/S)			
	0.25	0.5	1	2
Sample	rice husk	rice husk	rice husk	rice husk
Catalyst	10%Ni-Dolomite	10%Ni-Dolomite	10%Ni-Dolomite	10%Ni-Dolomite
Water injection rate (ml hr ⁻¹)	6	6	6	6
Particle size (µm)	1405-2800	1405-2800	1405-2800	1405-2800
Temperature (°C)	950	950	950	950
Nitrogen flow rate (ml min ⁻¹)	100	100	100	100
H ₂ (mmoles g ⁻¹ of biomass)	25.90	25.44	25.69	25.95
Mass balance (wt.%)				
Gas/(biomass+water)	27.35	26.30	26.47	28.47
Solid/(biomass+water)	13.12	13.02	13.13	13.56
Mass balance	94.71	96.65	95.54	99.24
Gas/(biomass)	66.20	63.64	63.53	67.69
Solid/(biomass)	31.75	31.50	31.50	32.25

It is suggested that unlike the other parameters e.g. temperature and water injection rate, under the studied conditions, catalyst to sample ratio does not seem to have a significant effect on gas yield perhaps due to higher temperatures used in this study. Results presented in this study are in agreements with the findings of Wu et al. [116] who researched the catalyst (Ni/CeO₂/Al₂O₃) to sample ratio of polypropylene using two-stage pyrolysis gasification reactor at 800 °C. They also reported slight variations in gas yield in relation to the weights of polypropylene and reacted water. Gas yield increased

from 90.10 wt.% for 0.25 catalyst to sample ratio to 91.90 for catalyst to sample ratio of 2.0.

Contrary to the trends observed in this study, Wang and colleagues [117] investigated the catalytic pyrolysis of douglas fir pellets in microwave reactor in the presence of ZSM-5 catalyst. Gas yield was found to be increased from 51.63 % to 55.90 % when catalyst to biomass ratio was increased from 1.32 to 4.68.

5.4.4.2 The influence of catalyst to sample ratio on gas composition and hydrogen production

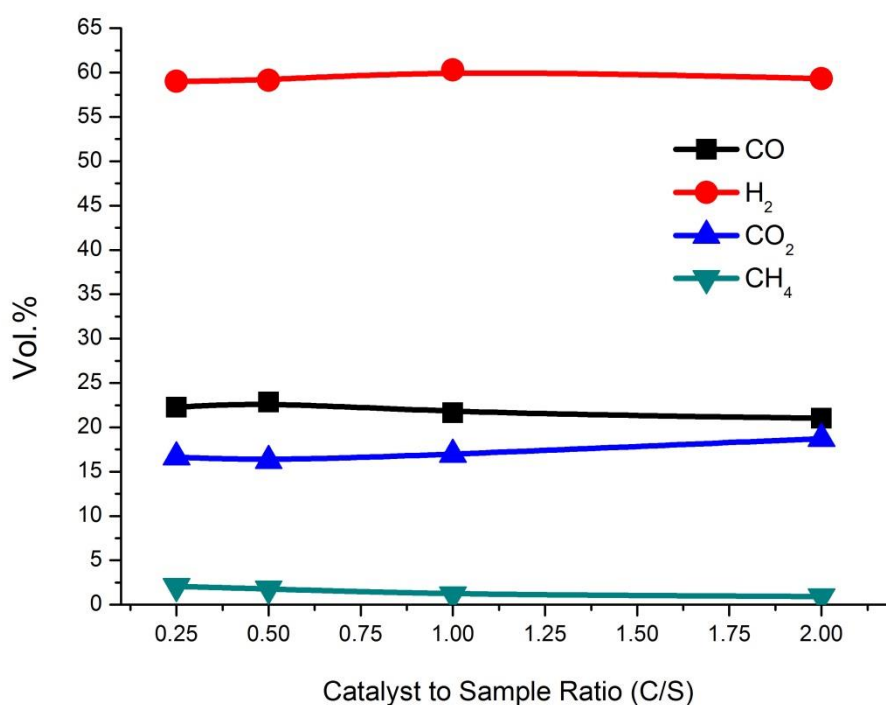


Figure 5-23 The effect of catalyst to sample ratio on gas composition during the pyrolysis-gasification of rice husk

The composition of gases derived from different catalyst to sample ratios during the pyrolysis/gasification of rice husk is shown in Figure 5-23. From these results, it is clear that gas composition varied slightly with the increase in catalyst to sample ratio. Hydrogen concentration was increased from 59 vol.% for C/S of 0.25 to 59.32 vol.% for C/S of 2.0, however the highest concentration of hydrogen (60.29 vol.%) was recovered using a C/S ratio of 1.0. A slight increase in hydrogen concentration with the increase in catalyst to sample ratio was also reported in [118].

Hydrogen gas yield results, shown in Table 5-15, were almost constant at ~26 mmoles g^{-1} with the increase in C/S ratio from 0.5 to 2.0. It is suggested that in this study, the combination of higher temperature (950 °C) along with the presence of steam and catalyst in the gasification stage provide effective environment to obtain higher hydrogen yield from biomass.

5.4.5 The influence of carrier gas flow rate

5.4.5.1 Product yield

The influence of carrier gas flow rate on product yield from the two-stage pyrolysis/gasification of rice husk was investigated. Four different flow rates of 50, 100, 200 and 400 ml min^{-1} were investigated. As the total volume of the reactor was 294.60 cm^3 , by increasing the carrier gas flow rate, residence time (reactor volume divided by the nitrogen volumetric flow rate) for all the volatiles, tars and gases was varied from 5.89 min for 50 ml min^{-1} to 2.95 min for 100 ml min^{-1} , to 1.47 min for 200 ml min^{-1} and finally to 0.74 min for a carrier gas flow rate of 400 ml min^{-1} .

Results from the influence of carrier gas (nitrogen) on product yield are shown in Table 5-16. It is clear that with the increase in carrier gas flow rate, gas yield in relation to biomass and water was almost constant at ~26 wt.%. Similar findings were reported by Onay et al. [40] who investigated the influence of carrier gas flow rate on product yield. It was noticed the gas yield was almost constant with the increase in carrier gas flow rate from 50 to 400 ml min^{-1} .

Table 5-16 The influence of carrier gas flow rate on pyrolysis-gasification of rice husk

Sample	Carrier gas flow rate (ml min ⁻¹)			
	50	100	200	400
	rice husk	rice husk	rice husk	rice husk
Catalyst	10%Ni-Dolomite	10%Ni-Dolomite	10%Ni-Dolomite	10%Ni-Dolomite
Catalyst weight (g)	2	2	2	2
Water injection (ml hr ⁻¹)	6	6	6	6
Particle size (µm)	1405-2800	1405-2800	1405-2800	1405-2800
Temperature (°C)	950	950	950	950
H ₂ (mmoles g ⁻¹ of biomass)	23.28	25.05	26.27	24.42
Mass balance (wt.%)				
Gas/(biomass+water)	23.71	26.30	26.86	25.85
Solid/(biomass+water)	12.30	13.02	13.66	12.54
Mass balance	90.80	96.65	94.43	93.85
Gas/(biomass)	60.70	63.64	64.40	64.42
Solid/(biomass)	31.50	31.50	32.75	31.25

5.4.5.2 The influence of carrier gas flow rate on gas composition and hydrogen production

The influence of carrier gas flow rate on gas composition was shown in Figure 5-24, As shown in Figure 5-24, in terms of hydrogen concentration, increasing the nitrogen flow rate does not showed any improvement in gas composition. The hydrogen concentration was fairly constant at ~59 vol.% for all nitrogen flow rates. Hydrogen production results (shown in Table 5-16) also showed similar behaviour. The amount of produced hydrogen was almost constant at around 25 mmoles g⁻¹ of rice husk sample. As shown in Figure 5-24, the concentration of other gases was also nearly constant for all the nitrogen flow rates researched in this study.

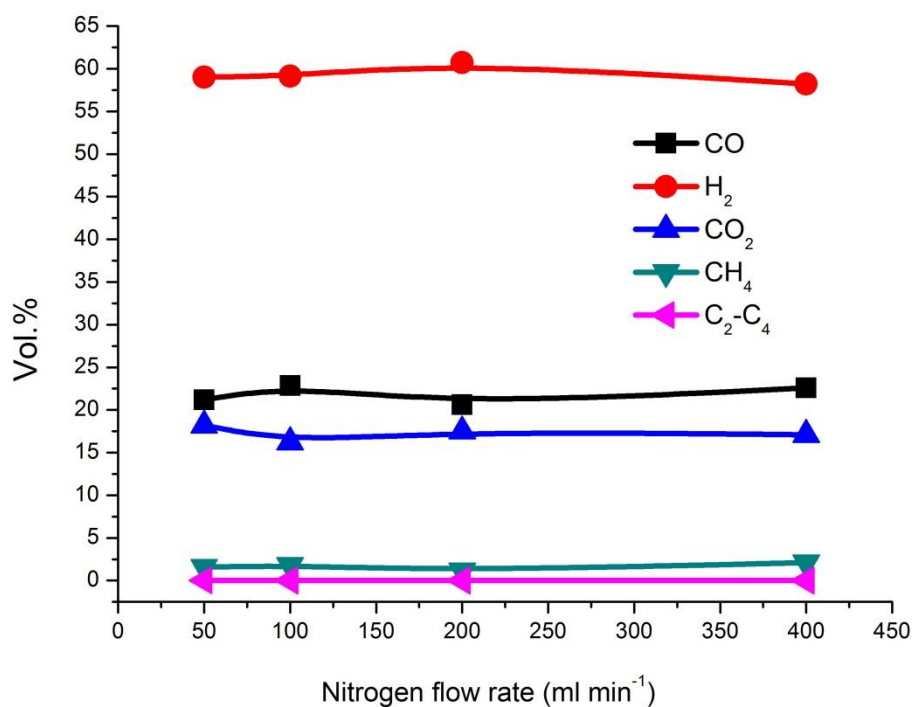


Figure 5-24 The effect of carrier gas flow rate on gas composition during the pyrolysis-gasification of rice husk

5.4.6 Conclusions for section 5.4

In this section, the influence of various process conditions such as temperature, water injection rate and catalyst to sample ratio on hydrogen production from the two-stage pyrolysis/gasification of rice husk was investigated. The following conclusions can be drawn from this study.

- With the increase in temperature from 850 °C to 1050 °C, hydrogen yield was significantly increased from 20.03 to 30.62 mmoles per gram of rice husk. Gas yield was also increased with the increase in temperature. Hydrogen concentration in the gas mixture was increased from 53.95 vol.% to 65.18 vol.%. A decrease in CH₄ and lighter hydrocarbons (C₂-C₄) concentration indicate the effectiveness of steam reforming and thermal cracking reactions at higher temperatures. The amount of deposited coke on the catalyst was also reduced from 2.46 wt.% for 850 °C to zero at 1000 °C except for 1050 °C where 3.89 wt.% of coke was observed perhaps due to the soot formation.

- With the increase in water injection rate from 2 ml hr⁻¹ to 10 ml hr⁻¹, hydrogen yield was considerably increased from 22.31 to 27.86 mmoles per gram of rice husk. Gas yield in relation to biomass was also increased from 61.61 wt.% to 64.23 wt.%. Hydrogen concentration in the gas mixture was also improved from 56.29 vol.% to 61.88 vol.%.
- The influence of biomass particle size on hydrogen production was also investigated. It was found that with the decrease in particle size from the range of 2800 - 3350 to 212 - 500 μm, hydrogen yield was improved from 25.05 to 29.13 mmoles per gram of rice husk. Gas yield was also increased with the decrease in biomass particle size. Hydrogen concentration in the gas mixture was increased from 59.45 vol.% to 63.12 vol.%. The concentration of CO and CH₄ were slightly reduced however CO₂ concentration was almost constant.
- No significant differences in hydrogen yield and gas yield were observed when C/S ratio was varied from 0.25 to 2.0. Hydrogen yield was almost constant at 26 mmoles per gram of rice husk. Hydrogen concentration was also constant around 60 vol.%. It was suggested that under the studied conditions of higher temperature in the presence of steam, even the small amount of catalyst was sufficient for effective gasification of volatiles.
- The carrier gas flow rate was varied from 50 to 400 ml min⁻¹. It was found that the nitrogen flow rate did not show any influence on gas yield as well as on hydrogen yield. The hydrogen yield was almost constant at ~25 mmoles g⁻¹ and gas yield in relation to biomass and water was also constant at ~26 wt.%.

5.5 Chapter references

- [1] K. Raveendran, A. Ganesh, and K. C. Khilar, "Influence of mineral matter on biomass pyrolysis characteristics," *Fuel*, vol. 74, pp. 1812-1822, 1995.
- [2] C. Wu, Z. Wang, V. Dupont, J. Huang, and P. T. Williams, "Nickel-catalysed pyrolysis/gasification of biomass components," *Journal of Analytical and Applied Pyrolysis*, vol. 99, pp. 143-148, 1// 2013.
- [3] P. T. Williams and S. Besler, "The pyrolysis of rice husks in a thermogravimetric analyser and static batch reactor," *Fuel*, vol. 72, pp. 151-159, 1993.
- [4] H. Yang, R. Yan, H. Chen, D. H. Lee, and C. Zheng, "Characteristics of hemicellulose, cellulose and lignin pyrolysis," *Fuel*, vol. 86, pp. 1781-1788, 2007.
- [5] K. Slopiecka, P. Bartocci, and F. Fantozzi, "Thermogravimetric analysis and kinetic study of poplar wood pyrolysis," *Applied Energy*.
- [6] S. S. Idris, N. A. Rahman, K. Ismail, A. B. Alias, Z. A. Rashid, and M. J. Aris, "Investigation on thermochemical behaviour of low rank Malaysian coal, oil palm biomass and their blends during pyrolysis via thermogravimetric analysis (TGA)," *Bioresource Technology*, vol. 101, pp. 4584-4592, 2010.
- [7] A. Ounas, A. Aboukhas, K. El harfi, A. Bacaoui, and A. Yaacoubi, "Pyrolysis of olive residue and sugar cane bagasse: Non-isothermal thermogravimetric kinetic analysis," *Bioresource Technology*, vol. 102, pp. 11234-11238, 2011.
- [8] E. Biagini, A. Fantei, and L. Tognotti, "Effect of the heating rate on the devolatilization of biomass residues," *Thermochimica Acta*, vol. 472, pp. 55-63, 2008.
- [9] M. Van de Velden, J. Baeyens, A. Brems, B. Janssens, and R. Dewil, "Fundamentals, kinetics and endothermicity of the biomass pyrolysis reaction," *Renewable Energy*, vol. 35, pp. 232-242, 2010.
- [10] A. O. Aboyade, T. J. Hugo, M. Carrier, E. L. Meyer, R. Stahl, J. H. Knoetze, *et al.*, "Non-isothermal kinetic analysis of the devolatilization of corn cobs and sugar cane bagasse in an inert atmosphere," *Thermochimica Acta*, vol. 517, pp. 81-89, 2011.
- [11] A. O. Aboyade, J. F. Görgens, M. Carrier, E. L. Meyer, and J. H. Knoetze, "Thermogravimetric study of the pyrolysis characteristics and kinetics of coal blends with corn and sugarcane residues," *Fuel Processing Technology*, vol. 106, pp. 310-320, 2013.
- [12] K. S. Shanmukharadhy and K. Ramachandran, "Thermal degradation behaviour of bagasse particles," *Journal of the Energy Institute*, vol. 82, pp. 120-122, 2009.
- [13] H. Lu, E. Ip, J. Scott, P. Foster, M. Vickers, and L. L. Baxter, "Effects of particle shape and size on devolatilization of biomass particle," *Fuel*, vol. 89, pp. 1156-1168, 2010.
- [14] T. Mani, P. Murugan, J. Abedi, and N. Mahinpey, "Pyrolysis of wheat straw in a thermogravimetric analyzer: Effect of particle size and heating rate on devolatilization and estimation of global kinetics," *Chemical Engineering Research and Design*, vol. 88, pp. 952-958, 2010.
- [15] E. Eftimie and E. Segal, "Basic language programs for automatic processing non-isothermal kinetic data," *Thermochimica Acta*, vol. 111, pp. 359-367, 1987.

- [16] I. I. Ahmed and A. K. Gupta, "Hydrogen production from polystyrene pyrolysis and gasification: Characteristics and kinetics," *International Journal of Hydrogen Energy*, vol. 34, pp. 6253-6264, 2009.
- [17] A. T. Harris and Z. Zhong, "Non-isothermal thermogravimetric analysis of plywood wastes under N₂, CO₂ and O₂ atmospheres," *Asia-Pacific Journal of Chemical Engineering*, vol. 3, pp. 473-480, 2008.
- [18] N. Y. Harun and M. T. Afzal, "Thermal Decomposition Kinetics of Forest Residue," *Journal of Applied Sciences*, vol. 10, pp. 1122-7, 2010.
- [19] P. Luangkiattikhun, C. Tangsathitkulchai, and M. Tangsathitkulchai, "Non-isothermal thermogravimetric analysis of oil-palm solid wastes," *Bioresource Technology*, vol. 99, pp. 986-997, 2008.
- [20] K. G. Mansaray and A. E. Ghaly, "Determination of kinetic parameters of rice husks in oxygen using thermogravimetric analysis," *Biomass and Bioenergy*, vol. 17, pp. 19-31, 1999.
- [21] A. Saddawi, J. M. Jones, A. Williams, and M. A. Wójtowicz, "Kinetics of the Thermal Decomposition of Biomass," *Energy & Fuels*, vol. 24, pp. 1274-1282, 2010/02/18 2009.
- [22] G. b. Várhegyi, H. Chen, and S. Godoy, "Thermal Decomposition of Wheat, Oat, Barley, and Brassica carinata Straws. A Kinetic Study," *Energy & Fuels*, vol. 23, pp. 646-652, 2009/02/19 2009.
- [23] S. S. Daood, S. Munir, W. Nimmo, and B. M. Gibbs, "Char oxidation study of sugar cane bagasse, cotton stalk and Pakistani coal under 1% and 3% oxygen concentrations," *Biomass and Bioenergy*, vol. 34, pp. 263-271, 2010.
- [24] A. S. Jamaluddin, "Estimation of kinetic parameters for char oxidation," *Fuel*, vol. 71, pp. 311-317, 3// 1992.
- [25] R. H. Hurt and J. M. Calo, "Semi-global intrinsic kinetics for char combustion modeling," *Combustion and Flame*, vol. 125, pp. 1138-1149, 5// 2001.
- [26] Z. Li, W. Zhao, B. Meng, C. Liu, Q. Zhu, and G. Zhao, "Kinetic study of corn straw pyrolysis: Comparison of two different three-pseudocomponent models," *Bioresource Technology*, vol. 99, pp. 7616-7622, 2008.
- [27] M. X. Xiaodong Zhang, Rongfeng Sun and Li Sun, "Study on Biomass Pyrolysis Kinetics," *Journal of Engineering for Gas Turbines and Power*, vol. 128, pp. 493-496, 2006.
- [28] K. Sasaki, X. Qiu, Y. Hosomomi, S. Moriyama, and T. Hirajima, "Effect of natural dolomite calcination temperature on sorption of borate onto calcined products," *Microporous and Mesoporous Materials*, vol. 171, pp. 1-8, 2013.
- [29] S. Lowell and J. Shields, "Adsorption isotherms," in *Powder Surface Area and Porosity*, ed: Springer Netherlands, 1984, pp. 11-13.
- [30] K. Sing, D. Everett;, R. Haul;, L. M. ;, R. P. ;, J. R. ;, *et al.*, "Reporting Physisorption data for Gas/Solid systems with Special Reference to the Determination of Surface Area and Porosity," *Pure and Applied Chemistry*, vol. 57, pp. 603-619, 1985.
- [31] B. Yoosuk, P. Udomsap, and B. Puttasawat, "Hydration–dehydration technique for property and activity improvement of calcined natural dolomite in heterogeneous biodiesel production: Structural transformation aspect," *Applied Catalysis A: General*, vol. 395, pp. 87-94, 2011.
- [32] É. Kristóf-Makó and A. Z. Juhász, "The effect of mechanical treatment on the crystal structure and thermal decomposition of dolomite," *Thermochimica Acta*, vol. 342, pp. 105-114, 1999.

- [33] J. Srinakruang, K. Sato, T. Vitidsant, and K. Fujimoto, "Highly efficient sulfur and coking resistance catalysts for tar gasification with steam," *Fuel*, vol. 85, pp. 2419-2426, 2006.
- [34] J. Srinakruang, K. Sato, T. Vitidsant, and K. Fujimoto, "A highly efficient catalyst for tar gasification with steam," *Catalysis Communications*, vol. 6, pp. 437-440, 2005.
- [35] M. S. Abu Bakar and J. O. Titiloye, "Catalytic pyrolysis of rice husk for bio-oil production," *Journal of Analytical and Applied Pyrolysis*.
- [36] Q. Sun, S. Yu, F. Wang, and J. Wang, "Decomposition and gasification of pyrolysis volatiles from pine wood through a bed of hot char," *Fuel*, vol. 90, pp. 1041-1048, 2011.
- [37] L. Burhenne, J. Messmer, T. Aicher, and M.-P. Laborie, "The effect of the biomass components lignin, cellulose and hemicellulose on TGA and fixed bed pyrolysis," *Journal of Analytical and Applied Pyrolysis*.
- [38] E. Kırtay, "Recent advances in production of hydrogen from biomass," *Energy Conversion and Management*, vol. 52, pp. 1778-1789, 2011.
- [39] O. Onay and O. Mete Koçkar, "Fixed-bed pyrolysis of rapeseed (*Brassica napus* L.)," *Biomass and Bioenergy*, vol. 26, pp. 289-299, 2004.
- [40] O. Onay and O. M. Kockar, "Slow, fast and flash pyrolysis of rapeseed," *Renewable Energy*, vol. 28, pp. 2417-2433, 2003.
- [41] M. García-Pérez, A. Chaala, and C. Roy, "Co-pyrolysis of sugarcane bagasse with petroleum residue. Part II. Product yields and properties," *Fuel*, vol. 81, pp. 893-907, 2002.
- [42] X. Xu, J. Enchen, W. Mingfeng, L. Bosong, and Z. Ling, "Hydrogen production by catalytic cracking of rice husk over Fe₂O₃/γ-Al₂O₃ catalyst," *Renewable Energy*, vol. 41, pp. 23-28, 5// 2012.
- [43] D. Neves, H. Thunman, A. Matos, L. Tarelho, and A. Gómez-Barea, "Characterization and prediction of biomass pyrolysis products," *Progress in Energy and Combustion Science*, vol. 37, pp. 611-630, 2011.
- [44] Y. Chen, H. Yang, X. Wang, S. Zhang, and H. Chen, "Biomass-based pyrolytic polygeneration system on cotton stalk pyrolysis: Influence of temperature," *Bioresource Technology*, vol. 107, pp. 411-418, 2012.
- [45] M. Becidan, Ø. Skreiberg, and J. E. Hustad, "Products distribution and gas release in pyrolysis of thermally thick biomass residues samples," *Journal of Analytical and Applied Pyrolysis*, vol. 78, pp. 207-213, 2007.
- [46] Luo, Wang, Liao, and Cen, "Mechanism Study of Cellulose Rapid Pyrolysis," *Industrial & Engineering Chemistry Research*, vol. 43, pp. 5605-5610, 2004/09/01 2004.
- [47] J. P. Diebold, "A unified, global model for the pyrolysis of cellulose," *Biomass and Bioenergy*, vol. 7, pp. 75-85, // 1994.
- [48] J. L. Banyasz, S. Li, J. Lyons-Hart, and K. H. Shafer, "Gas evolution and the mechanism of cellulose pyrolysis," *Fuel*, vol. 80, pp. 1757-1763, 10// 2001.
- [49] Y.-C. Lin, J. Cho, G. A. Tompsett, P. R. Westmoreland, and G. W. Huber, "Kinetics and Mechanism of Cellulose Pyrolysis," *The Journal of Physical Chemistry C*, vol. 113, pp. 20097-20107, 2009/11/19 2009.
- [50] M. Balat, "Mechanisms of Thermochemical Biomass Conversion Processes. Part 1: Reactions of Pyrolysis," *Energy Sources, Part A: Recovery, Utilization, and Environmental Effects*, vol. 30, pp. 620-635, 2008/03/03 2008.
- [51] E.-J. Shin, M. R. Nimlos, and R. J. Evans, "Kinetic analysis of the gas-phase pyrolysis of carbohydrates," *Fuel*, vol. 80, pp. 1697-1709, 10// 2001.

- [52] F. J. K. a. A. Broido, "Speculations on the nature of cellulose pyrolysis," *Pyro-dynamics*, vol. 2, pp. 151-163, 1965.
- [53] W. F. Fassinou, L. Van de Steene, S. Toure, G. Volle, and P. Girard, "Pyrolysis of Pinus pinaster in a two-stage gasifier: Influence of processing parameters and thermal cracking of tar," *Fuel Processing Technology*, vol. 90, pp. 75-90, 1// 2009.
- [54] J. F. González, S. Román, G. Engo, J. M. Encinar, and G. Martínez, "Reduction of tars by dolomite cracking during two-stage gasification of olive cake," *Biomass and Bioenergy*, vol. 35, pp. 4324-4330, 10/15/ 2011.
- [55] J. Šulc, J. Štojd, M. Richter, J. Popelka, K. Svoboda, J. Smetana, *et al.*, "Biomass waste gasification – Can be the two stage process suitable for tar reduction and power generation?," *Waste Management*, vol. 32, pp. 692-700, 4// 2012.
- [56] C. Wu, L. Wang, P. T. Williams, J. Shi, and J. Huang, "Hydrogen production from biomass gasification with Ni/MCM-41 catalysts: Influence of Ni content," *Applied Catalysis B: Environmental*, vol. 108–109, pp. 6-13, 10/11/ 2011.
- [57] X. Xiao, X. Meng, D. D. Le, and T. Takarada, "Two-stage steam gasification of waste biomass in fluidized bed at low temperature: Parametric investigations and performance optimization," *Bioresource Technology*, vol. 102, pp. 1975-1981, 1// 2011.
- [58] H. Yang, R. Yan, H. Chen, D. H. Lee, D. T. Liang, and C. Zheng, "Pyrolysis of palm oil wastes for enhanced production of hydrogen rich gases," *Fuel Processing Technology*, vol. 87, pp. 935-942, 2006.
- [59] J. Herguido, J. Corella, and J. Gonzalez-Saiz, "Steam gasification of lignocellulosic residues in a fluidized bed at a small pilot scale. Effect of the type of feedstock," *Industrial & Engineering Chemistry Research*, vol. 31, pp. 1274-1282, 1992/05/01 1992.
- [60] L. Devi, K. J. Ptasinski, and F. J. J. G. Janssen, "A review of the primary measures for tar elimination in biomass gasification processes," *Biomass and Bioenergy*, vol. 24, pp. 125-140, 2// 2003.
- [61] M. Balat, "Mechanisms of Thermochemical Biomass Conversion Processes. Part 2: Reactions of Gasification," *Energy Sources, Part A: Recovery, Utilization, and Environmental Effects*, vol. 30, pp. 636-648, 2008/03/03 2008.
- [62] I. I. Ahmed and A. K. Gupta, "Sugarcane bagasse gasification: Global reaction mechanism of syngas evolution," *Applied Energy*, vol. 91, pp. 75-81, 2012.
- [63] C. Xu, J. Donald, E. Byambajav, and Y. Ohtsuka, "Recent advances in catalysts for hot-gas removal of tar and NH₃ from biomass gasification," *Fuel*, vol. 89, pp. 1784-1795, 2010.
- [64] P. Simell, E. Kurkela, P. Ståhlberg, and J. Hepola, "Catalytic hot gas cleaning of gasification gas," *Catalysis Today*, vol. 27, pp. 55-62, 1996.
- [65] J. Wang, B. Xiao, S. Liu, Z. Hu, P. He, D. Guo, *et al.*, "Catalytic steam gasification of pig compost for hydrogen-rich gas production in a fixed bed reactor," *Bioresource Technology*.
- [66] J. Corella, J. Herguido, J. Gonzalez-Saiz, F. J. Alday, and J. L. Rodriguez-Trujillo, "Fluidized Bed Steam Gasification of Biomass with Dolomite and with a Commercial FCC Catalyst," in *Research in Thermochemical Biomass Conversion*, A. V. Bridgwater and J. L. Kuester, Eds., ed: Springer Netherlands, 1988, pp. 754-765.
- [67] A. Olivares, M. P. Aznar, M. A. Caballero, J. Gil, E. Francés, and J. Corella, "Biomass Gasification: Produced Gas Upgrading by In-Bed Use of Dolomite,"

- Industrial & Engineering Chemistry Research*, vol. 36, pp. 5220-5226, 1997/12/01 1997.
- [68] S. Rapagnà, N. Jand, and P. U. Foscolo, "Catalytic gasification of biomass to produce hydrogen rich gas," *International Journal of Hydrogen Energy*, vol. 23, pp. 551-557, 1998.
- [69] I. F. Elbaba and P. T. Williams, "High yield hydrogen from the pyrolysis-catalytic gasification of waste tyres with a nickel/dolomite catalyst," *Fuel*, vol. 106, pp. 528-536, 2013.
- [70] A. Corujo, L. Yermán, B. Arizaga, M. Brusoni, and J. Castiglioni, "Improved yield parameters in catalytic steam gasification of forestry residue; optimizing biomass feed rate and catalyst type," *Biomass and Bioenergy*, vol. 34, pp. 1695-1702, 2010.
- [71] P. H. Blanco, C. Wu, J. A. Onwudili, and P. T. Williams, "Characterization and evaluation of Ni/SiO₂ catalysts for hydrogen production and tar reduction from catalytic steam pyrolysis-reforming of RDF," *Applied Catalysis B: Environmental*.
- [72] I. F. Elbaba, C. Wu, and P. T. Williams, "Hydrogen production from the pyrolysis-gasification of waste tyres with a nickel/cerium catalyst," *International Journal of Hydrogen Energy*, vol. 36, pp. 6628-6637, 6// 2011.
- [73] C. Wu, Z. Wang, J. Huang, and P. T. Williams, "Pyrolysis/gasification of cellulose, hemicellulose and lignin for hydrogen production in the presence of various nickel-based catalysts," *Fuel*, vol. 106, pp. 697-706, 2013.
- [74] C. Wu and P. T. Williams, "A novel Ni-Mg-Al-CaO catalyst with the dual functions of catalysis and CO₂ sorption for H₂ production from the pyrolysis-gasification of polypropylene," *Fuel*, vol. 89, pp. 1435-1441, 7// 2010.
- [75] S. Wang, "A Comprehensive Study on Carbon Dioxide Reforming of Methane over Ni/ γ -Al₂O₃ Catalysts," *Industrial & Engineering Chemistry Research*, vol. 38, pp. 2615-2625, 1999/07/01 1999.
- [76] M. A. Goula, A. A. Lemonidou, and A. M. Efstathiou, "Characterization of Carbonaceous Species Formed during Reforming of CH₄ with CO₂ over Ni/CaO-Al₂O₃ Catalysts Studied by Various Transient Techniques," *Journal of Catalysis*, vol. 161, pp. 626-640, 1996.
- [77] J. Sehested, "Four challenges for nickel steam-reforming catalysts," *Catalysis Today*, vol. 111, pp. 103-110, 2006.
- [78] P. Wang, E. Tanabe, K. Ito, J. Jia, H. Morioka, T. Shishido, *et al.*, "Filamentous carbon prepared by the catalytic pyrolysis of CH₄ on Ni/SiO₂," *Applied Catalysis A: General*, vol. 231, pp. 35-44, 2002.
- [79] S. Natesakhawat, R. B. Watson, X. Wang, and U. S. Ozkan, "Deactivation characteristics of lanthanide-promoted sol-gel Ni/Al₂O₃ catalysts in propane steam reforming," *Journal of Catalysis*, vol. 234, pp. 496-508, 2005.
- [80] V. C. H. Kroll, H. M. Swaan, and C. Mirodatos, "Methane Reforming Reaction with Carbon Dioxide Over Ni/SiO₂ Catalyst: I. Deactivation Studies," *Journal of Catalysis*, vol. 161, pp. 409-422, 1996.
- [81] L. Kępiński, B. Stasińska, and T. Borowiecki, "Carbon deposition on Ni/Al₂O₃ catalysts doped with small amounts of molybdenum," *Carbon*, vol. 38, pp. 1845-1856, 2000.
- [82] D. L. Trimm, "Catalysts for the control of coking during steam reforming," *Catalysis Today*, vol. 49, pp. 3-10, 1999.
- [83] C. Wu and P. T. Williams, "Investigation of coke formation on Ni-Mg-Al catalyst for hydrogen production from the catalytic steam pyrolysis-gasification

- of polypropylene," *Applied Catalysis B: Environmental*, vol. 96, pp. 198-207, 4/26/ 2010.
- [84] L. Emami Taba, M. F. Irfan, W. A. M. Wan Daud, and M. H. Chakrabarti, "The effect of temperature on various parameters in coal, biomass and CO-gasification: A review," *Renewable and Sustainable Energy Reviews*, vol. 16, pp. 5584-5596, 2012.
- [85] Q. Xie, S. Kong, Y. Liu, and H. Zeng, "Syngas production by two-stage method of biomass catalytic pyrolysis and gasification," *Bioresource Technology*, vol. 110, pp. 603-609, 4// 2012.
- [86] S. Septien, S. Valin, C. Dupont, M. Peyrot, and S. Salvador, "Effect of particle size and temperature on woody biomass fast pyrolysis at high temperature (1000–1400°C)," *Fuel*, vol. 97, pp. 202-210, 2012.
- [87] K. Qin, W. Lin, P. A. Jensen, and A. D. Jensen, "High-temperature entrained flow gasification of biomass," *Fuel*, vol. 93, pp. 589-600, 2012.
- [88] J. J. Hernández, R. Ballesteros, and G. Aranda, "Characterisation of tars from biomass gasification: Effect of the operating conditions," *Energy*, vol. 50, pp. 333-342, 2013.
- [89] L. Devi, K. J. Ptasinski, F. J. J. G. Janssen, S. V. B. van Paasen, P. C. A. Bergman, and J. H. A. Kiel, "Catalytic decomposition of biomass tars: use of dolomite and untreated olivine," *Renewable Energy*, vol. 30, pp. 565-587, 2005.
- [90] V. Skoulou, A. Swiderski, W. Yang, and A. Zabaniotou, "Process characteristics and products of olive kernel high temperature steam gasification (HTSG)," *Bioresource Technology*, vol. 100, pp. 2444-2451, 2009.
- [91] P. Lahijani and Z. A. Zainal, "Gasification of palm empty fruit bunch in a bubbling fluidized bed: A performance and agglomeration study," *Bioresource Technology*, vol. 102, pp. 2068-2076, 2011.
- [92] C. Franco, F. Pinto, I. Gulyurtlu, and I. Cabrita, "The study of reactions influencing the biomass steam gasification process," *Fuel*, vol. 82, pp. 835-842, 2003.
- [93] J. Sehested, J. A. P. Gelten, I. N. Remediakis, H. Bengaard, and J. K. Nørskov, "Sintering of nickel steam-reforming catalysts: effects of temperature and steam and hydrogen pressures," *Journal of Catalysis*, vol. 223, pp. 432-443, 2004.
- [94] J. Sehested, "Sintering of nickel steam-reforming catalysts," *Journal of Catalysis*, vol. 217, pp. 417-426, 2003.
- [95] J. Sehested, J. A. P. Gelten, and S. Helveg, "Sintering of nickel catalysts: Effects of time, atmosphere, temperature, nickel-carrier interactions, and dopants," *Applied Catalysis A: General*, vol. 309, pp. 237-246, 2006.
- [96] T. W. Hansen, A. T. DeLaRiva, S. R. Challa, and A. K. Datye, "Sintering of Catalytic Nanoparticles: Particle Migration or Ostwald Ripening?," *Accounts of Chemical Research*, 2013.
- [97] I. F. Elbaba, C. Wu, and P. T. Williams, "Catalytic Pyrolysis-Gasification of Waste Tire and Tire Elastomers for Hydrogen Production," *Energy & Fuels*, vol. 24, pp. 3928-3935, 2010/07/15 2010.
- [98] X. Xiao, D. D. Le, K. Morishita, S. Zhang, L. Li, and T. Takarada, "Multi-stage biomass gasification in Internally Circulating Fluidized-bed Gasifier (ICFG): Test operation of animal-waste-derived biomass and parametric investigation at low temperature," *Fuel Processing Technology*, vol. 91, pp. 895-902, 2010.
- [99] X. Meng, W. de Jong, N. Fu, and A. H. M. Verkooijen, "Biomass gasification in a 100 kWth steam-oxygen blown circulating fluidized bed gasifier: Effects of

- operational conditions on product gas distribution and tar formation," *Biomass and Bioenergy*, vol. 35, pp. 2910-2924, 2011.
- [100] G. Hu, S. Xu, S. Li, C. Xiao, and S. Liu, "Steam gasification of apricot stones with olivine and dolomite as downstream catalysts," *Fuel Processing Technology*, vol. 87, pp. 375-382, 2006.
- [101] X. T. Li, J. R. Grace, C. J. Lim, A. P. Watkinson, H. P. Chen, and J. R. Kim, "Biomass gasification in a circulating fluidized bed," *Biomass and Bioenergy*, vol. 26, pp. 171-193, 2004.
- [102] M. K. Karmakar and A. B. Datta, "Generation of hydrogen rich gas through fluidized bed gasification of biomass," *Bioresource Technology*, vol. 102, pp. 1907-1913, 2011.
- [103] J. R. Rostrup-Nielsen, *Steam Reforming Catalysts*. Copenhagen: Danish Technical Press, 1975.
- [104] D. Duprez, M. C. DeMicheli, P. Marecot, J. Barbier, O. A. Ferretti, and E. N. Ponzi, "Deactivation of steam-reforming model catalysts by coke formation: I. Kinetics of the Formation of Filamentous Carbon in the Hydrogenolysis of cyclopentane on Ni/Al₂O₃ Catalysts," *Journal of Catalysis*, vol. 124, pp. 324-335, 1990.
- [105] I. F. Elbaba and P. T. Williams, "Two stage pyrolysis-catalytic gasification of waste tyres: Influence of process parameters," *Applied Catalysis B: Environmental*, vol. 125, pp. 136-143, 8/21/ 2012.
- [106] J. J. Hernández, G. Aranda-Almansa, and A. Bula, "Gasification of biomass wastes in an entrained flow gasifier: Effect of the particle size and the residence time," *Fuel Processing Technology*, vol. 91, pp. 681-692, 2010.
- [107] S. Luo, B. Xiao, X. Guo, Z. Hu, S. Liu, and M. He, "Hydrogen-rich gas from catalytic steam gasification of biomass in a fixed bed reactor: Influence of particle size on gasification performance," *International Journal of Hydrogen Energy*, vol. 34, pp. 1260-1264, 2009.
- [108] Y. Wang and C. M. Kinoshita, "Kinetic model of biomass gasification," *Solar Energy*, vol. 51, pp. 19-25, 1993.
- [109] B. V. Babu and A. S. Chaurasia, "Modeling for pyrolysis of solid particle: kinetics and heat transfer effects," *Energy Conversion and Management*, vol. 44, pp. 2251-2275, 2003.
- [110] J. Li, Y. Yin, X. Zhang, J. Liu, and R. Yan, "Hydrogen-rich gas production by steam gasification of palm oil wastes over supported tri-metallic catalyst," *International Journal of Hydrogen Energy*, vol. 34, pp. 9108-9115, 2009.
- [111] L. Wei, S. Xu, L. Zhang, H. Zhang, C. Liu, H. Zhu, *et al.*, "Characteristics of fast pyrolysis of biomass in a free fall reactor," *Fuel Processing Technology*, vol. 87, pp. 863-871, 2006.
- [112] J. M. Encinar, J. F. González, and J. González, "Steam gasification of *Cynara cardunculus* L.: influence of variables," *Fuel Processing Technology*, vol. 75, pp. 27-43, 2002.
- [113] S. Rapagnà and A. Latif, "Steam gasification of almond shells in a fluidised bed reactor: the influence of temperature and particle size on product yield and distribution," *Biomass and Bioenergy*, vol. 12, pp. 281-288, 1997.
- [114] W. Zou, C. Song, S. Xu, C. Lu, and Y. Tursun, "Biomass gasification in an external circulating countercurrent moving bed gasifier," *Fuel*.
- [115] R. Yin, R. Liu, J. Wu, X. Wu, C. Sun, and C. Wu, "Influence of particle size on performance of a pilot-scale fixed-bed gasification system," *Bioresource Technology*, vol. 119, pp. 15-21, 2012.

- [116] C. Wu and P. T. Williams, "Effects of Gasification Temperature and Catalyst Ratio on Hydrogen Production from Catalytic Steam Pyrolysis-Gasification of Polypropylene," *Energy & Fuels*, vol. 22, pp. 4125-4132, 2008/11/19 2008.
- [117] L. Wang, H. Lei, S. Ren, Q. Bu, J. Liang, Y. Wei, *et al.*, "Aromatics and phenols from catalytic pyrolysis of Douglas fir pellets in microwave with ZSM-5 as a catalyst," *Journal of Analytical and Applied Pyrolysis*, vol. 98, pp. 194-200, 2012.
- [118] C. Wu and P. T. Williams, "Pyrolysis–gasification of post-consumer municipal solid plastic waste for hydrogen production," *International Journal of Hydrogen Energy*, vol. 35, pp. 949-957, 2// 2010.

CHAPTER 6 CATALYST SELECTION & PYROLYSIS/GASIFICATION OF BAGASSE

6.1 Introduction

Sugarcane bagasse is one of the major biomass wastes in sugarcane producing countries. As mentioned in chapter 3, the proximate analysis of the three biomasses; rice husk, bagasse and wheat straw showed that the bagasse contains the highest volatiles with the lowest ash contents. This makes it a perfect biomass for production of hydrogen from pyrolysis/gasification. In this chapter, two-stage pyrolysis/gasification of bagasse was carried out with the aim to obtain higher hydrogen yield. In the two-stage process, bagasse was pyrolysed at 950 °C in the first stage. Volatiles, liquids and tar components evolving from the first stage were gasified in the presence of steam and catalyst at higher temperature from 950 - 1000 °C.

Several Ni-based catalysts were prepared in the laboratory and tested for the production of hydrogen. Fresh and reacted catalysts were characterized for catalytic activity and stability using various techniques including scanning electron microscope (SEM), transmission electron microscope (TEM), and X-ray diffraction (XRD). The surface properties of fresh and reacted catalysts were also investigated using nitrogen adsorption/desorption at 77 K. The best performing catalyst was chosen based on the highest quantity of hydrogen produced for further investigation. In order to enhance the catalytic activity and stability, the influence of Ni-loading and calcination temperature on the catalyst was also investigated. The influence of process conditions i.e. gasification temperature, water injection rate and catalyst to biomass sample ratio (C/S) on hydrogen production was also investigated in this chapter.

The catalyst selection from various Ni-based catalysts included Ni-dolomite, Ni-MgO, Ni-SiO₂, Ni-Al₂O₃, and Ni-Ce-dolomite is outlined in section 6.2. The influence of gasification temperature and Ni-loading is reported in section 6.3 and section 6.4 respectively. The influence of water injection rate from 6 - 35ml hr⁻¹ is explained in section 6.5. The effect of calcination temperature and catalyst to sample ratio is mentioned in section 6.6 and 6.7.

6.2 Catalyst selection for hydrogen production from pyrolysis-gasification of sugarcane bagasse

In this section, seven different Ni-based catalysts; Ni-dolomite, Ni-MgO, Ni-SiO₂, Ni-Al₂O₃, 2 wt.% Ce - Ni-dolomite, 5 wt.% Ce - Ni-dolomite and 10 wt.% Ce - Ni-dolomite were prepared in the laboratory by wet impregnation method. The Ni contents in all these catalysts were kept constant at 10 wt.%. All the catalysts were dried overnight at 105 °C and were calcined at 900 °C for 3 hours in an air environment. All these catalysts were then grinded and sieved to achieve the particle size between 50 - 212 µm.

6.2.1 Characterisation of the fresh researched catalysts

Surface properties of selected fresh catalysts are outlined in Table 6-1. It is evident that the 10 wt.% Ni-Al₂O₃ showed the highest BET surface area of 76.82 m² g⁻¹. Similar surface area of 77 m² g⁻¹ for 10 wt.% Ni-Al₂O₃ calcined at 900 °C was reported by Darvell et al. [1]. The 10 wt.% Ni-MgO catalyst also showed significantly higher surface area of 53.9 m² g⁻¹. The other catalysts like 10 wt.% Ni-dolomite, 10 wt.% Ni-SiO₂ and 2 wt.% Ce – 10 wt.% Ni-dolomite showed lower surface area of less than 10 m² g⁻¹.

Table 6-1 Surface properties of fresh catalysts

Fresh Catalyst	BET surface area	BJH pore volume	Average pore size
	m ² g ⁻¹	cm ³ g ⁻¹	nm
10% Ni-Al ₂ O ₃	76.82	0.2792	5.64
10% Ni-dolomite	5.56	0.0308	3.78
2%Ce-10% Ni-dolomite	7.37	0.0229	2.96
10% Ni-MgO	53.90	0.3939	36.08
10% Ni-SiO ₂	8.16	0.0253	2.17

Average pore size and pore volume results shown in Table 6-1 also indicate that the 10 wt.% Ni-MgO has the largest pores resulting in the highest pore volume. The 10 wt.% Ni-Al₂O₃ catalyst, on the other hand, also showed significantly larger pore volume but the average pore size was significantly smaller (5.64 nm) as compared to 36.08 nm for

10 wt.% Ni-MgO. This suggests that the Al₂O₃ support used in the 10 wt.% Ni-Al₂O₃ catalyst is highly porous as compared to the other catalysts. The pore size distribution results presented in Figure 6-1 also confirm the highly porous nature of the 10 wt.% Ni-Al₂O₃ catalyst by indicating the presence of a larger proportion of smaller diameter pores in the range of 4 - 7 nm. The pore size distribution curve for 10 wt.% Ni-MgO indicates the presence of relatively larger pores. The other catalysts showed very little porosity as compared to these two catalysts.

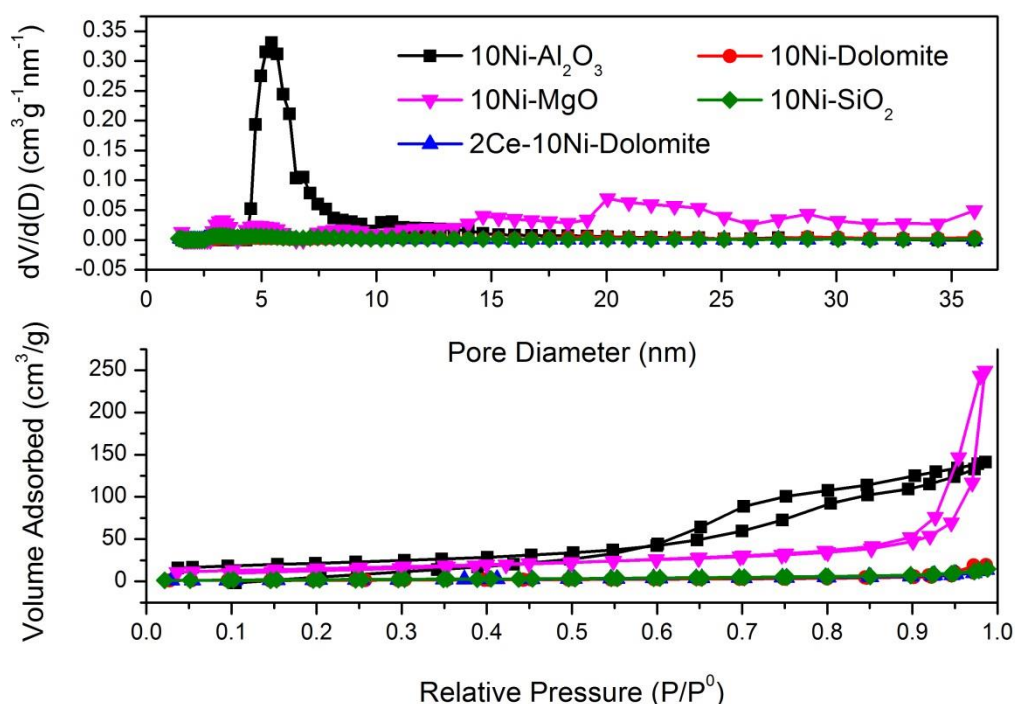


Figure 6-1 Pore size distribution (a), and N₂ adsorption/desorption isotherms of the fresh catalysts (b)

The N₂ adsorption/desorption results for different freshly prepared catalysts are presented in Figure 6-1. These adsorption/desorption curves conform to one of the six types proposed by the IUPAC classification system [2]. It was found that the 10 wt.% Ni-Al₂O₃ catalyst showed the type IV isotherm. A hysteresis loop (adsorption-desorption hysteresis) is observed at higher relative pressure. The presence of a hysteresis loop indicates that the evaporation of N₂ from a pore is a different process from the condensation in it [3]. From the IUPAC classification, type H4 hysteresis loop

was assigned to this isotherm which is the characteristics of adsorbent containing slit shape pores mainly in the micropores range. This hysteresis loop is associated with the capillary condensation in mesopore structures. The 10 wt.% Ni-MgO catalyst showed type V isotherm indicating the presence of type H1 hysteresis loop. This suggests that the cylindrical shape channels with narrow distribution of uniform pores were present in this catalyst [4].

As an initial investigation, each one of these catalysts was mixed with the bagasse (at catalyst to sample ratio of 0.5) and the influence of every catalyst on bagasse thermal degradation was investigated using thermogravimetric analysis (TGA). The weight loss in relation to temperature in a nitrogen environment was determined using TGA. The results of weight loss in relation to temperature are shown in Figure 6-2. As indicated in Figure 6-2, the 10 wt.% Ni-Al₂O₃ catalyst considerably promoted the thermal degradation of bagasse as compared to the other catalysts. The relatively better performance of the 10 wt.% Ni-Al₂O₃ catalyst was perhaps due to its highly porous nature and well dispersed Ni phase. The other catalysts showed little influence on thermal degradation of sugarcane bagasse under the particular experimental conditions of the thermogravimetric analyser.

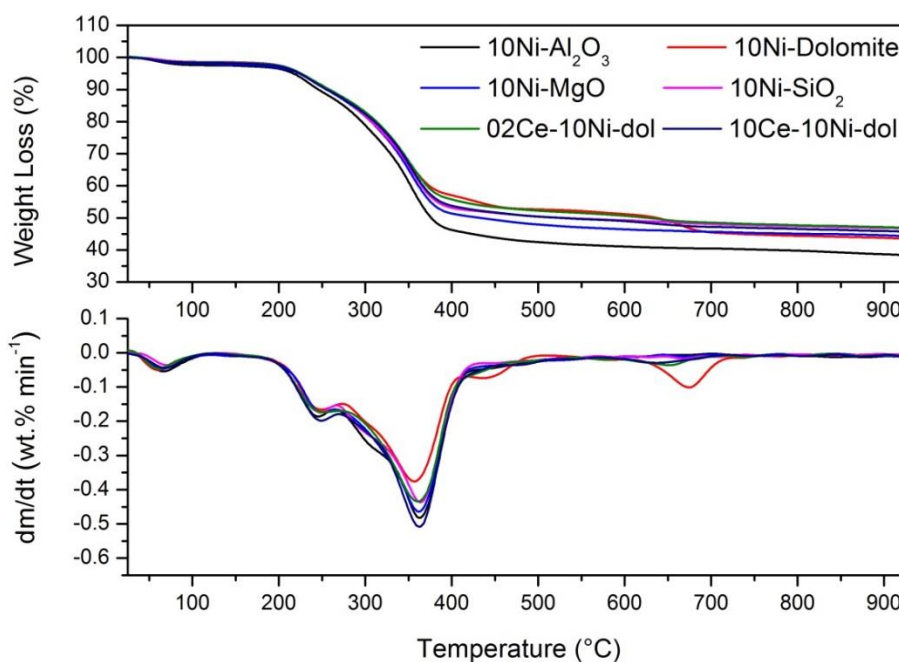


Figure 6-2 TGA results for mixture of bagasse and each produced catalyst

6.2.2 Product yield

The influence of different catalysts on hydrogen production from the two-stage pyrolysis/gasification of sugarcane bagasse was investigated in this section. Seven different Ni-based catalysts; Ni-dolomite, Ni-MgO, Ni-SiO₂, Ni-Al₂O₃, 2 wt.% Ce - Ni-dolomite, 5 wt.% Ce - Ni-dolomite and 10 wt.% Ce - Ni-dolomite were investigated and the results were compared with the product yield obtained from silica sand as a blank substitute. Product yield results are shown in Table 6-2. From these results, it is clear that the presence of catalyst instead of silica sand improved the gas yield as well as hydrogen yield. The gas yield in relation to biomass (corrected for no input water) increased significantly from 63.72 wt.% for sand (no catalyst) to 77.71 wt.% for 10 wt.% Ni-Al₂O₃ catalyst. This higher catalytic activity of 10 wt.% Ni-Al₂O₃ was most likely due to the higher surface area compared to the other catalysts. The metal support interaction between Ni and Al₂O₃ also might have played a role for better dispersion and to prevent Ni sintering [5]. Miccio et al. [6] also reported the effectiveness of Ni-Al₂O₃ catalyst over the other catalysts for the higher hydrogen yield with lower tar contents from the gasification of spruce wood in a fluidized bed reactor.

The other catalysts, 10 wt.% Ni-dolomite and 10 wt.% Ni-SiO₂ moderately increased the gas yield from 63.72 wt.% for sand (no catalyst) to 70.24 wt.% for 10 wt.% Ni-dolomite and 69.19 wt.% for 10 wt.% Ni-SiO₂. Addition of Cerium (Ce) into 10 wt.% Ni-dolomite did not show any noticeable improvements in terms of gas yield. 10 wt.% Ni-MgO showed the lowest catalytic activity in terms of gas yield and hydrogen yield. This lower yield was perhaps due to the amalgamation of Ni²⁺ into the lattice of the MgO support to form MgO based NiO-MgO solid solution [7]. Xie et al. [8] compared the performance of different mineral based catalysts i.e. dolomite and olivine with Ni-based catalyst during the two-stage pyrolysis-gasification of pine sawdust. It was found that the Ni supported on Al₂O₃ showed the highest surface area and the highest H₂:CO ratio. Li et al. [9] used two-stage system for the production of syngas from municipal solid waste using Ni based catalyst supported in Al₂O₃. They reported a significant increase in gas yield from 1.26 to 2.18 Nm³ kg⁻¹ at 800 °C. The tar yield was also reduced dramatically from 34.6 to 0.24 g/Nm³.

Table 6-2 Results of pyrolysis (950 °C) - gasification (950 °C) of sugarcane bagasse with or without different catalysts

	Gasification catalyst							
	Sand	10%Ni- Al ₂ O ₃	10%Ni- Dolomite	10%Ni- MgO	10%Ni- SiO ₂	2%Ce+10% Ni-Dolomite	5%Ce+10% Ni-Dolomite	10%Ce+10% Ni-Dolomite
Sample weight (g)	4.00	4.00	4.00	4.00	4.00	4.00	4.00	4.00
Sample particle size (µm)	1405-2800	1405-2800	1405-2800	1405-2800	1405-2800	1405-2800	1405-2800	1405-2800
Catalyst weight (g)	2	2	2	2	2	2	2	2
Water injection rate (ml hr ⁻¹)	6	6	6	6	6	6	6	6
Nitrogen flowrate (ml min ⁻¹)	100	100	100	100	100	100	100	100
H ₂ (mmoles g ⁻¹ of biomass)	21.18	29.62	25.41	23.31	24.21	28.25	25.01	24.51
Mass balance (wt.%)								
Gas/(biomass+water)	27.38	29.94	28.04	23.93	26.56	29.40	27.25	28.43
Solid/(biomass+water)	9.67	9.15	8.98	9.70	8.54	9.28	9.06	9.21
Mass balance	95.91	96.03	96.80	92.67	91.92	94.45	95.53	97.88
Gas/(biomass)	63.72	77.71	70.24	58.57	69.19	71.29	67.65	73.28
Solid/(biomass)	22.50	23.75	22.50	23.75	22.25	22.50	22.50	23.75

Table 6-3 The influence of different catalysts on product yield from pyrolysis (950 °C) -gasification (1000 °C) of sugarcane bagasse

	Gasification catalyst			
	Sand	10%Ni-Al ₂ O ₃	10%Ni-Dolomite	2%Ce+10%Ni-Dolomite
Sample weight (g)	4.00	4.00	4.00	4.00
Sample particle size (µm)	1405-2800	1405-2800	1405-2800	1405-2800
Catalyst weight (g)	2	2	2	2
Water injection rate (ml hr ⁻¹)	6	6	6	6
Nitrogen flow rate (ml min ⁻¹)	100	100	100	100
H ₂ (mmoles g ⁻¹ of biomass)	25.07	29.93	28.19	28.15
Mass balance (wt.%)				
Gas/(biomass+water)	27.56	28.80	30.04	25.23
Solid/(biomass+water)	8.52	8.97	8.81	8.61
Mass balance	95.80	97.08	101.30	97.11
Gas/(biomass)	74.40	74.67	78.40	71.79
Solid/(biomass)	23.00	23.25	23.00	24.50

As a general trend, the higher gasification temperature of 1000 °C instead of 950 °C led to enhanced gas yield as well as hydrogen yield. As shown in Table 6-3, with the increase in gasification temperature from 950 to 1000 °C, the gas yield for the sand bed, in relation to biomass (corrected for no input water) increased from 63.72 wt.% to 74.40 wt.%. This significant increase in gas yield for the sand bed indicated that the increase in temperature promoted the thermal cracking and other gas phase endothermic reactions. When 10 wt.% Ni-Al₂O₃ catalyst was used instead of the sand bed, the gas yield slightly improved to 74.67 wt.%. This lower gas yield for 10 wt.% Ni-Al₂O₃ catalyst was most likely due to the loss of surface area (Table 6-4) caused by sintering of the alumina support [10-12] as evident from SEM images in Section 6.3.3. For 10 wt.% Ni-dolomite catalyst, gas yield also increased from 70.24 wt.% to 78.40 wt.%. However, for 2 wt.% Cerium (Ce) – dolomite catalyst, the increase in temperature from 950 to 1000 °C, did not improve the gas yield (71.29 wt.% to 71.79 wt.%).

6.2.3 The influence of different catalysts on gas composition and hydrogen production

The influence of various catalysts on gas composition especially hydrogen is reported in Figure 6-3. All the concentrations are reported in vol.% and on a nitrogen free basis. It is clear that the H₂ concentration in the product gas mixture was enhanced from 54 vol.% for sand (no catalyst) to ~ 60 vol.% for 10 wt.% Ni-Al₂O₃. The hydrogen yield obtained using various catalysts is shown in Table 6-2. It is evident that the hydrogen yield increased from 21.18 mmoles g⁻¹ for sand (no catalyst) to the highest 29.62 mmoles g⁻¹ for 10 wt.% Ni-Al₂O₃. The lowest increase in hydrogen yield from 21.18 mmoles g⁻¹ for sand (no catalyst) to 23.31 mmoles g⁻¹ was observed for 10 wt.% Ni-MgO catalyst.

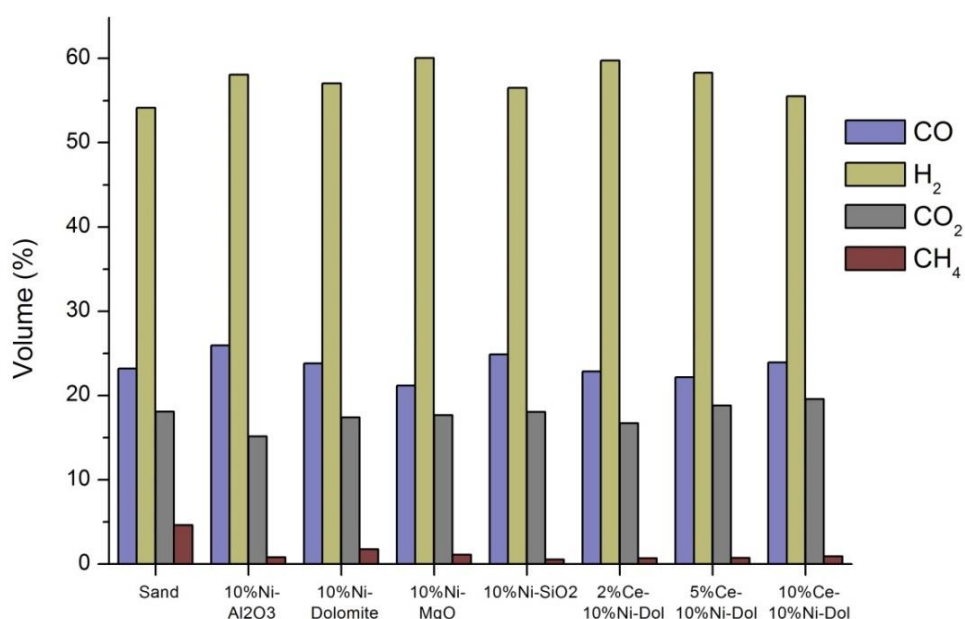


Figure 6-3 Composition of gases in the product mixture at 950 °C

The other catalysts; 10 wt.% Ni-dolomite and 10 wt.% Ni-SiO₂ showed little change in hydrogen yield (25.41 and 24.21 mmoles g⁻¹ respectively). Addition of 2 wt.% Ce to the 10 wt.% Ni-dolomite further improved hydrogen yield from 25.41 to 28.25 mmoles g⁻¹, however further increase in Ce contents to 5 wt.% and to 10 wt.% reduced the gas yield as well as hydrogen yield. Isha et al. [7] reported that the addition of 5 % Ce to a 5 %

Ni-Al₂O₃ catalyst enhanced CH₄ conversion to hydrogen to 98 % but further increases in Ce to 10 wt.% and 15 wt.% lead to a slight decrease in CH₄ conversion to 96 % [7].

As shown in Figure 6-3, the presence of 10 % Ni-Al₂O₃ catalyst instead of silica sand enhanced the H₂ concentration in the product gas to ~ 60 vol.%. The concentration of CO increased from 23.2 vol.% for no catalyst to 25.94 vol.% for 10 % Ni-Al₂O₃ catalyst and CO₂ concentration reduced from 18 vol.% to 15.16 vol.%. The increase in CO concentration along with the decrease in CO₂ suggests that the presence of catalyst slightly shifted the equilibrium of the Boudouard reaction towards CO formation. The CH₄ concentration was also significantly reduced from 4.61 vol.% to 0.79 vol.% when silica sand was replaced by 10 % Ni-Al₂O₃ catalyst. This suggests that the presence of 10 % Ni-Al₂O₃ catalyst also improved the steam reforming of CH₄. Similar trends were observed for the other catalysts, 10 % Ni-dolomite, 10 % Ni-MgO and 10 % Ni-SiO₂ but the catalytic activity of these catalysts was lower perhaps due to the lower surface area of these catalysts. Miccio et al. [6] also reported that the Ni catalyst supported on alumina was effective in increasing hydrogen concentration in the product gaseous mixture. Compared to mineral based catalyst like olivine and dolomite, alumina supported Ni catalyst showed a significant increase in H₂ and CO concentration along with the reduction in CO₂ and CH₄ concentrations.

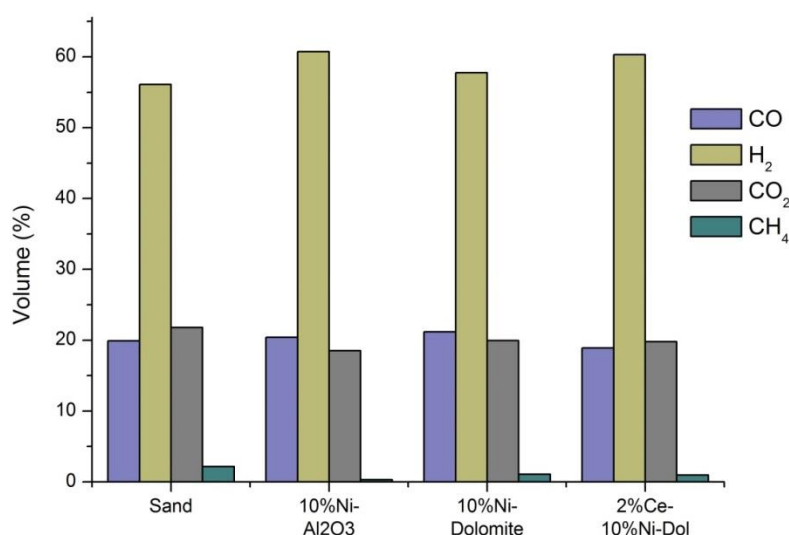


Figure 6-4 Gas composition showing the influence of different catalyst at 1000 °C

As shown in Figure 6-4, the influence of the four different catalysts on product gas composition was investigated at higher gasification temperature of 1000 °C. Addition of 10 % Ni-Al₂O₃ catalyst instead of the sand bed improved the hydrogen concentration in the product gas mixture from 56 vol.% to more than 60 vol.%. Although the use of 10 % Ni-dolomite at 1000 °C enhanced the gas yield significantly from 74.40 wt.% for the sand bed to 78.40 wt.% (shown in Table 6-3) but this increase does not translate into the higher hydrogen concentration in the gas mixture as H₂ concentration slightly increased from 56.11 vol.% to 57.75 vol.%. As shown in Table 6-3, the highest hydrogen yield of 29.93 mmol per gram of biomass was obtained using 10 % Ni-Al₂O₃ catalyst. The use of 10 % Ni-dolomite and 2 % Ce-10 % Ni-dolomite improved the gas yield to 28.19 and 28.15 as compared to 25.07 mmol per gram of biomass obtained using the sand bed. This higher hydrogen yield obtained from 10 % Ni-Al₂O₃ catalyst was most likely due to the higher surface area of this catalyst as compared to the other catalysts. The highly porous support (i.e. alumina) effectively dispersed the Ni particles resulting in higher yields. The strong metal-support interaction is also thought to have played an important role, producing higher gas and hydrogen yields.

6.2.4 Characterisation of reacted catalyst

Table 6-4 Comparison of surface area of fresh and reacted catalyst

Catalyst	BET surface area (m ² g ⁻¹)		
	Fresh catalyst	Reacted 950 °C	Reacted 1000 °C
10% Ni-Al ₂ O ₃	76.82	34.23	25.26
10% Ni-MgO	53.90	8.03	nd*
10% Ni-SiO ₂	8.16	3.23	nd*
10% Ni-dolomite	5.56	nd*	2.80
2%Ce-10% Ni-dolomite	7.37	3.22	1.13

* *not determined*

The BET surface area of different freshly prepared and reacted catalysts was analysed with the aim to investigate the influence of process conditions on the catalytic activity of these catalysts. Results shown in Table 6-4 indicate that the reacted catalysts showed a loss in surface area. For example, BET surface area of the 10 % Ni-Al₂O₃ catalyst was reduced to 34.23 m² g⁻¹ when used during gasification at 950 °C. This decrease in

surface area upon heat treatment was due to the changes in crystalline structure and hence a decrease in porosity of the material [12]. The other catalysts, 2 % Ce - 10 % Ni-dolomite also showed loss in surface area from 7.37 to 3.22 for the catalyst reacted at 950 °C to 1.13 m² g⁻¹ for 1000 °C. The 10 % Ni-MgO catalyst showed the highest loss in surface area of more than 85 %. This severe loss of surface area for 10 % Ni-MgO explains the lower catalytic activity of this catalyst in terms of gas yield and hydrogen yield (as shown in Table 6-2).

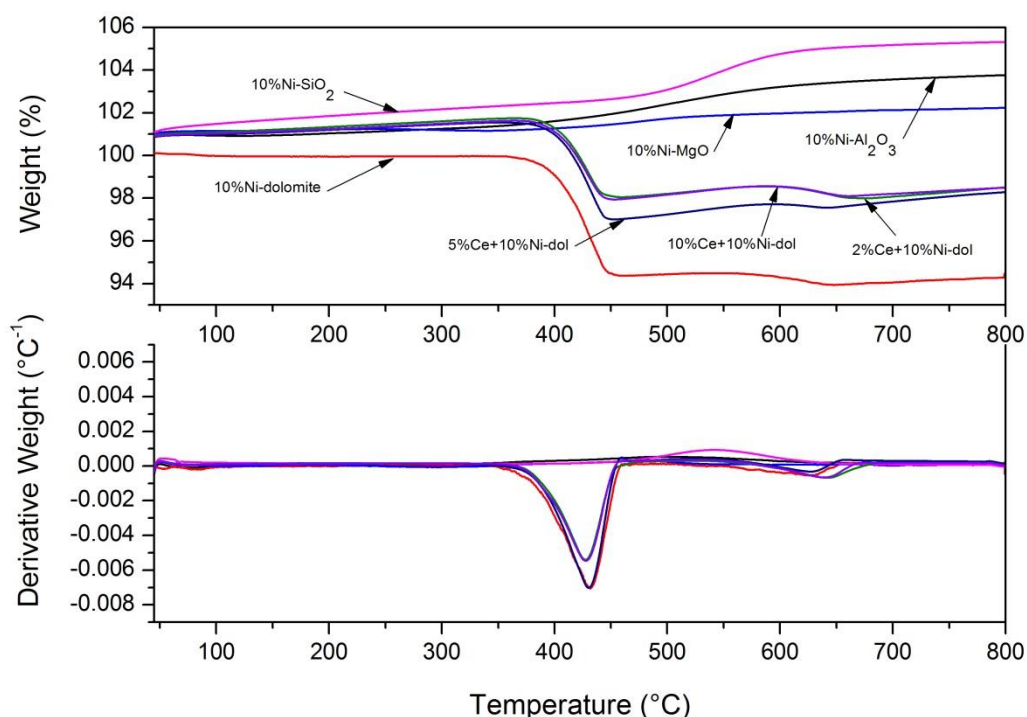


Figure 6-5 TGA-TPO and DTG-TPO results of different coked catalyst during the pyrolysis-gasification of bagasse at 950 °C

Thermogravimetric analysis (TGA) was used to investigate the coke deposition on the reacted catalysts. Temperature programmed oxidation (TGA-TPO) and their derivative curves (DTG-TPO) for the catalyst used at gasification temperature of 950 and 1000 °C are shown in Figure 6-5 and Figure 6-6 respectively. As shown in Figure 6-5, all the dolomite based catalysts showed a noticeable weight loss peak around 450 °C with a slight decrease in weight around 650 °C. According to the literature [13], these weight loss curves observed at two different temperatures indicate the presence of two different

kinds of carbons (amorphous and graphite) deposited on the reacted catalysts. It was suggested that the first peak around 450 °C was due to the oxidation of amorphous carbon while the second peak around 650 °C was due to the oxidation of graphite carbon deposited on the reacted catalyst [14]. The highest amount of carbon deposits of 5.54 wt.% were found on 10 % Ni-dolomite catalysts while addition of Ce in 10 % Ni-dolomite inhibited the carbon deposition on the catalyst to around 2.5 wt.%.

The other catalysts, 10 % Ni-SiO₂, 10 % Ni-MgO and 10 % Ni-Al₂O₃ catalyst did not show any weight loss over the entire temperature range. Instead a slight increase in catalyst weight was observed at temperatures above 400 °C. This increase in catalyst weight was due to the conversion of metallic Ni into NiO in the oxidation environment as NiO contained in freshly prepared catalyst was reduced to metallic Ni in the reducing environment during gasification [15].

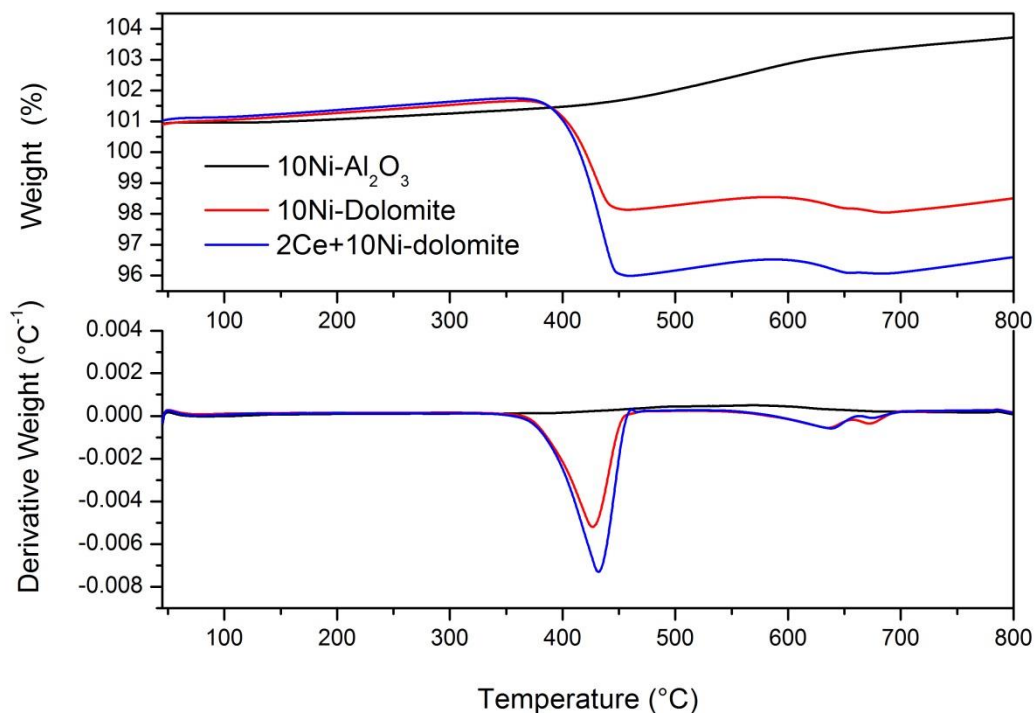


Figure 6-6 TGA-TPO and DTG-TPO results of different coked catalyst during the pyrolysis-gasification of bagasse at 1000 °C

The TGA-TPO and DTG-TPO thermograms of reacted catalysts at a gasification temperature of 1000 °C are shown in Figure 6-6. No weight loss was recorded for reacted 10 % Ni-Al₂O₃ catalyst indicating the effectiveness of this catalyst during steam gasification. A slight weight increase was most likely due to the oxidation of metallic Ni into NiO.

10 % Ni-dolomite and 2 % Ce - 10 % Ni-dolomite showed a weight loss of 2.27 and 4.33 wt.%. Compared to the TGA-TPO results at 950 °C shown in Figure 6-5, it was noticed that the increase in gasification temperature from 950 °C to 1000 °C enhanced the catalytic activity of 10 % Ni-dolomite catalyst resulting in an increase in the gas and hydrogen yield (Table 6-3) with the lower carbon deposits on 10 % Ni-dolomite catalyst.

An increase in gasification temperature to 1000 °C showed a negative effect on the 2 % Ce - 10 % Ni-dolomite catalyst. It is suggested that this catalyst was deactivated at the higher gasification temperature of 1000 °C was due to the severe loss of surface area (Table 6-4) which resulted in higher carbon deposits on the catalyst surface and lower gas and hydrogen yield (Table 6-3). It was noticed that the amount of deposited carbon on 2 % Ce - 10 % Ni-dolomite catalyst was increased from 2.42 to 4.33 wt.% indicating the deactivation of this catalyst.

High resolution scanning electron microscopy (SEM) at 100,000X resolution was used to characterize the morphology of fresh and reacted catalysts. SEM images of seven fresh and reacted catalysts are compared in Figure 6-7, Figure 6-8, and Figure 6-9. As indicated by the TGA-TPO results (Figure 6-5 and Figure 6-6), high temperature steam gasification was very effective and only less than 6 wt.% carbon deposits were formed on the dolomite based catalysts while other catalysts, 10 % Ni-SiO₂, 10 % Ni-MgO and 10 % Ni-Al₂O₃ did not show the presence of any carbon deposits. These SEM images confirm these findings as no carbon deposits were observed for these catalysts. In terms of morphology of fresh and reacted catalysts, no major differences were observed for these catalysts. However, the dolomite based catalysts showed an increase in catalyst particle size (Figure 6-7a-b, Figure 6-8c-f and Figure 6-9) which explains the loss of surface area of reacted catalysts as shown in Table 6-4. The 10 % Ni-SiO₂, and 10 % Ni-Al₂O₃ catalysts did not show any morphological changes after gasification (Figure 6-7c-d and Figure 6-8a-b) while the comparison of fresh and reacted 10 % Ni-MgO

catalysts indicated some structural damage after exposure to higher gasification temperature (Figure 6-7e-f).

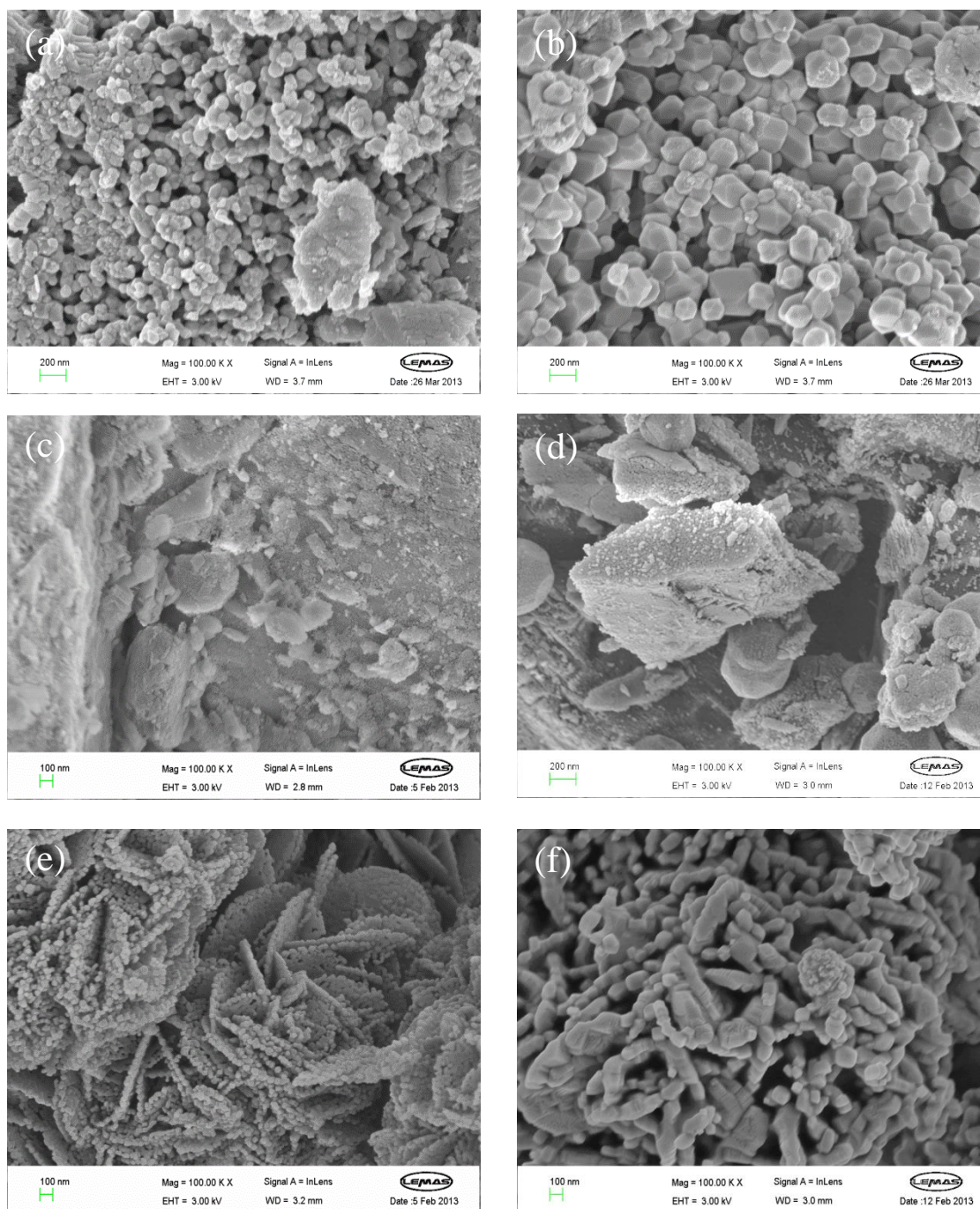


Figure 6-7 SEM images of fresh and reacted catalysts (a) fresh 10 wt.% Ni-dolomite , (b) reacted 10 wt.% Ni-dolomite at 950 °C, (c) fresh 10 % Ni-Al₂O₃ , (d) reacted 10 % Ni-Al₂O₃, (e) fresh 10 wt.% Ni-MgO, and (f) reacted 10 wt.% Ni-MgO

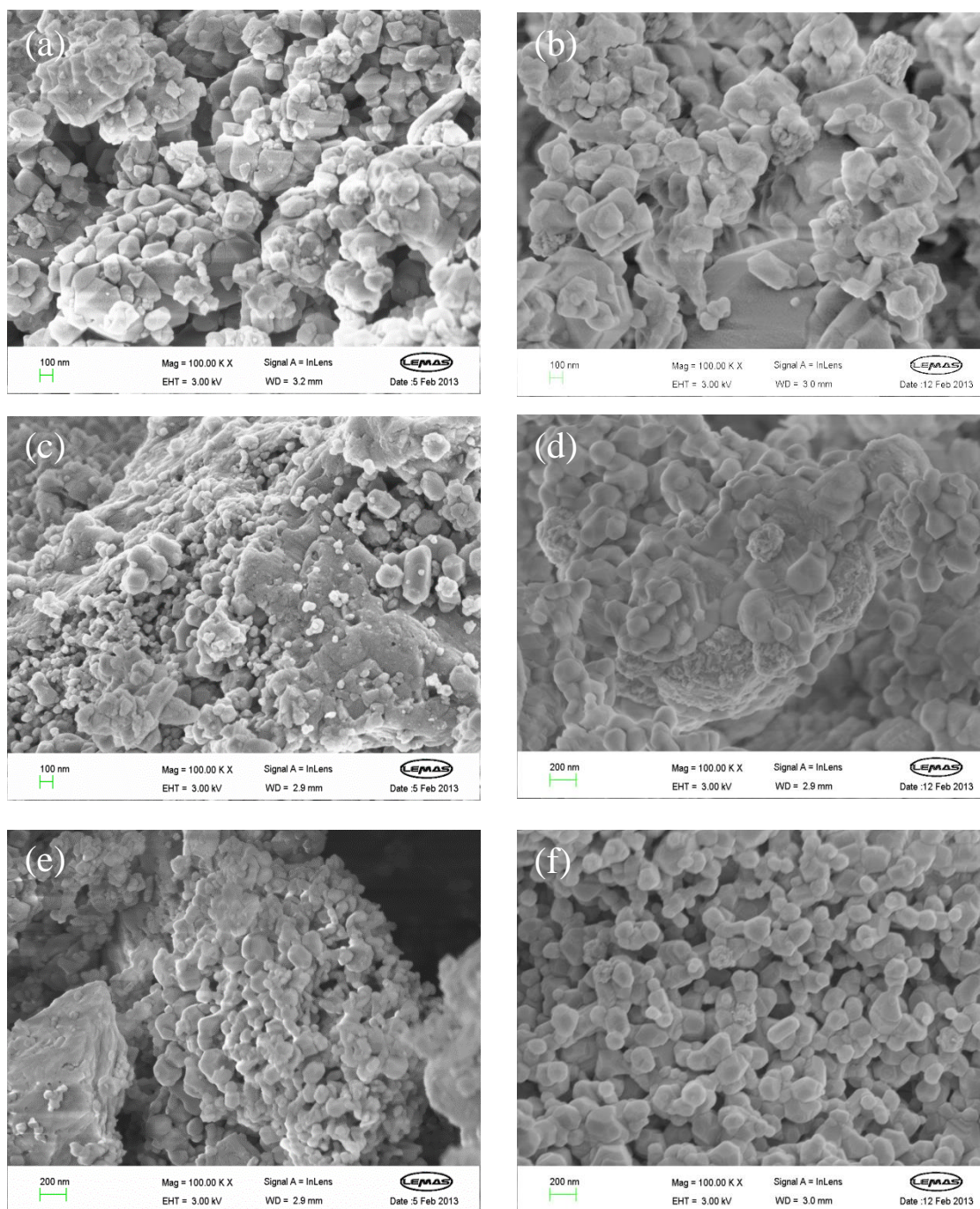


Figure 6-8 SEM images of fresh and reacted catalysts (a) fresh 10 wt.% Ni-SiO₂, (b) reacted 10 wt.% Ni-SiO₂ at 950 °C, (c) fresh 2 % Ce -10 % Ni-dolomite, (d) reacted 2 % Ce - 10 % Ni-dolomite, (e) fresh 5 % Ce - 10 wt.% Ni-dolomite and (f) reacted 5 % Ce - 10 wt.% Ni-dolomite

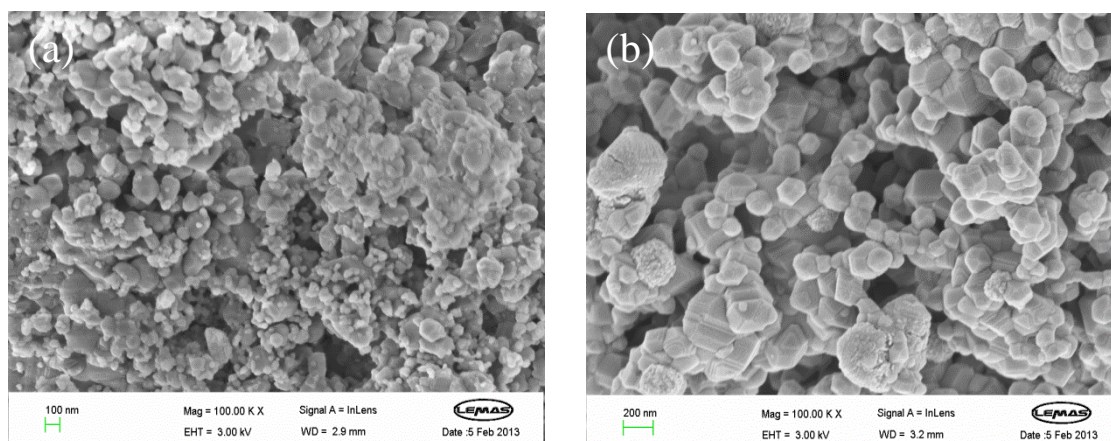


Figure 6-9 SEM of fresh and reacted catalysts (a) fresh 10 % Ce - 10wt.%Ni-dolomite and (b) reacted 10 % Ce - 10wt.%Ni-dolomite

6.3 The influence of gasification temperature

6.3.1 Product yield

In the previous section, it was found that 10 % Ni-Al₂O₃ was the most effective catalyst in terms of hydrogen production during the high temperature pyrolysis/gasification of bagasse. In this section, the influence of gasification temperature on pyrolysis-gasification of sugarcane bagasse was investigated using a 10 % Ni-Al₂O₃ catalyst. For this set of experiments, the temperature of the pyrolysis stage was kept constant at 950 °C while the temperature of the gasification stage was varied from 800 to 1050 °C with an increment of 50 °C.

The product yield results shown in Table 6-5 indicate that the gas yield in relation to biomass and water varied slightly. Initially the gas yield increased from 29.53 wt.% for 800 °C to 29.94 wt.% at 950 °C and then reduced to 24.62 wt.% at 1050 °C. This reduction in gas yield at higher temperature was most likely due to the loss of surface area of 10 wt.% Ni-Al₂O₃ catalyst.

Table 6-5 The influence of gasification temperature on pyrolysis-gasification of sugarcane bagasse (pyrolysis temperature of 950 °C)

	Temperature (°C)					
	800	850	900	950	1000	1050
Sample weight (g)	4.00	4.00	4.00	4.00	4.00	4.00
Biomass particle size (µm)	1405-2800	1405-2800	1405-2800	1405-2800	1405-2800	1405-2800
Catalyst	10%Ni-Al ₂ O ₃					
Catalyst weight (g)	2	2	2	2	2	2
Water injection rate (ml hr ⁻¹)	6	6	6	6	6	6
Nitrogen flow rate (ml min ⁻¹)	100	100	100	100	100	100
H ₂ (mmoles g ⁻¹ of biomass)	21.17	22.74	26.10	29.62	29.73	35.65
Mass balance (wt.%)						
Gas/(biomass+water)	29.53	27.47	25.54	29.94	26.38	24.62
Solid/(biomass+water)	9.24	9.52	9.43	9.15	9.14	9.41
Mass balance	97.91	98.00	93.36	96.03	91.86	93.59
Gas/(biomass)	73.54	67.11	64.29	77.71	64.97	64.07
Solid/(biomass)	23.00	23.25	23.75	23.75	22.50	24.50

6.3.2 The influence of temperature on gas composition and hydrogen production

Although the increase in gasification temperature did not influence the gas yield greatly but it significantly did improve the gas composition in terms of hydrogen production. As shown in Table 6-5, hydrogen yield increased from 21.17 mmol g⁻¹ at 800 °C to 35.65 mmol g⁻¹ at 1050 °C. The product gas composition results shown in Figure 6-10 also indicate a similar trend. The hydrogen concentration in the product gas mixture increased from 50.32 vol.% at 800 °C to 67.41 vol.% at 1050 °C. Similar trends were also reported by other researchers [16, 17]. Skoulou et al. [17] performed steam gasification of olive kernel in a fixed bed gasifier. They also reported an increase in hydrogen gas concentration from less than 10 vol.% at 750 °C to ~ 42 vol.% at 1050 °C.

When compared with the steam gasification results of rice husk using 10 % Ni-dolomite in section 5.4.1, it was noticed that the gasification of sugarcane bagasse using 10 % Ni-Al₂O₃ catalyst produced a higher hydrogen yield of 35.65 mmol per gram of bagasse compared to 30.62 mmol per gram of rice husk at 1050 °C. This shows that the gasification of bagasse using 10 % Ni-Al₂O₃ is a better option as compared to the gasification of rice husk using 10 % Ni-dolomite.

The increase in hydrogen concentration with the increase in temperature can be explained by the fact the higher temperature favours endothermic reactions (e.g. water gas reaction and Boudouard reaction) [18]. Steam reforming and dry reforming of methane and other higher hydrocarbons also contribute towards the higher hydrogen concentration. Thermal cracking of various tar components also leads to enhanced hydrogen yield at higher gasification temperatures [19].

As shown in Figure 6-10, the concentration of CO initially increased from 23.63 vol.% at 800 °C to 25.94 vol.% at 950 °C. Meanwhile, the CO₂ concentration reduced from 20.14 vol.% at 800 °C to 15.16 vol.% at 950 °C. This suggests that the higher temperature of 950 °C shifted the equilibrium of the endothermic Boudouard reaction leading to the formation of CO. The other reactions including the endothermic water gas, steam methane reforming, dry reforming and thermal cracking of heavy tar components also had played an important role producing higher hydrogen yield. It is also worth mentioning that the extent of equilibrium of each reaction depends on many

factors as various competing parallel reactions are taking place simultaneously in the gasifier.

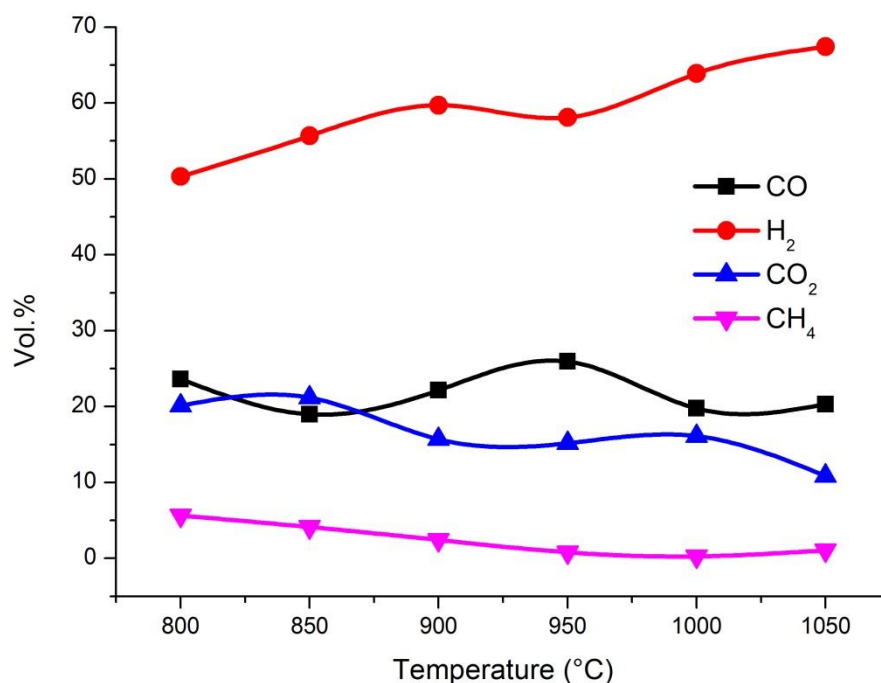


Figure 6-10 The influence of gasification temperature on gas composition during the pyrolysis-gasification of sugarcane bagasse

The CO₂ concentration in the gaseous mixture gradually reduced from 20.14 vol.% at 800 °C to 10.87 vol.% at 1050 °C. This decrease in CO₂ concentration can be attributed to the endothermic Boudouard and dry reforming reactions favourable at higher temperatures [19]. CH₄ concentration also decreased from 5.64 vol.% at 800 °C to 0.25 vol.% at 1000 °C. This decrease was mainly due to the endothermic methane steam reforming reaction leading to the enhanced hydrogen and CO production. Further increase in temperature to 1050 °C slightly increased the CH₄ concentration to 1.05 vol.%. This was most likely due to the shift in equilibrium of the methanation reaction. The higher concentration of hydrogen present in the product gas mixture caused this shift in the equilibrium of the methanation reaction, producing more CH₄. No C₂-C₄ hydrocarbons were detected throughout the investigated range of temperature indicating the effectiveness of the two-stage process for hydrogen production. Franco et al. [20]

performed the steam gasification of wood biomass. A decrease in the concentrations of CH₄ and other lighter hydrocarbons was reported with the rise in temperature.

6.3.3 Characterization of reacted 10 % Ni-Al₂O₃ catalyst

In order to investigate the influence of gasification temperature, the BET surface area of reacted catalysts was compared to that of fresh catalyst. As indicated in Table 6-6, a linear trend of reduction in surface area with the increase in temperature was observed. This loss of surface area was due to the loss of support surface area and loss of Ni surface area [21]. The morphological change in alumina support due to sintering was the most probable reason for the loss of support surface area [10, 11]. The loss of Ni surface area was also most likely due to sintering.

Table 6-6 The influence of gasification temperature on surface area of catalyst

Catalyst	Reaction Temperature	BET surface area
	(°C)	m ² g ⁻¹
Fresh 10 wt.% Ni-Al ₂ O ₃	-	76.82
Reacted 10 wt.% Ni-Al ₂ O ₃	800	60.86
Reacted 10 wt.% Ni-Al ₂ O ₃	950	34.23
Reacted 10 wt.% Ni-Al ₂ O ₃	1000	25.26
Reacted 10 wt.% Ni-Al ₂ O ₃	1050	7.85

The scanning electron microscope (SEM) images shown in Figure 6-12 also showed the sintering of Ni particles and alumina support. It is evident from Figure 6-12 that the Ni particle size increased from ~100 nm for 800 °C to ~200 nm for higher temperatures. As reported by other authors [10, 11], the morphological change in alumina support was most likely due to the sintering. These changes were observed in the SEM images (Figure 6-12 e-f).

Various studies [22, 23] have been conducted to understand the mechanism of sintering. It was reported that the sintering of Ni based catalyst depend on different factors including time on stream, temperature, atmosphere and Ni-support interaction [24]. It is widely accepted that the sintering of Ni particles follow one of the two mechanisms namely particle migration and coalescence (PMC) and Ostwald ripening (OR) [22]. During particle migration and coalescence, a Ni crystallite migrates over the support

followed by coalescence whereas during Ostwald ripening (also known as atomic migration or vapour transport) is characterized by the absence of any translatory motion of Ni particles. Instead metal species emitted from one crystallite are captured by other crystallites via gas phase.

It has been suggested by Sehested et al. [22] that the increase in the rate of sintering at higher temperature was due to the change of sintering mechanism from particle migration to Ostwald ripening. Hansen et al. [23] used an in-situ TEM technique to investigate the mechanism of sintering of nanoparticles. They suggested the presence of three phases of sintering. During phase I, the catalyst rapidly lost its catalytic activity due to the Ostwald ripening mechanism. During phase II, slowdown of sintering was observed. They reported the combination of particle migration and Ostwald ripening was observed in this phase. During phase III, stable catalytic activity was observed after particle growth and support restructuring.

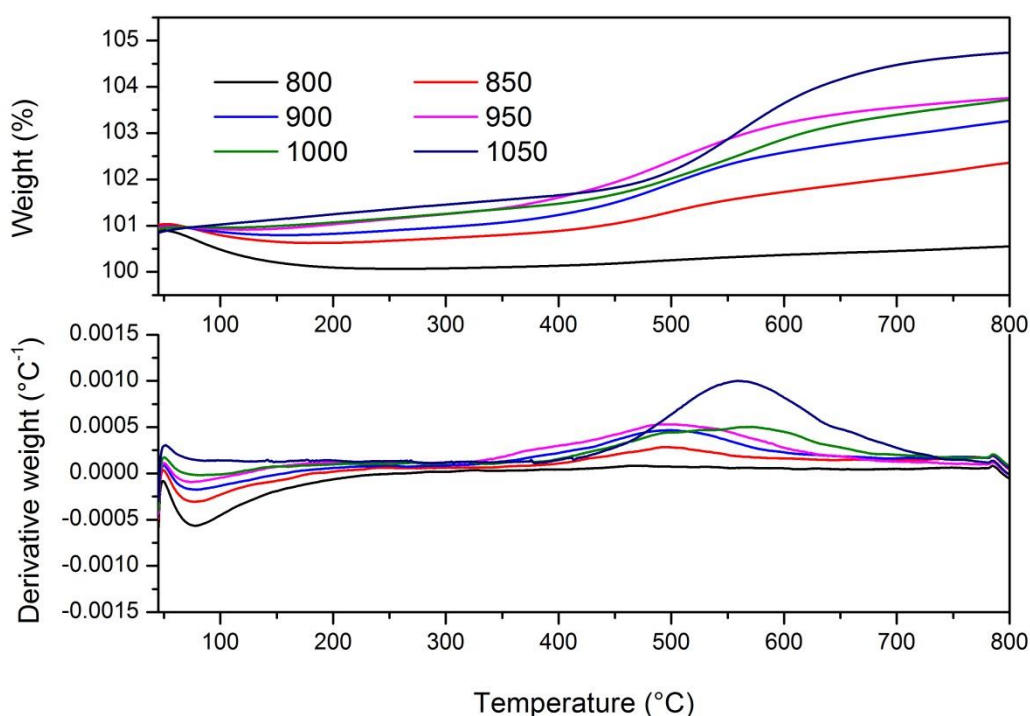


Figure 6-11 TGA-TPO and DTG-TPO results showing the effect of temperature on reacted 10 wt.%Ni-Al₂O₃ catalyst during the pyrolysis-gasification of sugarcane bagasse

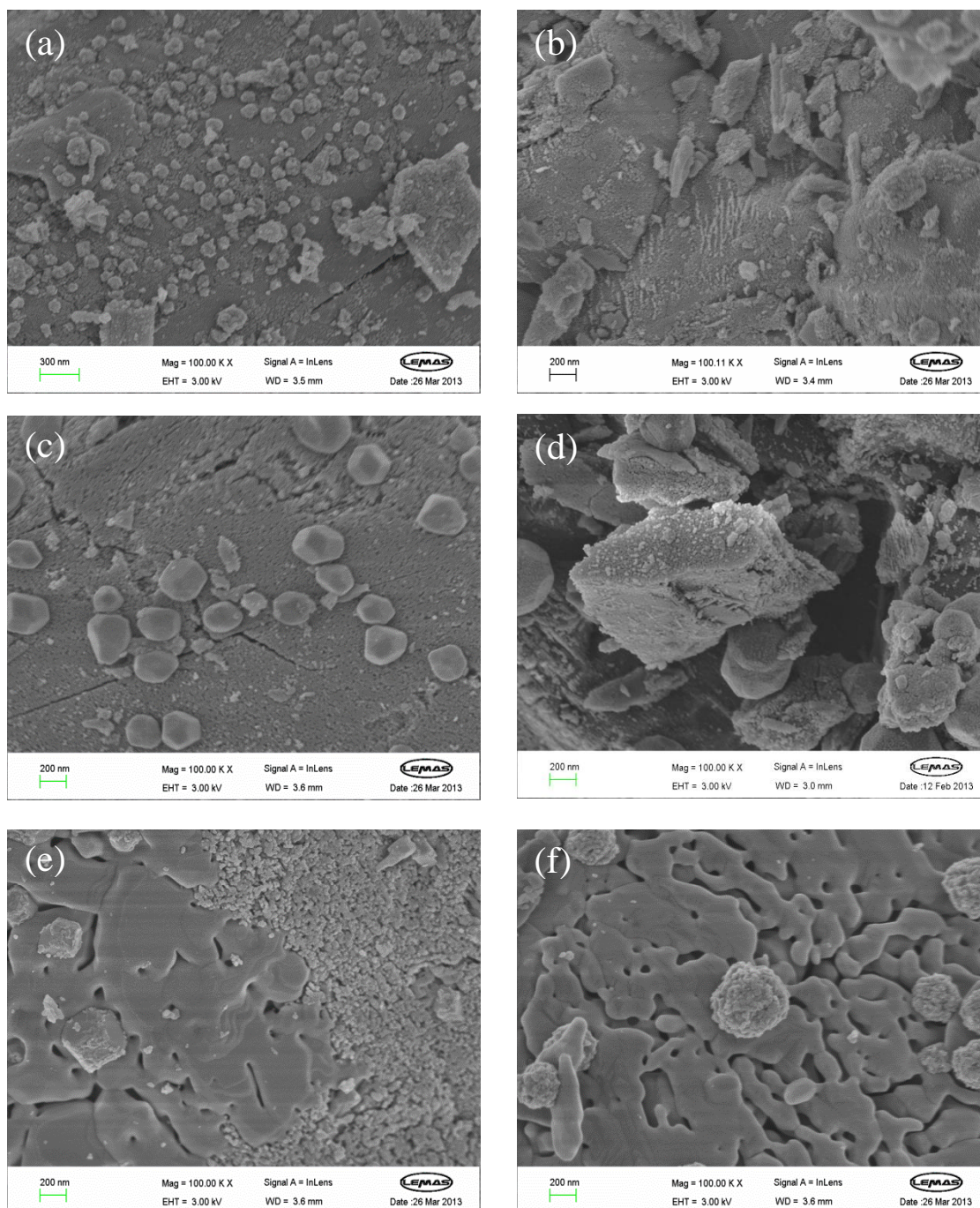


Figure 6-12 SEM images of reacted 10 % Ni-Al₂O₃ catalysts reacted at different temperatures (a) at 800 °C, (b) at 850 °C, (c) at 900 °C, (d) at 950 °C, (e) at 1000 °C, and (f) at 1050 °C

The reacted 10 % Ni-Al₂O₃ catalysts were characterized by thermogravimetric analysis with the aim to investigate the amount and nature of carbon deposits. The TGA-TPO and DTG-TPO curves are shown in Figure 6-11. These results indicate that no carbon

deposits were found on any of the reacted catalysts. The SEM images shown in Figure 6-12 also confirm these findings as no carbon deposits were seen on these images. The slight weight loss around 100 °C was due to the evaporation of water from the sample surface. The minor increase in catalyst weight was observed after 400 °C. This increase in catalyst weight was probably due to the oxidation of metallic Ni particles which were formed by the reduction of NiO in the hydrogen-rich environment during steam gasification.

6.4 The influence of Ni loading

6.4.1 Product yield

The influence of different Ni contents on gas yield and hydrogen production during two-stage pyrolysis/gasification of bagasse was investigated. The experimental conditions and product yield results are shown in Table 6-7.

Table 6-7 The effect of Ni-loading on pyrolysis (950 °C) - gasification (950 °C) of bagasse

	Ni loading			
	5 wt.%	10 wt.%	20 wt.%	40 wt.%
Sample weight (g)	4.00	4.00	4.00	4.00
Sample particle size (µm)	1405-2800	1405-2800	1405-2800	1405-2800
Catalyst	Ni-Al ₂ O ₃			
Catalyst weight (g)	2	2	2	2
Water injection rate (ml hr ⁻¹)	6	6	6	6
Nitrogen flow rate (ml min ⁻¹)	100	100	100	100
H ₂ (mmoles g ⁻¹ of biomass)	27.27	29.62	27.59	26.06
Mass balance (wt.%)				
Gas/(biomass+water)	28.80	29.94	27.69	28.54
Solid/(biomass+water)	9.87	9.54	9.48	9.35
Mass balance	98.58	96.03	92.36	95.24
Gas/(biomass)	70.76	77.71	69.37	73.29
Solid/(biomass)	24.25	24.75	23.75	24.00

The product yield results shown in Table 6-7 indicate that by increasing the Ni contents in the catalyst does not show any significant improvements in terms of gas yield and hydrogen yield. The gas yield in relation to biomass (corrected for no input water) improved from 70.76 wt.% to 77.71 wt.% when nickel contents were increased from 5 wt.% to 10 wt.%. The increase in nickel loading from 5 wt.% to 10 wt.% most likely enhanced the number of available catalytic sites thereby increasing the gas yield by improving thermal cracking and steam reforming of tar compounds and hydrocarbons. Further increase in nickel contents to 20 wt.% and 40 wt.% did not show any positive effect on the gas yield. It is suggested that the increase in nickel contents from 5 wt.% to 10 wt.% lead to a saturation point where further increase in nickel contents does not have any positive effect on gas yield and hydrogen yield. Srinakruang et al. [25] investigated the influence of various Ni loading on steam gasification of tar model compounds. It was suggested that the performance of catalyst contain 15 wt.% Ni was better than the catalyst containing 20 wt.% and 10 wt.% nickel. Bangala et al. [26] performed the steam reforming of naphthalene using Ni-Al₂O₃ catalyst. It was reported that by increasing the nickel contents from 5 wt.% to 10 wt.% and to 15 wt.% the gas yield and conversion increased. Further increase in nickel content did not improve the gas yield.

It is also interesting to note that in this study, the higher pyrolysis and gasification temperature used in the two-stage configuration already significantly improved the hydrogen production by accelerating thermal cracking and reforming of hydrocarbons and tar. As shown in Figure 6-13, only less than 1 % of methane was found for a nickel loading of 10 wt.% or above. No other hydrocarbons were observed for all nickel loadings. These findings are in agreement with Nassos et al. [27], who reported that the influence of nickel loading is more pronounced at lower temperature (500 - 600 °C) than at higher temperatures (> 700 °C).

6.4.2 The influence of Ni-loading on gas composition and hydrogen production

The product gas composition derived from the pyrolysis/gasification of bagasse using different Ni:Al₂O₃ ratios are shown in Figure 6-13. From these results, it is evident that the increase in nickel contents did not have any significant influence on hydrogen gas

yield. It was found that the hydrogen concentration was around 60 vol.% in the product gas mixture. The hydrogen yield results shown in Table 6-7 also showed no significant improvement with the increase in nickel contents from 5 wt.% to 40 wt.%. The highest hydrogen yield of 29.62 mmol g^{-1} of bagasse was obtained using 10 wt.% nickel.

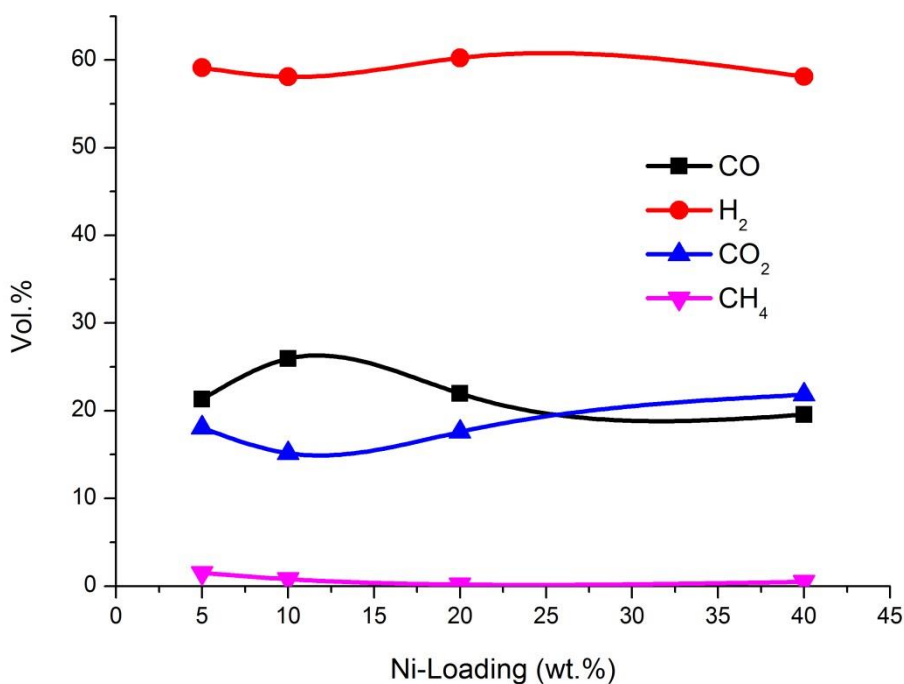


Figure 6-13 The influence of Ni loading on gas composition during the pyrolysis-gasification of bagasse

It is suggested that under the investigated conditions, the composition of the product gas mixture is not influenced by the increase in nickel contents. As the final percentage of each individual gas (CO, CO₂, H₂ and CH₄) mainly depends on the equilibrium of different reactions hence it is proposed that under the studied conditions, the equilibria of these reactions are not influenced by the different nickel loadings. It is well established that the equilibria of these reactions are dependent on numerous other factors such as reaction temperature and steam to biomass ratio.

6.4.3 Characterization of reacted Ni-Al₂O₃ catalysts

The surface analysis of reacted catalysts was performed and the results are shown in Figure 6-14. It was noticed that the BET surface area of the reacted catalysts was reduced. This reduction in surface area was most likely due to the sintering as no carbon deposits were observed from scanning electron microscope images (Figure 6-16) and temperature programmed oxidation results (Figure 6-15).

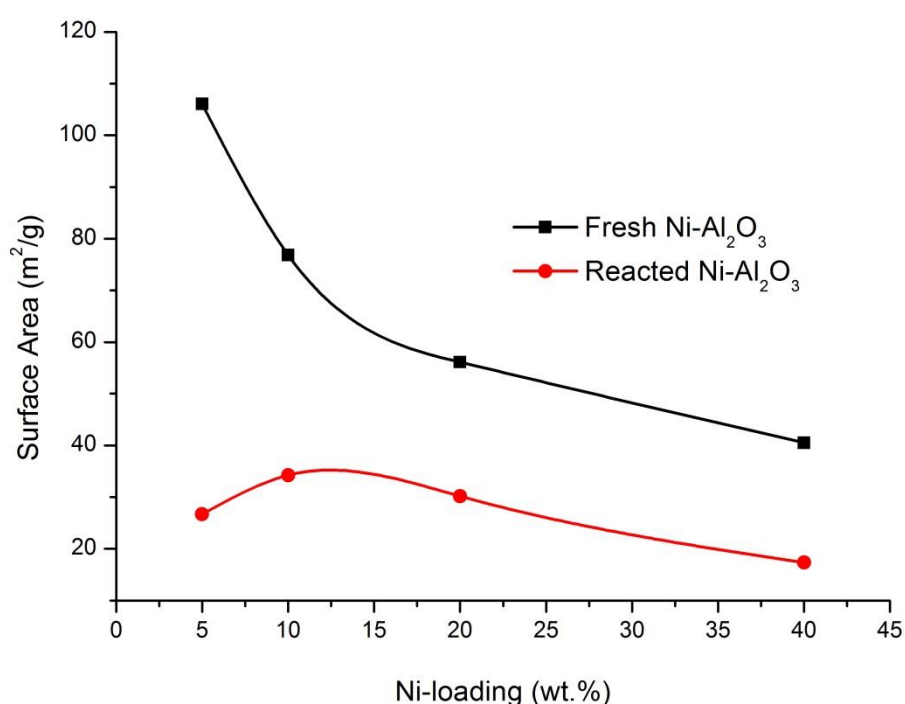


Figure 6-14 The influence of Ni-loading on surface area of fresh and reacted catalysts

As indicated in Figure 6-14, compared to the catalysts containing 5 wt.% and 10 wt.% nickel, a smaller reduction in surface area of catalysts containing 20 % and 40 % nickel contents was observed. It is suggested that for the higher nickel concentrations of 20 wt.% and 40 wt.%, strong metal-support interaction between nickel particles and alumina support resulted in the formation of nickel aluminate and inhibited the process of sintering [28].

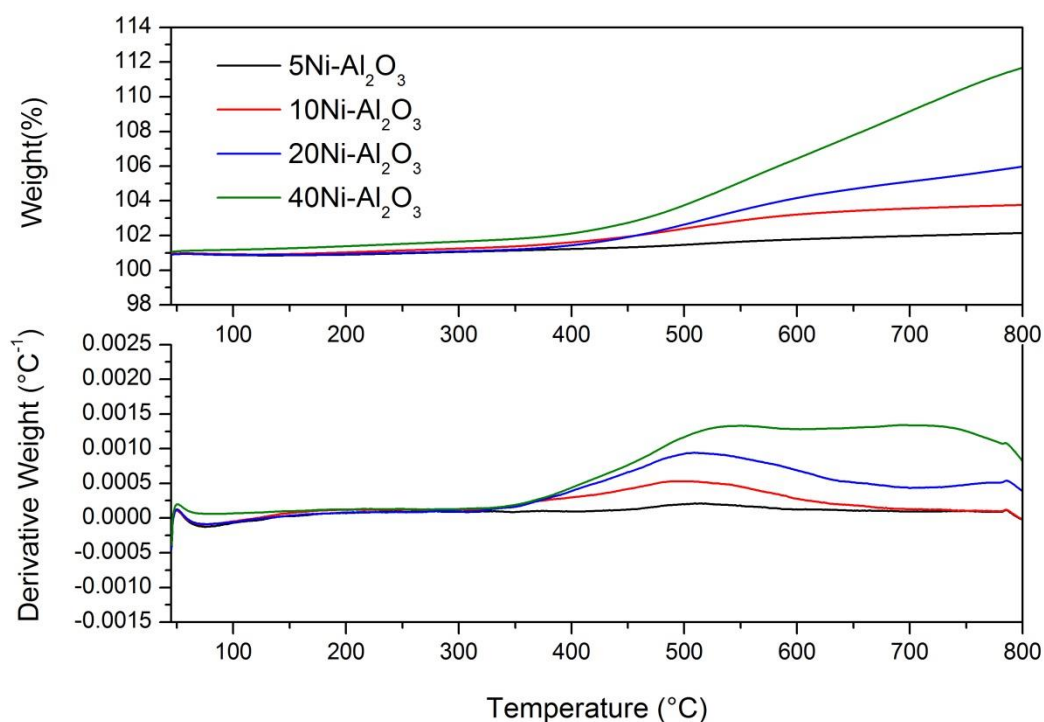


Figure 6-15 TGA-TPO and DTG-TPO results showing the effect of Ni-loading on reacted Ni-alumina catalyst during the pyrolysis-gasification of bagasse

Temperature programmed oxidation of reacted catalysts was performed to investigate the presence of any carbon deposits however no weight loss was observed from TGA-TPO and DTG-TPO results (shown in Figure 6-15) indicate the absence of any carbon deposits. The scanning electron microscope images (Figure 6-16) also confirm the absence of any carbon deposits on the catalyst surface. A systematic increase in catalyst weight with the increase in nickel loading suggest that the metallic nickel was oxidised during temperature programmed oxidation as the higher oxidation curve was observed for catalysts containing higher nickel contents.

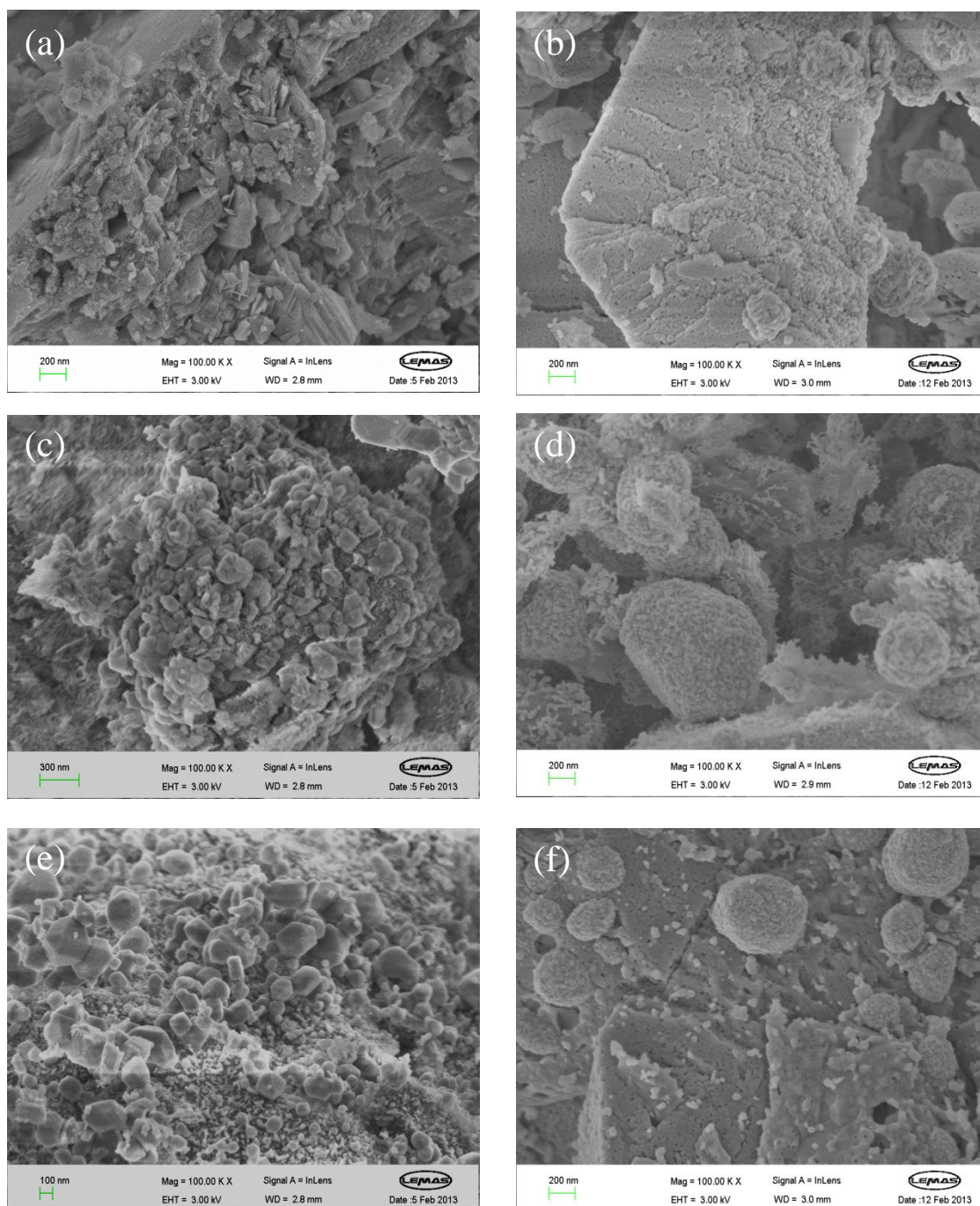


Figure 6-16 SEM images of fresh and reacted catalysts (a) fresh 5 wt.% Ni-Al₂O₃ , (b) reacted 5 wt.% Ni-Al₂O₃, (c) fresh 20 wt.% Ni-Al₂O₃ , (d) reacted 20 wt.% Ni-Al₂O₃, (e) fresh 40 wt.% Ni-Al₂O₃ and (f) reacted 40 wt.% Ni-Al₂O₃

6.5 The influence of water/steam injection rate

6.5.1 Product yield

The influence of water/steam injection rate on the product yield and hydrogen production was investigated. The gasification stage containing 10 wt.% Ni-Al₂O₃ catalyst was heated up to 1000 °C first and the bagasse sample was pyrolysed in the first stage from room temperature to 950 °C at a constant heating rate of 20 °C min⁻¹. The injection of steam into the gasification stage was also started with the pyrolysis of bagasse. Volatiles, liquids and gases evolved from the pyrolysis stage were made to react with the catalyst at high temperature in the presence of steam. The product gas and hydrogen yield results obtained using different water injection rates of 6, 15, 25 and 35 ml hr⁻¹ are shown in Table 6-8.

Table 6-8 The influence of water injection rate on pyrolysis (950 °C) - gasification (1000 °C) of sugarcane bagasse

	Water Injection rate (ml hr ⁻¹)			
	6	15	25	35
Sample weight (g)	4.00	4.00	4.00	4.00
Sample particle size (µm)	1405-2800	1405-2800	1405-2800	1405-2800
Catalyst	10%Ni-Al ₂ O ₃	10%Ni-Al ₂ O ₃	10%Ni-Al ₂ O ₃	10%Ni-Al ₂ O ₃
Catalyst weight (g)	2	2	2	2
Calcination temperature (°C)	900	900	900	900
Nitrogen flow rate (ml min ⁻¹)	100	100	100	100
H ₂ (mmoles g ⁻¹ of biomass)	29.93	41.92	42.46	44.47
Mass balance (wt.%)				
Gas/(biomass+water)	28.80	15.41	9.76	7.35
Solid/(biomass+water)	8.97	4.92	3.23	2.50
Mass balance	97.08	92.92	94.01	94.74
Gas/(biomass)	74.67	74.33	70.96	69.81
Solid/(biomass)	23.25	23.75	23.50	23.75

From the results shown in Table 6-8, it is clear that the increase in water injection rate showed a significant improvement in terms of hydrogen yield however, the gas yield was almost unaffected. The gas yield in relation to biomass + water reduced with the increase in water injection rate as the amount of water/steam injected was increased for the same amount of biomass. The gas yield in relation to biomass only (corrected for no input water) was slightly decreased from 74.67 to 74.33 wt.% with the increase in water injection rate from 6 to 15 ml hr⁻¹. Further increase in water injection rate to 25 and 35 ml hr⁻¹ had no effect on gas yield (~70 wt.%). It is suggested the excessive steam injection resulted in loss of energetic efficiency and hence the gas yield [29]. Lv et al. [30] reported a decrease in gas quality and reaction temperature with the excessive steam injection.

6.5.2 The influence of water injection rate on gas composition and hydrogen production

The product gas composition results presented in Figure 6-17 show that the increase in water/steam injection rate improved the hydrogen gas concentration. The hydrogen gas concentration increased from 60.73 to 72.92 vol.% with the increase in water/steam injection rate from 6 to 35 ml hr⁻¹. The hydrogen production result shown in Table 6-8 also indicated a substantial increase in hydrogen yield from 29.93 to 44.47 mmoles g⁻¹. The increase in hydrogen yield was due to the effective tar destruction and steam reforming reactions. The CO concentration in the gaseous mixture was sharply reduced from 20.43 to 9.37 vol.%. The increase in hydrogen concentration with the decrease in CO concentration suggests that the increasing water injection rate shifted the equilibrium of the water gas shift reaction towards hydrogen formation. This statement was confirmed by the increase in H₂:CO ratio. With the increase in water/steam injection rate from 6 to 35 ml hr⁻¹, the H₂:CO ratio was considerably increased from 2.97 to 7.78. The concentration of CO₂ did not show any substantial variation. It slightly reduced from 18.52 to 16.13 vol.% with the increase in water injection rate from 6 to 35 ml hr⁻¹. Franco et al. [20] investigated the influence of steam to biomass ratio during the steam gasification of pine wood at 800 °C. They also reported an increase in hydrogen concentration in the gas mixture with the decrease in CO concentration. No significant changes in CO₂ concentration were observed. Xiao et al. [29] studied the influence of steam to feedstock ratio in a multi-stage fluidised bed

reactor. It was observed that the increase in steam to biomass ratio resulted in an increase in hydrogen concentration with a decrease in CO concentration.

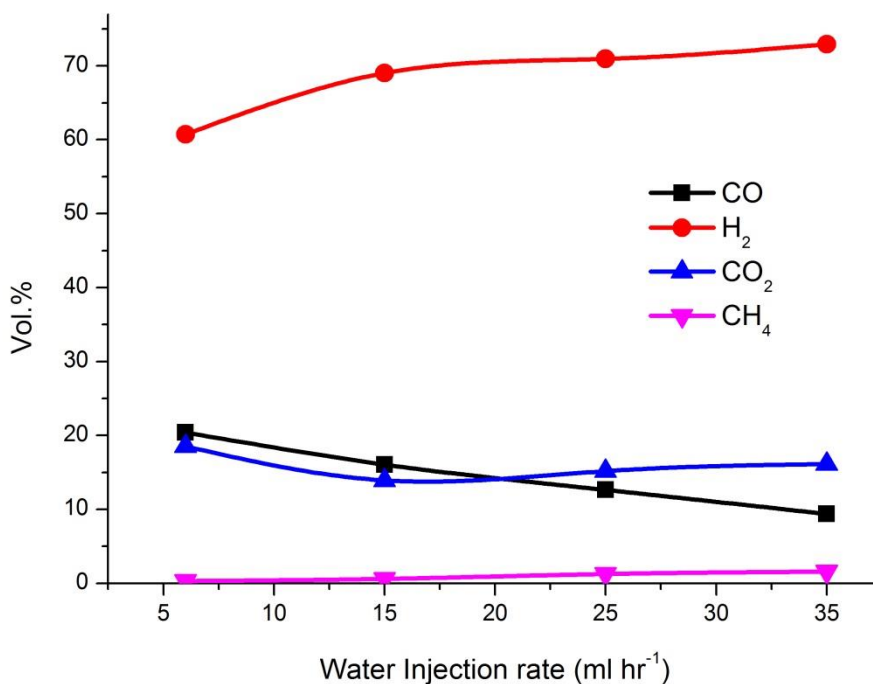


Figure 6-17 The influence of water injection rate on gas composition

It is suggested that the presence of steam or increase in steam concentration affects the equilibrium of various reactions. It is interesting to note that the increase in water/steam injection rate from 6 to 35 ml hr⁻¹ led to a slight increase in methane concentration from 0.32 to 1.58 vol.%. This increase in methane concentration at higher water injection rate was most likely due to the shift of equilibrium of the methane formation reaction. Franco et al. [20] also suggested that the increase in methane concentration at higher steam to biomass ratios was due to the methanation reaction.

The TGA-TPO and DTG-TPO thermograms of reacted catalysts are plotted in Figure 6-18. From these results it is evident that the process of gasification was efficient under these conditions and no carbon deposits were observed on the reacted catalysts. As the higher gasification temperature of 1000 °C was used during this study, catalyst was

slightly affected by the sintering of the alumina support. This behaviour is previously shown in SEM images of reacted catalysts during the temperature study (Figure 6-12e).

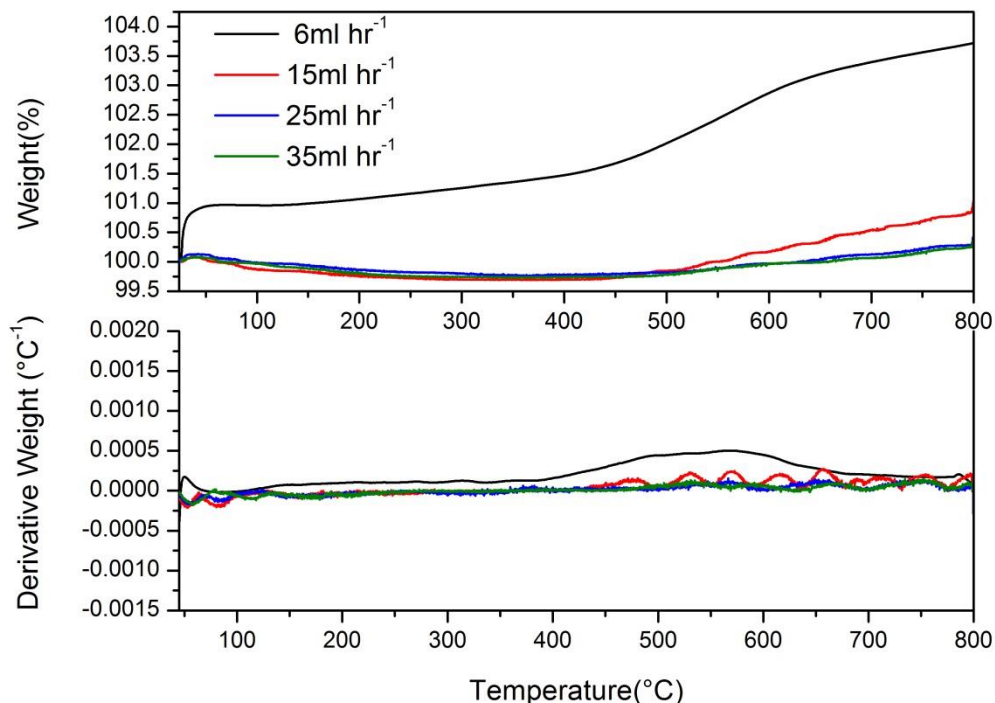


Figure 6-18 TGA-TPO and DTG-TPO results showing the effect of water injection rate on reacted 10 wt.% Ni-Al₂O₃ catalyst during the pyrolysis-gasification of sugarcane bagasse

6.6 The influence of calcination temperature

6.6.1 Characterization of fresh catalysts

The surface properties of freshly prepared 10 % Ni-Al₂O₃ catalysts calcined at different temperatures were investigated using a Quatachrome Nova 2200 analyser. The pore size distribution and N₂ adsorption/desorption isotherms are shown in Figure 6-19. The pore size distribution results indicate that the higher number of mesopores with smaller diameter (3 - 10 nm) were present in these catalysts. As shown in Table 6-9, with the increase in calcination temperature from 700 to 1000 °C the pore diameter was considerably increased from 3.78 nm to 7.85 nm. A decline in BET surface area from

118.90 to 64.77 $\text{m}^2 \text{g}^{-1}$ was also witnessed with the increase in calcination temperature (Table 6-9). As the surface area of the catalyst depends on the number of pores and the size of each pore, it is suggested that at higher calcination temperatures, lower BET surface area was most likely due to the merger of large number of small pores forming a relatively small number of large pores (Figure 6-19-(a)).

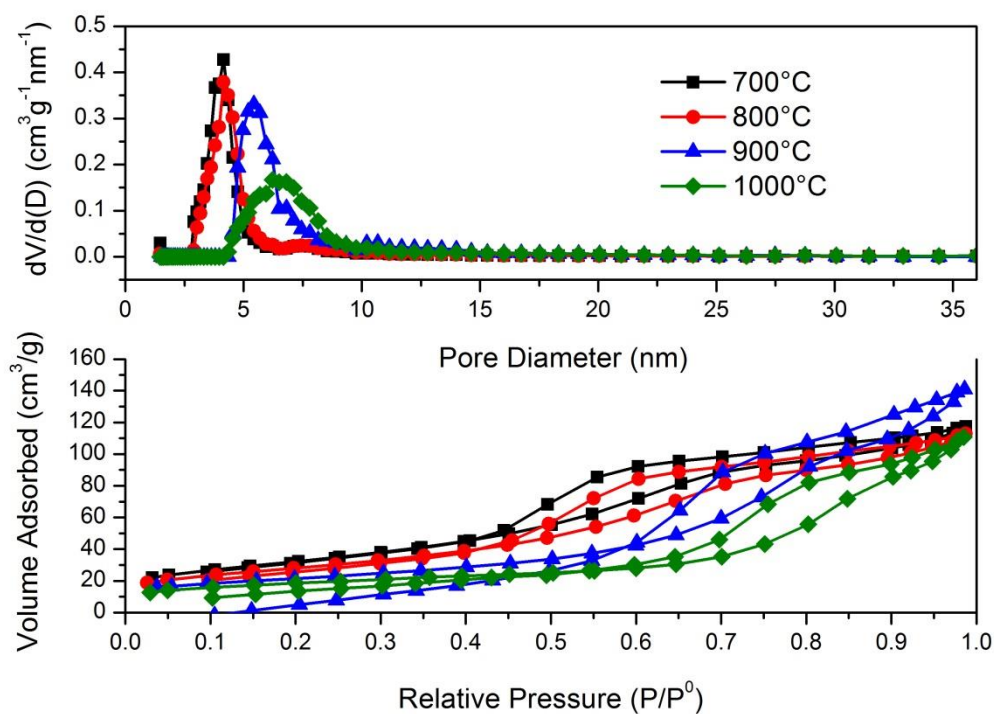


Figure 6-19 Pore size distribution (a), and N_2 adsorption/desorption isotherms of the fresh catalysts (b)

Table 6-9 Surface properties of fresh catalysts

Fresh catalyst	Calcination temp	BET surface area	BJH pore volume	Average pore size
	($^{\circ}\text{C}$)	$\text{m}^2 \text{g}^{-1}$	$\text{cm}^3 \text{g}^{-1}$	nm
10% Ni- Al_2O_3	700	118.90	0.1994	3.78
	800	102.90	0.1974	4.30
	900	76.82	0.2792	5.64
	1000	64.77	0.1903	7.85

The N₂ adsorption/desorption isotherms shown in Figure 6-19 indicate the type 4 isotherms demonstrating hysteresis loop [2]. The type 4 isotherm is characteristic of mesoporous materials. The hysteresis loop present is type H4 which is often associated with the capillary condensation taking place in narrow slit-like pores [2]. As indicated in Figure 6-19, with the increase in calcination temperature, the volume of gas adsorbed/desorbed per gram was reduced and hysteresis loop was shifted towards higher relative pressure. The lower volume of gas adsorbed/desorbed at higher calcination temperature indicate the reduction in number of pores and hence the surface area while the shift of hysteresis loop towards higher relative pressure was probably due to the presence of larger pore produced at higher calcination temperatures [31].

6.6.2 Product yield

Table 6-10 The effect of calcination temperature on pyrolysis (950 °C) - gasification (1000 °C) of sugarcane bagasse

	Calcination temperature (°C)			
	700	800	900	1000
Sample weight (g)	4.00	4.00	4.00	4.00
Sample particle size (µm)	1405-2800	1405-2800	1405-2800	1405-2800
Catalyst	10%Ni-Al ₂ O ₃			
Catalyst weight (g)	2	2	2	2
Water injection rate (ml hr ⁻¹)	25	25	25	25
Nitrogen flow rate (ml min ⁻¹)	100	100	100	100
H ₂ (mmoles g ⁻¹ of biomass)	35.72	42.29	42.46	42.06
Mass balance (wt.%)				
Gas/(biomass+water)	9.63	9.87	9.76	9.60
Solid/(biomass+water)	3.43	3.34	3.23	3.34
Mass balance	95.28	94.43	94.04	93.32
Gas/(biomass)	68.80	71.62	70.96	70.47
Solid/(biomass)	24.50	24.25	23.50	24.50

In this section, the influence of catalyst calcination temperature on product yield was investigated. The gas yield and hydrogen production results are shown in Table 6-10.

From these results, it is clear that under the investigated experimental conditions, calcination temperature showed very little influence in terms of gas yield and hydrogen production. The product gas yield in relation to biomass + water initially increased slightly from 9.63 to 9.87 wt.% with the increase in calcination temperature from 700 to 800 °C. Further increase in calcination temperature to 900 and 1000 °C resulted in a slight reduction in gas yield to 9.76 wt.% and 9.60 wt.%. With the increase in calcination temperature from 700 to 800 °C, hydrogen production also showed an initial increase from 35.72 to 42.29 mmoles g⁻¹ of biomass however; further increase in calcination temperature to 900 and 1000 °C did not show any improvements in terms of gas yield and hydrogen yield.

Calcination temperature is one of the important factors in determining the catalytic activity and long term effectiveness of a catalyst. Catalysts calcined at lower calcination temperature show lower stability while higher calcination temperature may lead to a lower surface area and hence lower gas and hydrogen yield [32, 33]. One possible explanation for lower catalytic activity at higher calcination temperature is the formation of stable compounds due to the strong metal support interaction. Although these compounds help reduce the sintering effect because these compounds are difficult to reduce back into active metal hence the catalytic activity of such catalysts was reduced [34]. Similar findings were reported by Srinakruang et al. [25] who investigated the influence of calcination temperature on Ni/dolomite during tar gasification. It was found that the catalysts calcined at lower temperatures of 500 and 750 °C showed higher activity due to the presence of a large amount of active metallic Ni while catalyst calcined at higher temperature of 950 °C showed the presence of NiMgO₂ which was difficult to reduce.

6.6.3 The influence of calcination temperature on gas composition and hydrogen production

In this section, the influence of catalyst calcination temperature on product gas composition was studied. The product gas composition results shown in Figure 6-20 indicate that under the investigated experimental conditions, calcination temperature showed little or no influence on product gas distribution. The hydrogen concentration initially increased slightly from 67.99 to 71.04 vol.% with the increase in calcination

temperature from 700 to 800 °C however further increases in calcination temperature did not shown any changes in hydrogen gas concentration.

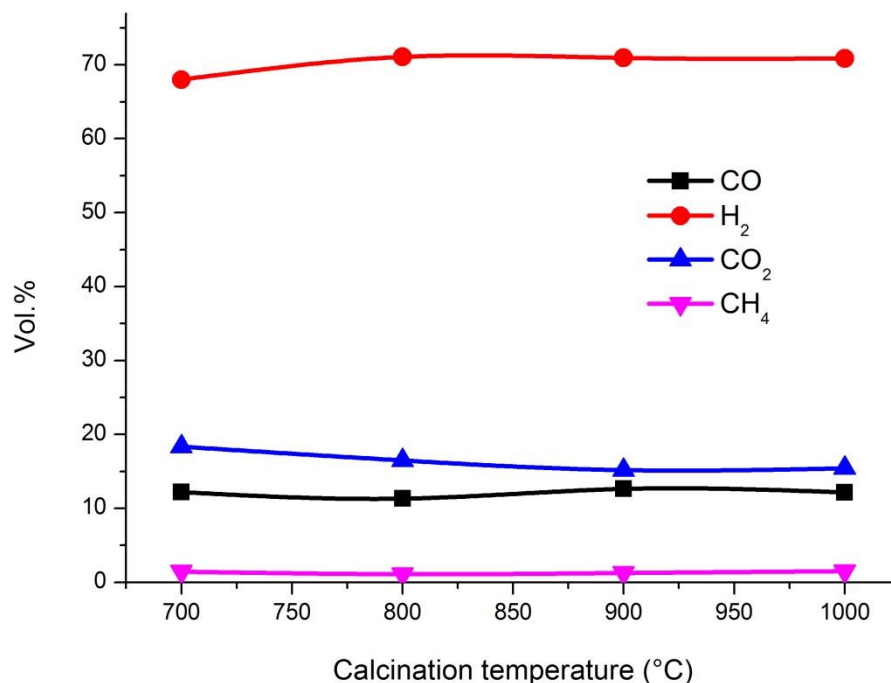


Figure 6-20 The influence of calcination temperature on gas composition

As shown in Figure 6-20, the concentration of other gases including CO, CO₂ and CH₄ also showed little or no influence of calcination temperature. The concentration of CO, CO₂ and CH₄ in the product gas mixture was found to be ~12, ~16 and ~1.5 vol.% respectively. The influence of calcination temperature on the surface area of fresh and reacted catalyst was plotted in Figure 6-21. It is clear from these results that catalyst calcined at lower temperatures of 700 and 800 °C showed significant loss of surface area after the gasification process. But the catalyst calcined at higher temperature of 900 and 1000 °C showed relatively lesser reduction of surface area. It is suggested that the catalyst calcined at lower temperature, when exposed to the higher gasification temperature (in this case 1000 °C) initially showed higher catalytic activity and deactivated due to the significant loss of surface area perhaps due to sintering. Similar findings were reported by Xu et al. [34] who investigated the catalytic cracking of rice husk over iron oxide supported on alumina. It was reported that the catalyst calcined at

600 °C showed higher initial catalytic activity however, catalytic activity was significantly reduced by the end of the experiment. It is suggested that the catalysts calcined at higher temperature of 900 and 1000 °C, showed lower loss of surface area perhaps due to the formation of nickel aluminate which prevented sintering.

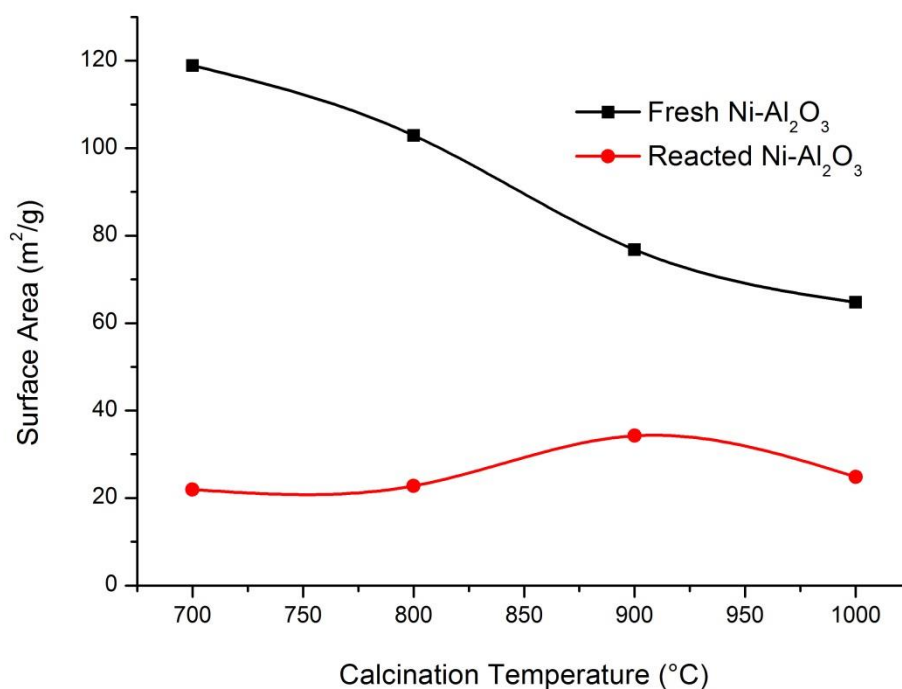


Figure 6-21 The influence of calcination temperature on surface area of fresh and reacted catalysts

6.7 The influence of catalyst to sample ratio

6.7.1 Product yield

In this section the influence of catalyst to sample ratio on product yield and hydrogen production was studied. In order to obtain different catalyst to sample ratios, the mass of the biomass was kept constant while the mass of the catalyst was varied. To achieve catalyst to sample ratios of 0.1, 0.5 and 2.0, the amount of catalyst used during the gasification was 0.4, 2 and 8 grams. During each experiment, 4 grams of biomass was pyrolysed at 950 °C. The volatiles, liquids and gases evolved from the pyrolysis stage

were gasified in the second stage already maintained at 1000 °C in the presence of catalyst and steam. The product yield and hydrogen yield results (Table 6-11) were also compared with the blank experiment. During the blank experiment, all the experimental conditions were identical however no biomass was placed inside the reactor.

Table 6-11 The effect of catalyst to sample ratio on pyrolysis (950 °C) - gasification (1000 °C) of sugarcane bagasse

	Catalyst to sample ratio			
	Blank	0.1	0.5	2
Sample weight (g)	NA*	4.00	4.00	4.00
Sample particle size (µm)	NA*	1405- 2800	1405- 2800	1405- 2800
Catalyst	10%Ni- Al ₂ O ₃			
Catalyst weight (g)	2.00	0.40	2.00	8.00
Water injection rate (ml hr ⁻¹)	25	25	25	25
Nitrogen flow rate (ml min ⁻¹)	100	100	100	100
H ₂ (mmoles g ⁻¹ of biomass)	6.33	39.18	42.46	44.70
Mass balance (wt.%)				
Gas/(biomass+water)	0.32	9.49	9.76	9.93
Solid/(biomass+water)	NA*	3.36	3.23	3.31
Mass balance	97.69	94.39	94.01	95.05
Gas/(biomass)	NA*	69.15	70.96	71.24
Solid/(biomass)	NA*	24.50	23.50	23.75

*NA – Not Applicable

The product yield results shown in Table 6-11, did not show any significant improvement in terms of product gas yield and hydrogen yield. In addition, with the increase in catalyst to sample ratio from 0.1 to 0.5 and 2.0, gas yield in relation to biomass and water also showed little influence. The gas yield in relation to biomass only (corrected for no input water) was also only marginally influenced, when C/S ratio was increased from 0.1 to 0.5 and to 2.0. Li et al. [9] suggested that the higher quantity of catalyst inside the reactor prolonged the gas residence time and promoted various gasification reactions. An increase in gas yield with the increase in C/S ratio was reported by other researchers. For example, Li et al. [9] researched the catalytic steam

gasification of municipal solid waste (MSW) in a two-stage fixed-bed reactor system. It was reported that with the increase in catalyst to MSW ratio from 0.5 to 2.0, the gas yield slightly improved from 2.1 to 2.25 m³ kg⁻¹. García et al. [35] also studied the influence of catalyst to sample ratio. They suggested using the catalyst to sample ratio of 0.65 or higher. It was reported that during the catalytic steam gasification of pine sawdust, for catalyst to sample ratio of less than 0.65, a decrease in total gas yield was observed due to the catalyst deactivation.

As indicated in Table 6-11, when compared with the identical condition experiment with C/S of 0.5, during the blank experiment (no biomass was placed inside the reactor), only a small amount of gas (0.32 wt.%) in relation to steam was attained as compared to the normal experiment where 9.76 wt.% of gas in relation to biomass and water was obtained. Also for the blank experiment, only 6.33 mmoles were obtained as compared to 42.46 mmoles found for the steam gasification experiment with biomass. The small amount of gas and hydrogen obtained during the blank experiment was perhaps due to the gasification of a small amount of carbon and tar components present inside the reactor as small concentration of CO₂ (along with the hydrogen) in the product gaseous mixture was also detected during the blank experiment. Bimbela et al. [36] explored the influence of catalyst weight to sample flow rate during the catalytic steam reforming of model pyrolysis liquid compounds. It was found that the gas yield as well as carbon conversion was increased with the increase in catalyst to sample ratio.

6.7.2 The influence of catalyst to sample ratio on gas composition and hydrogen production

The influence of catalyst to sample ratio on product gas composition is shown in Figure 6-22. From the results shown in Figure 6-22, it is clear that under the investigated experimental conditions, the increase in catalyst to sample ratio showed little or no influence of product gas composition. The hydrogen concentration slightly varied from 69.73 vol.% for the C/S ratio of 0.1 to 72.39 vol.% for the C/S ratio of 2.0. The hydrogen production results shown in Table 6-11 also presented a slight increase from 39.18 mmoles per gram of bagasse to 44.70 mmoles per gram of bagasse. The decrease in CH₄ concentration from 2.07 to 1.08 vol.% was also observed. The increase in

hydrogen concentration along with the decrease in CH_4 concentration suggests that the methane steam reforming was promoted due to the increase in the number of available active catalyst sites with the increase in C/S ratio. The concentrations of CO and CO_2 in the product gas mixture remain unchanged around 11 and 16 vol.% respectively.

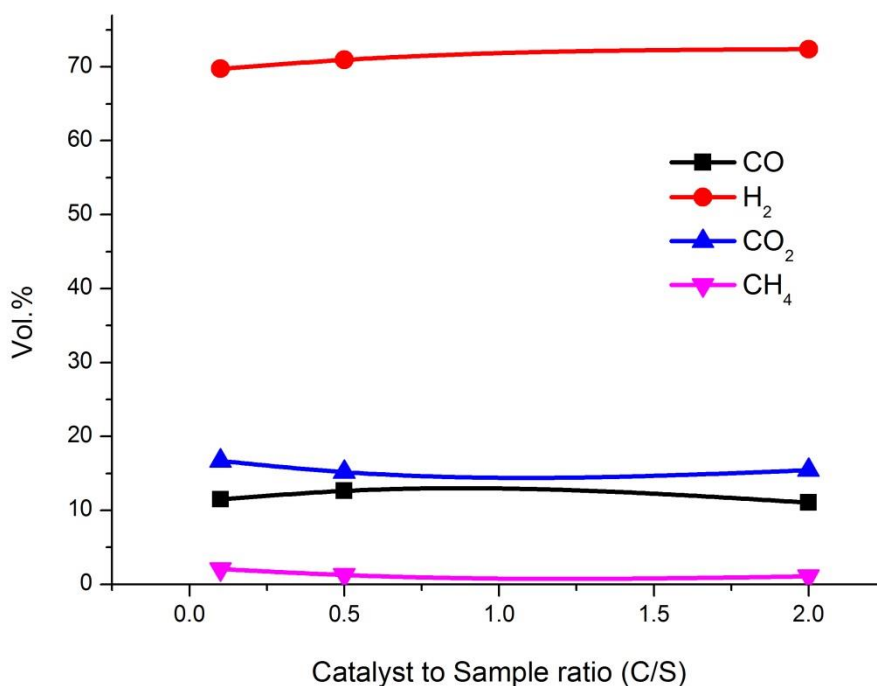


Figure 6-22 The influence of catalyst to sample ratio on gas composition

Li et al. [9] also reported similar trends of product gas composition obtained from the catalyst to sample ratio of 0.5 to 2.0 during steam gasification at 800 °C. They reported an increase in hydrogen gas concentration along with the decrease in methane and other lighter hydrocarbons. The concentration of CO and CO_2 was almost unchanged at around 20 vol.%.

6.8 Conclusions

In this chapter catalyst selection and several other process conditions were researched with the aim to maximize the hydrogen yield from two-stage pyrolysis/gasification of sugarcane bagasse. The following conclusions can be made from this chapter.

- During the catalyst selection process (Section 6.2), seven different Ni-based catalysts; 10 % Ni-dolomite, 10 % Ni-MgO, 10 % Ni-SiO₂, 10 % Ni-Al₂O₃, 2 wt.% Ce – 10 % Ni-dolomite, 5 wt.% Ce – 10 % Ni-dolomite and 10 wt.% Ce – 10 % Ni-dolomite were investigated. When compared with the silica sand as a substitute, the 10 % Ni-Al₂O₃ catalyst produced the highest hydrogen yield of 29.62 mmoles per gram of bagasse (Table 6-2) at a gasification temperature of 950 °C. Compared to the other catalysts, the higher hydrogen yield obtained using the 10 % Ni-Al₂O₃ catalyst was due to the higher surface area of this catalyst. Hence the 10 % Ni-Al₂O₃ catalyst was selected for further investigation of other process conditions like gasification temperature, water injection rate.
- The gasification temperature showed a positive influence on hydrogen yield. The hydrogen yield increased from 21.17 mmoles g⁻¹ at 800 °C to 35.65 mmoles g⁻¹ at 1050 °C. It was noticed that the hydrogen concentration in the product gas mixture was also increased from 50.31 vol.% at 800 °C to 67.40 vol.% at 1050 °C. The increase in hydrogen concentration with the increase in gasification temperature was due to the enhanced thermal cracking and catalytic reforming of tar and hydrocarbons. Higher gasification temperatures also favoured different endothermic reactions resulting in higher gas yield and hydrogen yield.
- In section 6.4, the influence of nickel loading on Ni-Al₂O₃ catalyst was researched. The amount of nickel in catalyst was increased from 5 wt.% to 10 wt.%, 20 wt.% and to 40 wt.%. The increase in nickel contents shows little or no influence on hydrogen yield. The highest hydrogen yield of 29.62 mmoles g⁻¹ was obtained using the 10 wt.% Ni-Al₂O₃ catalyst. The concentration of hydrogen was also unchanged at around 60 vol.%.

- Increasing water/steam injection rate dramatically improved hydrogen yield from 29.93 mmol g⁻¹ using 6 ml hr⁻¹ to 44.47 mmol g⁻¹ using 35 ml hr⁻¹. By increasing water/steam injection rate, the equilibrium of the water gas shift reaction was shifted towards hydrogen formation. The increase in water injection rate also promoted steam reforming of methane and tar components. A sharp increase in hydrogen concentration from 60.72 vol.% for 6 ml hr⁻¹ to 72.92 vol.% for 35 ml hr⁻¹ water injection rate was obtained. The increase in H₂:CO ratio from 2.97 to 7.78 confirmed the positive influence of water injection rate on the water gas shift reaction.
- In section 6.6, the influence of calcination temperature on hydrogen yield was investigated. Initial characterization of fresh catalysts revealed that with the increase in calcination temperature from 700 to 1000 °C, average pore size was increased while BET surface area was reduced from 118.90 to 64.77 m² g⁻¹. Hydrogen yield was initially increased from 35.72 to 42.29 mmol g⁻¹ with the increase in calcination temperature from 700 to 800 °C, however further increase in calcination temperature to 900 and 1000 °C did not show any improvements in hydrogen yield.
- The increase in catalyst to biomass sample ratio slightly improved hydrogen yield. With the increase in C/S ratio from 0.1 to 2.0, hydrogen yield was increased from 39.18 to 44.70 mmol per gram of bagasse. It was reported that this increase in hydrogen yield along with the decrease in methane concentration was due to the promotion of reforming reactions caused by the increase in the number of available catalyst sites.

6.9 Chapter references

- [1] L. I. Darvell, K. Heiskanen, J. M. Jones, A. B. Ross, P. Simell, and A. Williams, "An investigation of alumina-supported catalysts for the selective catalytic oxidation of ammonia in biomass gasification," *Catalysis Today*, vol. 81, pp. 681-692, 2003.
- [2] K. Sing, D. Everett;, R. Haul;, L. M. ;, R. P. ;, J. R. ;, *et al.*, "Reporting Physisorption data for Gas/Solid systems with Special Reference to the Determination of Surface Area and Porosity," *Pure and Applied Chemistry*, vol. 57, pp. 603-619, 1985.
- [3] P. A. Webb, Orr, Clyde,, *Analytical methods in fine particle technology*: Micromeritics Instrument Corporation, 1997.
- [4] J. E. S. S. Lowell, Martin A. Thomas, Matthias Thommes, *Characterization of Porous Solids and Powders: Surface Area, Pore Size and Density*: Springer Netherlands, 2004.
- [5] V. L. B. J. Requies, J. F. Cambra, M. B. Guemez, P. L. Arias, M. A. Pena, and J. L. G. Fierro, "Methane Catalytic Wet Partial Oxidation Using Nickel Supported on Basic Oxides," *Journal of New Materials for Electrochemical Systems*, vol. 12, pp. 161-166, 2009.
- [6] F. Miccio, B. Piriou, G. Ruoppolo, and R. Chirone, "Biomass gasification in a catalytic fluidized reactor with beds of different materials," *Chemical Engineering Journal*, vol. 154, pp. 369-374, 2009.
- [7] R. Isha and P. T. Williams, "Hydrogen production from catalytic steam reforming of methane: influence of catalyst composition," *Journal of the Energy Institute*, vol. 85, pp. 29-37, 2012.
- [8] Q. Xie, S. Kong, Y. Liu, and H. Zeng, "Syngas production by two-stage method of biomass catalytic pyrolysis and gasification," *Bioresource Technology*, vol. 110, pp. 603-609, 4// 2012.
- [9] J. L. Jianfen Li, Shiyan Liao, Xiaorong Zhou, Rong Yan "Syn-Gas Production from Catalytic Steam Gasification of Municipal Solid Wastes in a Combined Fixed Bed Reactor," 2010, pp. 530-534.
- [10] C. S. Nordahl and G. L. Messing, "Sintering of α -Al₂O₃-seeded nanocrystalline γ -Al₂O₃ powders," *Journal of the European Ceramic Society*, vol. 22, pp. 415-422, 4// 2002.
- [11] J.-P. Ahn, J.-K. Park, and H.-W. Lee, "Effect of compact structures on the phase transition, subsequent densification and microstructure evolution during sintering of ultrafine gamma alumina powder," *Nanostructured Materials*, vol. 11, pp. 133-140, 2// 1999.
- [12] K. Hessam;, D. Trimm;, M. Wainwright;, and N. Cant, "Phase-transformation of gamma-alumina to alpha-alumina as an industrial catalyst support," *International Journal of Engineering*, vol. 4, pp. 1-12, 1991.
- [13] S. Wang and G. Q. Lu, "Role of CeO₂ in Ni/CeO₂-Al₂O₃ catalysts for carbon dioxide reforming of methane," *Applied Catalysis B: Environmental*, vol. 19, pp. 267-277, 12/7/ 1998.
- [14] C. Wu and P. T. Williams, "Hydrogen production by steam gasification of polypropylene with various nickel catalysts," *Applied Catalysis B: Environmental*, vol. 87, pp. 152-161, 4/7/ 2009.
- [15] P. H. Blanco, C. Wu, J. A. Onwudili, and P. T. Williams, "Characterization and evaluation of Ni/SiO₂ catalysts for hydrogen production and tar reduction from

- catalytic steam pyrolysis-reforming of refuse derived fuel," *Applied Catalysis B: Environmental*, vol. 134–135, pp. 238-250, 2013.
- [16] J. F. González, S. Román, G. Engo, J. M. Encinar, and G. Martínez, "Reduction of tars by dolomite cracking during two-stage gasification of olive cake," *Biomass and Bioenergy*, vol. 35, pp. 4324-4330, 10/15/ 2011.
- [17] V. Skoulou, A. Swiderski, W. Yang, and A. Zabaniotou, "Process characteristics and products of olive kernel high temperature steam gasification (HTSG)," *Bioresource Technology*, vol. 100, pp. 2444-2451, 2009.
- [18] L. Emami Taba, M. F. Irfan, W. A. M. Wan Daud, and M. H. Chakrabarti, "The effect of temperature on various parameters in coal, biomass and CO-gasification: A review," *Renewable and Sustainable Energy Reviews*, vol. 16, pp. 5584-5596, 2012.
- [19] P. Lahijani and Z. A. Zainal, "Gasification of palm empty fruit bunch in a bubbling fluidized bed: A performance and agglomeration study," *Bioresource Technology*, vol. 102, pp. 2068-2076, 2011.
- [20] C. Franco, F. Pinto, I. Gulyurtlu, and I. Cabrita, "The study of reactions influencing the biomass steam gasification process," *Fuel*, vol. 82, pp. 835-842, 2003.
- [21] J. Sehested, "Sintering of nickel steam-reforming catalysts," *Journal of Catalysis*, vol. 217, pp. 417-426, 2003.
- [22] J. Sehested, "Four challenges for nickel steam-reforming catalysts," *Catalysis Today*, vol. 111, pp. 103-110, 2006.
- [23] T. W. Hansen, A. T. DeLaRiva, S. R. Challa, and A. K. Datye, "Sintering of Catalytic Nanoparticles: Particle Migration or Ostwald Ripening?," *Accounts of Chemical Research*, 2013.
- [24] J. Sehested, J. A. P. Gelten, and S. Helveg, "Sintering of nickel catalysts: Effects of time, atmosphere, temperature, nickel-carrier interactions, and dopants," *Applied Catalysis A: General*, vol. 309, pp. 237-246, 2006.
- [25] J. Srinakruang, K. Sato, T. Vitidsant, and K. Fujimoto, "Highly efficient sulfur and coking resistance catalysts for tar gasification with steam," *Fuel*, vol. 85, pp. 2419-2426, 2006.
- [26] D. N. Bangala, N. Abatzoglou, and E. Chornet, "Steam reforming of naphthalene on Ni–Cr/Al₂O₃ catalysts doped with MgO, TiO₂, and La₂O₃," *AIChE Journal*, vol. 44, pp. 927-936, 1998.
- [27] S. Nassos, E. Elm Svensson, M. Boutonnet, and S. G. Järås, "The influence of Ni load and support material on catalysts for the selective catalytic oxidation of ammonia in gasified biomass," *Applied Catalysis B: Environmental*, vol. 74, pp. 92-102, 2007.
- [28] A. Z. M. Mohammad Zangouei, Mehdi Arasteh "The influence of nickel loading on reducibility of NiO/Al₂O₃ catalysts synthesized by sol-gel method," *Chemical Engineering Research Bulletin*, vol. 14, pp. 97-102, 2010.
- [29] X. Xiao, D. D. Le, K. Morishita, S. Zhang, L. Li, and T. Takarada, "Multi-stage biomass gasification in Internally Circulating Fluidized-bed Gasifier (ICFG): Test operation of animal-waste-derived biomass and parametric investigation at low temperature," *Fuel Processing Technology*, vol. 91, pp. 895-902, 2010.
- [30] P. M. Lv, Z. H. Xiong, J. Chang, C. Z. Wu, Y. Chen, and J. X. Zhu, "An experimental study on biomass air-steam gasification in a fluidized bed," *Bioresource Technology*, vol. 95, pp. 95-101, 2004.

- [31] K. Sasaki, X. Qiu, Y. Hosomomi, S. Moriyama, and T. Hirajima, "Effect of natural dolomite calcination temperature on sorption of borate onto calcined products," *Microporous and Mesoporous Materials*, vol. 171, pp. 1-8, 2013.
- [32] D. Sutton, B. Kelleher, and J. R. H. Ross, "Review of literature on catalysts for biomass gasification," *Fuel Processing Technology*, vol. 73, pp. 155-173, 2001.
- [33] C. Wu and P. T. Williams, "Ni/CeO₂/ZSM-5 catalysts for the production of hydrogen from the pyrolysis-gasification of polypropylene," *International Journal of Hydrogen Energy*, vol. 34, pp. 6242-6252, 8// 2009.
- [34] X. Xu, J. Enchen, W. Mingfeng, L. Bosong, and Z. Ling, "Hydrogen production by catalytic cracking of rice husk over Fe₂O₃/γ-Al₂O₃ catalyst," *Renewable Energy*, vol. 41, pp. 23-28, 5// 2012.
- [35] S. M. GarcPSa L, Arauzo J, Bilbao R, "Catalytic steam gasification of pine sawdust. Effect of catalyst weight/biomass flow rate and steam/biomass ratios on gas production and composition," *Energy and Fuels*, vol. 13, pp. 851-9, 1999.
- [36] F. Bimbela, M. Oliva, J. Ruiz, L. García, and J. Arauzo, "Catalytic steam reforming of model compounds of biomass pyrolysis liquids in fixed bed: Acetol and n-butanol," *Journal of Analytical and Applied Pyrolysis*, vol. 85, pp. 204-213, 2009.

CHAPTER 7 CHAR GASIFICATION

7.1 Introduction

In chapter 5 and 6, two-stage pyrolysis/gasification of rice husk, sugarcane bagasse and wheat straw was investigated at a pyrolysis temperature of 950 °C. Volatiles, liquids and tar components evolving from the first stage were gasified in the second stage, in the presence of steam and catalyst at higher temperature from 950 - 1000 °C. In this chapter, the residual char from pyrolysis of these three biomass samples was researched. The aim of this study is to enhance the hydrogen yield from per gram of biomass by gasifying the residual char samples at higher temperature with and without catalysts. During these experiments, the biomass char sample was mixed with the catalyst and placed inside the gasification stage on a quartz-wool bed. The gasification stage was heated up from room temperature to 950 °C in an inert atmosphere of nitrogen. Once the desired temperature was achieved, steam injection using a syringe pump was started. The unreacted steam was recovered using a glass condenser system. All non-condensable gases were collected using a gas bag and were analysed offline using gas chromatography.

Initially all three char samples (rice husk, sugarcane bagasse and wheat straw) were investigated using thermogravimetric analysis and an elemental analyser (section 7.2). The most suitable char sample was chosen in terms of higher carbon and lower ash contents. In section 7.3, high temperature (950 °C) steam gasification of the chosen biomass char was performed by mixing the char with different catalysts at catalyst to sample ratio of 1. The catalysts investigated in this study were 10 % Ni-dolomite, 10 % Ni-Al₂O₃ and 10 % Ni-MgO. The results were compared to the steam gasification of char without any catalysts. The most suitable catalyst was chosen in terms of the highest hydrogen yield for further investigation of other experimental conditions.

As the gasification temperature is one of the important parameters of char gasification, the influence of gasification temperature on gas yield and particularly hydrogen yield was investigated in section 7.4. The range of gasification temperature studied in this research was from 750 - 1050 °C with an increment of 100 °C. The influence of

water/steam injection rate on gasification of biomass char was also investigated in section 7.5. The steam injection rate was varied from 6 to 25 ml hr⁻¹ and the influence on hydrogen gas yield was investigated.

7.2 Characterization of char from rice husk wheat straw and sugarcane bagasse pyrolysis

In this section, residual chars obtained from the pyrolysis of rice husk, bagasse and wheat straw were characterised with the aim to select the best suited char sample in terms of higher carbon and lower ash contents. The elemental analysis of three bio-char samples was performed. The results of elemental analysis are shown in Table 7-1. From these results it is clear that the highest carbon contents of 81.55 wt.% were observed in bio-char from bagasse. The char from rice husk and wheat straw showed considerably lower carbon contents of 52 and 62.79 wt.% respectively. The percentage of other elements like hydrogen and nitrogen were almost similar in these three bio-char samples. The oxygen percentage was calculated by difference. The gross calorific value (GCV) results shown in Table 7-1 also indicate that the bagasse sample was the most favourable option for steam gasification.

Table 7-1 Elemental analysis of feedstock char

Elemental analysis					
Feed stock	C (wt.%)	H (wt.%)	N (wt.%)	O ^a (wt.%)	GCV MJ kg ⁻¹
Bagasse char	81.55	1.85	0.96	15.63	30.33
Rice husk char	52.00	1.24	0.62	46.13	19.41
Wheat straw char	62.79	1.87	1.33	34.01	23.91

^a Calculated by difference

These three bio-char samples were further investigated using thermogravimetric analysis. Approximately 5 mg of each bio-char samples was placed in the TGA in an air atmosphere and the weight loss curve and its derivative were recorded from ambient temperature to 935 °C with a hold time of 10 min. The aim of this research was to investigate the weight loss behaviour of these bio-char samples in an oxidative environment. The TGA and DTG thermograms of these three bio-char sample are plotted in Figure 7-1. These thermograms also provide some meaningful information

about the amount of residual ash left after oxidation at such a high temperature of 935 °C.

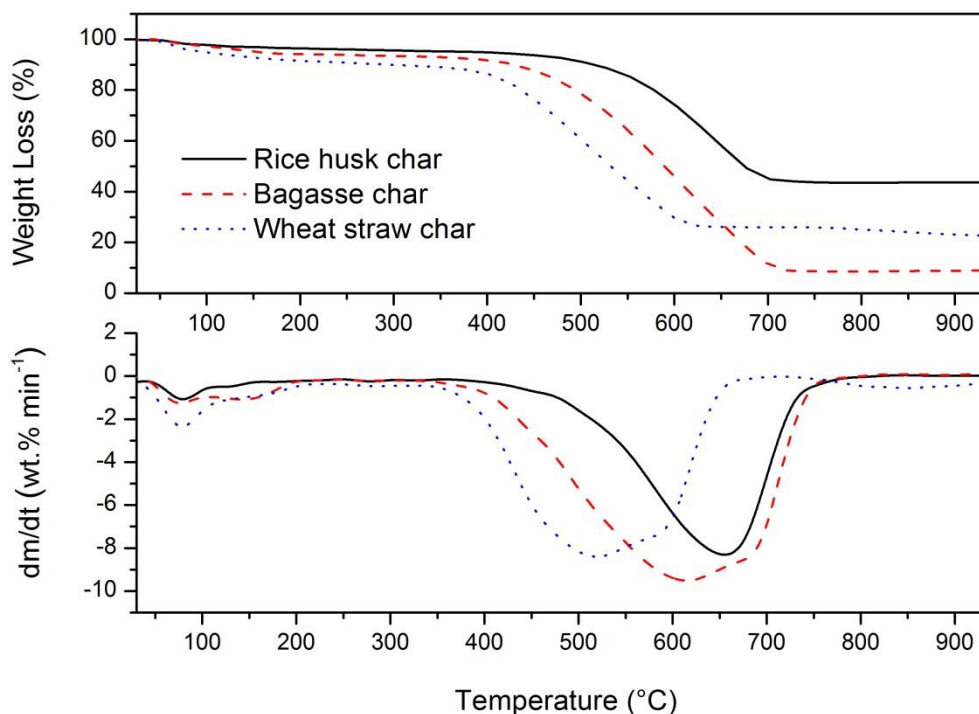


Figure 7-1 TGA and DTG thermograms of rice husk, sugarcane bagasse and wheat straw char at 25 °C min⁻¹

From the results shown in Figure 7-1, it is evident that the highest total weight loss was recorded for the sugarcane bagasse sample followed by wheat straw char and rice husk char respectively. Initially up to 100 °C, a slight weight loss was observed for all three samples which can be attributed to the loss of moisture from these samples. The main weight loss started at around 400 °C for all three samples and it was completed at 600 °C for wheat straw char and at 700 °C for rice husk and bagasse char respectively. After these temperatures, no significant weight loss was observed for these samples. The amount of residual ash calculated from the TGA data was 44.17, 22.66 and 9.44 wt.% for rice husk char, wheat straw char and bagasse char respectively. These TGA results when coupled with the elemental analysis results shown in Table 7-1 strongly indicate that the char obtained from the pyrolysis of bagasse was the most suitable candidate for the further investigation of hydrogen production from catalytic steam gasification of

bio-char at high temperatures. It is also interesting to note that from the pyrolysis of 4 grams of bagasse biomass (containing 45.5 wt.% carbon), ~ 1 g of char was obtained which contained around 81.55 wt.% of carbon. This indicates that around 50 % of the carbon contained in original biomass sample was still present in bio-char. From this fact, it can be inferred that the bio-char if completely gasified can produce an equal amount of hydrogen from gasification as compared to the original biomass.

Table 7-2 XRF analysis of ash from different biomass samples (wt.%)

	Wheat straw	Rice husk	Sugarcane bagasse
Al ₂ O ₃	10.46	1.27	9.08
BaO	0.04	-	0.1
CaO	5.43	2.34	9.4
Fe ₂ O ₃	0.58	0.95	3.48
K ₂ O	9.47	2.13	5.19
MgO	2.17	0.37	3.09
MnO	0.17	-	0.57
P ₂ O ₅	0.66	0.6	1.67
SiO ₂	59.38	86.88	47.84
SrO	0.05	0.01	0.18
TiO ₂	0.91	0.01	0.75

X-ray Fluorescence analysis (XRF) of ash (obtained from the oxidation of bio-char) was performed to investigate the presence of various metal oxides. The results of XRF are shown in Table 7-2. From these results it can be noticed that a large quantity of SiO₂ was present in all three samples however the ash obtained from rice husk char showed the highest quantity of 86.88 %. These findings were in agreement with the literature [1] where a higher proportion of around 90 % of silica was reported in rice husk ash.

It is also interesting to note that around 10 % Al₂O₃ was present in ash from bagasse and wheat straw while only 1.27 % of Al₂O₃ was present in rice husk ash. A significant quantity of CaO and K₂O was also present in wheat straw and sugarcane bagasse ash while rice hush ash contained only 2.34 % of CaO and 2.13 % of K₂O.

7.3 The influence of different catalysts on hydrogen production from gasification of sugarcane bagasse char at 950 °C

7.3.1 Product yield

In this section, the influence of different catalysts on hydrogen production from steam gasification of bio-char (obtained from the pyrolysis of sugarcane bagasse) was studied. Three different catalysts; 10 % Ni-MgO, 10 % Ni-Al₂O₃ and 10 % Ni-dolomite were mixed with the char sample at a catalyst to sample ratio of 1 and the results were compared to that of no catalyst. Various experimental conditions and hydrogen yield results are shown in Table 7-3. As 1gram of bio-char was obtained from the pyrolysis of 4 grams of sugarcane bagasse, hydrogen yield results are presented in Table 7-3, as mmoles per gram of char and mmoles per gram of biomass. These mmoles per gram of biomass results are calculated by dividing mmoles per gram of char results by 4.

Table 7-3 Gasification of sugarcane bagasse char at 950 °C using various catalysts

	Catalyst			
	no catalyst	10%Ni-Dolomite	10%Ni-Al ₂ O ₃	10%Ni-MgO
Bio-char particle size (µm)	212-500	212-500	212-500	212-500
Catalyst to sample ratio	0.00	1.00	1.00	1.00
Water injection rate (ml hr ⁻¹)	6	6	6	6
Nitrogen flowrate (ml min ⁻¹)	100	100	100	100
H ₂ (mmoles g ⁻¹ of biomass)	25.24	28.09	46.81	44.69
H ₂ (mmoles g ⁻¹ of char)	100.97	112.36	187.25	178.75
Mass balance (wt.%)				
Gas/(char + water injected)	23.83	21.84	11.80	12.77
Gas/(char)	274.74	265.88	225.53	237.82
Mass balance	95.26	92.95	96.11	94.83

From the results shown in Table 7-3, it is clear that the presence of catalyst significantly improved the hydrogen yield during gasification. When compared with the steam gasification without any catalyst, use of 10 % Ni-dolomite slightly improved the

hydrogen yield from 100.97 mmoles to 112.36 mmoles per gram of char. The addition of 10 % Ni-MgO showed an increase of 78 % as compared to no catalyst. The highest hydrogen yield of 187.25 mmoles per gram of char was obtained when the char sample was mixed with the 10 % Ni-Al₂O₃ catalyst. It is suggested that the higher hydrogen yield obtained using 10 % Ni-MgO and 10 % Ni-Al₂O₃ catalyst was most likely due to the higher surface area of these two catalysts. As already mentioned in chapter 6, the 10 % Ni-MgO and 10 % Ni-Al₂O₃ catalysts exhibited a higher surface area of 53.90 and 76.82 m² g⁻¹ respectively. The highly porous catalysts like 10 % Ni-MgO and 10 % Ni-Al₂O₃ when mixed with the char provided not only larger surface area with the active Ni sites but they also contributed towards shifting the chemical equilibria of various reactions to improve the hydrogen yield. The positive influence of different catalysts on char gasification has been reported in the literature. For example, Zhang et al. [2] reported that the addition of Ca and Na in the coal sample resulted in an increase in char conversion and hydrogen production. Kwon et al. [3] reported that the addition of K₂CO₃, Na₂CO₃, Li₂CO₃ catalysts with the char sample resulted in a change of order of reaction from one to zero. A significant improvement in terms of char conversion was also reported.

It has been suggested that in order to obtain a higher hydrogen yield, gasification of char containing higher fixed carbon and lower ash is recommended [4]. The catalytic role of various alkali and alkaline earth metals (AAEMs) was also reported. For example, Kajita et al. [5] investigated the steam gasification of a char sample obtained from the pyrolysis of cedar and bamboo biomass. The comparison of as-received char and acid-washed char revealed that the presence of AAEMs especially potassium strongly influence the conversion and reactivity of char samples by catalysing the various char conversion reactions. Otto et al. [6] also confirmed the catalytic effect of various metals like Pt, Rh, Ru and Pd. They reported that the addition of these catalysts strongly enhanced the gasification rate.

Moilanen et al. [7] reported the mechanism of gasification of solid a char particle. They suggested that the process of gasification of char starts by the diffusion of gasifying agent from atmosphere to particle surface and then to the inside of the particle resulting in adsorption onto the surface followed by the actual chemical reaction. Then the product gases desorbed from the reaction surface and diffuse back into the atmosphere. It was reported that for larger particle size diffusion is a rate limiting step [8]. If particle

size is very small such that there is no mass-transport limitation then the reaction is controlled by the chemical reactions (kinetic control) taking place onto the surface of the char. The smaller particle size of 212 – 500 μm was used in this study to enhance the gasification yield by minimizing the thermal gradient between the surface and inside the char particle. For smaller particle size, chemical reactions take place not only onto the surface of the char particle but also inside the char particle. Haykiri-Acma et al. [4] reported that the high temperature steam gasification of char is recommended for the production of hydrogen as the mechanism of gasification varies with the temperature. They reported that at lower temperature desorption of water takes place. At medium temperatures, production of CO was favoured along with the decomposition of hydroxide mineral while at high temperature production of hydrogen was favourable.

7.3.2 The influence of different catalysts on gas composition and hydrogen production

In this section the influence of catalyst on the product gas composition obtained from the steam gasification of sugarcane bagasse char was investigated. The product gas composition results are shown in Figure 7-2.

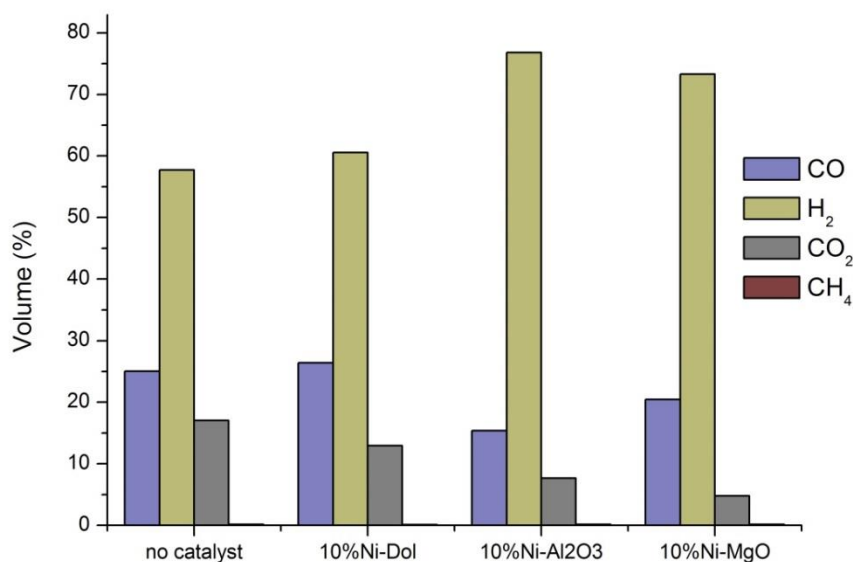


Figure 7-2 Composition of gases in the product mixture (nitrogen free) from gasification of sugarcane bagasse char using different catalysts

These results shown in Figure 7-2, clearly indicate that the presence of catalyst significantly improved the product gas composition in terms of H₂ production. The concentration of hydrogen was slightly improved from 57.74 vol.% for no catalyst to 60.54 vol.% for 10 % Ni-dolomite. Use of 10 % Ni-MgO further enhanced the hydrogen concentration to 73.30 vol.%. The highest hydrogen concentration of 76.81 vol.% was obtained when 10 % Ni-Al₂O₃ catalyst was used during gasification. It is interesting to note that the gasification of bio-char was strongly influenced by the presence of catalysts. It is suggested that these catalysts influenced the chemical equilibria of various reactions taking place inside the gasifier. Yang et al. [9] also reported that the hydrogen concentration was increased up to 1.8 times with the use of Au/Al₂O₃ catalyst during the steam gasification of char derived from the pyrolysis of *Dunaliella salina* biomass. Different chemical reactions taking place during the steam gasification of biomass char are listed in Chapter 2.

As shown in Figure 7-2, the highest concentration of hydrogen (76.81 vol.%) was achieved with the use of 10 % Ni-Al₂O₃ catalyst while a significant reduction in the concentration of CO from ~25 vol.% for no catalyst to ~15 vol.% for 10 % Ni-Al₂O₃ catalyst was observed. It is suggested that the presence of 10 % Ni-Al₂O₃ improved the hydrogen concentration by shifting the equilibrium of the water-gas shift reaction. The H₂:CO ratio was increased from 2.30 for no catalyst to 3.50 for 10 % Ni-MgO and to 5.00 for 10 % Ni-Al₂O₃ catalysts. The concentration of CO₂ was also sharply reduced from 17.05 vol.% for no catalyst to 7.67 vol.% for 10 % Ni-Al₂O₃ catalyst and to 4.77 vol.% for 10 % Ni-MgO catalyst. It is suggested that the higher gasifier temperature promoted the endothermic Boudouard reaction resulting in reduction of CO₂ concentration. The presence of catalyst does not seem to have any influence on the methanation reaction as the concentration of methane in the product gaseous mixture was almost constant at ~ 0.14 vol.% during all experiments.

7.4 The influence of temperature on char gasification

7.4.1 Product yield

In this section the effect of gasification temperature on catalytic steam gasification of sugarcane bagasse char was researched. The char sample was mixed with the 10 % Ni-Al₂O₃ catalyst placed inside the gasifier was heated up to the desired temperature from

750 - 1050 °C. Different experimental conditions and the results showing the influence of gasification temperature on hydrogen yield are outlined in Table 7-4. It is evident from Table 7-4 that with the increase in gasification temperature from 750 to 1050 °C hydrogen yield was significantly increased.

Table 7-4 The influence of temperature on gasification of bagasse char

	Temperature (°C)			
	750	850	950	1050
Bio-char particle size (µm)	212-500	212-500	212-500	212-500
Catalyst	10%Ni-Al ₂ O ₃			
Catalyst to sample ratio	1.00	1.00	1.00	1.00
Water injection rate (ml hr ⁻¹)	6	6	6	6
Nitrogen flow rate (ml min ⁻¹)	100	100	100	100
H ₂ (mmoles g ⁻¹ biomass)	11.33	30.21	46.81	42.86
H ₂ (mmoles g ⁻¹ char)	45.30	120.84	187.25	171.44
Mass balance (wt.%)				
Gas/(char + water injected)	5.05	14.72	11.80	17.19
Gas/(char)	94.59	293.50	225.53	288.40
Mass balance	96.40	95.86	96.11	99.07

When temperature was increased from 750 to 850 °C, hydrogen yield was sharply increased from 45.30 to 120.84 mmoles per gram of char. Further increase in temperature to 950 °C resulted in significant increase in hydrogen yield to 187.25 mmoles per gram of char. When the gasification temperature was increased to 1050 °C, the hydrogen yield was slightly reduced to 171.44 mmoles per gram of char sample. The initial increase in hydrogen yield with the increase in temperature up to 950 °C can be explained by the fact that with the increase in gasification temperature, various endothermic reactions for example, water gas reactions and Boudouard reaction were favoured.

It is also worth mentioning that with the increase in gasification temperature enhanced carbon conversion has been reported in the literature. For example, Yan et al. [10] reported that with the increase in gasification temperature from 600 to 850 °C, carbon contents in a char sample was reduced from 68.76 % to 3.17 % during the steam

gasification of pine sawdust char. An increase in conversion rate of biomass-derived char during steam gasification was reported by Nanou et al. [11]. They achieved 95 % conversion within 4.1 min at 800 °C as compared to 40 % conversion at 600 °C at 17.5 minute. An increase in carbon conversion with the increase in temperature was also reported by Encinar et al. [12].

A slight reduction in hydrogen yield when the temperature was increased from 950 to 1050 °C was most likely due to the reverse water-gas shift reaction (Equation 7-7). As the water gas shift reaction is slightly exothermic and is not favourable at such high temperature (1050 °C) for the production of hydrogen. A decrease in H₂:CO ratio from 5 to 4.06 was observed with the increase in temperature from 950 to 1050 °C.

7.4.2 The influence of temperature on gas composition and hydrogen production

The influence of gasification temperature on product gas composition is outlined in this section. Results shown in Figure 7-3 indicate that with the increase in temperature, hydrogen concentration in the gas mixture was improved at temperature up to 950 °C. It increased from 67.76 vol.% at 750 °C to the highest 76.81 vol.% at 950 °C. Further increase in gasification temperature to 1050 °C, resulted in a slight reduction of hydrogen concentration to 69.68 vol.%. Yan et al. [10] reported that with the increase in gasification temperature hydrogen concentration in the gas mixture was increased from 29.54 vol.% at 600 °C to 52.41 vol.% at 850 °C. Hydrogen yield was also increased significantly from 2.55 to 57.07 mol kg⁻¹ of biomass char.

With the increase in temperature, the concentration of CO was increased from 8.16 to 17.14 vol.% while the concentration of CO₂ was reduced from 23.71 vol.% at 750 °C to 10.86 vol.% at 1050 °C. The reduction in CO₂ concentration was mainly attributed to the Boudouard reaction and dry reforming reactions. The increase in CO concentration with the rise in temperature was contributed by many endothermic reactions such as oxidation reactions, water gas reaction and Boudouard reaction. A decrease in H₂:CO ratio from 5 to 4.06 at 1050 °C suggests that the reverse water-gas shift reaction also contributed towards this higher CO concentration at 1050 °C.

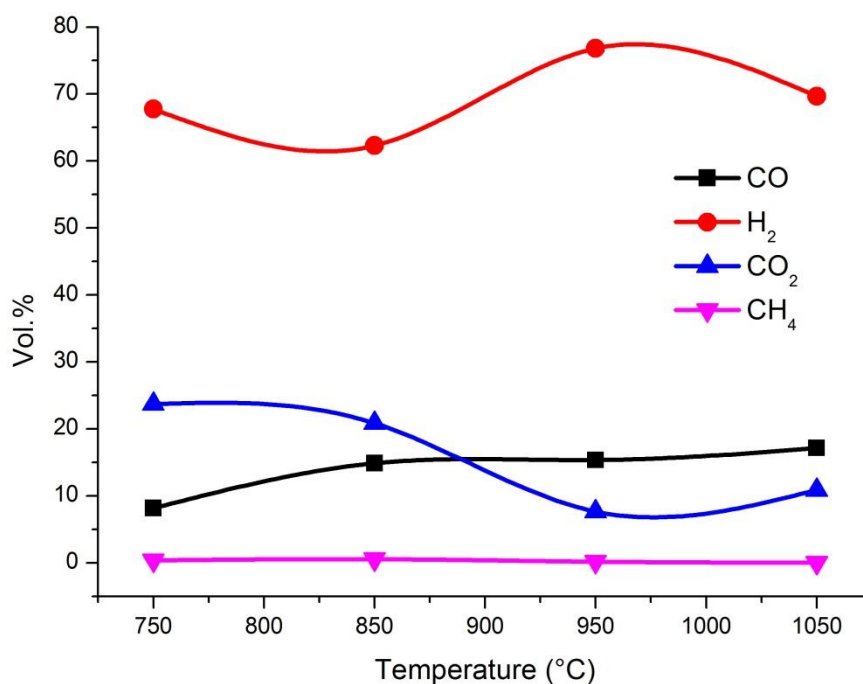


Figure 7-3 The influence of temperature on gas composition during steam gasification of sugarcane bagasse char

Howaniec et al. [13] reported an increase in hydrogen and CO concentration with the rise in temperature from 700 to 900 °C during steam gasification of *Salix Viminalis* biomass. With the increase in temperature, the concentration of hydrogen was increased from 60 to 64 vol.% while CO concentration was increased from 8 to 10 vol.% with the reduction in CO₂ concentration from 31 vol.% at 700 °C to 26 vol.% at 900 °C. Umeki et al. [14] also recommended the higher gasification temperature of 1173 K (900 °C) for higher hydrogen yield.

7.5 The influence of water/steam injection rate on gasification of char

7.5.1 Product yield

Like temperature, steam flow rate is one of the most important parameters in determining the overall gas yield and hence hydrogen yield. In order to enhance the hydrogen yield from steam gasification of biomass char, the influence of water/steam injection rate was researched in this section. Four different water/steam injection rates of 6, 15, 20 and 25 ml hr⁻¹ were investigated in this study. The hydrogen yield and mass balance results are shown in Table 7-5. These results indicate that with the initial increase in water injection rate from 6 to 15 ml hr⁻¹ the hydrogen yield was increased from 187.25 to 208.41 mmoles per gram of biomass char. However further increase in water injection rate resulted in a decrease in hydrogen yield to 168.58 mmoles for 20 ml hr⁻¹ and to 174.20 mmoles for 25 ml hr⁻¹.

It is suggested that the initial increase in hydrogen yield was due to the promotion of the water gas and the water gas shift reactions. Further increase in water injection rate lead to a decrease in hydrogen concentration due to the fact that the amount of char available was not sufficient for the amount of injected steam. Similar findings were reported by Yan et al. [10]. They investigated the influence of steam flow rate on gasification of pine sawdust char at 850 °C. They reported that initially with the increase in steam flow rate from 0 to 0.165 g min⁻¹ g⁻¹ of biomass char, hydrogen yield increased from 2.15 mol kg⁻¹ to 57.07 mol kg⁻¹. Further increase in steam flow rate to 0.357 g min⁻¹ g⁻¹ of biomass char resulted in a decrease in hydrogen yield to 37.47 mol kg⁻¹.

By increasing the steam injection rate during gasification, extra oxygen and hydrogen was made available into the system. Furthermore at high temperatures such as 950 °C, by increasing the water injection rate the equilibrium of water-gas shift reaction can be altered to enhance the hydrogen yield. Paviet et al. [15] investigated the kinetics of steam gasification of wood char. They performed char gasification in a tubular kiln reactor at various temperatures and steam flow rates. It was observed that with the increase in steam molar fraction, the char consumption rate was increased due to the lower diffusion resistance at higher steam flow rates.

Table 7-5 The influence of water injection rate on gasification of bagasse char

	Water injection rate (ml hr ⁻¹)			
	6	15	20	25
Bio-char particle size (µm)	212-500	212-500	212-500	212-500
Catalyst	10%Ni-Al ₂ O ₃	10%Ni-Al ₂ O ₃	10%Ni-Al ₂ O ₃	10%Ni-Al ₂ O ₃
Catalyst to sample ratio	1.00	1.00	1.00	1.00
Nitrogen flow rate (ml min ⁻¹)	100	100	100	100
H ₂ (mmoles g ⁻¹ of biomass)	46.81	52.10	42.15	43.55
H ₂ (mmoles g ⁻¹ of char)	187.25	208.41	168.58	174.20
Mass balance (wt.%)				
Gas/(char + water injected)	11.80	6.18	5.34	4.61
Gas/(char)	225.53	292.55	316.23	326.05
Mass balance	96.11	91.39	97.57	97.14

7.5.2 The influence of water injection rate on gas composition

The influence of increase in water injection rate on product gas composition is outlined in Figure 7-4. It was observed that under the studied experimental conditions, water injection rate was inversely proportional to the hydrogen concentration in the product gas mixture. It was observed that with the increase in water/steam injection rate, the concentration of hydrogen was gradually reduced. Initially it decreased slightly from 76.81 vol.% for 6ml hr⁻¹ to 73.95 vol.% for 15ml hr⁻¹. Further increase in water injection rate to 20 and to 25 ml hr⁻¹ reduced hydrogen concentration to 68.30 and 67.86 vol.% respectively.

Contrary to the above trend, the concentration of CO₂ was gradually increased from 7.67 to 14.13 vol.% with the increase in water injection rate. Yan et al. [10] also reported an increase in CO₂ concentration with the increase in steam flow rate. The concentration of CO was almost constant at ~15 vol.%. A slight but noticeable increase in CH₄ concentration (perhaps due to methanation reaction) with the increase in water injection rate was also observed. It increased from 0.16 to 0.21 to 0.25 and to 0.29 vol.% with the increase in water injection rate from 6 to 15, to 20 and to 25 ml hr⁻¹. It is suggested that the increase in water injection rate favoured the oxidation of char and CO which caused the increase in CO₂ concentration. Although it was speculated that the increase in water injection rate will favour the water gas shift reaction towards hydrogen

formation but a decrease in hydrogen concentration was noticed. It is inferred that due to the removal of CO by the oxidation reaction caused the reduction in hydrogen concentration by reverse water gas shift reaction [12]. The inhibition effect of syngas during steam gasification of char was also reported by some authors [5, 16]. For example, Fushimi et al. [16] investigate the influence of hydrogen partial pressure on gasification of wood char. It was found that the inhibition was caused by the reverse oxygen exchange reaction and dissociative hydrogen adsorption on the char. Yan et al. [10] reported that the water gas shift reaction, water gas reaction and methane steam reforming reactions had played important roles in determining the gas yield with the increase in steam flow rate.

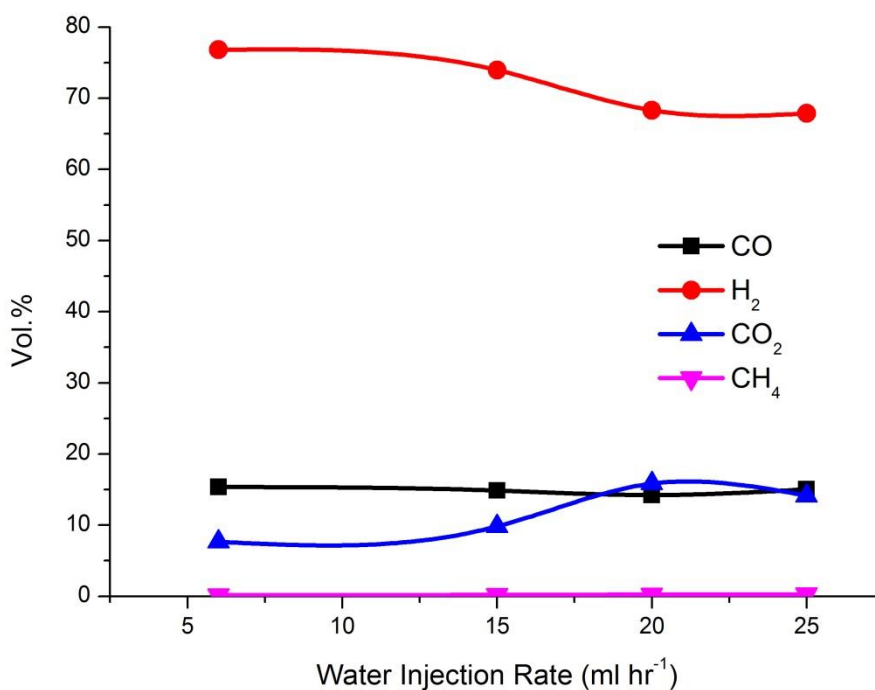


Figure 7-4 The influence of water injection rate on gas composition during gasification of sugarcane bagasse char

7.6 Conclusions

In this chapter, steam gasification of biomass chars derived from the pyrolysis of biomass was performed. The aim of this study was to enhance the hydrogen yield by utilizing the residual char. The following conclusions can be made from this study.

- Char samples obtained from the pyrolysis of three different biomass samples namely rice husk, wheat straw and sugarcane bagasse were characterised to find the most suitable char for further gasification studies. As compared to the rice husk and wheat straw, char from sugarcane bagasse with the highest elemental carbon of 81.55 wt.% and the lowest ash contents of less than 10 wt.% was the most suitable candidate for further research.
- In Section 7.3, steam gasification of bagasse char was carried out in the presence of various catalysts. It was found that the highest hydrogen yield of 187.25 mmoles g⁻¹ of char was obtained using 10 % Ni-Al₂O₃ catalyst. As compared to no catalyst, the hydrogen concentration in the product gas was increased from 57.74 to 76.81 vol.%. This higher hydrogen yield from 10 % Ni-Al₂O₃ catalyst was attributed to the large surface area of this catalyst. Compared to the no catalyst results, 87 % increase in hydrogen yield was recorded.
- The influence of gasification temperature on hydrogen yield revealed that the most suitable temperature to obtain the highest hydrogen yield was found to be 950 °C. Increase in gasification temperature from 750 to 950 °C favoured the endothermic reactions causing significant increase in hydrogen yield from just 45.30 at 750 °C to 187.25 mmoles g⁻¹ char at 950 °C.
- The influence of water/steam injection rate on hydrogen yield from steam gasification of bagasse char was studied in section 7.5. It was found that initially with the increase in water injection rate from 6 to 15 ml hr⁻¹ the hydrogen yield was increased from 187.25 to 208.41 mmoles per gram of biomass char. However further increase in water injection rate resulted in a decrease in hydrogen yield to 168.58 mmoles for 20ml hr⁻¹ and to 174.20 mmoles for 25ml hr⁻¹.

7.7 Chapter references

- [1] S. V. Vassilev, D. Baxter, L. K. Andersen, and C. G. Vassileva, "An overview of the chemical composition of biomass," *Fuel*, vol. 89, pp. 913-933, 2010.
- [2] L.-x. Zhang, S. Kudo, N. Tsubouchi, J.-i. Hayashi, Y. Ohtsuka, and K. Norinaga, "Catalytic effects of Na and Ca from inexpensive materials on in-situ steam gasification of char from rapid pyrolysis of low rank coal in a drop-tube reactor," *Fuel Processing Technology*, vol. 113, pp. 1-7, 2013.
- [3] T. W. Kwon, J. R. Kim, S. D. Kim, and W. H. Park, "Catalytic steam gasification of lignite char," *Fuel*, vol. 68, pp. 416-421, 1989.
- [4] H. Haykiri-Acma, S. Yaman, and S. Kucukbayrak, "Gasification of biomass chars in steam–nitrogen mixture," *Energy Conversion and Management*, vol. 47, pp. 1004-1013, 2006.
- [5] M. Kajita, T. Kimura, K. Norinaga, C.-Z. Li, and J.-i. Hayashi, "Catalytic and Noncatalytic Mechanisms in Steam Gasification of Char from the Pyrolysis of Biomass†," *Energy & Fuels*, vol. 24, pp. 108-116, 2010/01/21 2009.
- [6] K. Otto and M. Shelef, "Catalytic steam gasification of graphite: Effects of intercalated and externally added Ru, Rh, Pd and Pt," *Carbon*, vol. 15, pp. 317-325, 1977.
- [7] A. Moilanen, K. Saviharju, and T. Harju, "Steam Gasification Reactivities of Various Fuel Chars," in *Advances in Thermochemical Biomass Conversion*, A. V. Bridgwater, Ed., ed: Springer Netherlands, 1993, pp. 131-141.
- [8] M. Luo and B. Stanmore, "The combustion characteristics of char from pulverized bagasse," *Fuel*, vol. 71, pp. 1074-1076, 1992.
- [9] C. Yang, L. Jia, S. Su, Z. Tian, Q. Song, W. Fang, *et al.*, "Utilization of CO₂ and biomass char derived from pyrolysis of *Dunaliella salina*: The effects of steam and catalyst on CO and H₂ gas production," *Bioresource Technology*, vol. 110, pp. 676-681, 2012.
- [10] F. Yan, S.-y. Luo, Z.-q. Hu, B. Xiao, and G. Cheng, "Hydrogen-rich gas production by steam gasification of char from biomass fast pyrolysis in a fixed-bed reactor: Influence of temperature and steam on hydrogen yield and syngas composition," *Bioresource Technology*, vol. 101, pp. 5633-5637, 2010.
- [11] P. Nanou, H. E. Gutiérrez Murillo, W. P. M. van Swaaij, G. van Rossum, and S. R. A. Kersten, "Intrinsic reactivity of biomass-derived char under steam gasification conditions-potential of wood ash as catalyst," *Chemical Engineering Journal*, vol. 217, pp. 289-299, 2013.
- [12] J. M. Encinar, J. F. González, J. J. Rodríguez, and M. a. J. Ramiro, "Catalysed and uncatalysed steam gasification of eucalyptus char: influence of variables and kinetic study," *Fuel*, vol. 80, pp. 2025-2036, 2001.
- [13] N. Howaniec, A. Smoliński, K. Stańczyk, and M. Pichlak, "Steam co-gasification of coal and biomass derived chars with synergy effect as an innovative way of hydrogen-rich gas production," *International Journal of Hydrogen Energy*, vol. 36, pp. 14455-14463, 2011.
- [14] K. Umeki, T. Namioka, and K. Yoshikawa, "The effect of steam on pyrolysis and char reactions behavior during rice straw gasification," *Fuel Processing Technology*, vol. 94, pp. 53-60, 2012.
- [15] F. Paviet, O. Bals, and G. Antonini, "The effects of diffusional resistance on wood char gasification," *Process Safety and Environmental Protection*, vol. 86, pp. 131-140, 2008.

- [16] C. Fushimi, T. Wada, and A. Tsutsumi, "Inhibition of steam gasification of biomass char by hydrogen and tar," *Biomass and Bioenergy*, vol. 35, pp. 179-185, 1// 2011.

CHAPTER 8 CONCLUSIONS AND FUTURE WORK

8.1 Introduction

In this research work, a two-stage, ultra-high temperature (up to 1050 °C), pyrolysis/gasification reactor was designed and built to investigate the pyrolysis and gasification of different biomass samples with the aim to produce high hydrogen yield. Initially, biomass samples, sugarcane bagasse, rice husks and wheat straws were characterised using thermogravimetric analysis to find the most suitable biomass for hydrogen production. A comparative study of fast and slow pyrolysis conditions was performed to investigate the influence of pyrolysis conditions on product yield and gas composition. For all three biomass samples, pyrolysis, steam gasification and catalytic steam gasification using calcined dolomite and nickel impregnated dolomite were performed. The influence of various process conditions including temperature, steam injection rate, carrier gas flow rate, biomass particle size, and catalyst to sample ratio on pyrolysis/gasification of rice husk was investigated using 10 % Ni-dolomite catalyst.

In order to further enhance the hydrogen yield, the influence of seven different nickel based catalysts on hydrogen production from pyrolysis/gasification of sugarcane bagasse was researched. The key process parameters including gasification temperature, steam injection rate were also investigated. The other variables of catalyst calcination temperature and Ni loading were also studied. In order to get the maximum possible hydrogen yield, residual biomass char left from the pyrolysis was also gasified in the presence of steam and catalysts. Char samples from rice husks, bagasse and wheat straw were initially characterised in terms of the amount of fixed carbon and residual ash. The influence of catalyst, gasification temperature and steam injection rate was also investigated. The combined hydrogen yield from the gasification of original biomass and residual char showed that the two-stage gasification performed at ultra-high temperatures (950 - 1000 °C) is a promising option to obtain high hydrogen yield.

8.2 Conclusions

8.2.1 Pyrolysis of waste biomass: Investigation of fast pyrolysis and slow pyrolysis process conditions on product yield and gas composition

- Slow pyrolysis of the wood, rice husks and forestry residue was markedly different from that of fast pyrolysis. For wood, only 24.7 wt.% gas yield was obtained from slow pyrolysis as compared to 78.63 wt.% from fast pyrolysis. For rice husk 18.94 wt.% gas was obtained, for forestry residue 24.01 wt.% gas was obtained compared to 66.61 wt.% and 73.91 wt.% from fast pyrolysis respectively. There were correspondingly lower yields of oil and char from fast pyrolysis whereas for slow pyrolysis oil and char yields were higher.
- The composition of the product gases was also influenced by the heating rate. The higher CO:CO₂ ratio found for fast pyrolysis was due to the interaction of CO₂ present in the syngas with the solid particles present in the gas stream.
- The gas yield was increased with the increase in fast pyrolysis temperature between 750 – 1050 °C. A corresponding decreasing in char and oil yield was noticed. Maximum gas yields, on an ash-free basis were 91.71 wt.% for wood, 98.36 wt.% for rice husk and 90.80 wt.% for forestry residue. The higher gas yield at higher pyrolysis temperature was attributed to the enhanced thermal cracking of oil and tar compounds. The strong interaction between syngas and solid char must have played a role in enhanced gas yield.
- Addition of steam to the fast pyrolysis of wood produced increased yields of hydrogen. For example, hydrogen yield was 26.91 vol.% in the absence of steam increasing to 44.13 vol.% in the presence of steam at the reaction temperature of 750 °C. The presence of steam enhanced the hydrogen yield by increased reforming of methane and other hydrocarbons. Presence of steam also had some influence on the equilibrium of water gas reaction thereby increasing hydrogen yield.

8.2.2 Characterization of rice husk, sugarcane bagasse and wheat straw using thermogravimetric analysis

- On an ash-free basis, the highest volatiles of ~83 wt.% were found for sugarcane bagasse compared to rice husk and wheat straw. The rice husk biomass exhibited the lowest volatiles of ~77 wt.% and the highest ash contents of ~17 wt.%. However, the ultimate analysis results showed that highest carbon contents (~45 wt.%) were also present in bagasse. All three biomass samples showed hydrogen contents of around 5 wt.%.
- The study of heating rate indicated that with the increase in heating rate from 5 to 20 and to 40 °C min⁻¹, a lateral shift in the TGA thermograms was observed for all three biomass samples. This shift in the TGA thermogram was due to the heat transfer limitations at higher heating rates. Due to short reaction time at higher heating rates, higher temperature was required for the evolution of volatiles from biomass samples
- The study of different biomass particle sizes revealed that as compared to the smaller particles, higher char yield was obtained from the pyrolysis of larger particles. This can be explained by the fact that increase in particle diameter hinders the efficient heat transfer from the particle surface to the centre hence leading to a temperature gradient between the surface and centre of the biomass particle. The effect is minimal for smaller particle size but for the larger particles more time is required for complete conversion
- Kinetic parameters were calculated using Coats-Redfern method. For the main weight loss curve, order of reaction for rice husk and bagasse was found to be 0.5 while for wheat straw; it was 0.5 for 5 and 20 °C min⁻¹ heating rates. At higher heating rate of 40 °C min⁻¹, the order of reaction was changed to 2.0.

8.2.3 Hydrogen production from ultra-high temperature pyrolysis, steam gasification and catalytic steam gasification of rice husk, sugarcane bagasse and wheat straw

- Hydrogen yield was radically improved from ~ 2 mmoles g^{-1} for pyrolysis to ~ 21 mmoles g^{-1} of biomass during two-stage pyrolysis/gasification in the presence of steam at $950\text{ }^\circ\text{C}$. The presence of steam enhanced the hydrogen yield by increased reforming of methane, lighter hydrocarbons and tar. Presence of steam also had some influence on the equilibrium of water gas reaction thereby increasing hydrogen yield.
- The use of calcined dolomite and 10 % Ni-dolomite catalysts in second stage further increased gas yield and hydrogen yield. The hydrogen yield of 25.44 mmoles g^{-1} of biomass was obtained from the pyrolysis/gasification of rice husk using 10 % Ni-dolomite. The highest hydrogen concentration in the gas mixture was found to be 59.14 vol.%.
- 10 wt.% Ni dolomite catalyst used in this study was characterized using TGA-TPO, SEM and TEM techniques. TGA-TPO results showed that the significantly lower carbon deposits of less than 10 wt.% were found on reacted 10 wt.% Ni dolomite catalyst.

8.2.4 The influence of various process conditions on ultra-high temperature catalytic steam gasification of rice husk using 10 wt.% Ni-dolomite catalyst at $950\text{ }^\circ\text{C}$

- With the increase in temperature from $850\text{ }^\circ\text{C}$ to $1050\text{ }^\circ\text{C}$, hydrogen yield was significantly increased from 20.03 to 30.62 mmoles per gram of rice husk. Hydrogen concentration in the gas mixture was increased from 53.95 vol.% to 65.18 vol.%. The amount of deposited coke on catalyst was also reduced from 2.46 wt.% for $850\text{ }^\circ\text{C}$ to zero at $1000\text{ }^\circ\text{C}$. Higher gasification temperature favoured endothermic reactions. Steam reforming of hydrocarbons and tar was also improved at higher gasification temperatures leading to higher gas yield and hydrogen yield.
- With the increase in water injection rate from 2 ml hr^{-1} to 10 ml hr^{-1} , hydrogen yield was considerably increased from 22.31 to 27.86 mmoles per gram of rice

husk. Hydrogen concentration in the gas mixture was also improved from 56.29 vol.% to 61.88 vol.%. The increase in water injection rate shifted the equilibrium of the water gas shift reaction thereby enhancing the hydrogen yield.

- The influence of biomass particle size on hydrogen production was also investigated. It was found that with the decrease in particle size from the range of 2800 - 3350 to 212 - 500 μm , hydrogen yield was improved from 25.05 to 29.13 mmoles per gram of rice husk. Hydrogen concentration in the product gas mixture was increased from 59.45 vol.% to 63.12 vol.%. With the reduction in particle size, surface area to volume ratio of the particles was improved. This resulted in larger surface area available for pyrolysis/gasification thereby enhancing the gas and hydrogen yield.
- No significant differences in hydrogen yield and gas yield were observed when C/S ratio was varied from 0.25 to 2.0. Hydrogen yield was almost constant at 25.90 mmoles per gram of rice husk. Hydrogen concentration was also constant at around 60 vol.%.
- The carrier gas (nitrogen) flow rate was varied from 50 to 400 ml min^{-1} . No significant difference in product gas yield and hydrogen yield was observed with the increase in carrier gas flow rate, over the range investigated.

8.2.5 The influence of catalyst and other process conditions on ultra-high temperature catalytic steam gasification of sugarcane bagasse

- Seven different Ni-based catalysts; 10 % Ni-dolomite, 10 % Ni-MgO, 10 % Ni-SiO₂, 10 % Ni-Al₂O₃, 2 wt.% Ce - 10 % Ni-dolomite, 5 wt.% Ce - 10 % Ni-dolomite and 10 wt.% Ce - 10 % Ni-dolomite were compared with silica sand in terms of hydrogen yield from two-stage pyrolysis/gasification of bagasse. The 10 % Ni-Al₂O₃ catalyst produced the highest hydrogen yield of 29.62 mmoles per gram of bagasse at gasification temperature of 950 °C.
- The gasification temperature showed a positive influence on the two-stage pyrolysis/gasification of bagasse. The hydrogen yield was increased from 21.17 mmoles g⁻¹ at 800 °C to 35.65 mmoles g⁻¹ at 1050 °C using 10 % Ni-Al₂O₃ catalyst. The hydrogen concentration in the product gas mixture was also increased from 50.31 vol.% at 800 °C to 67.40 vol.% at 1050 °C.

- The amount of nickel in Ni-Al₂O₃ catalyst was increased from 5 wt.% to 10 wt.%, 20 wt.% and to 40 wt.%. The increase in nickel contents shows little or no influence on hydrogen yield. This suggests that the presence of small amount of Ni (~10 wt.%) was sufficient to carry out the pyrolysis/gasification of biomass under the researched high temperature conditions. The highest hydrogen yield of 29.62 mmol g⁻¹ was obtained. The concentration of hydrogen was also unchanged at around 60 vol.%.
- Increasing water/steam injection rate dramatically improved hydrogen yield from 29.93 mmol g⁻¹ using 6 ml hr⁻¹ to 44.47 mmol g⁻¹ using 35 ml hr⁻¹. A sharp increase in hydrogen concentration from 60.72 vol.% for 6 ml hr⁻¹ to 72.92 vol.% for 35 ml hr⁻¹ water injection rate was obtained. The increase in H₂:CO ratio from 2.97 to 7.78 confirmed the positive influence of water injection rate on the water gas shift reaction.
- With the increase in catalyst calcination temperature from 700 to 1000 °C, average pore size was increased while the BET surface area was reduced from 118.90 to 64.77 m² g⁻¹. This suggests that the lower calcination temperature of 700 - 800 °C was favourable for biomass gasification as large proportion of smaller particles was available at lower calcination temperature thereby producing a catalyst of higher surface area. The hydrogen yield was initially increased from 35.72 mmol g⁻¹ for 700 °C to 42.29 mmol g⁻¹ for 800 °C. However further increase in calcination temperature to 900 and 1000 °C did not show any improvements in hydrogen yield.
- The increase in catalyst to sample ratio (C/S) improved hydrogen yield. With the increase in C/S ratio from 0.1 to 2.0, hydrogen yield was increased from 39.18 to 44.70 mmol per gram of bagasse.
- In this research work, the highest hydrogen yield of 44.47 mmol g⁻¹ was obtained using 35 ml hr⁻¹ water injection rate from the two-stage pyrolysis/gasification of sugarcane bagasse in the presence of 10 % Ni-Al₂O₃ catalyst at gasification temperature of 1000 °C. However this two-stage pyrolysis/gasification process can be optimised to further enhance the hydrogen yield.

8.2.6 Catalytic steam gasification of residual biomass char

- Thermogravimetric and elemental analysis of three char samples (obtained from the pyrolysis of rice husk, bagasse and wheat straw) revealed that the sugarcane bagasse was the most suitable candidate with 81.55 wt.% elemental carbon and less than 10 wt.% ash.
- Compared to the 10 % Ni-dolomite and 10 % Ni-MgO, the highest hydrogen yield of 187.25 mmol g⁻¹ of char was obtained using 10 % Ni-Al₂O₃ catalyst. When compared with the no catalyst results, addition of 10 % Ni-Al₂O₃ catalyst increased the hydrogen yield by 87 %. The highly porous catalyst, 10 % Ni-Al₂O₃ when mixed with the char provided not only larger surface area with the active Ni sites but also contributed towards shifting the chemical equilibria of various reactions to improve the hydrogen yield.
- The increase in gasification temperature from 750 to 950 °C favoured the endothermic reactions causing significant increase in hydrogen yield from just 45.30 at 750 °C to 187.25 mmol g⁻¹ char at 950 °C.
- With the increase in water injection rate from 6 to 15 ml hr⁻¹ the hydrogen yield was increased from 187.25 to 208.41 mmol per gram of bagasse char. However further increase in water injection rate to 20 ml and 25 ml hr⁻¹ did not improve the hydrogen yield. The initial increase in hydrogen yield was due to the promotion of the water gas and the water gas shift reactions. Further increase in water injection rate did not improve the hydrogen concentration due to the fact that the amount of char available was not sufficient for the amount of injected steam.
- The highest hydrogen yield of 208.41 mmol g⁻¹ of char was obtained from the catalytic steam gasification of sugarcane bagasse char at 950 °C using 10 % Ni-Al₂O₃ catalyst with steam injection rate of 15 ml hr⁻¹. As ~1 gram of bio-char was obtained from the pyrolysis of 4 grams of sugarcane bagasse. The hydrogen yield in mmol per gram of biomass was calculated by dividing mmol per gram of char results by 4. Hence the maximum of 52.10 mmol of hydrogen were obtained in terms of per gram of biomass.
- As mentioned in section 8.2.5, the highest hydrogen yield of 44.47 mmol g⁻¹ was obtained from the two-stage pyrolysis/gasification of sugarcane bagasse. By combining these results with the char gasification results (52.10 mmol g⁻¹

biomass), a total of 96.57 mmoles of hydrogen per gram of biomass can be obtained. In other words, from the results of current research work ~ 200 g hydrogen yield can be obtained from 1 kg of sugarcane bagasse sample which is around 4 times higher than the original amount of hydrogen present (~ 50 grams per kg of biomass at 5 wt.%) in the biomass sample.

8.3 Future work

After the current research work, the following further investigations are suggested in the area of high temperature biomass gasification for hydrogen production.

- The process of high temperature pyrolysis/gasification can be optimised to obtain even higher hydrogen yield by converting the remaining CO into H₂. For example, even after obtaining the high hydrogen yield of ~ 200 g kg⁻¹ of biomass, around 10 vol.% and 15 vol.% CO is still present in the product gas mixture from the gasification of biomass and char respectively. Hydrogen yield can increase up to 250 g kg⁻¹ of biomass. The hydrogen concentration in the gas mixture can also be increased to above 90 vol.% by converting CO into H₂ using the water gas shift reaction and further absorption of CO₂ in CaO at ~ 700 °C.
- A four stage reactor is proposed to further enhance the hydrogen yield from the process by controlling the temperature of each zone independently. Zone 1 (from top to bottom) for pyrolysis of biomass at ~ 750 °C. Zone 2 for thermal cracking and catalytic steam gasification at ~ 1000 °C. Zone 3 for CO₂ absorption by CaO at ~ 700 °C. Zone 4 at $\sim 250 - 450$ °C to convert any remaining CO into H₂ by the water gas shift reaction. Reactor temperatures, steam injection rates, and different catalysts are recommended to be investigated in the above mentioned configuration.
- Further investigations on different catalyst preparation methods (For example, sol-gel method) are suggested. The research on different variables during catalyst preparation process, e.g. addition of different metals, solution stirring time, pH of the solution is also recommended to further optimise the catalyst.

- A mathematical model based on feed forward neural networks can be developed to estimate and predict the product gas composition from gasification of biomass under different process conditions. Once developed, the accuracy of such model can be enhanced by training these neural networks.

APPENDIX - A GAS CALCULATIONS

In order to calculate the concentration of different gases in the product gas mixture, calibration of GCs was performed with gas mixtures of known concentration. Three different cylinders containing permanent gases, alkanes and alkenes were obtained from Scientific & Technical Gases Ltd. Each cylinder contains 20 litres of standard gas at 300 psi.

The standard gas mixture for permanent gases was comprised of H₂, CO, N₂, O₂, and CO₂. The concentration of each gas was 1 vol% with balance nitrogen. The standard gas mixture for alkanes contains CH₄, C₂H₆, C₃H₈ and C₄H₁₀. The cylinder was 96 vol.% nitrogen with 1 vol.% of each gas. For alkenes, the concentration of ethane, propene, butene and butadiene was 1 vol.% with balance nitrogen. One ml of each standard gas mixture was injected into the GCs and the response peak area for each individual gas was obtained using Star chromatography workstation (version 6) software. A typical GC response area to standard gases is shown in Table A-1.

Table A-1 Peak area for standard gases

Gas	Concentration (vol.%)	Peak area
CO	1.0	37618
H ₂	1.0	501975
O ₂	1.0	65908
N ₂	96.0	3852873
CO ₂	1.0	11126
CH ₄	1.0	590908
C ₂ H ₄	1.0	1043634
C ₂ H ₆	1.0	1135268
C ₃ H ₆	1.0	1517754
C ₃ H ₈	1.0	1667632
C ₄ H ₈	2.0	1997072
C ₄ H ₁₀	1.0	2541354

Once the GCs are calibrated and peak area of the standard gases are known, one ml of synthesis gas obtained from the pyrolysis/gasification of biomass was injected. The peak area relevant to each individual gas in the product gas mixture was calculated by software. Each sample was injected three times to obtain the consistent and reliable

results. The concentration of individual gases can be calculated from the peak area of corresponding gas in the product gas mixture and the area of standard gas using the following formula.

$$C_x = \frac{A_{xp}}{A_{xc}} \times (\% \text{ of gas } X \text{ in calibration mixture}) \quad (A - 1)$$

Where C_x is the concentration of gas X, A_{xp} is the area of gas X in the product gas mixture and A_{xc} is the area of gas X in the calibration gas mixture.

Data analysis

A formula sheet in Excel was designed to calculate the concentration of individual gases. As each sample was injected three times into the GCs, the concentration of all gases was averaged and normalised to obtain the final concentration of product gases. Example calculations are shown in Table A-2.

During all the pyrolysis/gasification experiments, a constant flow of nitrogen was supplied for a known length of time. Hence the total volume of the nitrogen gas injected into the system can be calculated as follows.

$$\begin{aligned} \text{Total vol. of nitrogen} \\ = \text{flow rate of nitrogen (ml min)} \times \text{total time (min)} \quad (A - 2) \end{aligned}$$

In example calculations in Table A-2,

$$\text{Total vol. of nitrogen} = 100 \text{ (ml /min)} \times 140 \text{ (min)} = 14000 \text{ (ml)} = 14 \text{ liters}$$

Once the total volume of nitrogen and the percentage of nitrogen in the product gas mixture are known (78.67 vol.% in Table A-2), the total volume of gas can be calculated using the following formula.

$$\begin{aligned} \text{Total gas volume (liters)} \\ = \frac{100}{\text{nitrogen conc. (vol\%)}} \times \frac{\text{total nitrogen vol. (ml)}}{1000} \quad (A - 3) \end{aligned}$$

$$\text{Total gas volume (liters)} = \frac{100}{78.67} \times \frac{14000}{1000} = 17.80 \text{ (litres)} \quad (A - 4)$$

Because the concentration of each gas is already known, the number of moles of each gas is calculated using this formula (assuming gas volume of 22.4 litres at standard temperature and pressure conditions (PV = nRT)).

$$\text{Moles of gas X} = \frac{\text{Conc. of Gas X (vol\%)}}{100} \times \frac{\text{Total gas volume (lit)}}{22.4} \quad (A - 5)$$

For example, for hydrogen gas with the concentration of 12.61 vol% (from Table A-2)

$$\text{Moles of hydrogen} = \frac{12.61}{100} \times \frac{17.80}{22.4} = 0.10 \text{ moles} \quad (A - 6)$$

Once the number of moles of each gas are known, the number of grams of each individual gas can be calculated using the following formula.

$$\begin{aligned} \text{Weight of gas X (grams)} \\ = (\text{Molecular weight of gas X}) \times (\text{moles of gas X}) \end{aligned} \quad (A - 7)$$

For hydrogen example,

$$\text{Weight of hydrogen (grams)} = (2.01) \times (0.10) = 0.201 \quad (A - 8)$$

The total weight of the gas can be calculated by adding the number of grams of each individual gas.

Table A-2 Example calculations for gas composition

Gas	Peak area	Gas conc. (vol.%)	# of moles	Gas weight (g)	N ₂ free gas conc. (vol.%)
CO	171544	4.87	0.039	1.08	22.84
H ₂	5581320	12.61	0.100	0.20	59.14
N ₂	2796547	78.67	0.625		
CO ₂	39995	3.46	0.028	1.21	16.24
CH ₄	208781	0.38	0.003	0.05	1.78
Gas collection (min)		140	Total gas volume (lit)		17.80
N ₂ flow (ml min ⁻¹)		100	Total gas weight (g)		2.55

Finally nitrogen free gas composition can be calculated by

$$N_2 \text{ free gas conc.} = \frac{\text{Gas conc. (vol\%)}}{\text{total gas vol\%} - N_2 \text{ conc. (vol\%)}} \times 100 \quad (A - 9)$$

For hydrogen example,

$$N_2 \text{ free H}_2 \text{ conc.} = \frac{12.61}{100 - 78.67} \times 100 = 59.14 \text{ (vol\%)} \quad (A - 10)$$

After knowing the total amount of gas (grams), gas yield can be calculated using the following formula

$$\text{Gas yield (wt. \%)} = \frac{\text{Total amount of gas (grams)}}{\text{Amount of biomass (grams)}} \times 100 \quad (A - 11)$$

While on an ash-free basis, gas yield was calculated using the following formula

$$\begin{aligned} \text{Gas yield (wt. \%)} & \text{ on ashfree basis} \\ & = \frac{\text{Total amount of gas (grams)}}{\text{Biomass (grams)} - \text{Ash (grams)}} \times 100 \quad (A - 12) \end{aligned}$$

Mass balance for pyrolysis was calculated using the following formula

$$\text{Mass balance} = \frac{\text{Gas (g)} + \text{Oil (g)} + \text{Solid (g)}}{\text{Biomass (g)}} \times 100 \quad (\text{A} - 13)$$

Mass balance for gasification experiments was calculated using the following formula

$$\text{Mass balance} = \frac{\text{Gas (g)} + \text{Oil (g)} + \text{Solid (g)}}{\text{Biomass (g)} + \text{Steam Injected (g)}} \times 100 \quad (\text{A} - 14)$$

Product yield in relation to biomass only was calculated using the following formulas

$$\text{Gas yield (wt. \%)} = \frac{\text{Total amount of gas (grams)}}{\text{Amount of biomass (grams)}} \times 100 \quad (\text{A} - 15)$$

$$\text{Oil yield (wt. \%)} = \frac{\text{Total amount of oil (grams)}}{\text{Amount of biomass (grams)}} \times 100 \quad (\text{A} - 16)$$

$$\text{Solid yield (wt. \%)} = \frac{\text{Total amount of Solid (grams)}}{\text{Amount of biomass (grams)}} \times 100 \quad (\text{A} - 17)$$

Product yield in relation to biomass + injected water was calculated using the following formulas

$$\text{Gas yield (wt. \%)} = \frac{\text{Total amount of gas (g)}}{\text{Biomass (g)} + \text{Steam Injected (g)}} \times 100 \quad (\text{A} - 19)$$

$$\text{Solid yield (wt. \%)} = \frac{\text{Total amount of solid (g)}}{\text{Biomass (g)} + \text{Steam Injected (g)}} \times 100 \quad (\text{A} - 20)$$

APPENDIX - B CALCULATION OF KINETIC PARAMETERS

A detailed description of processing non-isothermal kinetic data by using a modified Coats-Redfern method has been reported and discussed ^[1].

The basic kinetic equation is:

$$\frac{d\alpha}{dt} = kf(\alpha) \quad (\text{B-1})$$

where α is the conversion of the waste biomass, defined as the following:

$$\alpha = \frac{m_0 - m}{m_0 - m_\infty} \quad (\text{B-2})$$

where m_0 is the initial sample weight, m is the sample weight at time t , and m_∞ is the final sample weight.

The reaction rate constant, k is given by the Arrhenius equation:

$$k = A \exp\left(-\frac{E}{RT}\right) \quad (\text{B-3})$$

where A is pre-exponential factor (min^{-1}); E is apparent activation energy (kJ mol^{-1}); T is reaction temperature (K); R is gas constant, it equals to 8.314×10^{-3} ($\text{kJ mol}^{-1} \text{K}^{-1}$).

The reaction temperature can be expressed with:

$$T = T_0 + \beta \cdot t \quad (\text{B-4})$$

where T_0 is the initial temperature (K); β is the heating rate (K min^{-1});

Eq. (B-1) is changed as follows:

$$\frac{d\alpha}{dT} = \frac{A}{\beta} f(\alpha) \exp\left(-\frac{E}{RT}\right) \quad (\text{B-5})$$

¹ E. Eftimie, E. Segal. Basic language programs for automatic processing non-isothermal kinetic data. *Thermochimica Acta*, 111 (1987) 359-367

If $f(\alpha)$ is presented as:

$$f(\alpha) = (1-\alpha)^n \quad (\text{B-6})$$

where n is the reaction order.

A combination of Eq. (B-5) and Eq. (B-6), with the further integration, it becomes:

$$\int_0^\alpha \frac{d\alpha}{(1-\alpha)^n T^2} = \frac{AR}{\beta E} \left[\exp\left(-\frac{E}{RT}\right) - \exp\left(-\frac{E}{RT_0}\right) \right] \quad (\text{B-7})$$

because $\exp\left(-\frac{E}{RT_0}\right) \approx 0$, Eq. (B-7) can be reduced to:

$$\ln \int_0^\alpha \frac{d\alpha}{(1-\alpha)^n T^2} = \ln \frac{AR}{\beta E} - \frac{E}{RT} \quad (\text{B-8})$$

If a set of experimental data $(T_i, \alpha_i, i=1,2,\dots,m)$ were introduced into Eq. (B-8):

$$\ln \int_0^{\alpha_i} \frac{d\alpha}{(1-\alpha)^n T^2} = \ln \frac{AR}{\beta E} - \frac{E}{RT_i}, \quad i=1,2,\dots,m \quad (\text{B-9})$$

assigned y_i as:

$$y_i = \ln \int_0^{\alpha_i} \frac{d\alpha}{(1-\alpha)^n T^2} \quad (\text{B-10})$$

and x_i as:

$$x_i = \frac{1}{T_i} \quad (\text{B-11})$$

The following equation can be obtained:

$$y_i = ax_i + b \quad (i=1,2,\dots,m) \quad (\text{B-12})$$

where $a = -\frac{E}{R}$, $b = \ln \frac{AR}{\beta E}$.

Therefore, from Eq. (B-12), a and b could be solved as:

$$\begin{cases} a = \frac{m \sum_{i=1}^m x_i y_i - \sum_{i=1}^m x_i \sum_{i=1}^m y_i}{m \sum_{i=1}^m x_i^2 - (\sum_{i=1}^m x_i)^2} \\ b = \bar{y} - a\bar{x} \end{cases} \quad (\text{B-13})$$

where $\bar{y} = \frac{1}{m} \sum_{i=1}^m y_i$, $\bar{x} = \frac{1}{m} \sum_{i=1}^m x_i$, and:

$$E = -aR, \quad A = -a\beta \exp(b)$$

To calculate the y_i , the trapezoidal method for unequal distances is used. By introducing the notation:

$$\ln \int_0^{\alpha_i} \frac{d\alpha}{(1-\alpha)^n T^2} = P(\alpha_i) \quad (i=1,2,\dots,m) \quad (\text{B-14})$$

with $P(\alpha_0) = 0$, therefore:

$$P(\alpha_i) = P(\alpha_{i-1}) + \frac{1}{2}(\alpha_i - \alpha_{i-1})[g(\alpha_i) + g(\alpha_{i-1})] \quad (i=1,2,\dots,m) \quad (\text{B-15})$$

$$\text{where } g(\alpha_i) = \frac{1}{(1-\alpha_i)^n T_i^2}, \quad g(\alpha_{i-1}) = \frac{1}{(1-\alpha_{i-1})^n T_{i-1}^2}$$

with the selection of the value of reaction order, n , according to the trial calculation for several values between 0.5 and 2.0.

APPENDIX – C GLOSSARY OF COMMONLY USED TERMS

Pyrolysis

Pyrolysis is the process of conversion of biomass and waste materials into useful liquid, gaseous fuels and char. The process is carried out in the absence of oxygen. Thermal breakdown of biomass produces varying proportion of char, liquid oils and gaseous fuel. Depending upon the heating rate pyrolysis can be categorized into slow, fast or flash pyrolysis.

Slow pyrolysis

During slow pyrolysis, heating rate varies from 5 - 7 °C min⁻¹. This slow heating rate produces more solid char and lesser amounts of liquid oils and gaseous fuels. Output of the process varies with the increase in reaction temperature. Increasing temperature produces more oils up to 550 - 600 °C and less char.

Fast pyrolysis

A higher heating rate of around 300 °C min⁻¹ is used in fast pyrolysis. It favours production of more oils and less char. Fast pyrolysis is more successful with fluidized bed reactor in producing more oil yield.

Flash pyrolysis

Flash pyrolysis employs very high heating rates of > 100 °C s⁻¹ with reaction time of only few seconds or even less. Due to high heating rate and low reaction time, particle size is an important factor. Particle size from 105 - 250 µm is favourable for flash pyrolysis.

Gasification

Gasification is the process of conversion of biomass or organic waste feedstock into a combustible gas. This process is carried out at substoichiometric conditions typically at temperature varying from 500 - 850 °C.

Combustion

During combustion, biomass is burnt in an open atmosphere in the presence of excess amount of oxygen to produce carbon dioxide, water and heat. Heat generated from combustion of biomass can be used in various ways especially for electricity generation.

Temperature programmed oxidation

The temperature programmed oxidation (TPO) technique is used to characterise the reacted catalysts using a thermogravimetric analyser (TGA). This technique is used to investigate the amount of coke deposited on the spent catalyst from the process of pyrolysis/gasification. Around 15 mg of reacted catalyst is placed inside the crucible of the TGA and heated from room temperature to 800 °C at a heating rate of 15 °C min⁻¹ in an air atmosphere (50 ml min⁻¹). The weight loss of the sample is recorded in relation to time and temperature.

Synthesis gas or syngas

Mixture of gases produced during gasification of biomass is known as synthesis gas or syngas. It is a combination of hydrogen, carbon monoxide, carbon dioxide and methane and lighter hydrocarbons including ethane, ethene, propane, propene, butane, butene and butadiene.

Residence time

Residence time is the reactor volume divided by the carrier gas flow rate.

Fixed bed reactor

Fixed bed reactors are stationary reactors which are relatively easy to design and operate. In a fixed bed reactor the sample is normally introduced from the top of the reactor while the product gases leaves either from the top or from the bottom depending upon up draft or down draft configuration. These types of reactors are suitable for small to medium applications. Due to the absence of mixing medium, achieving a uniform temperature is difficult at large scale.

Fluidised bed reactor

Fluidised bed reactors use a moving bed of inert material such as sand or silica. Feedstock is introduced from the bottom of the reactor and fluidised using air, nitrogen, steam, recycled product gases or a combination. Product gases leave the reactor from the upper part. Due to the fluidisation, heat transfer increases which in turn leads to better reaction rates and improved conversion efficiency. Fluidised bed reactors are suitable for medium to large applications and they can be easily scaled to megawatt applications.